Effect of Z-shaped Steel Plate Connectors on Out-of-Plane Flexural Behaviour of Precast Insulated Concrete Panels

by

Nabi Goudarzi

A thesis submitted in partial fulfillment of the requirements for the degree of

Doctor of Philosophy

in

STRUCTURAL ENGINEERING

Department of Civil and Environmental Engineering
University of Alberta

ABSTRACT

Precast Insulated Concrete Panels (PICP) consist of an insulation layer sandwiched between two concrete layers. The concrete layers of PICP are attached to each other by interlayer mechanical connectors. These panels are widely used in North America as cladding system to provide thermal insulation for the buildings and protect the building envelope against moisture ingress. These panels are subject to out-of-plane wind and seismic loading.

The out-of-plane shear strength and stiffness of PICP depend on the shear strength and stiffness of the interlayer mechanical connectors. Interlayer mechanical connectors with sufficient shear stiffness mobilize flexural composite behaviour between the concrete layers. The connectors that mobilize large degree of composite action are called *shear connectors*. As the out-of-plane flexural composite action of PICP is increased their out-of-plane deflection under out-of-plane service loading is decreased and their out-of-plane strength is improved. Most common shear connectors include truss and grid type connectors made of steel or composite material. While these connectors have proved to induce large degree of composite action, they are susceptible to buckling. Thus the full strength of their material is not efficiently mobilized.

Z-shaped Steel Plate Connectors (ZSPC) have recently been utilized in PICP and they reach their plastic shear strength before buckling. Thus, ZSPC is structurally more efficient than the existing truss and grid connectors in mobilizing composite action in PICP. In this research experimental and analytical studies are conducted on ZSPC to examine their shear behaviour, and to determine the effect of their width and thickness on their shear behaviour. An analytical method is proposed and validated to estimate the shear strength and stiffness of ZSPC, which can be used for optimal design of these connectors for PICP.

In this research, out-of-plane flexural tests are conducted to determine the effect of ZSPC on the out-of-plane strength and stiffness of non-loadbearing PICP with and without end-beams. These tests showed that PICP with ZSPC can achieve out-of-plane strength and stiffness of a fully-composite panel. Moreover, the tested PICP with end-beams achieved the out-of-plane strength and stiffness of a fully-composite panel even with the smallest ZSPC used in these tests.

A Multistep Linear Elastic (MLE) analysis method is proposed to estimate the out-of-plane flexural behaviour of PICP with different interlayer mechanical connectors with and without end-beams. This method is verified by the experimental results of the tested PICP in this research and previous studies. It is shown that the MLE analysis method can estimate the out-of-plane flexural behaviour of PICP with different interlayer connectors with and without end-beams. Based on the MLE method, an analytical approach is developed to estimate the out-of-plane deflection, cracking and ultimate out-of-plane flexural strengths of simply supported PICP with and without end-beams. The analytical results showed that end-beams absorb a large portion of the interlayer shear forces, thereby reducing the shear demand on the interlayer mechanical connectors. Moreover, end-beams improve the interlayer shear stiffness of PICP and induce at least 80% degree of composite action regardless of the shear stiffness of the interlayer mechanical connectors.

DEDICATION

Dedicated to my parents Floria Sobhi and Mortaza Goudarzi for all the support and encouragement they gave me without which my academic achievement would not be possible.

ACKNOWLEDGEMENTS

This research was funded by Civil and Environmental Engineering Department of University of Alberta. The experimental program of this work was conducted at I.F Morrison Structures Laboratory of University of Alberta. Part of this research was funded by Natural Sciences and Engineering Research Council (NSERC) of Canada through an industrial partnership with Read Jones Christoffersen (RJC) Consulting Engineers. The insulation and Z-shaped connectors used in the experiments and parts of the funding throughout this research were provided by Fero Corporation.

I like to thank my first supervisor Dr. Yasser Korany for his support of this research throughout my studies. He helped me define this research project and design the experimental program. After he left the university, he continued to give me invaluable comments on processing and interpreting the experimental and analytical results. I also thank my second supervisor, Dr. Samer Adeeb, who supported this research and helped me in the numerical analysis conducted in this research. He also gave invaluable comments on the discussions of the experimental and numerical results. I also thank my co-supervisor Dr. Roger Cheng for supporting this research. He gave me precious insights into the experimental and numerical results of this research, including shear behaviour of Z-shaped connectors, flexural behaviour of insulated panels, and application of the numerical results of this research to other types of structures.

I would also like to thank the technicians of I.F. Morrison Structures Laboratory, Greg Miller and Cameron West for assisting me in design and implementation of the experimental program of this research. I also thank the technician of the concrete laboratory, Rizaldy Mariano, for helping me in casting and testing the concrete for the experimental part of this research.

Last but not least, I thank my friends in structures group who helped me in casting concrete during the experimental program of this research. These wonderful friends include but are not limited to: Amir Jamshidi, Diana Abdulhameed, Fereshte Talaei, Mohamad Najari, Mohammad Ahmed, Mohammad J.T. Kian, Montazar Rabiei, Pouya Salem, Sadegh Naserkhaki, Sina Ghazizadeh, Syed Mobeen.

Table of Contents

List of Tables

List of Figures

List of Major Symbols

A_l = cross sectional area of concrete layer

$A_{l,cr}$ = cross sectional area of cracked concrete layer

A_s = area of longitudinal reinforcement

b = width of insulated panel

b_{tie} = width of the tension tie

c = depth of uncracked part of the cross section

D = diagonal length of the unembedded part of Z-shaped connectors

d = depth of reinforcement from compressive side of cross section

E = modulus of elasticity of steel used in Z-shaped connectors

E_c = modulus of elasticity of concrete

F = total vertical load (Chapter 8)

f_a = flexural stress

f_c = compressive strength of concrete

f_r = tensile strength of concrete

f_u = ultimate strength of steel

f_v = average shear stress

f_y = yield strength of steel

h_c = distance between the centroids of the concrete layers

I_l = moment of inertia of concrete layer

$I_{l,cr}$ = moment of inertia of cracked concrete layer

K = total interlayer shear stiffness

K_0 = basic interlayer shear stiffness

K_a = shear stiffness of tension tie model due to its axial deformation

K_b = shear stiffness of simplified plate model under pure in-plane bending moment

$K_{c,pl}$ = shear stiffness of simplified model due to concrete-connector interaction

$K_{c,tie}$ = shear stiffness of tension tie due to concrete-connector interaction

K_{pl} = secant shear stiffness of simplified plate model

K_s = experimental secant shear stiffness of Z-shaped connectors (Chapter 4)

= shear stiffness of simplified plate model under pure in-plane shear force (Chapter 6)

K_{tie} = secant shear stiffness of tension tie model

L = length of unembedded part of Z-shaped connectors (Chapter 4, 5, 6)

= length of panel (Chapter 7, 8, 9)

M = in-plane bending moment (Chapter 6)

= out-of-plane bending moment (Chapter 7, 8, 9)

M_0 = plastic in-plane bending moment

M_l = out-of-plane bending moment of concrete layer

M_t = total out-of-plane bending moment

n = modular ratio of steel to concrete

P = total vertical force on the middle concrete layer in the push-off tests (Chapter 4, 5, 6)

= axial force (Chapter 7, 8, 9)

q_{cr} = out-of-plane cracking strength of panel

q_s = out-of-plane service load

q_u = out-of-plane ultimate strength of panel

t = thickness of Z-shaped connector

V = in-plane shear force of Z-shaped connectors

V_0 = plastic in-plane shear force using Tresca yield shear stress

V_{bm} = interlayer shear force taken by end-beam

V_c = total interlayer shear force of fully-composite panel

V_p = plastic in-plane shear strength of Z-shaped connector

V_t = total interlayer shear force

V_{tie} = shear strength of Z-shaped connector using tension tie model

W = width of Z-shaped connector along the direction of in-plane shear force

α = aspect ratio

β = degree of composite action

Δ_c = out-of-plane deflection of fully-composite panel

Δ_{nc} = out-of-plane deflection of non-composite panel

Δ_v = shear deformation of Z-shaped connectors (Chapter 4, 5, 6)

= vertical deflection of the mid-span of panel (Chapter 7, 8, 9)

θ = angle of the tension tie of Z-shaped connector with the connector width

λ = slenderness parameter

τ_y = yield shear stress

ϕ = curvature

Part 1: Introduction

1. Introduction and Research Objectives

1.1. Introduction to PICP

Precast Insulated Concrete Panels (PICP) is a type of insulated walls consisting of two concrete layers with insulation in between; the concrete layers are connected to each other by interlayer mechanical connectors (Figure 1-1). These panels are widely used as cladding system to provide thermal and acoustic insulation and protect the building envelope from moisture ingress. These panels are more durable and structurally more efficient than other cladding systems. Since PICP are installed on the perimeter of the building, they are subject to wind loading. Also PICP, as well as other wall or panel systems, are subject to out-of-plane seismic and explosion loads. In some PICP systems the top and bottom ends of the panels - where they are connected to the structural frame or floors of a building - are enclosed by concrete beams, called end-beams. End-beams are mostly used where loadbearing panels are connected to the floors to transfer the gravity loads to the panel. End-beams are also used in some panel systems to protect the panel from ingress of moisture and rainwater.

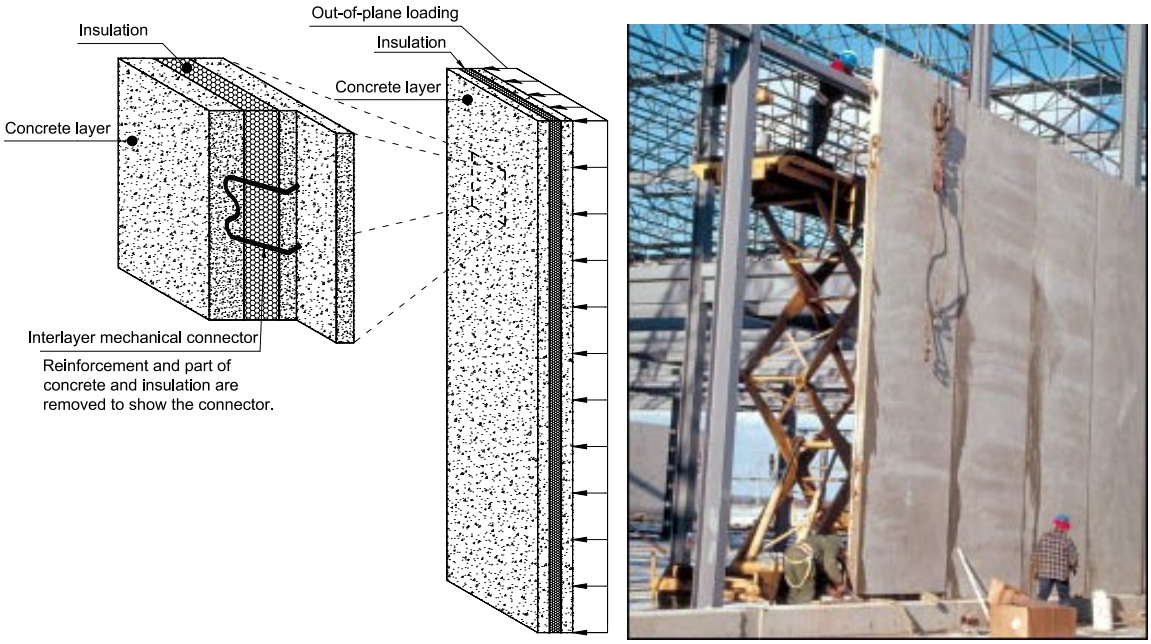

http://www.cpci.ca

Figure 1-1: Precast Insulated Concrete Panels.

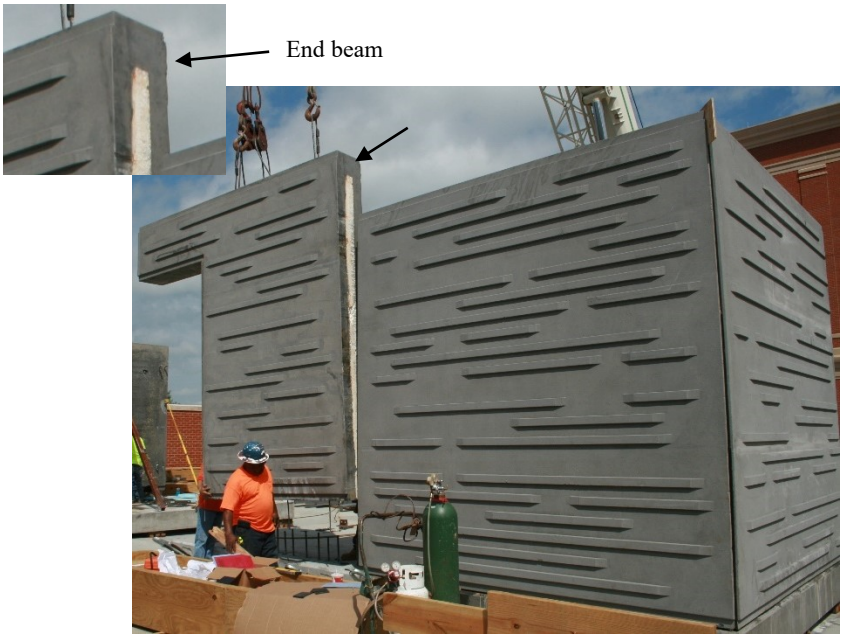

http://www.qarmazi.com/qa/57154/how-to-make-cement-wall/

Figure 1-2: Precast insulated concrete panels with end-beams.

Out-of-plane flexural behaviour of PICP

Out-of-plane flexural deformation of PICP is caused by either out-of-plane loading or out-of-plane buckling deformation of PICP under in-plane compressive forces. Therefore, it is important to understand the out-of-plane flexural behaviour of PICP. Theoretically, if the interlayer mechanical connectors possess infinitely large shear stiffness, the out-of-plane flexural behaviour of the panel resembles that of a Bernoulli beam, i.e. the plane sections remain plane across the entire depth of the panel. This behaviour is called fully-composite behaviour. Since the shear stiffness of the interlayer connectors is not infinite, the actual out-of-plane flexural behaviour of the panel resembles that of a Timoshenko beam, i.e. the plane sections do not remain plane across the entire depth of the panel and some shear slip occurs between the concrete layers. This behaviour is called partially-composite behaviour. But if the shear stiffness of the interlayer mechanical connectors is zero, the plane sections remain plane across the depth of individual concrete layers, but not across the entire depth of the panel. In other words, each concrete layer behaves as a Bernoulli beam. This behaviour is called non-composite behaviour. Therefore, the degree of out-of-plane flexural

composite behaviour depends on the shear stiffness of the interlayer mechanical connectors (Pessiki and Mlynarczyk, 2003).

In-plane and out-of-plane loading on PICP

Depending on the connection of panels to the floors of a building, PICP can be non-loadbearing or loadbearing (PCI, 2011). Non-loadbearing panels carry out-of-plane loads, but not gravity loads; these panels are connected to the wall framing of the building (Figure 1-3). The structural frame carries the gravity loads, while the panels only resist the out-of-plane wind loads. The out-of-plane strength and stiffness of PICP depends on the shear strength and stiffness of the interlayer mechanical connectors (Einea et al., 1991).

Loadbearing panels are directly connected to the floor slabs or joists and carry the gravity loads (Figure 1-3). The height/thickness ratio of PICP is high, thus loadbearing panels can undergo out-of-plane buckling deformation under axial loads. Therefore, the axial behaviour of PICP is also affected by the degree of out-of-plane flexural composite action. Experimental results have shown that axial strength of loadbearing panels depends on the slenderness ratio of the panel and is improved by the presence of end-beams (Benayoune et al. 2007, Gara 2012). The presence of end-beams was found to impose fully-composite buckling shape in the panels under axial loads regardless of the number of connectors (Gara, 2012). The degree of out-of-plane flexural composite behaviour of PICP under axial loading was found to increase with the increase in slenderness ratio of PICP (Mohamad et al., 2012). Since the behaviour of loadbearing panels is an interaction of axial and out-of-plane flexural behaviour, each of these modes of behaviour should be understood. As described in Section 1.2 the author believes despite the body of research on this topic, the out-of-plane flexural behaviour of PICP is not completely understood, i.e. the out-of-plane flexural strength and stiffness of PICP with different connector systems cannot be estimated using the existing literature. Therefore, this mode of behaviour is the focus of this research.

a. 

http://www.lonestarprestress.com

b. 

http://www.frontdesk.co.in

Figure 1-3: An example of: a. non-loadbearing and b. loadbearing insulated concrete panels.

Experimental research has shown that PICP can also be used as lateral force resisting system in regions with moderate to high seismicity (Pavese et al., 2011). Failure of PICP under lateral loads is governed by crushing of concrete and buckling of reinforcement at the corners of the panel. This failure mode can be prevented by providing concrete columns on the sides of the panel with sufficient confinement reinforcement to prevent buckling of columns' longitudinal bars. Application of PICP as lateral force resisting system is rare and more research is yet to be done on this application of PICP.

Non-loadbearing PICP

As mentioned earlier, shear behaviour of interlayer mechanical connectors significantly affects the degree of out-of-plane flexural composite behaviour of PICP. This degree of composite behaviour of non-loadbearing PICP may vary throughout the loading history of the panel (PCI, 2011). In the early stages of loading, where all the materials have elastic behaviour, an insulated panel might exhibit fully-composite behaviour. This composite behaviour degrades by increased out-of-plane loading due to plastic deformation of the shear connectors and cracking of the concrete layers. Analyses by the author shows that composite behaviour of concrete layers in PICP can reduce the thickness of the concrete layers by up to 50% compared to that in non-composite insulated panels. Therefore, neglecting composite action between concrete layers results in uneconomical design and inefficient use of materials in PICP. Moreover, high thickness of concrete layers in non-composite panels adds to the overall weight of the building, which in turn requires heavier structure for the building. Therefore, to achieve structurally efficient non-loadbearing panel, the interlayer connectors should have sufficient shear strength and stiffness for the panel to have composite out-of-plane flexural strength and stiffness.

On the other hand, composite panels lead to differential thermal deformations of the concrete layers, resulting in bowing of insulated panels. This induces cracking in the walls and spoils the aesthetics of the building (Einea et al., 1991). Moreover, material and number of interlayer mechanical connectors affect the thermal efficiency of PICP (CPCI 2007, Salmon et al. 1997). Steel and concrete interlayer connectors form thermal bridges between the concrete layers of PICP, reducing the thermal efficiency of the panel (McCall 1985, Wade and Porter 1988). Where thermal performance of PICP is the governing design factor, FRP (Fiber Reinforced Polymers) connectors are used in design of PICP. FRP connectors reduce thermal bridging between the concrete layers, thus maintaining the thermal efficiency of the panel, but they are more expensive than steel connectors. Therefore, design of PICP is a balance between structural, architectural and thermal performance, and the cost of the panel. This thesis only focuses on the structural performance of non-loadbearing panels under out-of-plane loading.

Interlayer mechanical connectors

As mentioned earlier the shear strength and stiffness of interlayer mechanical connectors determines the out-of-plane flexural behaviour of PICP. Common interlayer mechanical connectors include pins, ties, grids and trusses. These connectors are described more in Chapter 2 and are shown in Figure 2-1. Interlayer connectors are made of steel or FRP materials. Truss type connectors are the most common type of connectors to mobilize composite flexural behaviour. Although these connectors possess sufficient strength and stiffness to induce composite flexural behaviour in PICP, compressive web members of truss connectors are prone to buckling, after which the interlayer shear forces are only carried by the tensile web members. Due to buckling of the compressive web members, the full plastic shear capacity of truss connectors is not mobilized; i.e. not all the members of the truss connectors reach their plastic strength. This is inefficient use of material.

Fero Corporation has recently utilized Z-shaped Steel Plate Connectors (ZSPC) for PICP. Different forms of Z-shaped connectors, also called Z-shaped anchors, are used in masonry structures to tie the veneer to the masonry wall, as shown in Figure 1-4. The application of Z-shaped connectors as an interlayer connector system for PICP is new. In this application, the flanges of ZSPC are tied to the reinforcement of the concrete layers. As shown in Figure 1-5, ZSPC are oriented such that the interlayer shear forces act along the connector's width so that the interlayer shear forces induce in-plane shear force in the connector's web. Due to large in-plane shear strength and stiffness of this system, ZSPC seems to have high efficiency in transferring interlayer shear forces, hence improving the composite action of the concrete layers. However, the large in-plane shear strength and stiffness of ZSPC might be affected by the interaction between the embedded part of the connectors and the concrete. Currently, there is only one study in the literature on the effect of ZSPC on the out-of-plane flexural behaviour of PICP, and that study is only limited to two flexural tests. That study is explained in more detail in Section 2.3. Also, there is no study on the shear behaviour of ZSPC. As mentioned earlier, shear strength and stiffness of interlayer mechanical connectors determines the out-of-plane flexural strength and stiffness of PICP. Therefore, for every connector system it is important to find its shear strength and stiffness in order to estimate the out-of-plane flexural behaviour of PICP.

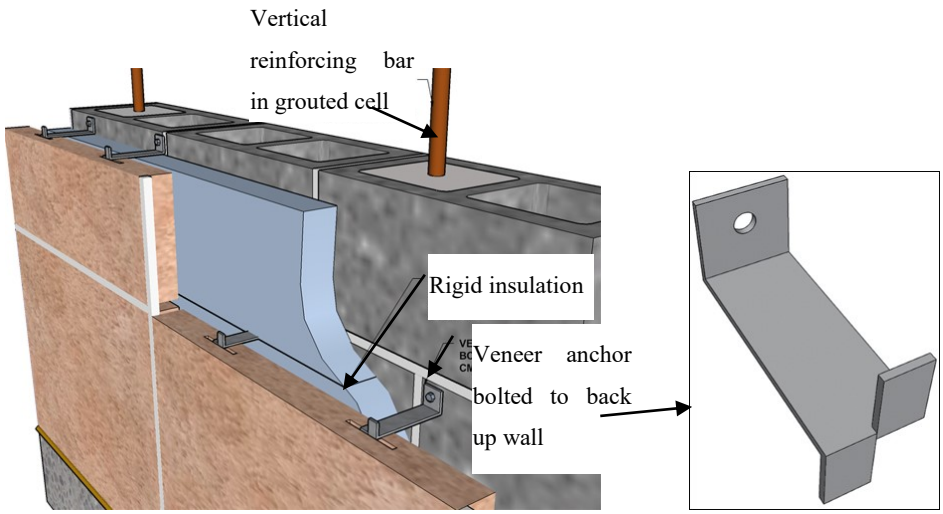

http://www.masonrysystems.org/wall-systems/cavity-wall-stone-slab-veneer-reinforced-concrete-block/

Figure 1-4: Connection of veneer to masonry wall by Z-shaped connectors.

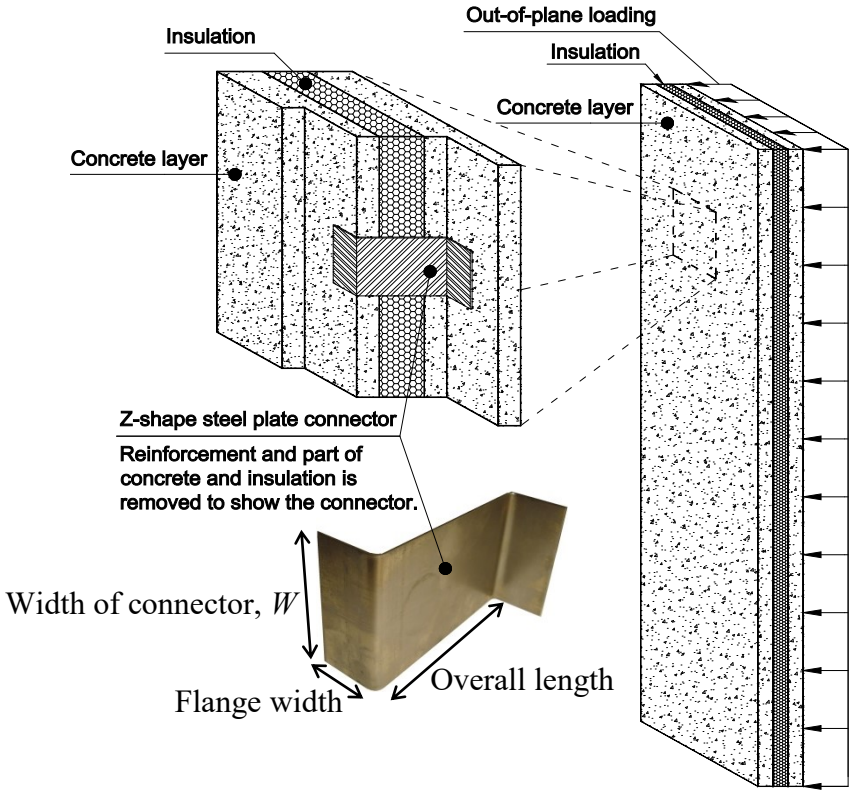

Figure 1-5: Schematic of Z-shaped connectors used in precast concrete panels.

Among the common connector systems, truss type connectors possess the largest shear strength and stiffness. These connectors are manufactured to the desired length, then placed in between the concrete layers before casting of concrete. However, Z-shaped connectors, as well as other discrete connectors are placed one by one at the designed spacing. Thus, using discrete connectors including Z-shaped connectors is more labor intensive than using truss connectors. However, to facilitate installation of Z-shaped connectors, these connectors can be placed at the designed spacing on a manufacturing bed and two bars can be hooked to the connector flanges, one bar at each flange. The flanges can then be welded to the bars. This assembly can then be placed between the concrete layers of PICP before casting of concrete.

1.2. Problem Statement

Many experimental and theoretical studies have shown that out-of-plane behaviour of Precast Insulated Concrete Panels (PICP) is significantly dependant on the shear strength and stiffness of the shear connectors, and that PICP with flexural fully-composite or partially-composite behaviour have significantly higher structural efficiency than PICP with non-composite behaviour (Pfeifer and Hansen, 1964). As a result many researchers have studied the effect of commonly used interlayer mechanical connectors on the degree of composite behaviour in PICP under out-of-plane loading.

A new mechanical connector system in PICP has recently been developed using Z-shaped Steel Plate Connectors (ZSPC) partially embedded in concrete, the structural behaviour of which has not yet been studied. Due to high in-plane shear and flexural behaviour of ZSPC, this type of connector is structurally efficient in providing interlayer shear strength and stiffness in PICP. Therefore, it is necessary to investigate the shear behaviour of ZSPC, and their effects on the degree of composite action of PICP under out-of-plane loading.

Moreover, in practice PICP are enclosed at top and bottom with reinforced concrete beams. However, the effect of these end-beams on out-of-plane behaviour of insulated panels is not fully investigated, and some studies have led to inconsistent results on the contribution of these beams to the composite behaviour of PICP. Therefore, more investigation is needed to be conducted on out-of-plane behaviour of PICP with RC end-beams to get a clear understanding of the effect of these beams on the degree of composite action between the concrete layers.

1.3. Scope and Objectives

In this research experimental and analytical investigations will be conducted on non-loadbearing Precast Insulated Concrete Panels (PICP) with Z-shaped Steel Plate Connectors (ZSPC). This research does not address loadbearing PICP. The objectives of this research are as follows:

1. Investigate the effect of ZSPC and RC end-beams on out-of-plane strength and stiffness of non-loadbearing PICP.

Specific Aim 1: Determine shear strength and stiffness of ZSPC partially embedded in concrete, as is the case in PICP.

Specific Aim 2: Determine the out-of-plane flexural behaviour of non-loadbearing PICP with ZSPC.

Specific Aim 3: Determine the out-of-plane flexural behaviour of non-loadbearing PICP with ZSPC and RC end-beams.

2. Propose an approach for structural design of ZSPC for non-loadbearing PICP with and without end-beams under out-of-plane loading.

Specific Aim 1: Propose an analytical approach to estimate the shear behaviour of ZSPC.

Specific Aim 2: Propose an analytical approach to estimate the out-of-plane flexural behaviour of PICP with ZSPC with and without end-beams.

1.4. Research Significance

Precast Insulated Concrete Panels are widely used as cladding for buildings due to their high concrete quality, durability, low maintenance cost, high speed of construction and high energy efficiency. These features have made PICP a suitable cladding system especially for regions with cold climate, such as Canada. These panels are subject to out-of-plane forces and their out-of-plane flexural behaviour depends on the shear behaviour of the interlayer mechanical connectors. Thus, it is necessary to design these mechanical connectors to obtain optimum structural and energy efficiency. As mentioned earlier, optimum design of these connectors to have composite behaviour will significantly increase the structural efficiency of the panel, which reduces their self-weight,

lowering the demand on the supporting structure. This significantly reduces the total cost of a construction project.

Due to large in-plane shear and flexural strength and stiffness of ZSPC, this connector system might be more efficient in providing interlayer shear strength and stiffness in PICP than other interlayer mechanical connectors. This connector system has not yet been studied in the literature. Therefore, it is important to understand the shear behaviour of ZSPC and their effect on the degree of composite action in PICP.

1.5. Thesis Outline

This thesis is written in four parts. Part 1 is the introductory part that contains four chapters. Chapter 1 gives an introduction to Precast Insulated Concrete Panels (PICP) and the effect of interlayer mechanical connectors on the out-of-plane behaviour of these panels. Then, it introduces Z-shaped Steel Plate Connectors (ZSPC) and explains the lack of knowledge on the shear behaviour of these connectors and their effect on the out-of-plane behaviour of PICP, thereafter outlines the scope and objectives of this research. Finally, it explains the significance of the conducted research for PICP industry.

Chapter 2 presents a brief overview of the previous experimental and analytical studies on PICP and the effect of various shear connectors on the out-of-plane behaviour of Precast Insulated Concrete Panels. Chapter 3 explains the methodology of this study to address the research objectives.

Part 2 presents the results of the investigations on the shear behaviour of ZSPC carried out in this research. This part is divided into three chapters. Chapter 4 describes the conducted push-off shear tests on ZSPC and gives discussions of these experimental results. Chapter 5 presents the numerical modeling of the tested shear specimens using Finite Element Method (FEM) and compares the results with the results of the push-off shear tests. Section 5.5 presents the results of the parametric study on the effect of width and thickness of ZSPC on their shear strength and stiffness using the numerical models developed in Chapter 5. Chapter 6, the last chapter of this part, compares the estimated shear behaviour of ZSPC using existing analytical models with the numerical results, and discusses the shortcoming of the existing models. Then it proposes a new analytical model to predict the shear behaviour of ZSPC based on the numerical results presented in Section 5.5.

Part 3 presents the results of the investigations on the out-of-plane behaviour of non-loadbearing PICP consisting of ZSPC. Two of the studied panels also included end-beams to evaluate the effect of these beams on the out-of-plane behaviour of these panels. This part is divided into three chapters. Chapter 7 describes the out-of-plane 4-point flexural tests on six PICP and gives discussions of these experimental results. Chapter 8 proposes Multistep Linear Elastic (MLE) method for nonlinear analysis of structures. This method is adopted in Chapter 8 to conduct nonlinear analysis of the tested PICP. The results of these analyses are compared with the results of the 4-point flexural tests. Chapter 9 give recommendations for structural design of PICP using simplified MLE method. Afterwards, Chapter 9 proposes an analytical model using degree of composite action to analyze simply supported PICP under out-of-plane uniform loading.

Part 4 includes Chapter 10, which summarizes the results of this research on the shear behaviour of ZSPC and their effect on out-of-plane flexural behaviour of non-loadbearing PICP. It also mentions unaddressed problems in this research and gives recommendations for future studies to complement and refine the results of this research.

2. Literature Review

2.1. Analysis and Design of PICP in Existing Codes and Practice

Leabu (1965) was one of the first researchers who proposed some guidelines for design of PICP, which has since been the basis of design codes such as the guide for precast concrete wall panels (ACI 533). He suggested in insulated panels the interlayer shear forces should not be transferred through the non-structural insulation layer. He also recommended that the slenderness (height/thickness) ratio of Insulated Concrete Panels be limited to 50 and their out-of-plane deflection be restricted to $h/240$. Moreover, the fasteners for lifting should be designed for 100% impact load (Leabu, 1965).

Nowadays some design provisions for PICP have been provided by ACI 533, ACI 318, CAN/CSA A23.3-04 and PCI design handbook. These documents give requirements on geometry, materials and construction method of these panels. They also require minimum amount of ties connecting these panels to the supporting floors and frames to ensure the integrity of the structure.

The Canadian standard for design of concrete structures (CAN/CSA-A23.3-04) standard requires that the concrete ingredients, reinforcement placement and concrete cover over the reinforcement comply with the requirements of CSA A23.4 and in corrosive environments the quality of concrete satisfy the requirements of CSA A23.1.

The CAN/CSA-A23.3-04 requires a minimum thickness of 140 mm and maximum height/thickness ratio of 65 for precast concrete panels. It also stipulates that the interaction between the concrete layers, thermal effects, thermal bridging and lifting stresses should be considered in designing PICP and their connections. Lifting stresses should be calculated using elastic uncracked analysis. Moreover, tension ties should be installed in the longitudinal and transverse directions of the structure to maintain the integrity of the structure. This standard limits the out-of-plane deflection of the panels to 1/100 of the height.

The guide for precast concrete wall panels (ACI 533) provides some general guidelines for fabrication of PICP and refers to the requirements of ACI 318 for structural design of these panels. According to ACI 533 the minimum required reinforcement should comply with ACI 318, but it should be greater than 0.1% of the cross sectional area of the panel. The requirements for shrinkage

reinforcement can be waived in one-way prestressed panels not wider than 3.7 m. ACI 533 also limits the out-of-plane deflection of non-load bearing PICP to 1/480 of its height.

The slenderness ratio (*h/t*) of insulated panels is limited to 150 by ACI-533, otherwise more precise analysis is required. According to this code the secondary effects of compressive forces ($p-\Delta$) in load bearing panels should be considered as per provisions of ACI 318. Interlayer shear forces can be calculated as the difference between the compressive and tensile forces at any section of the flexural member. Precast concrete wall panels are required to have at least two ties per panel with a minimum tensile strength of 44 kN per tie. Both American standard ACI 318 and Canadian standard CAN/CSA-A23.3-04 requires that forces due to creep, shrinkage, temperature differential, prestressing and handling be considered in design of PICP.

The most common method to calculate the shear demand of the connectors of PICP to ensure fully-composite action is based on the flexural capacity of the section, which is recommended by the Precast/Prestressed Concrete Institute (PCI 2011, CPCI 2007). In this method the maximum horizontal shear force is taken as the lesser of the compression resistance of the compression concrete layer and tension resistance of the tension concrete layer at mid-span (Naito et al. 2012). Thus the required shear capacity of the ties is calculated using the following equation:

$$V_{req} = min\left(A_s f_y, 0.85 f_c' b t_c\right) \quad \textbf{2-1}$$

Where A_s is the area of the non-prestressing reinforcement in the tension layer; f_y is the yield stress of the non-prestressing steel; f_c' is the compressive strength of concrete; b is the width of the panel; and t_c is the thickness of the compression concrete layer. To achieve a fully-composite response, the required number of shear ties can be determined using the shear strength of each shear tie and the required shear capacity of the ties. This method is based on assumption of full compatibility between the concrete layers (Naito et al. 2012). It should be noted that the shear demand cannot be determined assuming elastic response since it becomes inaccurate after cracking of the panel (Naito et al. 2012).

2.2. Shear Transfer between Concrete Layers

The stiffness and strength of interlayer mechanical connectors affect the degree of composite action in PICP. To evaluate the shear strength and stiffness of connectors direct shear tests (Mouser 2003) or push/pull out shear tests (Soriano & Rizkalla 2013, Naito et al. 2012, Salmon et al. 1997, Einea 1992) have been conducted on small PICP specimens. To investigate the effect of interlayer mechanical connectors on the out-of-plane flexural behaviour of PICP, panel specimens are usually tested under out-of-plane uniform loading (Einea 1992, Naito et al. 2012, Lee & Pessiki 2008) or 4-point loading (Basenbul et al. 1991, Soriano & Rizkalla 2013, Benayoune 2008, Frankl et al. 2011). In this section the shear behaviour of different interlayer connector systems and their effect on the flexural behaviour of PICP studied by previous researchers is summarized.

If a connector system possesses sufficient shear strength and stiffness to mobilize fully-composite or partially-composite action, it is called shear connector, otherwise it is called non-shear connector (PCI, 2011). Non-shear connectors only carry tensile forces to maintain the integrity of the layers during construction. However, the degree of composite action not only depends on shear behaviour of interlayer mechanical connectors, but also on panel length (Salmon & Einea 1995, Bush & Wu 1998), insulation thickness (Pfeifer & Hansen 1964, Frankl et al. 2008, Soriano & Rizkalla 2013), insulation type (Frankl et al. 2008, Soriano & Rizkalla 2013, Pfeifer & Hansen 1964) and number of connectors (Basunbul et al. 1991, Lee & Pessiki 2008).

Interlayer mechanical connectors are also divided into continuous connectors and discrete connectors (Einea et al. 1991). Figure 2-1 shows some common connector systems. Connectors are either made of steel, concrete, or composite materials (Einea et al. 1991, Naito et al. 2012). Composite materials are used when thermal efficiency of the panel is of high significance (Einea et al. 1991). Common types of continuous connectors include: truss connectors, concrete webs, grid connectors (Soriano & Rizkallah 2013, Naito et al. 2012, Bunn 2011) and ladder connectors (Carbonari et al. 2012, Naito et al. 2012).

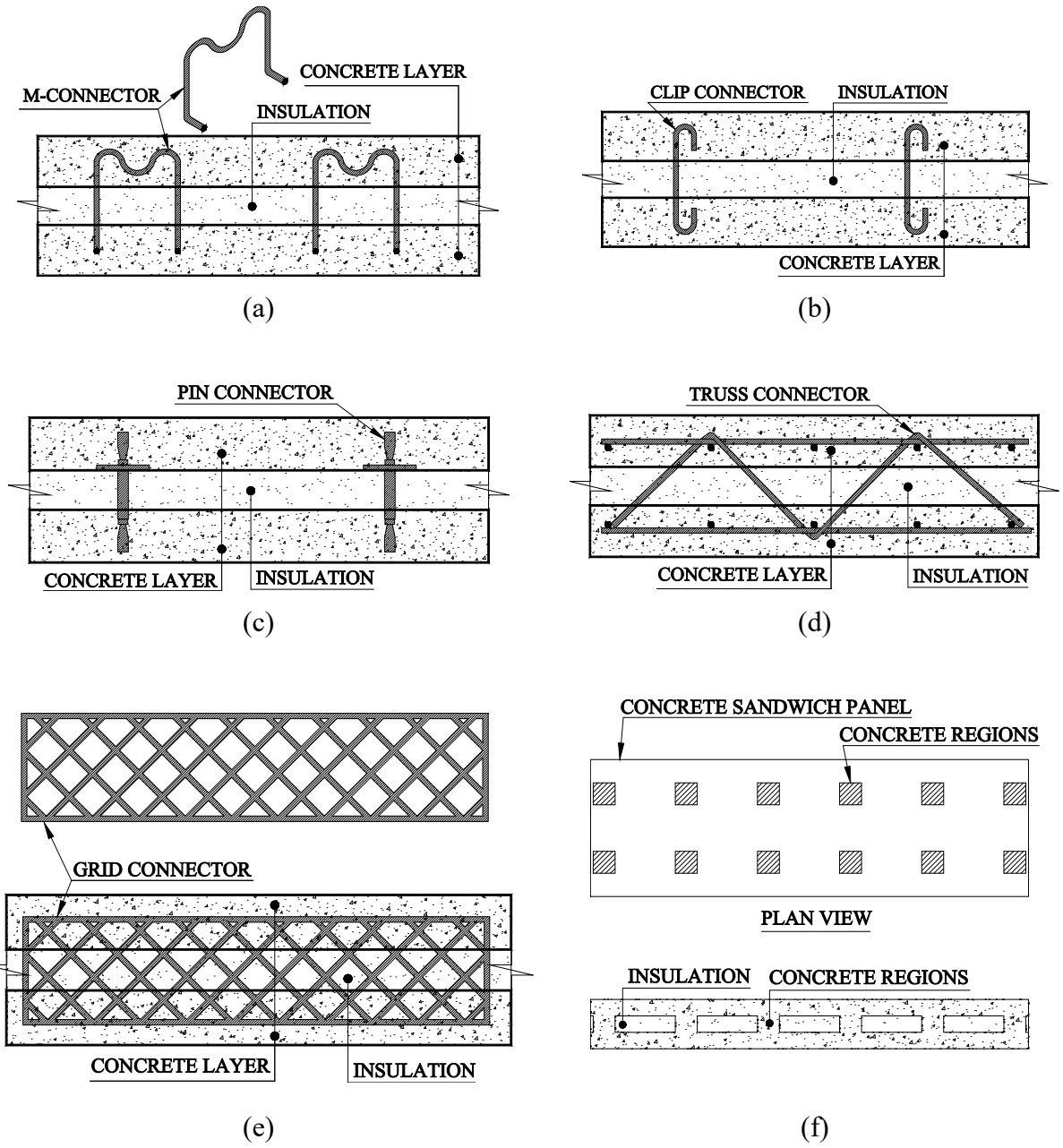

Figure 2-1. Different interlayer mechanical connector systems: a. M-ties, b. C-clips, c. pin, d. truss connector, e. grid connector, f. concrete regions.

Truss connectors can either made of bars or strips, and are made of FRP or steel (Salmon et al. 1997, Einea 1992, Naito et al. 2012). Truss connectors have larger shear strength and stiffness and energy absorption per unit length compared to pin connectors, grid connectors and ladder connectors (Naito et al. 2012, Einea 1992, Bush & Stine 1994). Failure mode of this connector system is buckling of compression legs and yielding of the tensile legs (Salmon et al. 1997, Einea et al. 1991). This depends on the compressive and tensile resistance of the legs, which depends on their material properties and diameter. Shear and flexural tests have shown that compression legs in steel trusses are susceptible to buckling due to the high length-to-diameter ratio of the compression legs (Salmon et al., 1997). After buckling of the compression legs the shear forces are taken by the tension legs of truss connectors. Thus shear behaviour of truss connectors is governed by the tensile behaviour of the diagonals. Since FRP is brittle tension legs in FRP truss connectors undergo brittle failure; conversely, since steel is ductile tension legs in steel truss connectors undergo ductile failure. Thus FRP truss connectors show brittle shear behaviour but steel truss connectors show ductile shear behaviour (Naito et al. 2012). Another mode of failure was found to be cracking of concrete layers of shear specimens (Einea 1992). This brittle failure mode occurs in shear specimens with high-strength truss connectors, which was observed in experiments by Einea (1992) on truss connectors with FRP material.

Flexural tests of PICP with truss connectors have shown that these connectors can mobilize partially-composite action depending on the number of trusses and cross sectional dimensions of trusses (Salmon et al. 1997). For example, experiments on PICP under out-of-plane uniform load by Salmon et al. 1997 showed that the shear stiffness of the tested panels to that of theoretical fully-composite panels was 72% and 27% for PICP with FRP and steel trusses, respectively. Moreover, due to ductility of steel, steel truss connectors redistribute the load after failure of the critical compression legs, which gives the panel a ductile failure mode. However, due to brittle nature of FRP material, FRP trusses do not redistribute the load after breakage of critical member thus leads to a brittle failure mode (Salmon et al. 1997).

Experiments by Pfeifer & Hansen (1964) and Lee & Pessiki (2008) have shown that concrete webs along the length of panels mobilize composite action in PICP due to their large shear strength and stiffness. However, increasing number of webs beyond the minimum required number to achieve fully-composite action does not improve the flexural behaviour of PICP (Lee & Pessiki 2008, Basenbul et al. 1991). Also, flexural tests have shown that PICP with concrete webs have ductile behaviour (Lee & Pessiki 2008). Although this connector system gives ideal out-of-plane flexural

behaviour to PICP, they reduce the thermal efficiency of the panel by making thermal bridges between the layers (Einea et al. 1991, PCI 2007) and increase the weight of the panel. Moreover, they rigidly connect the two concrete layers, which have different deformation, thus induce cracking on the panels (Einea et al. 1991, PCI 2007).

Grid connectors are made of metal sheets or composite materials (Soriano & Rizkalla 2013, Naito et al. 2002). The failure mode of FRP grid connectors includes rupture of tensile legs (Soriano & Rizkalla 2013) thus their shear behaviour is brittle (Natio et al. 2012). The failure modes of metal grid connectors, on the other hand, are buckling of compression legs and yielding of tensile legs (Naito et al. 2012, Mouser 2003). Since failure of metal grid connectors is governed by yielding of tensile legs the shear behaviour of this connector system is ductile (Naito et al. 2012). No pull-out of grid connectors was observed in shear tests on grid connectors (Soriano & Rizkalla 2013). Flexural tests have shown that grid connector systems can mobilize partially-composite to fully-composite behaviour depending in their material and number of connectors (Soriano & Rizkalla 2013, Frankl et al. 2011, Einea 1992).

Ladder connectors are a continuous non-shear connector system, investigated by shear tests and flexural tests by previous researchers. Because the connecting legs are perpendicular to the direction of the interlayer shear forces, they have low shear strength and stiffness, as shown by push-off shear tests (Naito et al. 2012, Gara et al. 2012). Therefore, ladder connector system does not mobilize composite action, as found by flexural tests on PICP under uniform loading (Carbonari et al. 2012). In the flexural tests conducted by Carbonari et al. 2012 on PICP with ladder connectors under uniform loading the initial stiffness of the tested PICP was only 8% of that of a theoretical fully-composite panel.

Common types of discrete connectors are M ties, Pins, C-shape ties and discrete concrete regions (Einea et al. 1991, Naito et al. 2012, Pessiki & Mlynarczyk 2003), which are shown in Figure 2-1. Most discrete connectors are non-shear connectors only used to maintain the integrity of PICP during handling.

C-shape steel ties and cross-shape ties have low shear strength and stiffness (Naito et al. 2012, Pfeifer & Hanson 1964) thus are non-shear connectors. C-shape steel ties undergo flexural and shear deformation at early stages of shear loading. With increased loading, these ties predominantly behave in tension, resulting in tensile yielding or pull-out failure of the tie depending on their embedment length (Naito et al. 2012, Woltman et al. 2013).

Composite pins with adequate diameter can have enough shear strength and stiffness to mobilize partially-composite out-of-plane flexural behaviour in PICP (Naito et al. 2012). The failure modes of these pins include shear or flexural failure, depending on the diameter/length ratio of the pin (Woltman et al. 2013). Shear failure mode is characterized by longitudinal cracks along the pin due to delamination of fibres and flexural failure is characterized by tensile rupture of fibres. No pull-out failure has been observed for these pins in shear tests by previous researchers (Woltman et al. 2013).

Shear tests have shown that M-ties have low shear strength and stiffness (Naito et al. 2012, Mouser 2003, Richmond 1997). Similar to C-shape steel ties, M-ties undergo large bending and shear deformations at early stages of loading. As shear deformation increases their behaviour changes to tension. This shifting of behaviour from shear and bending to tension is characterized by gradual increase in load after the first peak of shear force (Naito et al. 2012, Richmond 1997). Flexural tests have shown that PICP with M-ties exhibit non-composite behaviour (Mouser 2003, Pessiki & Mlynarczyk 2003). The out-of-plane flexural stiffness of panels tested by Pessiki & Mlynarczyk 2003 has only been 21% of that of a theoretical composite panel.

Discrete concrete regions is a connector system in which regions of concrete penetrate through insulation to connect the two concrete layers as shown in Figure 2-1. These regions have square, rectangular and circular shapes and are positioned at certain spacing across the panel. This connector system is rigid with high shear strength thus induce fully-composite action in PICP (Pessiki & Mlynarczyk 2003), however they significantly reduce the insulative efficiency of PICP due to thermal bridging and increases the weight of the panel (Einea et al. 1991). A certain type of discrete concrete region is reinforced beams at the top and bottom of PICP to keep out the rainwater. Flexural tests have shown that these end-beams have negligible effect on the degree of composite action in PICP (Carbonari et al. 2012, Pfeifer & Hansen 1964), which contradicts the findings by Salmon et al. 1997 that significant shear transfer occurs around the ends of PICP under out-of-plane loading.

Other than interlayer mechanical connectors shear transfer between concrete layers of PICP is affected by bonding and friction between insulation and concrete, handling inserts, thickness and type of insulation (Woltman et al. 2013, Soriano & Rizkalla 2013, Frankl et al. 2011). Bonding between insulation and concrete can take about 28% of the interlayer shear forces (Woltman et al.

2013), however this shear mechanism degrades during handling and over lifetime of the panel thus not recommended to rely on for design purposes (Pessiki & Mlynarczyk 2003, Einea et al. 1991).

Smaller insulation thickness in PICP improves the shear strength and stiffness of interlayer mechanical connectors (Soriano and Rizkalla 2013, Bunn 2011, Mouser 2003). For pin connectors, C-shape connectors and ladder connectors as the insulation thickness decreases the behaviour of the connector is dominated by shear, and as it increases the connector behaviour is dominated by bending (Woltman et al., 2013). Dominant shear behaviour corresponds to higher shear strength and stiffness. For connectors with inclined members, like truss connectors, smaller insulation thickness leads to smaller lengths of the inclined member, which improves buckling resistance of compression legs and longitudinal stiffness of all inclined members, which in turn increases shear strength and stiffness of the connector system.

Common types of insulation used in PICP include Expanded Polyurethane (EPS) and extruded polyurethane (XPS). Results of shear tests by previous researchers have proved PICP with EPS have higher shear strength due to more roughness of EPS surface (Soriano & Rizkalla 2013, Naito et al. 2012). Flexural tests on PICP have also revealed that PICP with EPS have improved flexural behaviour (Frankl et al. 2011, Soriano & Rizkalla 2013).

Analytical investigations by Salmon and Einea (1995) and Bush and Wu (1998) on PICP with truss connectors showed that as the length of panel increases, the effect of shear stiffness of connectors diminishes. Therefore, the degree of composite action increases with the length of the panel. This might be attributed to increased length or number of interlayer mechanical connectors along the panel with increased length, which leads to an overall higher shear transfer between the concrete layers.

2.3. Z-Shaped Steel Plate Connectors (ZSPC)

Z-shaped connectors were originally developed to connect masonry cladding to concrete or masonry wall (Figure 1-4). Recently Fero Corporation has utilized these connectors as interlayer mechanical connectors in PICP. These connectors are oriented such that the interlayer shear forces act along the web of the connectors, inducing in-plane shear forces in the webs. Therefore, the interlayer shear forces are transferred by the in-plane shear behaviour of the webs of ZSPC. Since steel plate possess large in-plane shear strength and stiffness, ZSPC are expected to mobilize high degree of composite action in PICP.

As a preliminary study, Fero Corporation conducted two 4-point out-of-plane tests on 1600 mm x 4000 (Width x length) PICP as shown in Figure 2-2 (Goudarzi et al., 2014). As shown in Figure 2-3, The two specimens were different in thickness of concrete layers and insulation. In the first specimen, P1, the thickness of the concrete layers was 75 mm and the overall thickness of the insulation was 75 mm, as well. In the second specimen, P2, the thickness of the concrete layers was 97 mm and the overall thickness of the insulation was 100 mm. In these tests 1.48 mm thick (16 gauge) and 76.2 mm wide ZSPC were installed at 600 mm spacing.

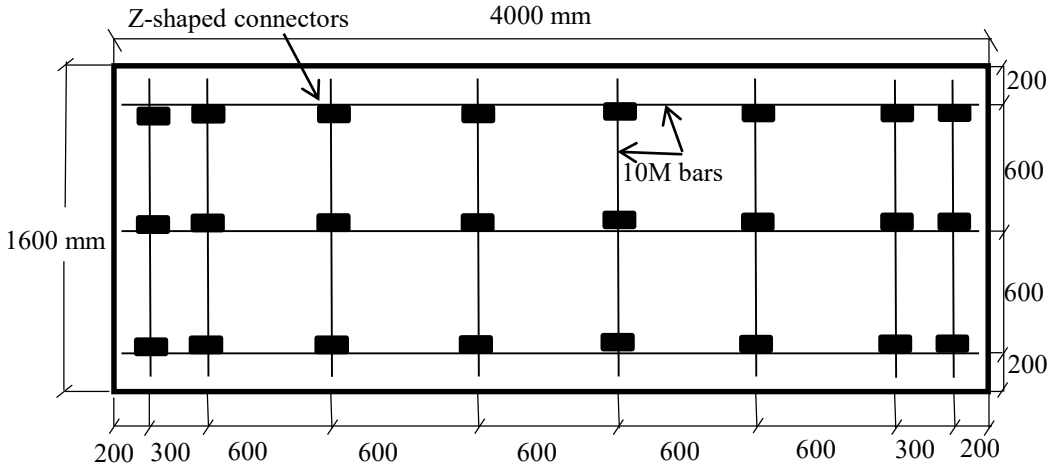

Figure 2-2: Plan view of PICP tested by Fero Corporation

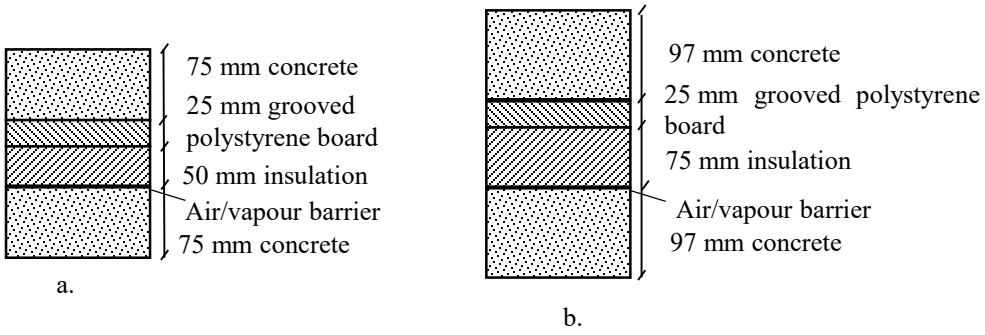

Figure 2-3: Details of a. P1 and b. P2, PICP specimens with ZSPC tested by Fero Corporation

Figure 2-4 shows the test setup of the PICP tested by Fero Corporation. As shown in this figure, the loading was applied by placing zinc ingots on two transfer beams that are sitting on two pipes. The pipes are 1306 mm apart. The zinc ingots were placed on the transfer beams until failure. At failure, the loading and mid-span out-of-plane deflection of the panels were recorded.

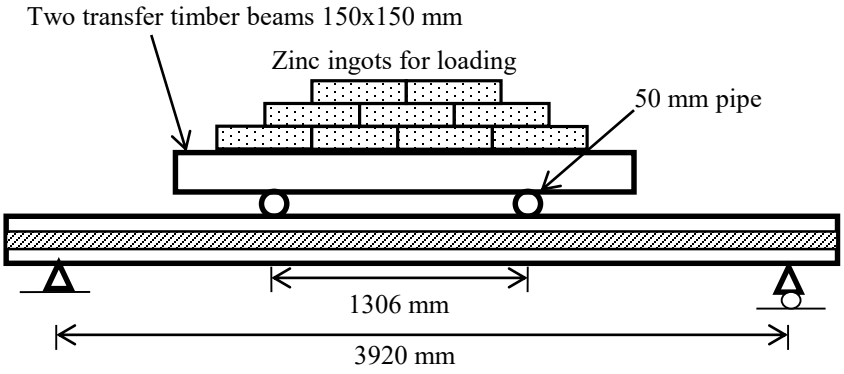

Figure 2-4: Test setup for out-of-plane 4-point flexural tests conducted by Fero Corporation

Table 2-1 summarizes the results of the two out-of-plane flexural tests conducted by Fero Corporation. This table also compares the experimental maximum out-of-plane bending moment at failure with the out-of-plane strength of a fully-composite panel estimated using CAN/CSA A23.3. As shown in this table, the experimental maximum out-of-plane bending moment of P1 was 24.08 kN.m and the flexural strength of a fully-composite panel using CAN/CSA A23.3 was 27 kN.m, which is 8.4% larger than the experimental results. Also, the experimental maximum out-of-plane bending moment of P2 was 31.45 kN.m and the flexural strength of a fully-composite panel using CAN/CSA A23.3 was 35.64 kN.m, which is 9.3% larger than the experimental results. This shows that the procedure given by CAN/CSA A23.3 overestimated the out-of-plane flexural strength of the tested PICP with ZSPC by average 8.8%. Another way to interpret this is that the tested PICP reached 88% of the theoretical flexural strength of a fully-composite panel; this suggests that PICP with ZSPC can reach high degree of out-of-plane flexural composite action.

However, the results of these two tests conducted by Fero corporation cannot be used to develop an analytical model to estimate the out-of-plane flexural behavior of PICP because the deflection of the panel was only recorded at the end of the test. So, the initial out-of-plane flexural stiffness of the panels at early stages of loading cannot be determined. This initial stiffness is required in design to check the out-of-plane deflection of the panels against the maximum acceptable deflection limits required by the design codes. Also, only one size of connector was used in these two tests. Therefore, the results cannot show the effect of the size of ZSPC on the out-of-plane flexural strength and stiffness of the panels. This effect is important to optimize the width and thickness of the connectors to achieve fully-composite action. Moreover, there was no shear test on the Z-shaped connectors. Therefore, the shear behavior of the connectors cannot be determined.

As mentioned earlier in this chapter, the shear strength and stiffness of the connectors significantly affects the out-of-plane strength and stiffness of PICP.

Table 2-1: Summary of results of PICP specimens tested by Fero Corporation

Parameter	P 1	P 2
Self-weight (kPa)	3.83	5.00
Failure load (kN)	18.15	29.43
Experimental bending moment at failure (kN.m)	24.08	31.45
Experimental mid-span deflection at failure (mm)	35.00	60.00
Theoretical bending moment at failure (kN.m) CAN/CSA A23.3†	27.00	35.64
(error %)	(8.4)	(9.3)

†Based on fully-composite cross section of the panel.

On the other hand, the flanges of the connectors and parts of the webs of ZSPC are embedded inside the concrete layers and, as mentioned earlier, the shear transfer between the concrete layers is through the unembedded parts of the connector's web, which is a rectangular steel plate. In other words, the shear transfer between the concrete layers is determined by the in-plane shear strength and stiffness of the web of Z-shaped connectors. Due to large in-plane shear strength and stiffness of steel plates, this connector is expected to have large shear strength and stiffness and thus mobilize fully-composite action in PICP. However, the in-plane shear strength and stiffness of these connectors are affected by the cracking of concrete around the connection of the connectors to concrete layers. Therefore, shear tests are needed to investigate the shear behaviour of Z-shaped connectors in PICP, and analytical models need to be developed to estimate this shear behaviour for different widths and thicknesses of the connectors. After estimating the shear behaviour of Z-shaped connectors in PICP, it can be related to the out-of-plane flexural behavior of PICP.

2.4. Analysis of PICP

2.4.1. Analytical Studies

Precast Insulated Concrete Panels belong to a broad category of sandwich panels, which consist of two relatively rigid facings with a flexible core in between. Flexural behaviour of sandwich panels depends on shear deformation of the core. Basic equations based on continuum mechanics have been proposed by previous researchers to account for these components of deformation in estimating out-of-plane flexural deformation of sandwich panels (Allen 1993, Gordaninejad & Bert 1989, Frostig & Baruch 1990, Challamel et al. 2010). In these approaches one assumption is that the shear stiffness of the core is much less than the skins, which is also valid for PICP with truss connectors (Bush & Wu 1998).

Holmberg & Plem 1986 developed one form of these basic equations which was adopted by Salmon & Einea 1995 to analyze PICP. According to Holmberg & Plem (1986) method out-of-plane deformation of sandwich panels has two components: 1. panel curvature $d\theta/dx$, 2. shear offset due to shearing deformation between the concrete layers q, as shown in Figure 2-5. Equilibrium of moments on the infinitesimal element shown in Figure 2-5 yields the following equation:

$$EIy_{,xx} = M + Eq_{,x}Bdr \qquad \text{2-2}$$

Where M is the external moment, I is the moment of inertia of the entire panel cross section, and B is the width of the panel. In this equation d, r, y and q are as shown in Figure 2-5. The shear stress in the connecting layer is taken as Kq, where K is the shear stiffness of the core.

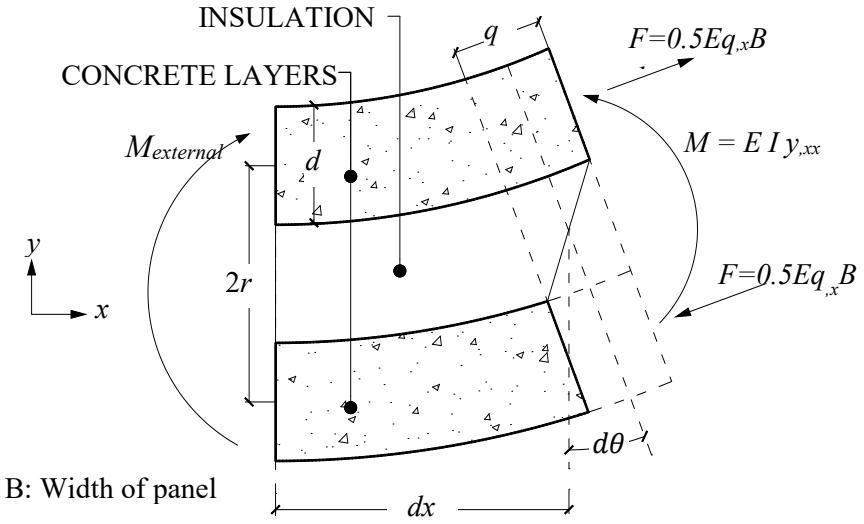

a.

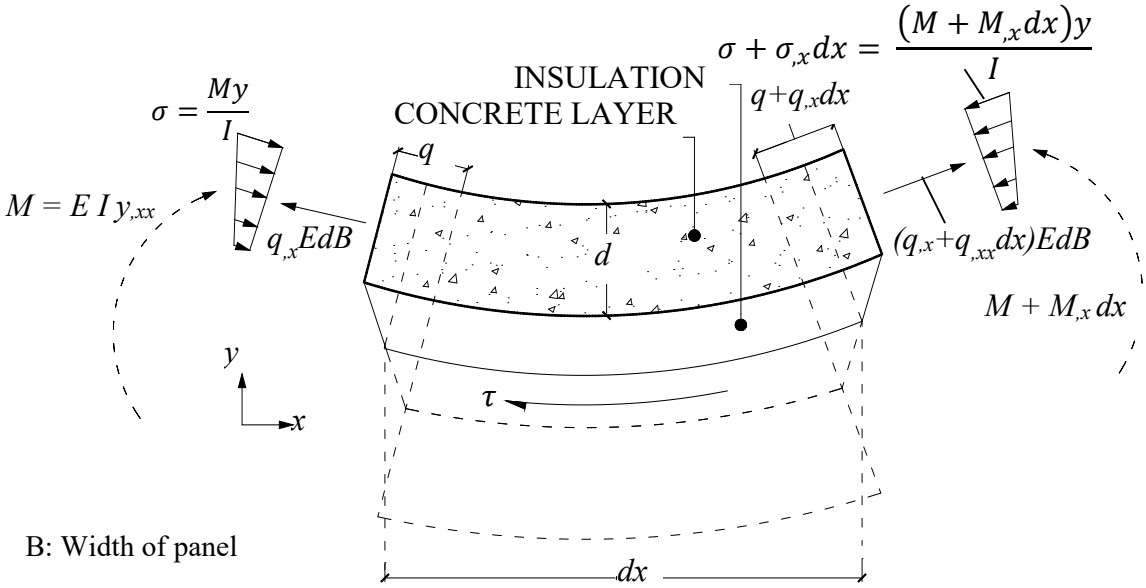

b.

Figure 2-5: Actions in an infinitesimal element of a concrete insulated panel: a. Forces and bending moments on cross section, b. shear stress between the concrete layers.

As shown in Figure 2-5 the shear stress in the core is produced by curvature of the panel plus the shear offset between the concrete layers, q. The former is calculated based on mechanics of materials. To calculate this interlayer shear stress equilibrium of horizontal forces is written as follows:

$$Edry_{,xxx} - 0.5Edq_{,xx} + Kq = 0 \quad \text{2-3}$$

Taking the derivative of equation 2-2 and substituting it in equation 2-3 and rearranging the equation gives the following equation:

$$\frac{2r}{EI} M_{,x} = \alpha^2 q_{,xx} - \beta^2 q \quad \text{2-4}$$

Where $\alpha^2 = 1 - Bdr^2/I$ and $\beta^2 = 2K/(Ed)$. Equation 2-32-4 can be solved for q, which can then be replaced in equation 2-3 to give y. To apply this theory to PICP, K can be calculated as follows (Salmon & Einea 1995, Bush and Wu 1998):

$$K = nK_{truss} + G_{ins} \quad \text{2-5}$$

Where K_{truss} is the shear stiffness per unit length of the connector, n is the number of truss connectors and G_{ins} is the shear modulus of the insulation. As mentioned earlier, the effect of the insulation material (G_{ins}) can be ignored since it deteriorates over time. The stiffness of truss connectors per unit length can be calculated by assuming the diagonal members of the connector as truss members pinned at the centre of concrete layers (Salmon & Einea 1995). This continuum-based method has been found to have maximum 1.0% error compared with Finite Element Analysis conducted by Salmon and Einea (1995). Whatsoever, continuum-based approaches are not convenient for design engineers to analyze PICP.

Previous researchers have proposed some analytical approaches incorporating shear strength of interlayer mechanical connectors to estimate the flexural resistance of PICP. Based on the results of out-of-plane flexural tests on PICP, Mouser (2003) proposed the following equation for estimating the flexural capacity of insulated concrete panels under out-of-plane loading.

$$M_r = M_{lt} + M_{lc} + (V_{con} + V_{ins})h_c \quad \text{2-6}$$

In this equation, M_r is the moment capacity of the insulated panel, M_{lt} and M_{lc} are the moment capacities of the tensile and compressive concrete layers, respectively, and V_{con} and V_{ins} are the shear capacities of the connectors and the concrete-insulation bonding, respectively. In this equation h_c is the distance between the centres of the concrete layers. It should be noted that this analytical approach is limited to PICP where the interlayer shear strength is smaller than the yield force of the longitudinal reinforcement. However, if the interlayer shear strength of PICP is larger than the yield force of the longitudinal reinforcement, the reinforcement yields earlier than the interlayer connectors, and thus $V_{con}+V_{ins}$ cannot be mobilized.

Hassan and Rizkallah (2010) proposed an iterative process for the design of insulated concrete panels with GFRP grid shear connectors with axial force applied on the leeward concrete layer. This guideline is based on the approach adopted by Newmark et al. (1951) for partially-composite steel beams. In this guideline it is assumed that the individual concrete layers have similar curvature and have linear strain distribution over their cross sections. The moment resistance of the panel is derived from the following equation.

$$M_r = M_{lt} + M_{lc} + V_t h_c \qquad \textbf{2-7}$$

Where, V_t and h_c are interlayer shear forces and the distance between the centres of the concrete layers, respectively. In the concrete layers, the equilibrium of forces along the panel should be satisfied according to equations 2-8 and 2-9, respectively.

$$\sum C - \sum T = P_u - V_c \qquad \textbf{2-8}$$

$$\sum C - \sum T = V_c \qquad \textbf{2-9}$$

Where $\sum C$ and $\sum T$ are the sum of compressive and tensile forces over the cross section of the concrete layers, respectively, P_u is the net axial force over the entire cross section of the panel. In these equations V_c is the interlayer shear force required for composite action, which is found

iteratively. Any interlayer force V_t less than V_c mobilizes partially-composite interaction. The degree of composite action is calculated as the ratio of V_t/V_c.

2.4.2. Numerical Studies

Many numerical studies using Finite Element Method (FEM) on insulated panels exist in literature, with different thin stiff skin and flexible core materials. However, there are a limited number of numerical studies using FEM on PICP. The FEM studies on PICP include 2D and 3D models. In these studies concrete and insulation layers are modeled by quadrilateral elements (Benayoune et al. 2008), Einea 1992) in 2D, solid elements (Lee 2003, Bush & Wu 1998, Newberry et al. 2010) or shell elements (Benayoune et al. 2008) in 3D. The truss connectors are modeled using truss element for metal truss connectors (Benayoune et al. 2008, Bush & Wu 1998) or beam element for FRP bent bar connectors (Einea, 1992). Also, Newberry et al. (2010) adopted Multiple Point Constraint (MPC) approach in modeling shear connectors, in which the shear connectors are modeled using tensile and shear springs with mechanical properties derived from shear tests. Reinforcing bars are usually modeled as embedded regions in the concrete layers.

The contact between the insulation and concrete layers was treated differently in previous studies. Einea (1992) modeled the insulation with quadrilateral elements in full contact with concrete layers in his 2D models. However, shear modulus of the insulation was given a small value to eliminate shear contribution of this layer to out-of-plane behaviour of the model. Lee (2003) modeled the insulation using gap element with zero tensile strength and stiffness capable of transferring compression forces. Newberry et al. (2010) applied zero friction at the insulation-concrete interface, since the interface shear contribution was accounted for in their MPC approach in modeling shear connectors.

In nonlinear FEA studies on PICP, metal connectors and reinforcement were modeled using either von Mises plasticity model, or non-linear stress-strain curves (Einea 1992, Benayoune 2008). In earlier studies, the nonlinear behaviour of concrete in 2D models was simulated using two nodal interface and control elements (Einea, 1992). Interface element allows separation under tension and control element is capable of resisting tension up to the tensile resistance of concrete. These two elements were used together to simulate cracking behaviour of concrete. Concrete crushing was not modeled in numerical analyses by Einea (1992), since he only studied out-of-plane

behaviour of PICP under service loads, where concrete crushing does not occur. In more recent models, concrete behaviour was modeled using either concrete damage plasticity (Newberry et al., 2010) or modified von Mises model (Benayoune et al. 2008). In the modified von Mises model, different compression and yielding properties were assigned to the material.

In most of the FEM models conducted so far, full contact was assumed between steel (reinforcement and connectors) and concrete material without any slippage observed in the experiments. This has resulted in stiffer load-displacement behaviour with higher ultimate load resistance in the FEM models (Benayoune et al., 2008). However, the FEM models by Benayoune et al. (2008) using shell elements for concrete layers have given close correlation with their experimental results.

3. Research Methodology

As mentioned earlier, Precast Insulated Concrete Panels (PICP) are used as a cladding system, therefore they are subjected to out-of-plane wind and earthquake loading, producing out-of-plane flexure in the panels. This flexure induces shear forces between the concrete layers, which is carried by the interlayer mechanical connectors. Hence, the shear behaviour of these connectors significantly affects the out-of-plane flexural behaviour of PICP. Moreover, in some PICP systems the top and bottom of the panels are enclosed by Reinforced Concrete (RC) beams, which affects the out-of-plane behaviour of PICP. Since the effects of ZSPC and RC end-beams have not been fully investigated previously, they are studied in this research with the scope and objectives given in Section 1.3. These objectives are addressed by the methodology outlined as follows.

3.1. Objective 1

Objective 1 is to investigate the effect of ZSPC and RC end-beams on out-of-plane strength and stiffness of non-loadbearing PICP.

Specific Aim 1

In this objective Specific Aim 1 is to determine shear strength and stiffness of ZSPC partially embedded in concrete, as is the case in PICP.

As explained in Chapter 2 push-off shear tests are commonly adopted to evaluate the shear behaviour of various interlayer mechanical connectors. A push-off shear test consists of small scale PICP with three concrete layers that sandwich two insulation layers as shown in Figure 4-2. The middle concrete layer is pushed down against the side concrete layers to apply shear on the interlayer mechanical connectors. Thus in this research, to study the shear behaviour of ZSPC, push-off shear tests were conducted on eleven shear specimens consisting of ZSPC. These specimens varied in width and thickness. Details of this experimental program and its results are presented in Chapter 4.

Numerical models of the tested shear specimens were also developed using FEM and were verified against the experimental results. These numerical models and their results are presented in Chapter 5. Based on these numerical models parametric studies were conducted on shear behaviour of ZSPC with variable width and thickness, the results of which are presented in Section 5.5.

Specific Aim 2

In this objective Specific Aim 2 is to determine the out-of-plane flexural behaviour of non-loadbearing PICP with ZSPC.

The out-of-plane flexural behaviour of PICP with ZSPC was experimentally investigated by four out-of-plane 4-point flexural tests on 1118 mm x 3556 mm (44.0 inch x 140 inch) panels. Details of these flexural tests and their results are presented in Chapter 7. An analytical model is proposed in Chapter 8 to conduct nonlinear analysis of PICP with ZSPC, by which the out-of-plane flexural behaviour of non-loadbearing PICP with ZSPC can be determined. The results of these numerical analyses are verified against the results of the out-of-plane flexural tests.

Specific Aim 3

In this objective Specific Aim 3 is to determine the out-of-plane flexural behaviour of non-loadbearing PICP with ZSPC and RC end-beams.

The out-of-plane flexural behaviour of PICP with ZSPC and RC end-beams was experimentally investigated by two out-of-plane 4-point flexural tests on 1118 mm x 3556 mm (44.0 inch x 140 inch) panels. Details of these flexural tests and their results are presented in Chapter 7.

Similarly, the analytical model proposed in Chapter 8 was adopted to conduct nonlinear analysis of PICP with ZSPC and end-beams, by which their out-of-plane flexural behaviour can be determined. The results of these numerical analyses are verified against the results of the out-of-plane flexural tests.

3.2. Objective 2

Objective 2 is to propose an approach for structural design of ZSPC for non-loadbearing PICP with and without end-beams under out-of-plane loading.

Specific Aim 1

In this objective Specific Aim 1 is to propose an analytical approach to estimate the shear behaviour of ZSPC.

The results of parametric studies on shear behaviour of ZSPC were compared to the estimated results using existing analytical models. Moreover, contours of shear and normal stresses in ZSPC

derived from the numerical models were examined to understand the shear behaviour of these connectors. Based on these analytical and numerical investigations, an analytical model is proposed to estimate the shear strength and stiffness of ZSPC partially embedded in concrete. These analytical models are discussed in Chapter 6.

Specific Aim 2

In this objective Specific Aim 2 is to propose an analytical approach to estimate the out-of-plane flexural behaviour of PICP with ZSPC with and without end-beams.

The analytical model proposed in Chapter 8 was adopted to estimate the behaviour of PICP with ZSPC with and without end-beams. Specific recommendations are also provided for the structural design of simply supported PICP with ZSPC with and without end-beams under out-of-plane uniform loading.

Part 2: Shear Behaviour of ZSPC

As mentioned earlier shear strength and stiffness of ZSPC affects the out-of-plane flexural behaviour of PICP. Therefore, experimental and numerical investigations were conducted to determine shear behaviour of these connectors in this part of the thesis. Based on these investigations, two analytical models using mechanics of materials were adopted to estimate the shear behaviour of ZSPC based on its width and thickness. These analytical models were verified against the numerical results.

This part of the thesis consists of three chapters that present the process and results of the experimental, numerical and analytical studies on the shear behaviour of ZSPC. Chapter 4 presents the setup and results of the shear tests on ZSPC as well as the material tests on the concrete, connectors and insulation. The experimental results are then adopted in Chapter 5 to verify the numerical model. Then the verified numerical models will be used to conduct parametric analysis to determine the effect of width and thickness of ZSPC on its shear strength and stiffness. The results of these parametric analyses are adopted in Chapter 6 to develop two analytical models to estimate the shear strength and stiffness of ZSPC based on its width and thickness.

4. Experimental Investigation of ZSPC in Shear

4.1. Introduction

The test setup and results of the shear tests on ZSPC are presented in this chapter. There is currently no standard shear test method to examine the shear behaviour of interlayer mechanical connectors. In this research, it was preferred that the shear test method had simple setup so the load path would be readily predictable and the connectors would be under pure shear force. The shear test also had to represent the behaviour of connectors in PICP as accurately as possible, so the results could be directly related to the behaviour of ZSPC in PICP. The two common shear tests on interlayer mechanical connectors in PICP include direct shear test (Mouser, 2003) and pull/push-off shear tests (Naito et al. 2012, Salmon et al. 1997). Of these two test methods, direct shear test was not chosen since it would induce uplift in the shear specimen. Pull-out and push-off shear tests both are simple test setups and their results can be related to the behaviour of ZSPC in PICP. Based on the available laboratory equipment, push-off shear tests was adopted for experimental study of the shear behaviour of ZSPC. The details of the push-off shear tests are given in Section 4.2. This section also provides the results of the material tests. Section 4.3 presents the results of the push-off shear tests and discusses the shear behaviour of ZSPC and their mode of failure. The results of these push-off tests will be adopted later in Chapter 5 to verify the numerical models. The numerical models will then be used to perform parametric analysis to identify the effect of width and thickness of ZSPC on its shear strength and stiffness.

4.2. Test Setup of Push-off Shear Tests

In this research push-off shear test was adopted to assess the shear behaviour of ZSPC. As shown in Figure 4-1, the shear specimens in push-off shear tests consisted of three layers of concrete sandwiched by two insulation layers. The middle concrete layer was connected by one mechanical connector to each of the side concrete layers. The middle concrete layer is pushed down by the force P against the other two concrete layers to exert shear force $V=0.5P$ on each connector. The displacement of the middle concrete layer Δ_v is the same as the shear deformation of each connector, thus the P- Δ_v graphs of push-off tests directly relates to V- Δ_v graphs for each ZSPC. The in-plane shear force in the connector produces in-plane bending moments, M, at the ends of the unembedded part of the connectors (Figure 4-1).

The bending moments at the ends of connector's web, *M*, produce in-plane tensile stresses in the tensile regions of the web, which tend to pull the connector out of the concrete layer. This pull-out action is resisted by two mechanisms: 1. Bonding between the web and concrete, 2. Pry-out strength of the concrete confined by the flange and the embedded part of the web (Figure 4-1). Concrete-connector bonding dissipates at early stages of loading due to slick surface of the connectors. At increased loading the pry-out strength of the confined concrete at the connector-concrete connection resists the pull-out action of the connectors. The larger width of the flange increases the size of the confined concrete, which improves the strength of connector-concrete connection. Also, if the flanges are hooked to the reinforcement of the concrete layers, the pry-out strength of the confined concrete is expected to improve. In this research the width of the flange was 50 mm, which is the common flange width of these connectors as indicated by the manufacturer.

The bending moments at the ends of the connector's web make the side concrete layers pivot about their bottom edges, i.e. the top of the side layers get closer to each other. If this pivoting happens freely the load-displacement behaviour of the shear test specimen will exhibit smaller strength and stiffness than when there is no pivoting. The pivoting of side concrete layers is partially restrained by the compressive behaviour of the insulation.

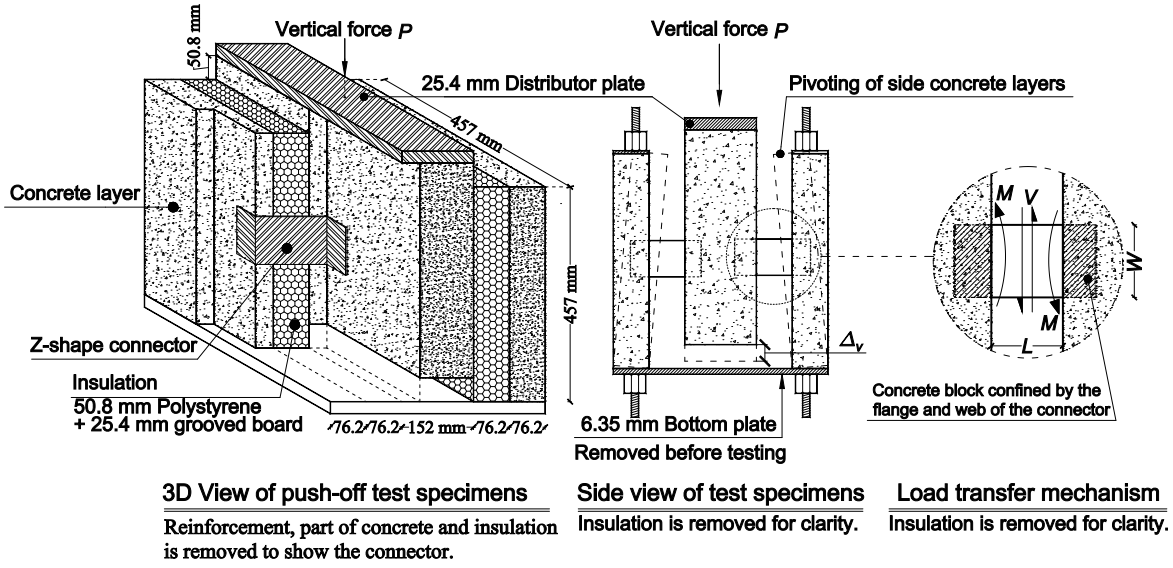

Figure 4-1: Schematic of push-off shear tests.

Eleven push-off shear tests were conducted on four groups of ZSPC with various widths and thicknesses, the details of which are summarized in Table 4-1. Each connector group in the shear test program is annotated hereafter as SHα-β, where α is the width of the ZSPC in inches and β is

the gauge number of the steel sheet. Individual specimens are referred to as SHα-β-γ, where γ is the specimen number. Three replicas of each connector group, except for SH6-16, were tested. Due to construction errors, the intended third replica of SH6-16 was ruined since one of the connectors was dislodged excessively in concrete during casting and vibrating.

Table 4-1: Details of the shear connectors

ZSPC designation	Shape of shear Connector	Width (*W*) mm	Thickness (*t*) Gauge# (mm)
SH3-16	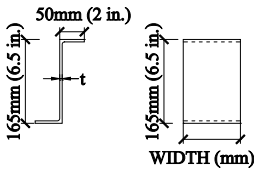	76.2	16 (1.47)
SH4-16		102	16 (1.47)
SH6-16		152	16 (1.47)
SH4-10		102	10 (3.21)

Wider and thicker ZSPC mobilize higher degree of composite action in PICP. The preliminary study on th flexural behaviour of PICP with ZSPC (Goudarzi et al., 2014) showed that the tested PICP with 76 mm wide and 1.48 mm thick ZSPC reached 88% of the theoretical flexural strength of a fully-composite panel. This suggests that this size of ZSPC might be capable of mobilizing high composite action in PICP. However, to investigate the effect of the width and thickness of ZSPC on the flexural behaviour of PICP, these parameters were varied in the shear tests in this chapter and flexural tests in Chapter 7. In this research the width of ZSPC varied from 76.2 mm to 152 mm and the thickness varied from 1.47 mm to 3.21 mm. Based on the results of the preliminary study, ZSPC with this range of width and thickness was believed to mobilize high degree of composite action in PICP. To optimize the number and cost of the experimental program, the shear tests were intended to include ZSPC with the selected minimum and maximum width and thickness; the shear behaviour of ZSPC with intermediate widths and thicknesses were then found by parametric analysis of the numerical models of these shear tests.

The schematic of the shear tests is shown in Figure 4-2. As shown in this figure each side concrete layer is connected to the middle concrete layer by one ZSPC. The specimens were composed of three 457 mm x 457 mm (width x height x thickness) concrete layers. The width and height of the concrete layers is representative of the typical spacing of the connectors in practice, which is between 400 mm to 600 mm. In practice the thickness of the concrete layers of PICP varies between 50.8 mm to 102 mm. In this experimental program the thicknesses of side and middle concrete layers were taken as 76.2 mm and 152 mm, respectively. The middle concrete layer was

taken twice as thick as the side concrete layers to provide enough embedment depth for the two ZSPC connecting to it from the side concrete layers.

The concrete layers were reinforced by grade 420, 10M bars (Figure 4-2). The minimum nominal concrete cover of the bars was set at 25.4 mm. As shown in Figure 4-2 the ZSPC were hooked to the bars in the side concrete layers, but due to fabrication errors they could not hook to the bars of the middle concrete layer, thus the connectors were tied to these bars by steel wires. For flexural panels, however, the fabrication quality was improved to hook the connectors to the bars of both layers, as described in Section 7, to maximize the connection strength and stiffness between ZSPC and concrete layers. The connections of ZSPC to the bars of the middle and side concrete layers are shown in Figure 4-3.

As shown in Figure 4-2, the side concrete layers are reinforced with 10 mm threaded rods at the edges. The threaded bars were installed to be used for handling the specimens in the laboratory. Four hooks were screwed onto these threaded bars. The specimens were then lifted and handled in the laboratory using these hooks. The side concrete layers were just sitting on the pedestal, thus were free to pivot about their bottom edges. Therefore, the bending moments imposed on the side concrete layers would not cause out-of-plane flexure in the side concrete layers; they would instead cause pivoting of the side concrete layers, which was resisted by the compressive behavior of the insulation. These threaded rods were assumed to have negligible effect on the load-displacement behavior of the shear specimens, since the side concrete layers were expected to be under negligible out-of-plane flexure.

The thickness of insulation commonly varies from 25.4 mm to 76.2 mm. As discussed earlier, thicker insulation results in lower interlayer shear strength and stiffness (Soriano and Rizkalla, 2013). In this study, the insulation thickness was taken as 76.2 mm to evaluate the least shear strength and stiffness of ZSPC that can be mobilized in common practice. The insulation is commonly made of either Extruded Polystyrene (XPS) or Expanded Polystyrene (EPS). Since plastic sheets were used in this research to eliminate unwanted shear path through insulation-concrete bonding, the material of insulation was not structurally important. However, insulation was used to facilitate construction of the specimens. The insulation consisted of one 50.8 mm layer of Extruded Polystyrene (XPS) foam panel and one 25.4 mm layer of grooved board intended to allow water to drain out of the panel. This combination is one of the PICP systems used in industry. As shown in Figure 4-2, plastic sheets were placed between concrete layers and insulation to

eliminate the undesired shear path of concrete-insulation bonding. This bonding significantly improves shear transfer between concrete layers. For example, Woltman et al. (2013) showed in their experiments that concrete-insulation bonding improves shear strength of GFRP pin connectors by 28%. Therefore, it is important to eliminate this undesired shear path to investigate the effect of shear connector only.

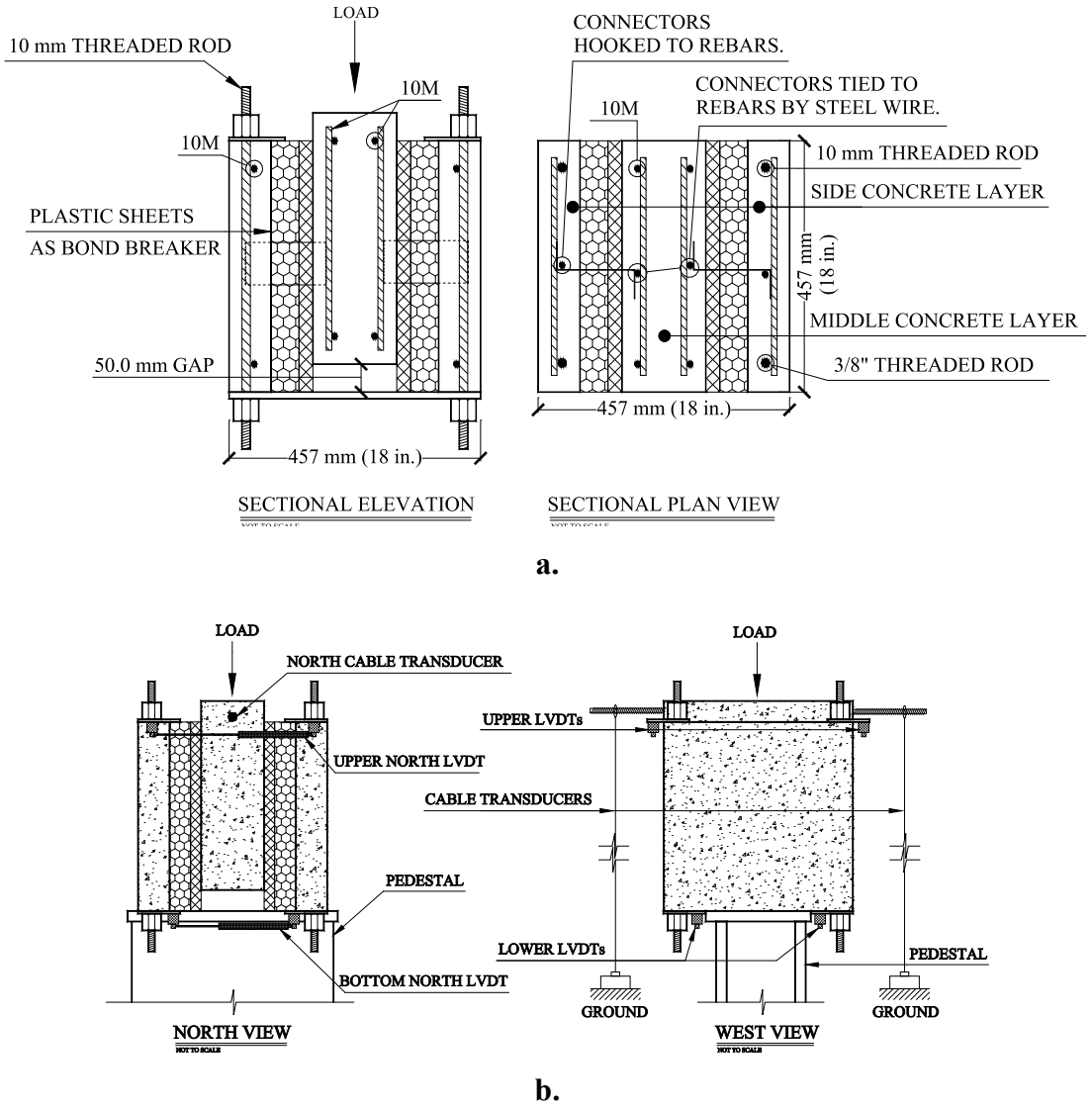

Figure 4-2: Design of push-off tests, a. specimen design, b. instrumentation.

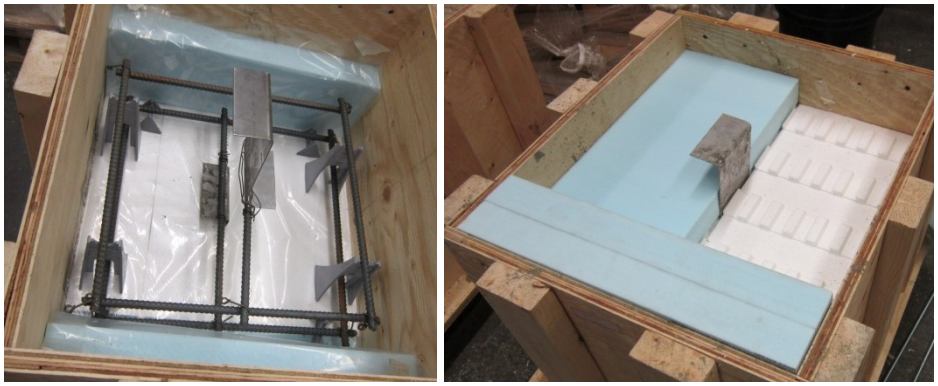

a. b.

Figure 4-3: Fabrication of shear specimens: a. Connection of connectors to the reinforcing bars, b. Placing of insulation around connectors.

Figure 4-4 shows the material tests conducted on concrete, insulation, reinforcing bars and ZSPC. As mentioned earlier, at increased loading the pull-out effect of the connectors on the concrete layers is resisted by the pry-out strength of the concrete confined by the flange and web of the connectors. Concrete with larger compressive strength possesses larger tensile strength, thus possess larger pry-out strength in push-off shear tests. The compressive strength of PICP is usually greater than 30 MPa (Leabu, 1965), therefore the 28-day compressive strength of concrete in these tests were designed to be minimum 30 MPa. Three compressive tests were conducted on 102 mm x 204 mm (diameter x height) concrete cylinders after 28 days in accordance with ASTM C39M-14. Modulus of Elasticity and Poisson's ratio were measured in accordance with ASTM C469M-10. The 28-day Compressive behaviour of concrete in shear specimens was as shown in Figure 4-5. The average compressive strength and modulus of elasticity of concrete were 41.77 MPa and 24.47 GPa, respectively and the Poisson ratio was 0.171. Since concrete hydration continues with low rate for several weeks after 28 days, the compressive strength of concrete slightly increases over time. Therefore, on the testing day of each shear specimen three compressive tests were conducted on concrete to obtain its compressive behaviour at the exact age just before the push-off shear test. The results of these tests are presented in Table 4-2. Moreover, eleven Brazilian split tests according to ASTM C496M-11 were conducted on 102 mm x 204 mm (diameter x height) concrete cylinders after 28 days. The average tensile strength of the concrete was 3.83 MPa with 12.16% coefficient of variation.

As mentioned earlier the load-displacement graph of the push-off shear test relates to the shear force - deformation of the shear connectors. The load-displacement behaviour of the push-off test specimens are affected by the compressive behaviour of the insulation. The compressive behaviour

of the insulation partially restrains the side concrete layers from pivoting. Hence the compressive behaviour of insulation should be measured by compression tests to be incorporated in numerical modeling of these tests. The compressive behaviour of the insulation material was tested in accordance with ASTM C165-07, the results of the insulation compressive tests are given in Figure 4-7. Nominal cross sectional dimensions of the tested foams were 125 mm x 125 mm. Three compression tests were carried out on 50.8 mm thick extruded polystyrene boards and three on the combined 50.8 mm thick extruded polystyrene boards and 25.4 mm grooved board, which is the same combination used in the push-off tests.

a.

b.

c.

d.

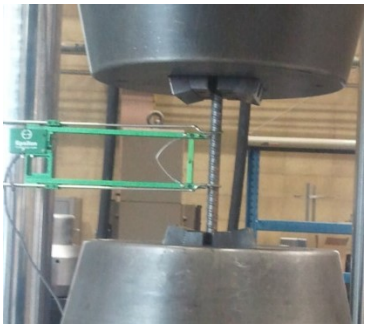

e.

Figure 4-4: Material tests: a. compressive test of concrete, b. split test of concrete, c. compressive test of insulation, d. tensile test of steel bars cut from ZSPC, e. tensile test of reinforcing bars.

The compressive stress against engineering strain for the insulation is shown in Figure 4-7. As shown in this figure, the extruded polystyrene had initial compressive stiffness of 8,727 kPa up to about 24,300 micro-strain, after which the stiffness gradually decreases. At 400,000 micro-strain the compressive stiffness of the insulation picks up again. The combination of grooved board and

extruded polystyrene had initial compressive stiffness of 314 kPa, and after about 70,000 micro-strain, the compressive stiffness ramps up to 1,113 kPa. At 120,000 micro-strain the compressive stiffness gradually decreases.

Three tensile tests of steel coupons from each connector group, totalling 9 coupons, were conducted according to ASTM A370-2013. The stress-strain curves of these coupons are shown in Figure 4-8 and the material properties of the connector groups are summarized in Table 4-2. As shown in this figure the ZSPC connector groups provided by the manufacturer have different material properties. The modulus of elasticity for SH3-16 is 188 GPa, for SH4-16 and SH6-16 is 201 GPa, and for SH4-10 is 194 GPa. The yield stress for SH3-16 is 350 MPa, for SH4-16 and SH6-16 is 195 MPa, and for SH4-10 is 308 MPa. And the ultimate stress for SH3-16 is 470 MPa, for SH4-16 and SH6-16 is 320 MPa, and for SH4-10 is 430 MPa. Since the yield stress for different ZSPC varies from each other the experimental shear strengths of these tests cannot be directly compared together. Therefore, to compare the shear strengths of ZSPC, their average shear stress, $\tau_{avg} = V/(tW)$, are divided by their yield shear stress, $\tau_y = f_y/\sqrt{3}$, which is presented in Section 4.3. The variability of the material properties of ZSPC is not a significant concern because, as mentioned in Section 4.1 the primary purpose of these tests is to verify the numerical models presented in Chapter 5. These numerical models will then be adopted to carry out parametric analysis on the effect of width and thickness of ZSPC on their shear strength and stiffness.

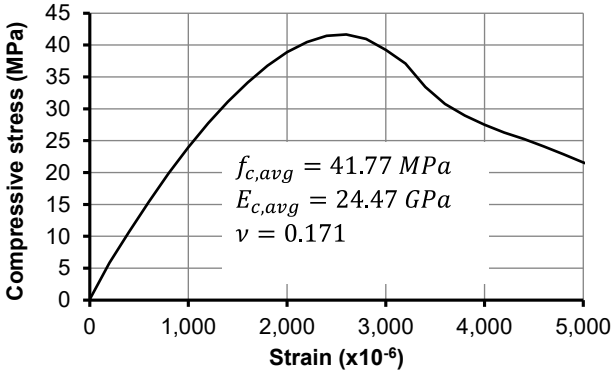

Figure 4-5: 28-day engineering compressive stress-strain behaviour of concrete for shear specimens.

The shear tests were conducted by placing the specimens on a pedestal and then the middle concrete layer was pushed down by a hydraulic jack. As shown in Figure 4-6 the force of the jack is transferred through a conical block to a 25.4 mm steel plate on the top of the middle concrete layer to distribute to force of the jack across the middle layer. To ensure full contact between the plate and concrete, plaster of Paris was applied on top of the middle concrete layer. The conical

plate was used to allow rotation of the middle layer in all direction, thus no undesired restraint would be applied to the specimen.

Since the shear connectors have low torsional stiffness, the middle concrete layer of the specimens are prone to twisting as shown in Figure 4-6. Therefore, a wooden containment box was used to restrain this twisting as shown in Figure 4-6. As shown in Figure 4-6, a 25.4 mm plate was placed on top of the middle concrete layer to distribute the force of the jack across the middle layer.

As shown in Figure 4-2, in our original design, there was a steel plate at the bottom of the specimen to provide a smooth seating for the specimen on the pedestal. The first specimen (SH4-16-1) was placed on the pedestal with this bottom plate. During this first test the plate was curved due to pivoting of the side layers at excessive post-failure loadings. Therefore the plate was removed for the remaining shear tests to eliminate any undesirable effect of the bottom plate on the specimen.

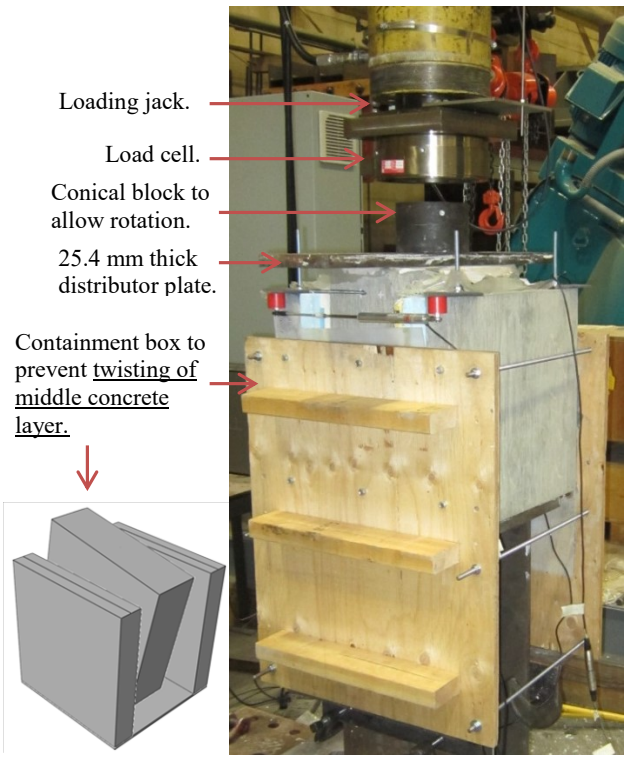

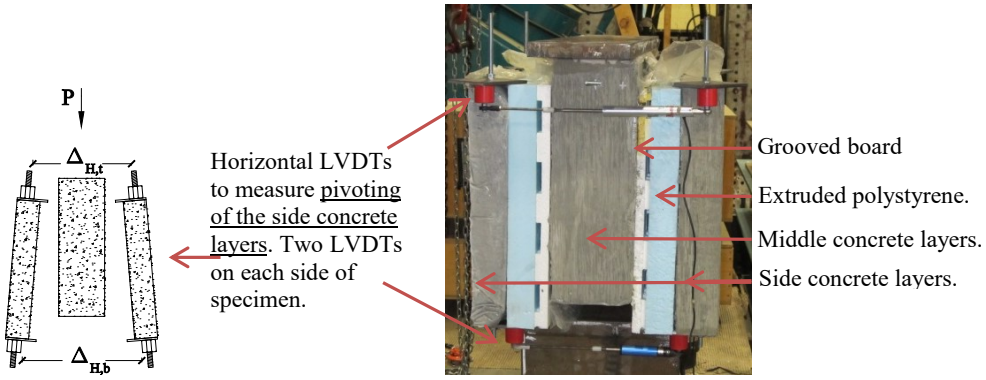

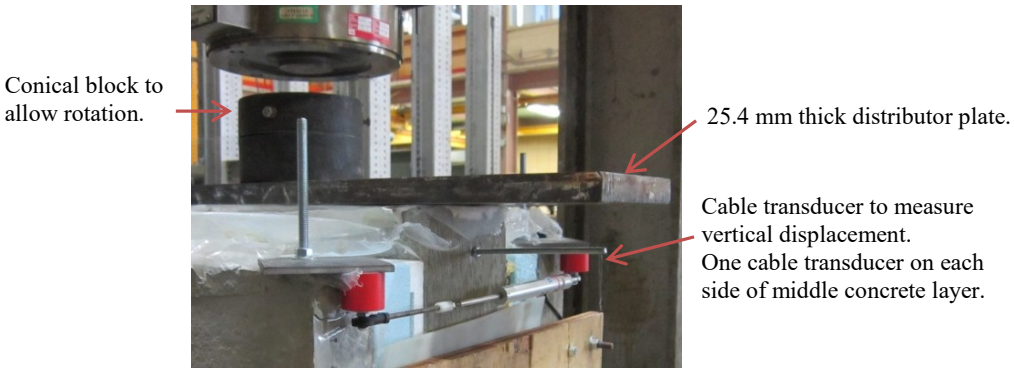

Figure 4-6: Test setup for push-off shear tests.

Vertical displacement of the middle concrete layers was monitored using one cable transducer attached to each side of the middle concrete layer of the specimen as shown in Figure 4-6. Moreover, the horizontal relative displacements of the top and bottom of the side concrete layers were measured by two LVDTs on each side of the specimen to monitor the pivoting of side concrete layers. The effect of pivoting on the shear behaviour of these tests is investigated Section 5.

Table 4-2: Material properties of ZSPC and concrete used in shear test specimens.

ZSPC designation	Test specimen number	$f_c\ (MPa)$	Steel properties			
			$f_y\ (MPa)$	$\tau_y\ (MPa)$[*1]	$f_u\ (MPa)$	$E\ (GPa)$
SH3-16	1	47.00	350	202	470	188
	2	46.17				
	3	44.62				
SH4-16	1	43.84	195	113	320	201
	2	48.52				
	3	47.17				
SH6-16[*2]	1	45.10	195	113	320	201
	3	45.82				
SH4-10	1	45.39	308	178	430	194
	2	46.67				
	3	48.44				

[*1] $\tau_y = f_y/\sqrt{3}$. [*2] Shear test specimen SH6-16-2 was not testable due to construction errors.

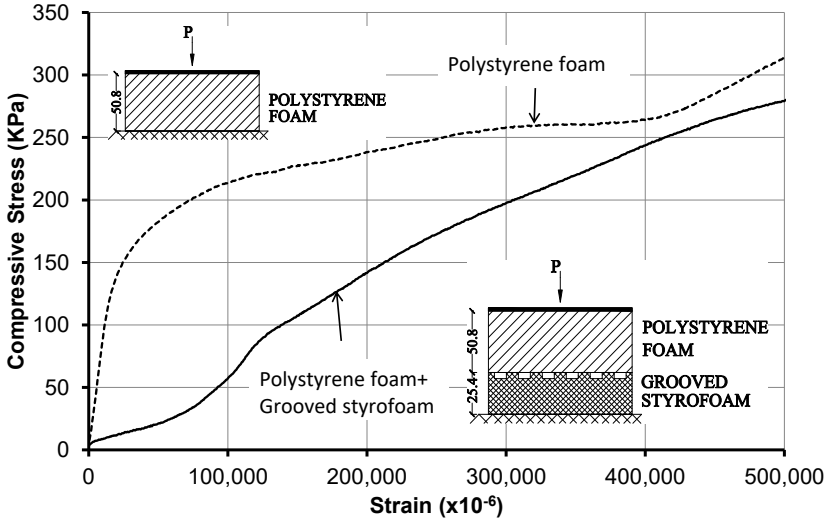

Figure 4-7: Engineering compressive stress-strain behaviour of insulation material.

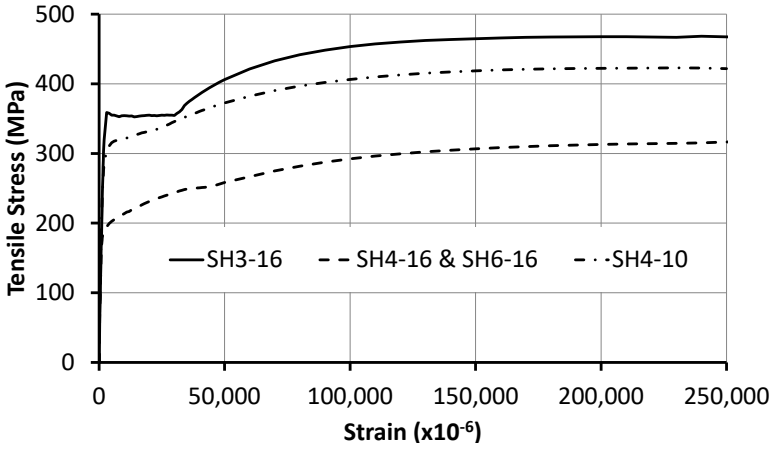

Figure 4-8: Engineering tensile stress-strain behaviour of ZSPC material.

4.3. Test Results and Discussion

The shear specimens were positioned on a pedestal supported by a beam and the vertical displacement of the middle concrete layers was measured using cable transducers that were referenced to the ground. This vertical displacement includes the vertical movement of the middle concrete layer and the vertical deflection of the supporting beam and pedestal, which should be subtracted from the readings of the cable transducers. Therefore, the supporting structure of the shear specimens were tested under loading and its load-deformation history was recorded, which is shown in Figure 4-9. This deformation was subtracted from the readings of cable transducers for all shear tests to obtain the vertical displacement of the middle concrete layer due to deformation of ZSPC only.

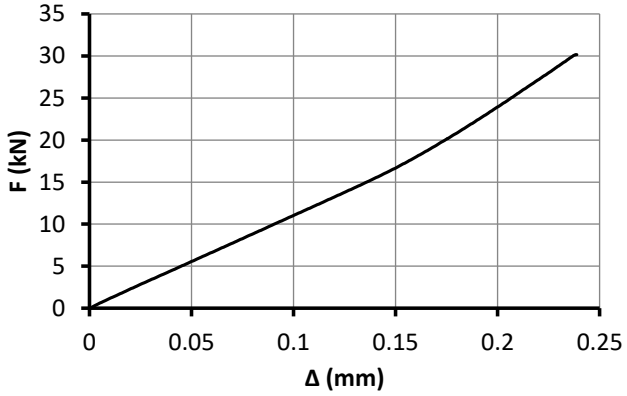

Figure 4-9: Load - deformation of the supporting beam.

Figure 4-10 shows the shear force (V) carried by one connector versus the vertical displacement (Δ_v) of the middle concrete layer for all connector groups. In this figure the shear force includes self-weight of the middle concrete layer and the weights of the loading distributor plate and the conical block. The weights of conical block and steel plate were 13.56 kg and 26.84 kg, respectively. The weight of the middle concrete layer was 77.88 kg. Thus the total load applied on the connectors before the start of the test was 1.16 kN.

As shown in Figure 4-10, for all connector groups the shear force increases to a maximum value, taken as the shear strength V_r herein, and gradually decreases afterwards. Figure 4-10 shows that the shear strength of specimens SH6-16-3 and SH4-10-1 are much lower than their corresponding replicas. Examination of these specimens after the test revealed that the embedment depth of ZSPC were only about 12 mm due to construction errors. Thus the results of these two specimens are not used in calculating average shear strength and stiffness of ZSPC. Since there is only one sound push-off shear test on SH6-16, no conclusion is drawn from its results. The results of this one specimen are reported only because they follow the same trend as all other test groups.

As shown in Figure 4-10, the V-Δ_v graphs for all shear specimens do not have distinct yield shear strength. This is more pronounced in SH3-16 test specimens and SH4-16-3, where the V-Δ_v behaviour gradually decreases in slope throughout the loading history until it reaches its shear strength V_r. For the connector groups with 1.47 mm (16 gauge) steel sheets, after the peak shear strength the shear force decreases to some shear force level, called residual shear strength hereafter, and remains constant with increased Δ_v. After the peak shear strength, the average shear forces in SH3-16, SH4-16 test specimens and in SH6-16-1 reduce to 9.0 kN, 11.6 kN and 14 kN, respectively. These residual shear strengths are 63%, 80% and 64% of the shear strengths of their respective connector groups. In other words, the residual shear strength of every tested 16 gauge connector group is more than 60% of its maximum shear strength (Figure 4-10). For shear specimen SH6-16-1, after the shear force reduced to 9.0 kN, it starts picking up again at around Δ_v of 4.6 mm and reaches 20 kN at 10.0 mm shear deformation. Judging by the deformed shape of the connectors after the end of the tests, as explained later, this secondary increase in shear force can be attributed to the tension field action in the SH6-16-1 connectors.

The fact that the tested 16 gauge connectors maintain more than 60% of their shear strengths suggests that these ZSPC are ductile and absorb considerable amount of energy. Ductility of interlayer mechanical connectors is a desirable behaviour in applications where the panel is under

blast loading (Naito et al., 2009). Connectors with higher ductility absorb more energy, thus dissipate the input energy of a blast. Ductility of ZSPC is out of the scope of this research, however, ZSPC tested in this research showed some energy absorption. The intent of our current tests, as mentioned earlier, was to determine the strength and stiffness of ZSPC, since these two parameters are important for design of PICP under wind and seismic loadings, which are the common loadings on non-loadbearing PICP. However, it is recommended that future research should focus on studying the ductility of ZSPC.

Figure 4-10 shows that in the shear behaviour of SH4-10 connector group there are multiple sudden drops around and after the peak shear force. The same ragged pattern with less intensity is observed in the shear behaviour of SH6-16-1 test specimen. This ragged pattern is not observed in the shear behaviour of SH3-16 and SH4-16 connector groups made of gauge 16 steel sheets. This ragged pattern can be attributed to the cracking of concrete around the connector-concrete connection, which is more intense for SH4-10 connector groups and gauge 16 connector groups. The reason behind this can be understood by explaining the load transfer mechanism between the ZSPC and the concrete layers as follows.

Since the flanges and parts of the web of each connector were embedded inside the concrete layers, the ends of the web were restrained against in-plane rotation. Thus, the in-plane shear forces in the connector produce in-plane bending moments at the ends of the connector's web (Figure 4-1). These In-plane bending moments in the connector's web induce in-plane tensile stresses in some regions of the connector's web. These in-plane tensile stresses tend to pull the connector's flanges out of the concrete layers. The connector-concrete connection resists this pull-out effect by two mechanisms; the first is the bonding between the connector and the concrete, and the second is the pry-out resistance of the concrete block confined by the connector's flange and the embedded part of the connector's web (Figure 4-1). This pry-out resistance is improved if the flanges of the connector are hooked to the reinforcing bar. Since these connectors have slick surfaces, the connector-concrete bonding is weak thus it diminishes at early stages of loading. Therefore, at increased loading the pry-out resistance of the confined concrete is the primary resistance of the connector-concrete connection.

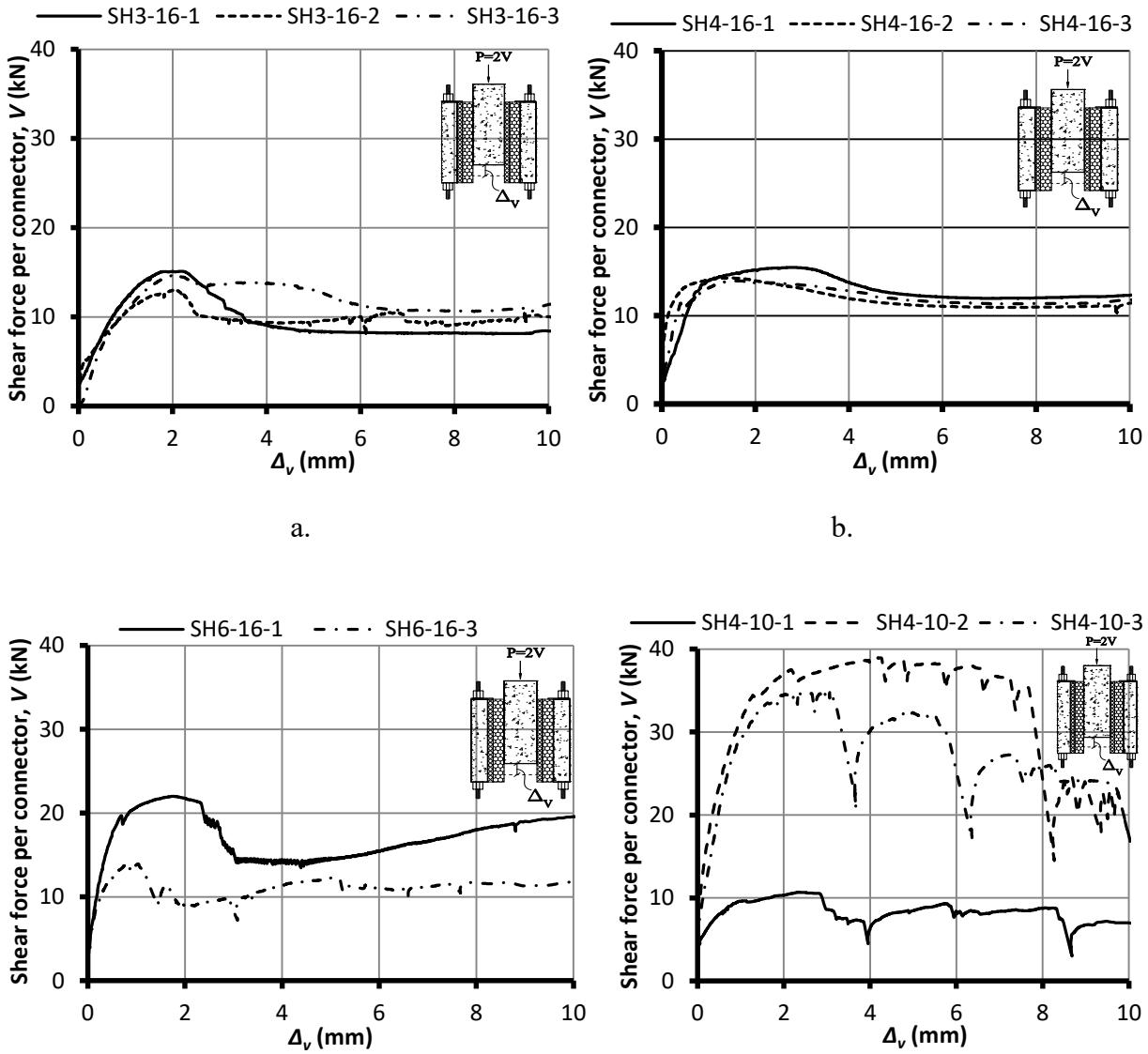

Figure 4-10: Shear behaviour of tested ZSPC for a. SH3-16, b. SH4-16, c. SH6-16, d. SH4-10.

Increase in the width and thickness of the ZSPC improves its shear stiffness, thus larger forces and bending moments are transferred to the connector-concrete connection. However, increase in width and thickness of the connector does not have the same effect on the resistance of the connector-concrete connection. The increase in the connector's width enlarges the size of the concrete block confined by the connector's flange, thus improves the pry-out resistance of the connector-concrete connection. But the increase in the connector's thickness does not change the size of the concrete block confined by the connector's flange, thus does not improve the pry-out resistance of the connector-concrete connection. Therefore, when the width of the connector is increased larger forces and bending moments are transferred to the concrete through the connector-concrete

connection with improved resistance. But when the thickness of the connector is increased larger forces and bending moments are transferred to the concrete through the connector-concrete connection with unimproved resistance, which intensifies cracking around the connection. In other words, increase in *t*/*W* ratio of ZSPC intensifies concrete cracking around the connector-concrete connection. If the thickness of the connector is excessively increased, the failure of the connector-concrete connection governs the shear behaviour of ZSPC.

Table 4-3 summarizes the experimental results of the push-off tests. As mentioned earlier, the tested ZSPC had different yield stress. To investigate the effect of width and thickness of Z-shaped connectors on their shear strength, the effect of their material difference on their shear strength should be eliminated. This is done by taking τ_{avg}/τ_y ratio for each connector group, where τ_{avg} is the average shear stress across the cross section of the connector, which is equal to $V_r/(tW)$; and τ_y is the von Mises yield shear stress of steel, which is equal to $f_y/\sqrt{3}$. Table 4-3 shows that τ_{avg}/τ_y is 0.63 for SH3-16 and SH4-10, and 0.88 for SH4-16 and SH6-16. This difference can be attributed to the effect of *t/W* on the resistance of the connector-concrete connection, explained earlier. Increasing connector's width improves the shear stiffness of ZSPC and improves the connector-concrete connection by enlarging the size of the confined concrete block (Figure 4-1). Increasing connector's thickness improves the shear stiffness of ZSPC but does not improve the resistance of the connector-concrete connection since increased thickness does not change the size of the confined concrete block at the connection. Therefore, thick connectors transfer large forces to the concrete layers through connector-concrete connection with relatively small resistance, which intensifies concrete cracking around the connection. This cracking affects the strength and stiffness of ZSPC. In the tested connector groups, SH3-16 and SH4-10 have larger *t/W*, hence smaller τ_{avg}/τ_y than SH4-16 and SH6-16.

Shear stiffness of the connector is used in design to calculate the out-of-plane deflection of PICP under service loads. Here, the experimental shear stiffness, K_s, for these tests are derived using the secant stiffness from zero shear force to the shear force level corresponding to the service wind load, i.e. $V_r/1.4$, where the factor 1.4 is the load factor for wind loading in the ultimate limit state as per NBCC (NRC 2010). The experimental shear strength, V_r, and the shear stiffness, K_s, for all test groups along with the corresponding coefficients of variation are summarized in Table 4-3. Figure 4-11 shows K_s versus the cross sectional area (tW) of the tested ZSPC.

Figure 4-11 and Table 4-3 show that K_s increases with the width and thickness of the connectors. For connector groups SH3-16, SH4-16 and SH4-16 the only variable is the width and for connector groups SH4-16 and SH4-10 the only variable is the thickness. As shown in Figure 4-11, K_s grows faster with width than thickness. For example, the area of SH4-16 is 33% larger than that of SH3-16, while K_s of SH4-16 is 91% greater than that of SH3-16. Whereas, the area of SH4-10 is 100% larger than that of SH4-16, but K_s of SH4-10 is only 68% larger than that of SH4-16. This shows that the increasing connector thickness has lower impact on K_s than increasing connector width, which may be attributed to intensified cracking around the connector-concrete connection for ZSPC with high *t/W*, explained earlier. It should be noted that the mentioned differences in the shear stiffness among the ZSPC groups are more than the coefficient of variation of shear stiffness within each group, which confirms the validity of the aforementioned argument.

Table 4-3: Summary of push-off test results.

Connector group	Specimen	V_r, kN	$V_{r,avg}$, kN (COV%)	τ_{avg} (MPa)	$\frac{\tau_{avg}}{\tau_y}$	K_s, kN/mm	$K_{s,avg}$, kN/mm (COV%)
SH3-16	**1**	15.07	14.22 (8.04)	127.04	0.63	14.45	13.42 (9.98)
	2	12.92				13.92	
	3	14.67				11.91	
SH4-16	**1**	15.41	14.52 (5.40)	98.17	0.87	18.35	28.66 (42.32)
	2	14.22				42.02	
	3	13.93				25.61	
SH6-16[*2]	**1**	21.99	21.99	99.17	0.88	44.33	44.33
	2[*1]	13.56	n.a.	n.a.	n.a.	52.97	n.a.
SH4-10	**1**	38.59	36.58 (2.83)	178	0.64	45.00	42.51 (8.27)
	2	34.58				40.02	
	3[*1]	10.53	n.a.	n.a.	n.a.	17.32	n.a.

[*1] Not considered in averaging due to premature failure of the specimen caused by construction errors. [*2] The third specimen of this connectors group was untestable due to construction errors.

Notes: n.a. = not applicable. COV = Coefficient of variation.

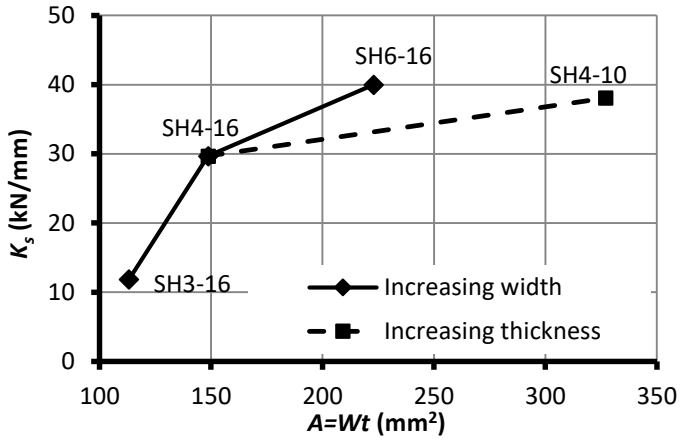

Figure 4-11: Experimental secant shear stiffness vs. the cross sectional area of the tested ZSPC shear specimens.

Figure 4-12 illustrates the deformed shape of the tested connectors after the end of the tests and shows that all ZSPC with 1.47 mm (16 gauge) steel sheet underwent significant buckling along the compression diagonal strut, and formed a tension-tie along the tension diagonal of the unembedded part of the connector's web. Since the compressive force of the compressive diagonal diminishes after buckling, the shear resistance of the connector decreases. However, after buckling, some of the compressive force of the buckled diagonal is transferred to the insulation, and thus the connector continues to carry some shear force after the drop in the shear resistance. This might explain the residual shear strength of the 16 gauge connectors shown in Figure 4-10. With increased loading, the tension-ties pull the side concrete layers toward the middle concrete layer, compressing the insulation, by which larger compression is produced in the insulation. This leads to gradual increase in shear resistance of 16 gauge connectors after buckling. This might explain the ascending portion of the V-Δ_v behaviour of SH6-16 (Figure 4-10).

As shown in Figure 4-12, the connectors in SH4-10, made of 3.21 mm (10 gauge) steel sheet, did not buckle, instead it underwent shear deformation. Figure 4-10 shows that ZSPC in SH4-10-2 deformed up to about 7.5 mm without significant drop in shear resistance. This large shear ductility compared to 16 gauge ZSPC might be due to plastic shear deformation of the connector. Due to high ductility of steel, plastic shear deformation of ZSPC leads to ductile shear behaviour. The ZSPC in SH4-10-3 could have the same shear ductility as SH4-10-2, if it was not for the sudden drops in shear resistance caused by cracking at the connector-concrete connection.

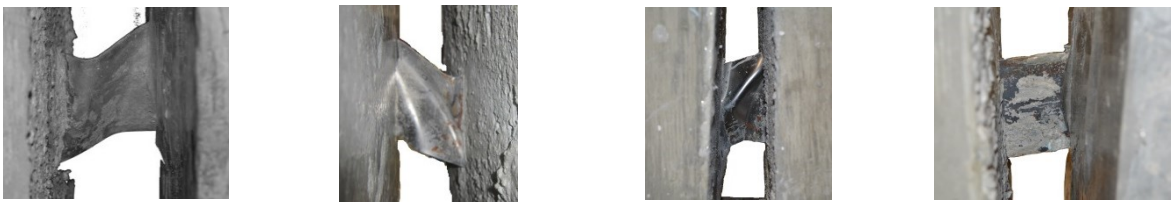

a. b. c. d.

Figure 4-12: Deformed shape of ZSPC for: a. SH3-16, b. SH4-16, c. SH6-16, and d. SH4-10.

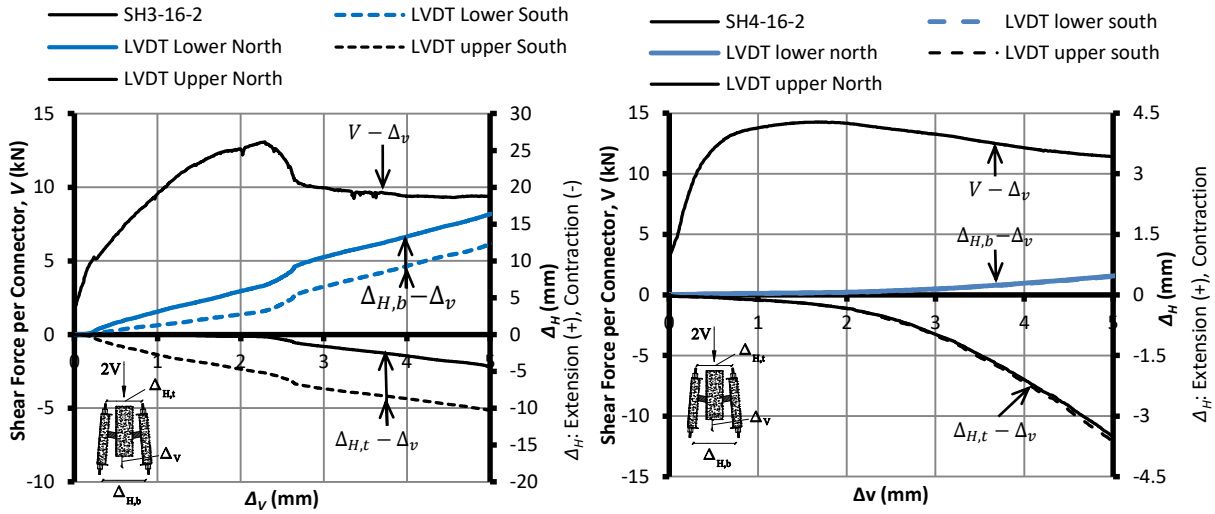

a. b.

Figure 4-13: Horizontal displacement side layers for a. SH3-16-2, b. SH4-16-2

As mentioned earlier, in push-off tests, the in-plane bending moments produced at the ends of the connector's web make the side concrete layers pivot about their bottom edges. Horizontal LVDTs at top and bottom of side concrete layers were used to monitor the horizontal displacements of these layers during loading (Figure 4-6). Figure 4-13 shows these horizontal displacements against Δ_v for SH3-16-2 and SH4-16-2. The horizontal displacements of side concrete layers for other shear specimens are given in Appendix A. As shown in Figure 4-13 under vertical loading the top of side concrete layers moves inwards and the bottom of side layers slides outward. For some of the tested shear specimens like SH4-16-2 the horizontal displacements of side concrete layers increase slowly before the peak shear force, after which these horizontal displacements increase faster. For some shear specimens like SH3-16-2, as shown in Figure 4-13 the top and bottom of the side concrete layers increase almost linearly throughout loading. For these specimens there is noticeable discrepancy between horizontal displacements of north and south sides of the concrete layers. This difference might be due to geometric imperfections and non-symmetries in the shear

specimens. The effect of pivoting of the side concrete layers on the shear strength and stiffness of the test specimens will be investigated in section 55.4.

4.4. Summary and Conclusion

Eleven push-off tests were conducted to study the effect of width and thickness of Z-shaped Steel Plate Connectors (ZSPC) on their shear strength and stiffness. The width of the connectors varied from 76.2 mm to 152.4 mm and the thickness varied from 1.47 mm (16 gauge) to 3.21 mm (10 gauge).

It was found that although increasing the width and thickness of ZSPC improves their shear strength and stiffness, increasing width is more effective than increasing thickness. This might be attributed to the effect of thickness-to-width (t/W) ratio of ZSPC on the resistance of the connector-concrete connection. Increase in the connector width improves the shear strength of ZSPC and the resistance of the connector-concrete connection. However, increase in thickness improves the shear strength of ZSPC without improving the resistance of the connector-concrete connection, which intensifies cracking of concrete around the connection, affecting the shear strength and stiffness of the connectors. This intensified cracking compromises some of the improvement in the connector's shear strength and stiffness caused by thickness increase of ZSPC. After the push-off tests the 16 gauge ZSPC were observed to have undergone significant buckling, forming a tension-tie along the tension diagonal of the connectors, similar to the tension field action in plate girders. This tension-tie might have contributed to the observed residual shear strength of ZSPC.

5. Numerical Analysis of Push-off Shear Tests

5.1. Introduction

In this research only a limited number of push-off tests were conducted on ZSPC as presented in Chapter 4. This limited number of tests is not sufficient to give a robust analytical model to estimate the shear strength and stiffness of ZSPC with different widths and thicknesses. Hence, complementary numerical models are needed to investigate the shear behaviour of ZSPC with wider variety of widths and thicknesses. These numerical models should first be verified by the experimental results of push-off tests presented in Chapter 4. The verified numerical models will then be adopted to conduct parametric analysis of ZSPC with varying widths and thicknesses. The results of these parametric analyses can then be adopted to develop analytical methods to estimate the shear strength and stiffness of ZSPC.

Section 5.2 of this Chapter describes the numerical modeling of the conducted push-off tests using Finite Element Method. The results of these models are compared with the experimental load-displacement behaviour of ZSPC in Section 5.3 to assess the validity of the FEM models. Section 5.4 investigates the effect of different factors on the numerical shear behaviour of ZSPC. The investigated factors include pivoting of side concrete layers, concrete-insulation interaction, connector-insulation interaction, and length of the unembedded part of the web. The effect of width and thickness of ZSPC on their shear behaviour is studied through parametric analysis presented in Section 5.6. In this parametric analysis the width of the connectors varies from 76.2 mm to 152.4 mm and the thickness varies from 1.47 mm to 3.21 mm. These limits of widths and thicknesses are the ones used in the push-off shear tests. Section 5.6 compares the shear behaviour of ZSPC with common existing interlayer connector systems studied by previous researchers and shows that the shear behaviour of ZSPC outperforms the shear behaviour of these existing connector systems.

5.2. Numerical Modeling of Push-off Shear Tests

Finite Element Method (FEM) was used to perform parametric analysis of ZSPC to investigate the effect of its width and thickness on its shear strength and stiffness. For this, the numerical models should be verified by the experimental results of the push-off shear tests described in Chapter 4.

Numerical modeling and analysis were performed using the software package of Abaqus/CAE (version 6.12-1).

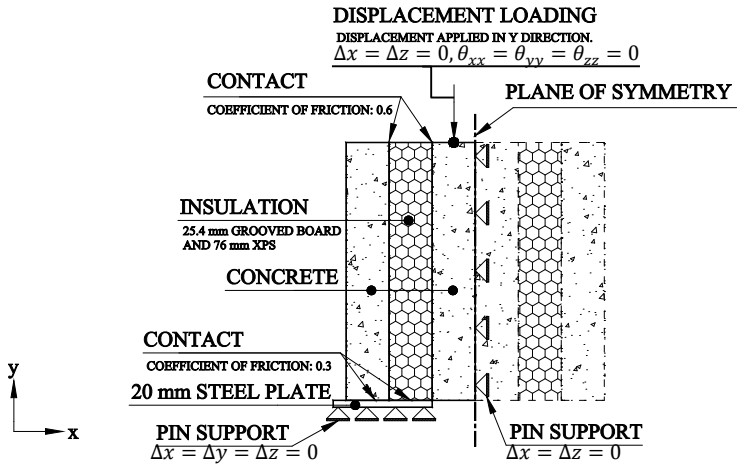

Figure 5-1: Assumptions used in numerical modeling of push-off shear tests.

Since the push-off shear test setup was symmetric about a plane going through the mid-thickness of the middle concrete layer, as shown in Figure 5-1, only the parts of the shear specimens on one side of the plane of symmetry were modeled. Therefore, the modeled shear specimens consist of half of the middle concrete layer and one side concrete layer with the corresponding insulation and Z-SPC (Figure 5-2). The intersection of the middle concrete layer and the plane of symmetry was restrained against translation in the x and z directions as shown in Figure 5-1. To apply loading in the numerical models the top of the middle concrete layer was tied to a rigid plate restrained against translations and rotations in all directions and a linearly increasing (ramp) displacement in y-direction was applied on this rigid plate.

The side concrete layer in the numerical model was resting on a 20.0 mm steel plate representing the pedestal used in the test. As shown in Figure 5-1 the bottom surface of this steel plate was restrained against translation in all directions. The interaction between the side concrete layer and the bottom steel plate was modeled as an impenetrable contact with a coefficient of friction of 0.3. The combination of grooved board and polystyrene insulation was modeled as a 76.2 mm thick solid layer. The interaction between this insulation layer and the concrete surfaces of the side and middle concrete layers was modeled as an impenetrable contact with a coefficient of friction of 0.6. The unembedded parts of the connectors were modeled with shell elements. The embedded parts of the connectors were modeled with solid element so that they could be assigned contact properties with the surrounding concrete that takes into consideration the effect of the embedded parts' thickness. The contact between the embedded parts of the connectors with the surrounding

concrete was modeled with bonding as shown in Figure 5-3, which is based on the experimental studies by Hotta et al. (1998) on the shear bonding behaviour of steel plates encased in concrete. After debonding of the interface, the concrete and connector were in contact with 0.45 coefficient of friction.

It was desired that the material model for these numerical analyses was capable of simulating concrete cracking and nonlinear behaviour of concrete in compression. There are three material models in Abaqus that can simulate cracking and compressive behaviour of concrete. The first one is brittle cracking that assumes linear compressive behaviour for concrete, thus was not selected for these analyses. The second material model for concrete is smeared cracking. This model can simulate nonlinear compressive behaviour, cracking and tension stiffening of concrete. In this model cracking is assumed to occur when the tensile stresses reach a failure surface called crack detection surface. When cracking occurs, the orientation of the cracking plane is stored for subsequent analyses. After cracking, the stiffness of the element in the direction of the cracking is reduced. Although this model had the desired capabilities to simulate the concrete material properties for the tested shear specimens, the analysis using smeared cracking model took long analysis time and it would often terminate at early stages of loading due to numerical instability.

The third model in Abaqus is concrete damage plasticity. Similar to smeared cracking, concrete damage plasticity can simulate nonlinear compressive behaviour, cracking and tension-stiffening of concrete. However, in concrete damage plasticity model when the stresses reach the failure surface, the stiffness of the element in all directions is reduced, which is not a realistic behaviour of concrete since in reality after cracking of concrete the material stiffness is only reduced normal to the crack direction. However, this problem with concrete damage plasticity can be circumvented by choosing finer mesh (Chaudhari and Chakrabarti, 2012). Contrary to using smeared cracking for numerical analysis, the numerical models of the shear tests using concrete damage plasticity continued up to failure of connectors, then the analysis terminated due to numerical instability. Therefore, concrete damage plasticity was adopted for numerical analysis of the shear tests.

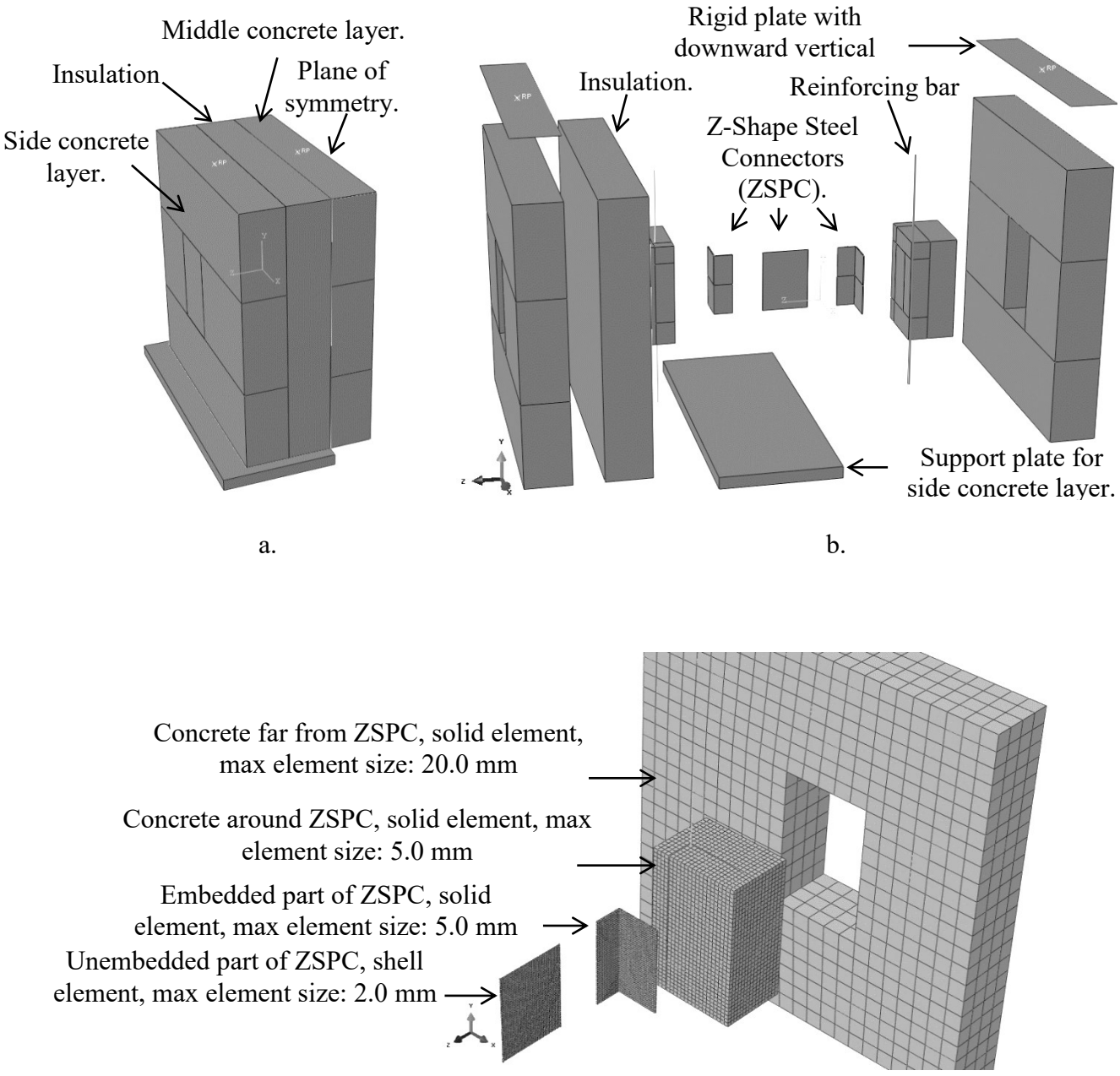

Figure 5-2: 3D rendering of the numerical models: a. whole model, b. different parts of model, c. mesh size of connector and concrete.

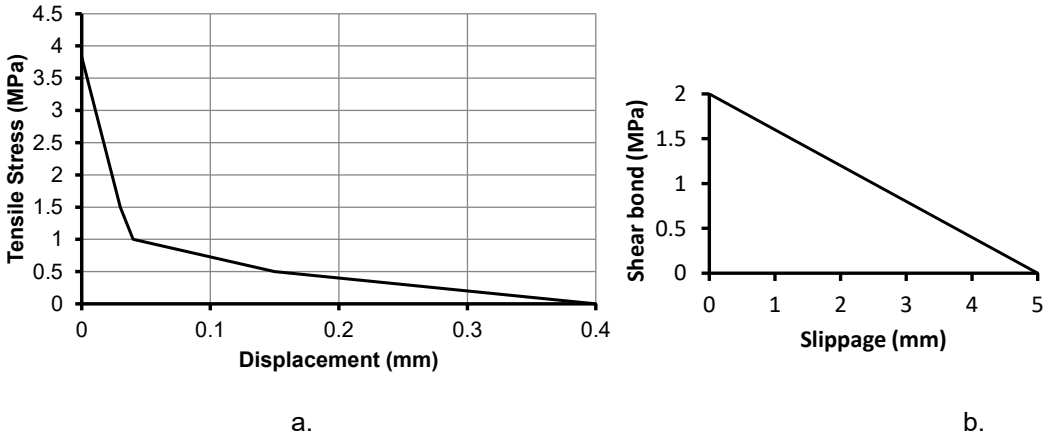

Figure 5-3: a. Tension softening behaviour of concrete, and b. bonding behaviour of ZSPC to concrete.

The details of the concrete damage plasticity in Abaqus are as presented by Lubliner et al. (1989). The softening behaviour of concrete under tension is modeled as shown in Figure 5-3, which is based on the experimental study by Cornelissen et al. (1986). In this figure the tensile strength of concrete is based on the tensile strength derived from Brazilian tests at 28 days of age, since the Brazilian split tests were not conducted on the testing day. Since the 28-day tensile strength was used for the tensile behaviour of the concrete, the compressive behaviour of the concrete was modeled as the 28-day compressive behaviour of the concrete shown in Figure 4-5 to be consistent. The material properties of the connectors were modeled as elastoplastic material with the von Mises yield criterion, with the true stress- true strain behaviour derived from the tensile tests, the results of which are shown in Figure 4-8. The steel plate holding the side concrete layer is modeled as an elastic material with modulus of elasticity of 200 GPa. The insulation material is defined as an elastoplastic material having the true stress-true strain behaviour as the experimental compressive behaviour of the combined grooved board and polystyrene shown in Figure 4-7.

The shear behaviour of the shear tests is dominated by the shear behaviour of the connectors and the cracking of the concrete around the connector-concrete connection. To find the optimum size of elements to obtain accurate results with economical cost of computation, 10 analyses were conducted on SH4-16 with different element sizes for ZSPC and concrete layers. Based on the results of this mesh-sensitivity analysis different components of the numerical models were discretized with finite elements with different sizes depending on the expected stress and strain concentration across the model. In the post-experiment examination of the shear specimens, concrete cracking and spalling was observed in the regions closer than 20.0 mm to 25.0 mm to the ZSPC, indicating high stresses in these regions. Therefore, the concrete regions around the connectors are discretized with a mesh finer than those far from the connectors. The maximum

element size for the concrete regions closer than 30.0 mm to the connectors is 5.0 mm and the maximum element size for the rest of the concrete is 20.0 mm. The maximum element size for the embedded and unembedded parts of the connectors is 2.5 mm (Figure 5-2).

5.3. Numerical vs. Experimental Results of Push-off Shear Tests

Figure 5-4 compares the numerical results for connector force (V) against the vertical displacement of the middle concrete layer (Δ_v) and Table 6-1 summarizes the numerical shear strength and secant shear stiffness, V_{FE} and K_{FE}, respectively. The secant stiffness of ZSPC is the secant stiffness of the $V - \Delta_v$ curve from the origin to $V_{FE}/1.4$, where the factor 1.4 is to reduce the shear strength to the shear force at service wind load. As shown in Table 5-1, V_r / V_{FE} varies between 0.91 to 1.12 with an average value of 1.04. This means the numerical models underestimated the experimental shear strengths by 4%. This table also shows that K_s/K_{FE} for the tested specimens varies between 0.83 to 1.3, with an average value of 1.18. This means the numerical models underestimated the experimental secant shear stiffness by 18%. Figure 5-4 shows that the numerical analyses were aborted shortly after reaching the peak shear force due to numerical instability.

Table 5-1: Comparison of experimental and numerical results for the push-off shear tests.

Connector group	Specimen	V_r, kN	V_{FE}, kN	V_r/V_{FE}	K_s, kN/mm	K_{FE}, kN/mm	K_s/K_{FE}
SH3-16	**1**	15.07	13.41	1.12	14.45	13.09	1.10
	2	12.92		0.96	13.92		1.06
	3	14.67		1.09	11.91		0.91
SH4-16	**1**	15.41	13.43	1.15	18.35	22.07	0.83
	2	14.22		1.06	42.02		1.90
	3	13.93		1.04	25.61		1.16
SH6-16[*2]	**1**	21.99	22.27	0.99	44.33	36.65	1.21
	2[*1]	13.56	n.a.	n.a.	52.97	n.a.	n.a.
SH4-10	**1**	38.59	37.97	1.02	45.00	34.68	1.30
	2	34.58		0.91	40.02		1.15
	3[*1]	10.53	n.a.	n.a.	17.32	n.a.	n.a.
Average				1.04			1.18

[*1] Not considered in averaging due to premature failure of the specimen caused by construction errors. [*2] The third specimen of this connectors group was untestable due to construction errors.

Notes: n.a. = not applicable.

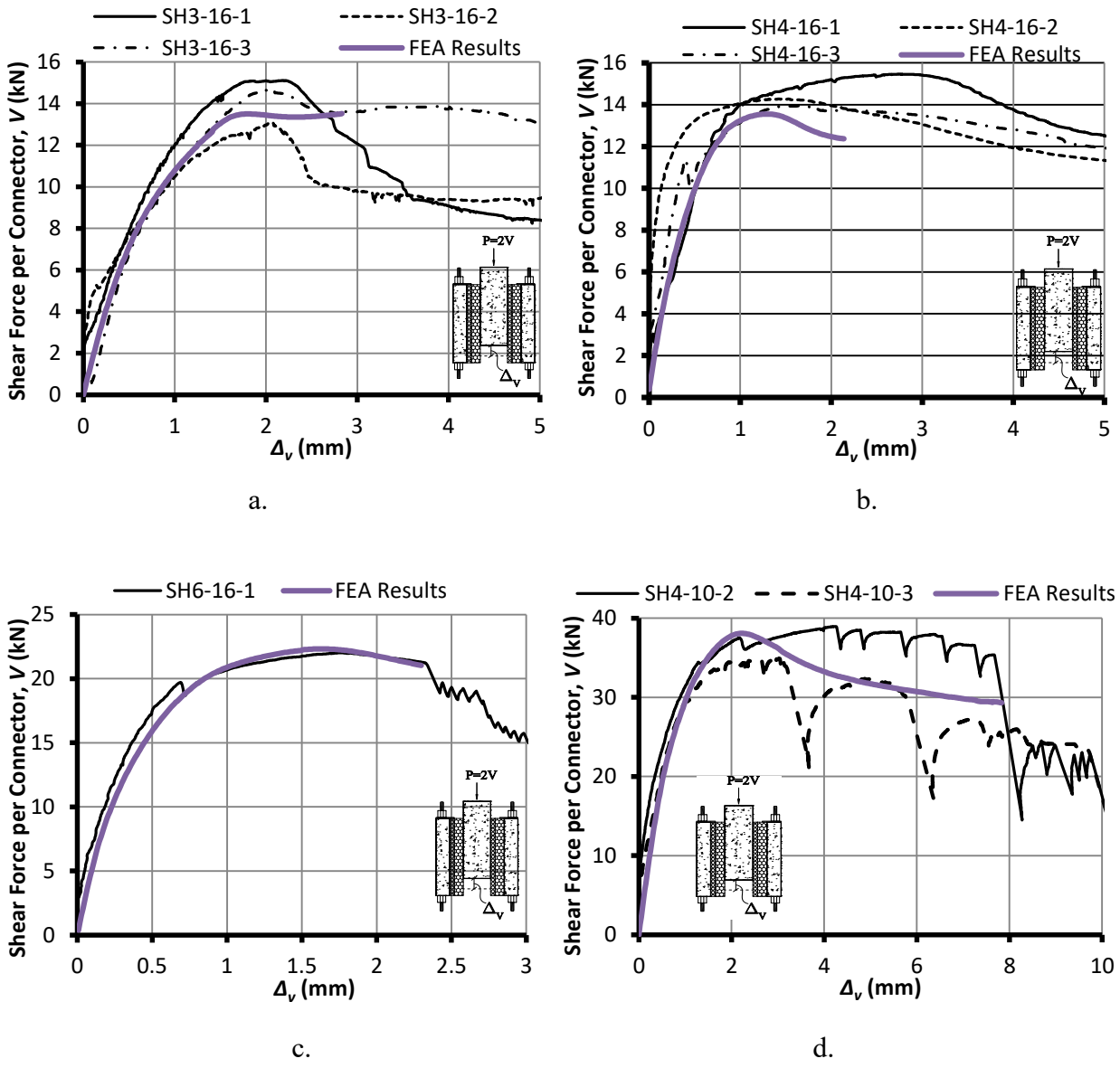

Figure 5-4: Comparison of FEA and experimental results for: a. SH3-16, b. SH4-16, c. SH6.16 and d. SH4-10.

These finite element models were able to predict the behaviour of the tested connector groups up to the peak point including shear stiffness and strength of the ZSPC, which are the two important mechanical properties of shear connectors for analysis of PICP. Thus these numerical models were adopted in the next section for the parametric analysis of ZSPC.

5.3.1. Distribution of In-Plane Normal and Shear Stresses

Distribution of in-plane horizontal stress, σ_x, and the in-plane shear stress, τ_{xy}, across the connector width close to the face of the middle concrete layer for the verified numerical models are shown in Figure 5-5. These stress distributions are taken at $\Delta_v = 0.25\ mm$ that is when the connector material is in elastic region. As shown in Figure 5-5, the distribution of normal stresses,

σ_x, is almost linear for SH3-16 and as the width and thickness of the connector increases this stress distribution becomes nonlinear. Moreover, the distribution of the shear stresses across the width for all the connector groups except SH6-16 is parabolic with maximum shear stress occurring at about 0.7 to 0.8 of the connector width. The shear stress distribution for SH6-16 has two maximum values occurring at 0.2 and 0.8 of the connector width.

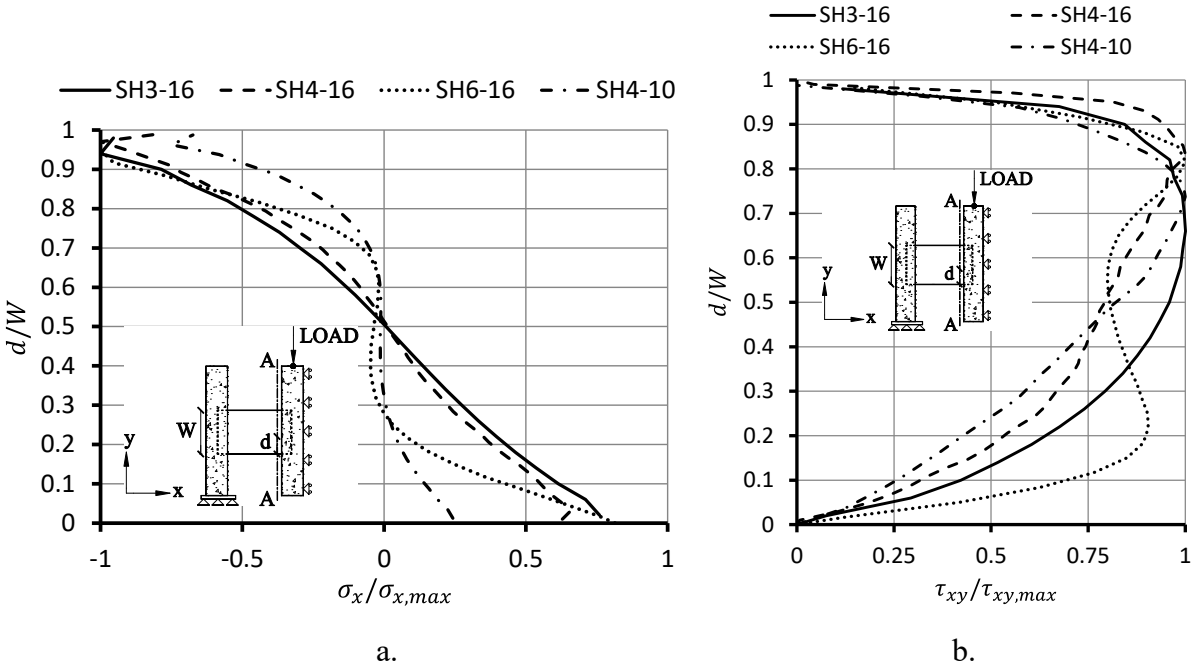

Figure 5-5: Stress distribution at connector-concrete interface (section A-A) when ZSPC material is in elastic region.

5.3.2. Connector-Concrete Bonding

Figure 5-6 shows the damage ratio of the bond between the embedded part of ZSPC and concrete derived from numerical model of SH3-16 at $\Delta_v = 0.2\ mm$. As shown in this figure, the concrete-connector bonding at regions far from the mid-width of connector failed, which shows that concrete-connector debonding happens at the very early stage of loading.

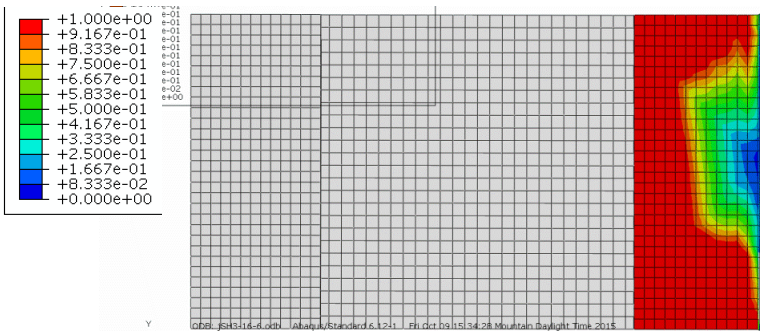

Figure 5-6: Damage ratio for bonding between concrete and ZSPC in numerical model of SH3-16.

5.3.3. Out-of-Plane Deformation of ZSPC under Shear Force

Figure 5-7 shows the out-of-plane deformation of the compressive corner of the connectors with respect to Δ_v. As shown in this figure out-of-plane deformation starts from the very early stages of loading and increases at higher rate with progression of loading. Figure 4-3.b. shows that the insulation was snugly placed on the sides of ZSPC during fabrication which could have somewhat restrained out-of-plane deformation of these connectors. The effect of this restraint is numerically studied in section 5.4.

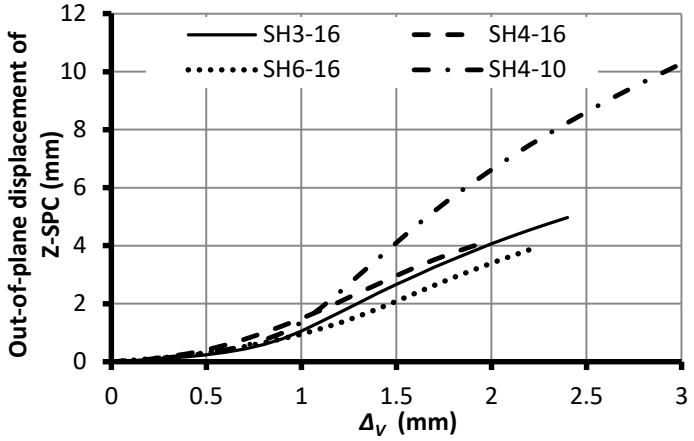

Figure 5-7: Numerical out-of-plane displacement of compressive corner of ZSPC.

Figure 5-8 shows the contour of out-of-plane deformation of the unembedded part of the tested ZSPC at their respective shear strength. As illustrated in this figure, the connectors in SH3-16 and SH4-16 shear specimens show formation of tension tie as the results of tension field action. However, there is no distinct tension tie in connectors of SH6-16 and SH4-10 shear specimens.

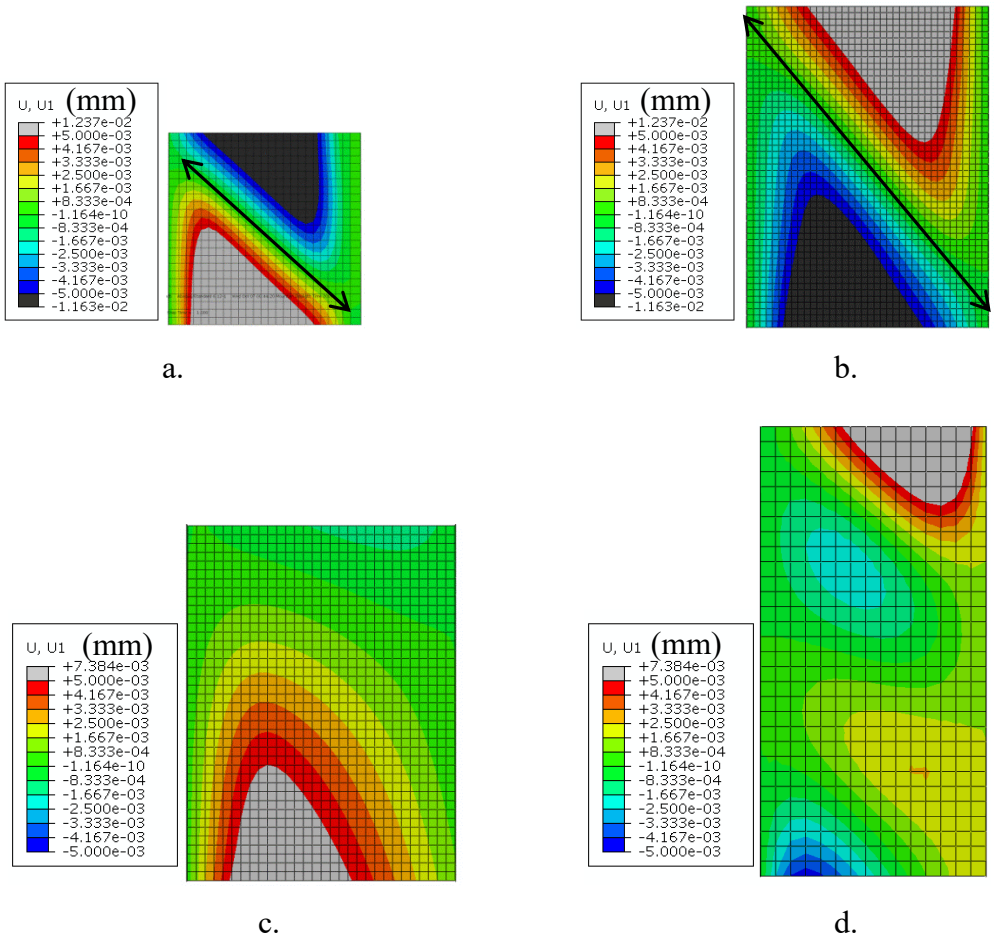

Figure 5-8: Contour of out-of-plane deformation of a. SH3-16, b. SH4-16, c. SH4-10 and d. SH6-16, from FEA models.

5.4. Factors Affecting Numerical Results of Push-off Shear Tests

The numerical results for the push-off tests are affected by many factors. Some of the factors that are either uncertain or were not determined in the experimental program are numerically studied here to investigate their effect on the shear strength and stiffness of ZSPC. For this, it was preferred to pick a numerical model in which the width of ZSPC is between the maximum and minimum widths of the tested ZSPC. However, the numerical model for SH4-16 was preferred over SH4-10 since 16 gauge ZSPC is more common in industry than 10 gauge ZSPC. Therefore, the numerical model for SH4-16 was taken as the benchmark model and designated FEA-1 with the attributes given in Table 5-2. Several modified versions of this model were made to investigate the effect of some factors on the shear strength and stiffness of ZSPC in the numerical model of SH4-16. The factors investigated here include pivoting of side concrete layers (FEA-2), concrete-insulation friction (FEA-3), connector-insulation interaction (FEA-4), and seepage of concrete mortar around the connector (FEA-5). The attributes of the modified numerical models are given in Table 5-2. The shear behaviour of ZSPC in SH4-16 by these numerical models is compared against the experimental results in Figure 5-9. Although these factors are not studied with experiments, these numerical investigations give us some insights into how these factors affect the shear behaviour of ZSPC. These effects might explain some of the differences between experimental and numerical results as well as between experimental results of the replicas of the same ZSPC group.

Table 5-2: Various numerical analyses of SH4-16.

	FEA-1	FEA-2	FEA-3	FEA-4	FEA-5
Pivoting of side concrete layers	free	restrained	free	free	free
Connector-insulation interaction	none	none	none	contact	none
Concrete-insulation coefficient of friction	0.6	0.6	0.0	0.6	0.6
Unembedded length of ZSPC (mm)	76	76	76	76	72

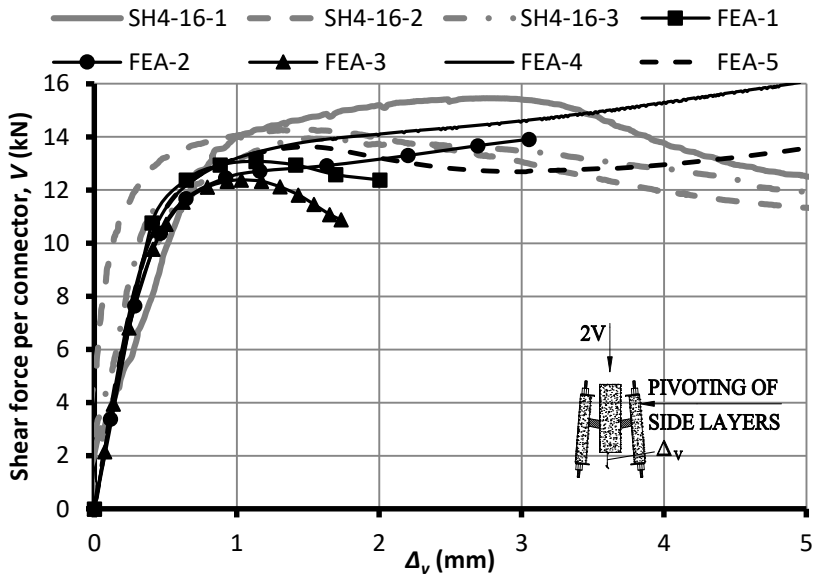

Figure 5-9: Factors affecting numerical results for shear behaviour of SH4-16.

5.4.1. Pivoting of Side Concrete Layers (FEA-2)

As mentioned in section 4.3 the side concrete layers underwent pivoting in the push-off tests. To study the effect of this pivoting, the numerical model for SH4-16 was modified to fully restrain the side concrete layer against any horizontal movement. This modified model is designated as FEA-2, the attributes of which are given in Table 5-2. Figure 5-9 compares the numerical results of FEA-2 with that of FEA-1, in which the side layers were pivot-free as in the tests. As shown in this figure, FEA-2 has the same shear stiffness as FEA-1. However, at $\Delta_v = 1.0\ mm$, where FEA-1 reaches its maximum shear strength, FEA-2 carries a 5% lower shear force. After this point the shear force in FEA-2 increases at lower rate up to 14.0 kN, where the analysis was terminated. This suggests that if the side concrete layers are fully restrained against pivoting the numerical model results in higher ductility and shear strength. In other words, relative movements of concrete layers result in reduced shear strength and ductility. Since in PICP the concrete layers are not fully restrained against relative movements with respect to each other, in this thesis, the numerical shear strength and stiffness of ZSPC are conservatively based on numerical push-off models without imposing restraint on pivoting of the side concrete layers.

5.4.2. Concrete-Insulation Friction (FEA-3)

As mentioned in section 4.2, the coefficient of friction for concrete-insulation interaction in the numerical models was arbitrarily taken as 0.6 based on engineering judgement of reported coefficients of friction between various materials. This value depends on the roughness of the concrete in contact with insulation, so it varies throughout the contact area and from one specimen to another. The effect of concrete-insulation friction was studied by defining frictionless surface for this contact in the numerical model for SH4-16. This modified model is designated as FEA-3 in Table 5-2. Figure 5-9 shows that FEA-3 has the same stiffness as FEA-1 but has 5% lower shear strength than FEA-1. In other words, concrete-insulation interaction with coefficient of friction of 0.6 contributes 5% to the numerical shear strength of SH4-16. For the parametric studies presented in 5.5, the coefficient of friction between the insulation and concrete is taken as 0.6.

5.4.3. Connector-Insulation Interaction (FEA-4)

As mentioned in Section 4.3 the insulation could have imposed some restraint against out-of-plane deformation of ZSPC. The effect of this restraint caused by connector-insulation interaction was investigated numerically for the verified model for SH4-16. In this analysis the numerical model for SH4-16 was modified to incorporate the connector-insulation interaction by modeling insulation on the sides of the unembedded part of ZSPC and defining impenetrable contact with 0.45 coefficient of friction between connector and insulation. This modified numerical model is designated as FEA-4 and its attributes are given in Table 5-2.

Figure 5-9 compares the shear behaviour of SH4-16 derived from push-off tests, the numerical model without connector-insulation interaction (FEA-1) and the modified numerical model with connector-insulation interaction (FEA-4). As shown in this figure, connector-insulation interaction had negligible effect on the numerical shear stiffness of ZSPC in SH4-16. Also at $\Delta_v = 1.0\ mm$ where FEA-1 reaches its shear strength of 13.1 kN, FEA-4 reaches the same shear force, however, it continues to pick up load at lower rate and exceeds the experimental shear strength of ZSPC in SH4-16. This suggests that the restraint on out-of-plane deformation of ZSPC enforced by the connector-insulation interaction in the push-off tests improves ductility and shear strength of the connector. Since in practice, the insulation might not be snugly placed around the connectors, in the parametric studies in Section 5.5 the effect of connector-insulation was conservatively ignored.

5.4.4. Seepage of Concrete Mortar around Connector

In the numerical modeling of push-off tests shown in Figure 5-2 thickness of insulation was taken as 76 mm, equal to that in the push-off tests. However, during concrete pour, some concrete mortar might have seeped around the connectors reducing the unembedded length of ZSPC. To examine the effect of this reduced unembedded length of ZSPC on its shear behaviour, the unembedded length of ZSPC in the numerical model for SH4-16 (FEA-1) was reduced to 72.0 mm. This modified model (FEA-5) accounts for 4.0 mm reduction of the unembedded part of the ZSPC due to seepage. For this modification, a line on the connector 4.0 mm from of the end of the ZSPC in FEA-5 is restrained from out-of-plane deformation as shown in Figure 5-10.

Figure 5-9 shows that the modified numerical model, FEA-5, has the same shear stiffness and ductility as the unmodified model, FEA-1, but has 6% higher shear strength than FEA-1. Also Δ_v at shear strength has increased 50% from 1.0 mm for FEA-1 to 1.5 mm for FEA-5. This suggests that seepage of concrete mortar around the connector improves the shear strength and ductility of ZSPC. In the parametric study in Section 5.5 seepage of mortar around connector was conservatively ignored.

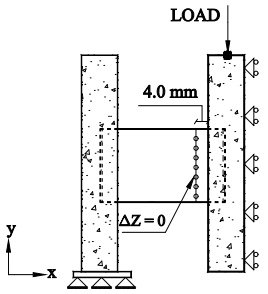

Figure 5-10: Numerical model with 4.0 mm reduced length of unembedded part of ZSPC (FEA-5).

5.5. Effect of Width and Thickness of ZSPC on its Shear Behaviour

The verified numerical models were adopted to perform parametric analysis to investigate the effect of width and thickness of ZSPC on their shear behaviour. The matrix for these parametric analyses is given in Table 5-3. In this table the models are designated as Zα-β, where α is the width of the connector in inch and β is the gauge number of the steel sheet of the connector. As shown in this table the thickness and width of the connectors vary from 1.47 mm to 3.42 mm and from 76.2 mm to 152 mm, respectively. These dimensions are within the range of the connectors tested as described in Chapter 4. For parametric analysis, the ZSPC was assigned the steel properties with

yield strength of 350 MPa, the same material as for SH3-16 shown in Figure 4-8. The connector with 350 MPa yield strength is more common for ZSPC used as interlayer connectors in PICP.

The numerical shear strength, V_{FE}, and secant shear stiffness, K_{FE}, of the ZSPC derived from the parametric analyses are summarized in Table 5-3 and are graphed in Figure 5-11. The secant shear stiffness of ZSPC is the secant stiffness of the $V - \Delta_v$ curve from the origin to $V_{FE}/1.4$, where the factor 1.4 is to reduce the shear strength to the shear force at service wind load. In Figure 5-11 the analyzed ZSPC are grouped by their widths and each group is denoted ZSPCα, where α is the width of the connector in inch. Figure 5-11.a. shows that shear strength of analyzed ZSPC increases linearly with cross sectional area, Wt, of the connector. This means the shear strength of the connector increases proportional to the width and thickness of ZSPC.

Table 5-3: Parametric analysis on shear behaviour of ZSPC.

$f_y = 355\ MPa$ $\quad\quad$ $\nu = 0.3$
$E = 187.9\ GPa$ $\quad\quad$ $G = 72.2\ GPa$

ZSPC Designation	Width (W) mm (in.)	Thickness (t) mm (gauge #)	Area (Wt) mm^2	V_{FE} (kN)	K_{FE}* (kN/mm)
Z3-16	76 (3)	1.48 (16)	112.48	12.92	18.33
Z3-14		1.9 (14)	144.40	16.63	16.80
Z3-12		2.66 (12)	202.16	27.82	17.17
Z3-10		3.42 (10)	259.92	37.58	16.70
Z4-16	101 (4)	1.48 (16)	149.48	17.78	24.70
Z4-14		1.9 (14)	191.90	26.38	27.06
Z4-12		2.66 (12)	268.66	40.74	25.62
Z4-10		3.42 (10)	345.42	54.20	24.75
Z5-16	127 (5)	1.48 (16)	187.96	24.76	36.68
Z5-14		1.9 (14)	241.30	35.85	41.21
Z5-12		2.66 (12)	337.82	53.48	45.13
Z5-10		3.42 (10)	434.34	71.30	46.60
Z6-16	152 (6)	1.48 (16)	224.96	31.18	47.24
Z6-14		1.9 (14)	288.80	44.18	54.54
Z6-12		2.66 (12)	404.32	66.86	61.91
Z6-10		3.42 (10)	519.84	87.61	64.90

*K is the secant stiffness from the origin to $V/1.4$ on the $V_{FE} - \Delta_v$ graph of ZSPC. The factor 1.4 is to reduce shear strength to shear force at service wind load.

Figure 5-11.b. shows the changes in the secant shear stiffness, K_{FE}, with changing the cross sectional area of ZSPC. In this figure each line represents one ZSPC group with the same width. As shown in this figure, the secant shear stiffness increases with width of ZSPC. Figure 5-11

demonstrates that the effect of thickness on K_{FE} depends on the width of the connector. For 76 mm wide, ZSPC3, and 101 mm wide, ZSPC4, the connector's thickness has negligible effect on K_{FE}. For 76 mm wide ZSPC increase in thickness has had negligible effect on the secant shear stiffness. But for 127 mm wide, ZSPC5, and 152 mm wide, ZSPC6, thickness increase leads to an improvement in the secant shear stiffness of ZSPC. And this positive effect of thickness for ZSPC6 is slightly higher than that for ZSPC5, which is depicted in Figure 5-11.b. by the higher slope of ZSPC6 compared to that of ZSPC5 throughout the curve. Also the ZSPC5 and ZSPC6 curves have negative curvatures, which means for 127 mm and 152 mm wide connectors as the thickness increases the stiffness increases at a lower rate.

As discussed in Section 4.3, the mentioned effects of thickness on the secant shear stiffness might be attributed to intensified cracking with increased thickness, i.e. as the thickness increases higher forces are transferred from the connector to the concrete without much increase in the pry-out strength of the connector-concrete connection, which increases the stresses in concrete, leading to intensified cracking. However, as the connector gets wider it increases the transferred forces from connector to concrete, and improves the pry-out strength of the connector-concrete connection, hence it does not intensify tensile cracking of concrete.

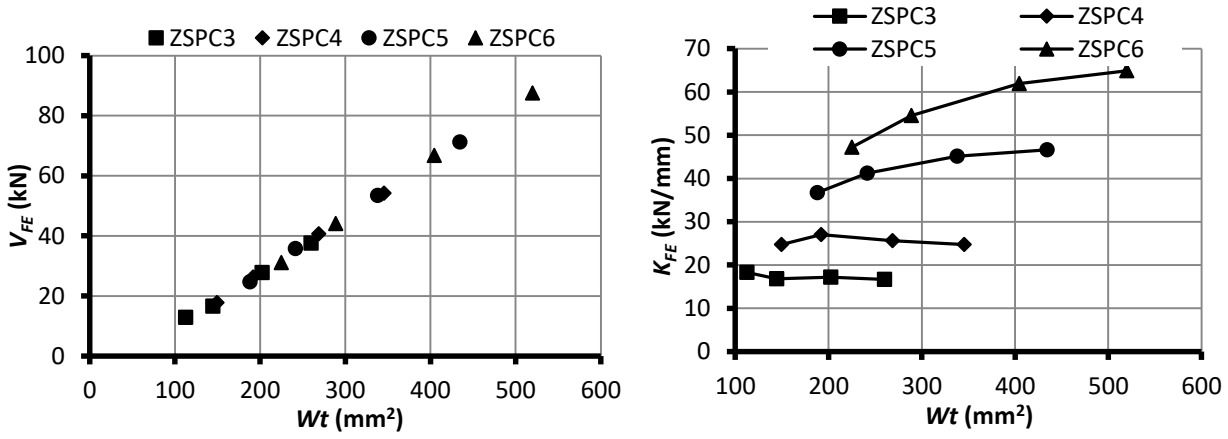

a. b.

Figure 5-11: Results of parametric analyses by FEM: a. shear strength of ZSPC, b. secant shear stiffness of ZSPC.

5.6. Shear Behaviour of ZSPC Compared with other Interlayer Connectors

As mentioned in Chapter 2, Naito et al. (2012) conducted pull-out tests on shear specimens with 50.0 mm thick insulation with various connector systems and discovered that truss connectors have the largest shear strength and stiffness than other steel connectors. Since the ZSPC in the numerical model for SH4-16 has almost the same cross sectional area (149.5 mm^2) as that for the tested truss connector (158.3 mm^2) by Naito et al. (2012), it was adopted and modified to compare the shear behaviour of ZSPC against that of the truss connector tested by Naito et al. (2012). In the modified model the insulation thickness was reduced from 76 mm to 50.0 mm and the connector material was assigned the properties of the steel with 355 MPa yield strength, i.e. the same material for SH3-16 shown in Figure 4-8. This material has lower yield strength than 1008 steel with a yield strength of 497 MPa that was used in the truss connector tested by Naito et al. (2012). Figure 5-12 compares the modified numerical model for SH4-16 against the experimental result for truss connector given by Naito et al. (2012). As shown in this figure both connector systems have the same shear stiffness, but ZSPC has 25% higher shear strength. Figure 5-12 also compares the shear behaviour of ZSPC against some of the existing interlayer mechanical connectors investigated by Naito et al. (2012) including M-tie, discrete GFRP grid, GFRP pin, CFRP truss. As shown in this figure ZSPC exhibits larger shear strength and stiffness than other common interlayer connectors.

It should be noted that although the ZSPC outperforms steel truss connectors in shear strength, installation of ZSPC, as well as other discrete connectors, is more labor intensive than truss connectors since discrete connectors are placed one by one during fabrication of PICP. But truss connectors are fabricated to the desired length, then the entire truss is placed between the concrete layers. This drawback of ZSPC can be overcome by the method described in Section 1.1.

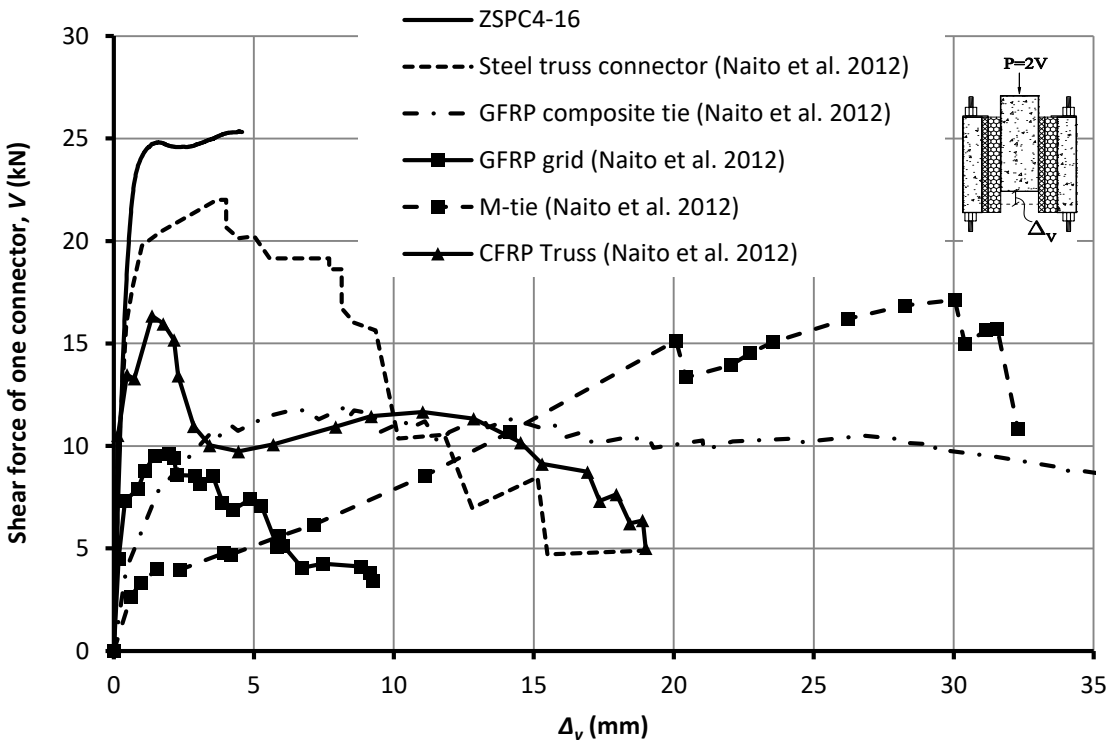

Note: the experimental V for continuous connectors is for 406 mm length of connector.

Figure 5-12: Comparison of shear behaviour of ZSPC with other interlayer mechanical connectors.

5.7. Summary and Conclusion

Finite Element Method (FEM) was adopted to model the push-off shear tests on ZSPC. The shear behaviour of ZSPC obtained from FEM models were in good agreement with the experimental shear behaviour of the connectors. These numerical models were adopted to investigate the effect of different factors on the shear behaviour of ZSPC; these factors included concrete-insulation friction, pivoting of side concrete layers, connector-insulation interaction, width and thickness of ZSPC.

It was found that concrete-insulation friction with a coefficient of friction of 0.6 contributes about 5% to the numerical shear strength of ZSPC. If pivoting of side concrete layers is restrained the concrete-insulation friction, hence the shear force transferred through concrete-insulation friction, diminishes because the restrained side concrete layers cannot pivot to compress the insulation to produce friction. Also, restrained pivoting of side concrete layers leads to improved ductility of ZSPC in the numerical models, which might be attributed to the tension field action developed after buckling of the thin connectors and the ductile shear deformation of the thick connectors.

Connector-insulation interaction was found to improve the numerical ultimate shear strength and ductility of ZSPC by restraining buckling of the connectors. This improvement, however, depends on how snugly the insulation is placed around ZSPC during construction.

The numerical shear strength of ZSPC was found to improve linearly by increasing the connector's width and thickness. But the numerical secant shear stiffness is affected differently when the connector's width or thickness is increased. Increase in the width of ZSPC significantly improves the shear stiffness of the connector, but increase in the thickness of ZSPC improves the connector's shear stiffness by negligible amount. For ZSPC with small width, increase in thickness was found to make no improvement in the connector's shear stiffness. This might be attributed to the effect of the thickness-to-width ratio of ZSPC on the resistance of the connector-concrete connection. As the connector width is increased, the confined concrete block in the connector-concrete connection is enlarged, hence the resistance of the connection is improved. But as the connector's thickness is increased, the size of the confined concrete block at the connector-concrete connection and thus the resistance of the connection remain unchanged. In this case, the connector with increased thickness transfers large forces to the concrete layers through connector-concrete connection with unimproved resistance. This intensifies concrete cracking around the connection, affecting the shear stiffness of ZSPC. Therefore, Z-shaped connectors with low thickness-to-width ratio are more efficient in providing interlayer shear strength and stiffness than connectors with high thickness-to-width ratio.

The numerical shear behaviour of ZSPC was compared with the experimental shear behaviour of steel truss connectors studied previously. It was found that with the same volume of steel, ZSPC has larger shear strength than steel truss connectors, but both connector systems have the same shear stiffness. Therefore, ZSPC is more efficient in providing interlayer shear strength in PICP than steel truss connectors. Also, it was shown that the shear behaviour of ZSPC outperformed the shear behaviour of some of the common existing interlayer connectors.

6. Analytical Models for ZSPC Shear Behaviour

6.1. Introduction

This Chapter presents two analytical models including simplified plate model and tension-tie model to estimate the shear strength and stiffness of ZSPC. The simplified model (Section 6.2) assumes the unembedded part of the ZSPC's web as a rectangular plate whose width is the same as the connector width and length equals the thickness of the insulation. The in-plane shear strains are assumed to have parabolic distribution and in-plane normal strains are assumed to have linear distribution across the width of the simplified plate. The theoretical yield shear strength of this plate using von Mises yield criterion and the theoretical plastic shear strength of this plate are shown to have good agreement with the numerical shear strength of ZSPC (Section 6.4). The simplified plate model is also adopted to estimate the shear stiffness of ZSPC. Following the observed buckling shape of gauge 16 ZSPC in push-off shear tests, a tension-tie model is developed to estimate the shear stiffness of ZSPC (Section 6.3); this model idealizes the unembedded part of the ZSPC's web as a tension-tie along its tension diagonal. To account for the effect of connector-concrete connection on the shear stiffness of ZSPC, the numerical results presented in Chapter 5 were adopted to modify the analytical expressions for ZSPC's shear stiffness using simplified plate model and tension-tie model (Section 6.4).

6.2. Simplified Plate Model

In this model the shear behaviour of the unembedded part of the web of the Z-shaped connectors is assumed to resemble the shear behaviour of a plate with the length, width and thickness of L, W and t, respectively (Figure 6-1). The vertical load P in the push-off tests induces in-plane shear force, V, and bending moment, M, in the unembedded part of the connector's web. The critical locations of the web are the two ends of the unembedded part of the web, that are under the combined effects of the in-plane shear force V and the in-plane bending moment M. The V and M are acting on the $W \times t$ cross section of the web, where W and t are the width and thickness of the connector, respectively (Figure 6-1).

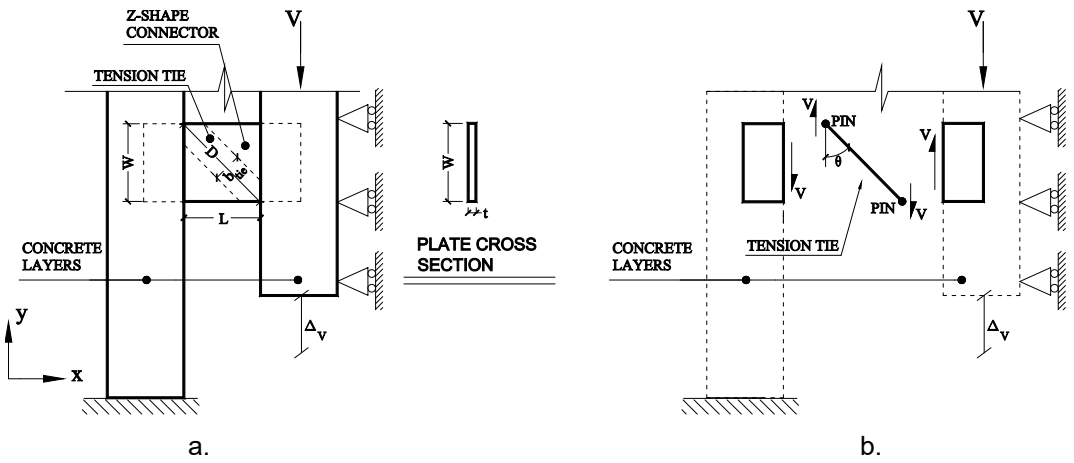

Figure 6-1. Schematics of: a. simplified plate model and b. tension-tie model.

6.2.1. Buckling Resistance of ZSPC

In the model shown in Figure 6-1, under loading the top right and bottom left corners are under compressive flexural stresses. As the loading increases, buckling starts from these compression corners and spreads throughout the connector, forming a tension field mechanism. If the steel sheet is very thin buckling of these corners governs the maximum shear resistance of ZSPC. Since the shear behaviour of this simplified plate model resembles that of shear tabs in steel structures, the analytical method proposed by Muir and Thornton (2004) for buckling resistance of shear tab connections is adopted herein to check the buckling resistance of the tested ZSPC. In this method, a slenderness parameter λ is defined by equation 6-1.

$$\lambda = \frac{W\sqrt{f_y}}{10t\sqrt{475 + 280(W/L)^2}} \qquad \textbf{6-1}$$

Where t, W and L are thickness, width and length of the unembedded part of the connector, respectively. In this equation, f_y is the yield stress of the steel plate. In this method, if $\lambda < 0.7$ buckling is not the governing mode of failure (Muir and Thornton, 2004), which is the case for sufficiently thick plates. In that case yielding of the plate governs the shear behaviour of the connector. The slenderness parameter given by equation 6-1 is higher for plates with smaller thickness and width, and larger length, i.e. thinner and longer plates with smaller width are more prone to buckling.

6.2.2. Yield Shear Strength of ZSPC Using von-Mises Yield Crieterion

In the simplified plate model, the von Mises yield criterion was adopted to calculate the theoretical yield strength of ZSPC, V_{VM}. For a general state of stress in steel, the von Mises yield criterion predicts yielding of the material when the σ_{VM}-an invariant of the stress tensor- reaches the value of f_y. The yield criterion is expressed using equation 6-2.

$$\sigma_{VM} = \sqrt{1/2 \times \left[\left(\sigma_{xx} - \sigma_{yy}\right)^2 + (\sigma_{xx} - \sigma_{zz})^2 + \left(\sigma_{yy} - \sigma_{zz}\right)^2\right] + 3\left(\tau_{xy}^2 + \tau_{xz}^2 + \tau_{yz}^2\right)} \leq f_y \qquad \textbf{6-2}$$

Where σ_{xx}, σ_{yy} and σ_{zz} are the normal stresses, τ_{xy}, τ_{xz} and τ_{yz} are the shear stresses in a three dimensional state of stress, and f_y is the yield stress of the steel material. In the simplified plate model, the shear connectors are assumed to be under a two dimensional state of stress with τ_{xy} and σ_{xx} being the only non-zero components of the stress matrix. Since the normal and average shear stresses are assumed to have linear and uniform distributions, respectively, across the plate width, $\sigma_{xx} = 3VL/(tW^2)$ and $\tau_{xy} = V/(tW)$, where V is the shear force applied on the connector. By denoting the maximum shear force by V_{VM}, equation 6-2 can be rearranged in the following form:

$$\left(\frac{f_a}{f_y}\right)^2 + \left(\frac{f_v}{\tau_y}\right)^2 = 1 \qquad \textbf{6-3}$$

Where $f_a = 3V_{VM}L/(tW^2)$ is the applied flexural stress and $f_v = V_{VM}/(tW)$ is the applied average shear stress and $\tau_y = f_y/\sqrt{3}$.

6.2.3. Plastic Shear Strength of ZSPC Using Tresca Yield Criterion

The theoretical plastic shear strength of the simplified plate model is estimated using the Tresca yield criterion, in which the plastic shear strength of the connectors, V_p is calculated based on a fully plastic section of a rectangular plate under uniaxial bending moment and shear force. The plastic shear strength is calculated by equation 6-4 as presented by Drucker (1956).

$$\frac{M}{M_0}+\frac{3}{4}\left(\frac{V}{V_0}\right)^2=1 \qquad \textbf{6-4}$$

Where M is the exerted moment on the connector, i.e. $M = V\,L/2$ and M_0 is the plastic bending moment, i.e. all normal stresses under bending moment have reached f_y, hence $M_0 = 0.25 f_y t W^2$. Moreover V_0 is the plastic shear resistance, i.e. all shear stresses have reached Tresca yield shear stress, $0.5f_y$, thus $V_0 = 0.5 f_y t W$. This equation can be rearranged to give the plastic shear strength by equation 6-5.

$$V_p=\frac{f_y t W}{3\alpha}\left(\sqrt{1+3\alpha^2}-1\right) \qquad \textbf{6-5}$$

Where, α is the aspect ratio W/L.

6.2.4. Secant Shear Stiffness of ZSPC

To estimate the secant shear stiffness of ZSPC using simplified plate model, K_{pl}, it is assumed that bending, shear and concrete-connector interaction work together like three springs in series. Moreover, the normal stress, i.e. σ_{xx} in Figure 6-1, is assumed to vary linearly across the connector's width. Using these assumptions K_{pl} is calculated as:

$$K_{pl}=\left(\frac{1}{K_b}+\frac{1}{K_s}+\frac{1}{K_{c,pl}}\right)^{-1} \qquad \textbf{6-6}$$

Where, $K_b = 12EI/L^3$ is the bending stiffness of the plate and $K_s = GA/(1.5L)$ is the average shear stiffness of the plate. In these expressions E and G are the tensile and shear moduli of elasticity of the steel, respectively, and I and A are the moment of inertia and area of the cross section of the plate, respectively, as shown in Figure 6-1. In equation 6-6, $K_{c,pl}$ is the stiffness of concrete-connector interaction accounting for interfacial debonding and concrete cracking. This value will be derived in Section 6-3 using the FEA results of the parametric analyses.

6.3. Tension-Tie Model

Based on the observed buckling pattern of the connectors shown in Figure 6-1, a tension-tie model is proposed herein to estimate the secant shear stiffness of ZSPC as an alternative to the method based on the simplified plate model given by equation 6-6. This model assumes a tension-tie along the diagonal of the unembedded part of the connector as shown in Figure 6-1. The thickness of this tension-tie, t, is equal to the thickness of the Z-shape connector, and the effective width of the tension-tie is b_{tie}. The length of the tension-tie, D, is equal to the diagonal length of the unembedded part of the connector's web, therefore D is equal to $(L^2+W^2)^{0.5}$.

6.3.1. Shear Stiffness of ZSPC Using Tension-Tie Model

To estimate the secant shear stiffness of ZSPC using the tension-tie model, K_{tie}, it is assumed that the tension-tie and the concrete-connector interaction work together like two springs in series. Moreover the ends of the tension-tie are assumed to move only in the y direction with respect to each other, as shown in Figure 6-1. Therefore, K_{tie} is calculated as follows:

$$K_{tie} = \left(\frac{1}{K_a} + \frac{1}{K_{c,tie}}\right)^{-1} \quad \textbf{6-7}$$

Where $K_{c,tie}$ is the stiffness of concrete-connector interaction accounting for interfacial debonding and concrete cracking, which will be derived in Section 6-3 using FEA results of parametric analyses. In equation 6-7, K_a is the stiffness of the tension-tie shown in Figure 6-1 in the y direction derived from the following equation.

$$K_a = \frac{Etb_{tie}}{D} cos^2(\theta) \quad \textbf{6-8}$$

Where, b_{tie} and θ are the tension-tie width and tension -tie angle with the vertical, respectively, as shown in Figure 6-1, and D and t are the length and thickness of the tension-tie, respectively. The width of the tension-tie, b_{tie}, is suggested to be calculated using the plastic shear strength of ZSPC given in Section 6.2.3. For this, the shear strength of the ZSPC using the tension-tie model is first

calculated assuming the shear strength is reached when the cross section of the tie is at yield stress, which leads to the following equation.

$$V_{tie} = f_y t b_{tie} \cos(\theta) \quad \textbf{6-9}$$

Where, V_{tie} is the shear strength of the connector using the tension-tie model. Then by replacing V_{tie} with V_p given in Section 6.2.3 and rearranging equation 6-9 the tension-tie width is calculated as follows:

$$b_{tie} = \frac{V_p}{f_y \, t \, cos(\theta)} \quad \textbf{6-10}$$

Where V_p is given by equation 6-5.

6.4. Comparison of Analytical and Numerical Results

6.4.1. Buckling and Shear Strengths of ZSPC

Table 6-1 summarizes the analytical results of simplified plate model for buckling and shear strengths of ZSPC studied in Section 5.5 and compares them with the numerical results presented in Section 5.5. As shown in this table, the slenderness ratio, λ, given by equation 6-1 is less than 0.7 for all of the investigated connectors. As discussed in Section 6.2.1, this means elastic buckling does not govern the shear failure of the connectors. Although the numerical results presented in Figure 5-7 showed that out-of-plane deformation of the connectors started from the onset of loading, it did not lead to elastic buckling failure predicted by equation 6-1. This is also proved by the average ratio of numerical shear strength to plastic shear strength, V_{FE}/V_p, in Table 6-1. This average ratio is 1.04, which means the studied connectors reached their analytical plastic shear strengths despite their out-of-plane deformations. Therefore, the buckling modes observed in the experiments after the test shown in Figure 4-12 might have been plastic buckling.

As mentioned in Section 6.2.1 thinner and longer plates with smaller width are more prone to buckling. The common minimum thickness and width of connectors are 1.48 mm (gauge 16) and 76 mm, respectively, and the common maximum insulation thickness of PICP - which is the

unmebedded length of ZSPC - are 152 mm. The ZSPC with these extreme dimensions is Z3-16, which has the slenderness ratio of 0.13, as given by Table 6-1. This means for common PICP with common dimensions of ZSPC buckling will not govern the shear failure of the connector.

The numerical and analytical results for the ZSPC studied in Section 5.5 are graphed in Figure 6-2 and are compared together in Table 6-1. Figure 6-2 shows that analytical plastic shear strength, V_p, and analytical yield shear strength, V_{VM}, give almost accurate estimates of the numerical shear strength of the studied ZSPC, V_{FE}. Table 6-1 gives V_{FE}/V_p and V_{FE}/V_{VM} for the studied connectors and shows that the average V_{FE}/V_p and V_{FE}/V_{VM} is 1.04 and 1.11, respectively, which means yield shear strength using the von Mises criterion (equation 6-3) and plastic shear strength using the Tresca criterion (equation 6-5) underestimate the numerical shear strength of the studied connectors by 4% and 11%, respectively. The estimation error for V_{VM} and V_p measured by coefficient of variation given in Table 6-1 is 0.95% and 1.72%, respectively. Since the analytical plastic shear strength, V_p, given by equation 6-5 gives better estimate of numerical shear strength of the studied ZSPC with smaller error, it is the preferred method in this thesis to predict the shear strength of ZSPC.

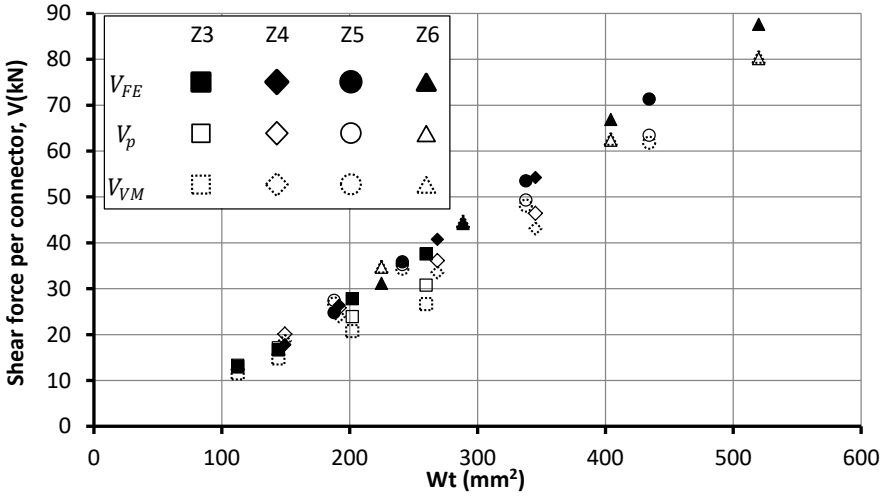

Figure 6-2: Numerical and analytical results for shear strength of ZSPC.

Table 6-1: Comparison between numerical and analytical results.

ZSPC designation	λ	V_p (kN)	V_{FE}/V_p	V_{VM} (kN)	V_{FE}/V_{VM}
Z3-16	0.13	13.31	0.97	11.53	1.12
Z3-14	0.10	17.09	0.97	14.80	1.12
Z3-12	0.07	23.92	1.16	20.72	1.34
Z3-10	0.06	30.76	1.22	26.64	1.41
Z4-16	0.13	20.09	0.88	18.65	0.95
Z4-14	0.10	25.80	1.02	23.94	1.10
Z4-12	0.07	36.11	1.13	33.52	1.22
Z4-10	0.06	46.43	1.17	43.10	1.26
Z5-16	0.13	27.45	0.90	26.75	0.93
Z5-14	0.10	35.24	1.02	34.34	1.04
Z5-12	0.07	49.33	1.08	48.07	1.11
Z5-10	0.06	63.43	1.12	61.81	1.15
Z6-16	0.12	34.68	0.90	34.85	0.89
Z6-14	0.09	44.52	0.99	44.75	0.99
Z6-12	0.07	62.33	1.07	62.64	1.07
Z6-10	0.05	80.14	1.09	80.54	1.09
Average			**1.04**		**1.11**
Coefficient of variation			**0.95%**		**1.72%**

6.4.2. Secant Shear Stiffness of ZSPC

Simplified plate model

The secant shear stiffness of ZSPC using the simplified plate model, K_{pl}, is related to the stiffness accounting for concrete-connector interaction, $K_{c,pl}$, by equation 6-6. To estimate $K_{c,pl}$, the numerical secant shear stiffness, K_{FE}, of the studied connectors given by Table 5-3 are substituted for K_{pl} in equation 6-6 and this equation is solved for $K_{c,pl}$. Figure 6-3.a. shows $K_{c,pl}$ against the aspect ratio, $\alpha = W/L$, for the studied connectors. As given by this figure, $K_{c,pl}$ can be estimated by equation 6-11 with 95.83% coefficient of determination, i.e. the square of correlation coefficient.

$$K_{c,pl} = 20.94\ \alpha^{1.91}, \quad (K_{c,pl} \text{ is in kN/mm}) \qquad \textbf{6-11}$$

In this equation α is the aspect ratio equal to W/L.

Tension-tie model

The secant shear stiffness of ZSPC using the tension-tie model, K_{tie}, is related to the stiffness accounting for concrete-connector interaction, $K_{c,tie}$, by equation 6-12. To estimate $K_{c,tie}$, the numerical secant shear stiffness, K_{FE}, of the studied connectors given by Table 5-3 are substituted for K_{tie} in equation 6-7 and this equation is solved for $K_{c,tie}$. Figure 6-3.b. shows $K_{c,tie}$ against D/L for the studied connectors. As given by this figure, $K_{c,tie}$ can be estimated by equation 6-12 with 95.72% coefficient of determination, i.e. the square of the correlation coefficient.

$$K_{c,tie} = 7.67\,(D/L)^{3.12}, \quad (K_{c,tie} \text{ is in kN/mm}) \qquad \textbf{6-12}$$

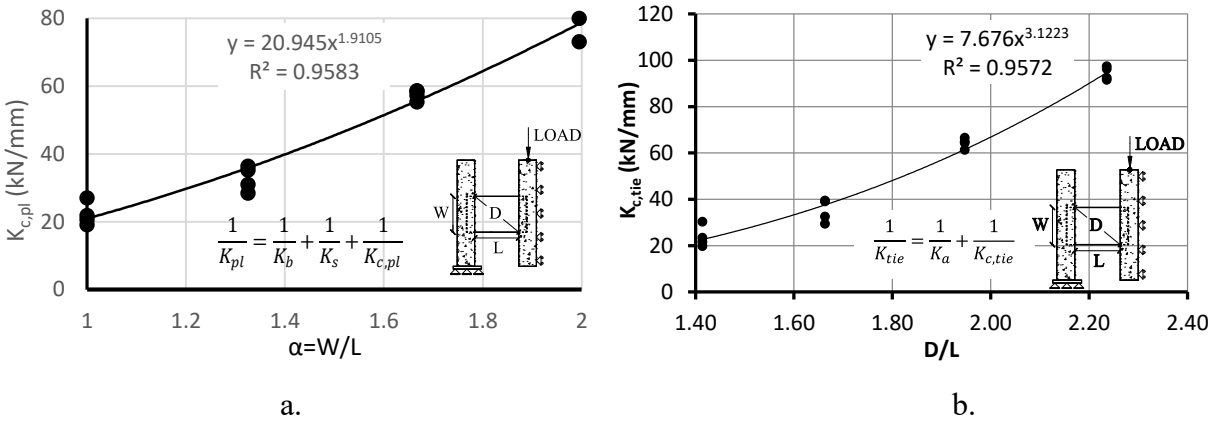

a. b.

Figure 6-3: Estimation of K_c in: a. simplified plate model and b. tension tie model.

6.5. Summary and Conclusion

A simplified plate model and a tension-tie model were presented to estimate the shear strength and stiffness of ZSPC. The simplified plate model assumes the unembedded part of the ZSPC as a rectangular plate. Based on the buckling shape observed after the push-off tests of gauge 16 ZSPC, a tension tie model was developed to estimate the shear stiffness of Z-shaped connectors. The analytical expressions for shear stiffness of ZSPC presented in this chapter were modified using the numerical results to account for the effect of connector-concrete interaction on the shear stiffness of ZPSC.

The von Mises yield shear strength and Tresca plastic shear strength of the simplified plate model proved to have good agreement with the numerical shear strengths of ZSPC. The Tresca plastic shear strength of the simplified plate model agrees with the numerical shear strength of ZSPC with 0.95% coefficient of variation, which is more accurate than the von Mises yield shear strength. Therefore, the plastic shear strength of the simplified plate model using Tresca yield criterion is recommended to estimate the shear strength of ZSPC. It was also found that elastic buckling does not govern the shear behaviour of ZSPC. Hence, the buckling shape observed after the push-off tests of gauge 16 connectors is considered as plastic buckling. It was also shown that the analytical expressions for the shear stiffness of ZSPC based on the simplified plate and tension-tie models have the same accuracy in estimating the shear stiffness of ZSPC. There is no preference for any of these two models in terms of accuracy to estimate the shear stiffness of ZSPC. However, the author prefers the simplified plate model, since it has fewer steps to calculate the shear stiffness of ZSPC.

Part 3: Out-of-Plane Flexural Behaviour of PICP with ZSPC

After identifying the shear behaviour of Z-shaped Steel Plate Connectors (ZSPC), its effect on the out-of-plane flexural behaviour of Precast Insulated Concrete Panels (PICP) should be examined. For this, 4-point flexural tests are conducted on PICP with ZSPC with and without end-beams. Although the loading condition in these tests are different than out-of-plane uniform wind loads that occur in practice, the results of 4-point loading tests are insightful since they directly give the experimental moment-curvature diagram of PICP, which will be compared against the theoretical moment-curvature diagrams of fully- and non-composite panels. The results of 4-point flexural tests will also be adopted to verify the proposed analytical model to estimate the out-of-plane behaviour of PICP. Afterwards, the proposed analytical model is compared against the experimental results of PICP tested by previous researchers under out-of-plane uniform loads, which is the actual loading condition of PICP under wind loads.

This part of the thesis presents the conducted experimental and analytical studies on the effect of ZSPC and end-beams on the out-of-plane flexural behaviour of PICP. Chapter 7 presents the results of out-of-plane 4-point flexural tests on four PICP with ZSPC without end-beams and two PICP with ZSPC and end-beams. The ZSPC in these six panels varied in width and thickness. The experimental out-of-plane flexural behaviour of these panels, their cracking patterns, deformation mechanism of the panels and the connectors during the tests are discussed in this chapter.

In Chapter 8 an analytical model is proposed for nonlinear numerical analysis of the tested panels. This analytical model is verified by the experimental results. This analytical model is adopted in Chapter 9 to propose general recommendations for structural design of PICP with ZSPC with and without end-beams. These recommendations can be extended to PICP with other types of interlayer mechanical connectors. Specific recommendations are provided in Chapter 9 for structural design of simply supported PICP with ZSPC with and without end-beams under out-of-plane uniform loading.

7. Experimental Investigation of PICP under Out-of-Plane Bending

7.1. Introduction

This Chapter presents the results of six out-of-plane 4-point flexural tests on PICP with ZSPC with and without end-beams. Although the loading condition in these tests are different than out-of-plane uniform wind loads that occur in practice, the results of these 4-point flexural tests are helpful since they directly give the experimental moment-curvature diagram of PICP, which will be compared against the theoretical moment-curvature diagrams of fully- and non-composite panels. The results of the 4-point flexural tests will also be adopted to verify the proposed analytical model in Chapter 8 to estimate the out-of-plane behaviour of PICP. In Chapter 9, the proposed analytical model is compared against the experimental results of PICP tested by previous researchers under out-of-plane uniform loads, which is the actual loading condition of PICP under wind loads.

Section 7.2 of Chapter 7 gives the details of the experimental program for the tested panels. The results of these flexural tests including the out-of-plane behaviour of the tested panels and deformation mechanism of the panels and ZSPC during the tests are discussed in Section 7.3. Section 7.4 summarizes the main findings of the flexural tests.

7.2. Setup of Out-of-Plane 4-Point Bending Tests on PICP

Out-of-plane 4-point flexural tests were conducted on six 1,118 mm x 3,556 mm (width x length) Insulated Concrete Panels to evaluate the effect of ZSPC and end-beams on the out-of-plane flexural behaviour of PICP. The matrix of these tests is given in Table 7-1. As given in this table, four of these tests were to examine the effect of width and thickness of ZSPC on the out-of-plane flexural behaviour of PICP. These four test specimens are called P-series and denoted by Pα-β, where α is the width of ZSPC in inch and β is the gauge number of the steel sheet used in the connector. The ZSPC used in these flexural tests were the same size as the ones used in the push-off shear tests to examine the effect of the shear behaviour of these ZSPC on the out-of-plane behaviour of PICP. Two of the flexural tests were enclosed by end-beams to study the effect of end-beams on the out-of-plane flexural behaviour of PICP. These two specimens are called PB-series and denoted by PBα-β, where α and β are defined similar to P-series test specimens. The

width of the connectors in these six panels varies from 76.2 mm to 152 mm and the thickness is 1.47 mm and 3.21 mm.

Table 7-1: Details of flexural tests

Panel designation	Shape of shear connectors	Width (W) mm	Thickness (t) Gauge # (mm)	End conditions
P3-16	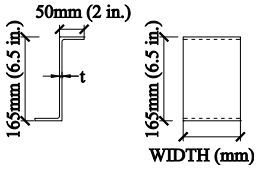	76.2	16 (1.47)	Without end-beams
P4-16		102	16 (1.47)	
P6-16		152	16 (1.47)	
P4-10		102	10 (3.21)	
PB3-16		76.2	16 (1.47)	With end-beams
PB6-16		152	16 (1.47)	

The typical thickness of concrete layers in PICP varies from 51 mm to 102 mm. In this study, the thickness of the concrete layers was taken as 76.2 mm. The typical thickness of insulation varies from 25.4 mm to 101 mm (PCI, 2011). Soriano and Rizkalla (2013) showed that smaller thickness of insulation increases shear strength and stiffness of the interlayer mechanical connectors. In this study, the insulation thickness was taken as 76.2 mm. The insulation in this study consisted of 51 mm extruded Polystyrene and 25 mm grooved board; this grooved board is to drain out the rainwater from the panel.

If there are too few interlayer mechanical connectors or too many longitudinal bars in the concrete layers of PICP, the interlayer mechanical connectors yield first, after which the panel would exhibit non-composite behaviour. Then the concrete layers deform following a non-composite behaviour until the individual concrete layers fail under flexure. On the other hand, if there are too few longitudinal bars in the concrete layers and too many interlayer mechanical connectors, the PICP will have partially- to fully-composite behaviour and the panel fails by yielding of the longitudinal bars in the tensile concrete layer prior to yielding of interlayer mechanical connectors. It is structurally efficient to have PICP with composite behaviour such that the failure of PICP occurs before failure of the panel. However, in short panels, where the panel length cannot accommodate sufficient number of connectors, the failure of the panel is governed by the failure of the connectors. This is not a problem since in short panels out-of-plane bending moments are small and can be resisted by non-composite PICP with minimum thickness of concrete layers and reinforcement required by design codes.

In this research, to study the effect of the shear behaviour of ZSPC on the out-of-plane behaviour of PICP, the panels were designed such that yielding of the connectors governs the failure of the

panels. Thus in the design of the panels, the theoretical maximum interlayer shear forces, which is equal to the sum of yield tensile strengths of the tensile reinforcement, were larger than the sum of plastic shear strengths of ZSPC located from mid-span to one end of the panel. There are six connectors from mid-span to one end of the panel. Therefore, the design of the panel is such that:

$$6V_r < A_s f_y \quad \text{7-1}$$

Where V_r is the strength of connectors, A_s is the area of the longitudinal steel and f_y is the yield strength of steel bars in these tests.

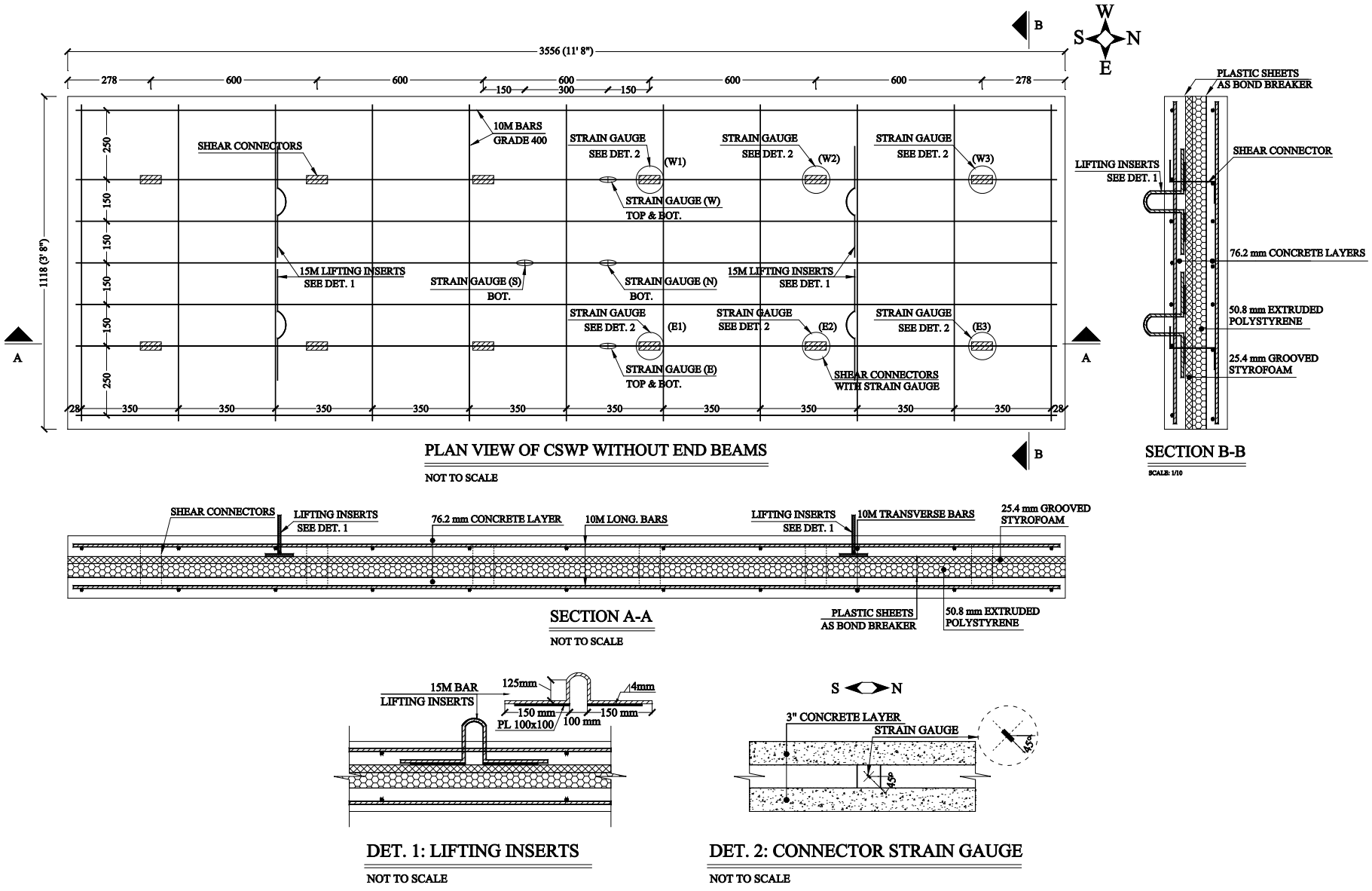

Figure 7-1: Design and instrumentation of panels without end-beams.

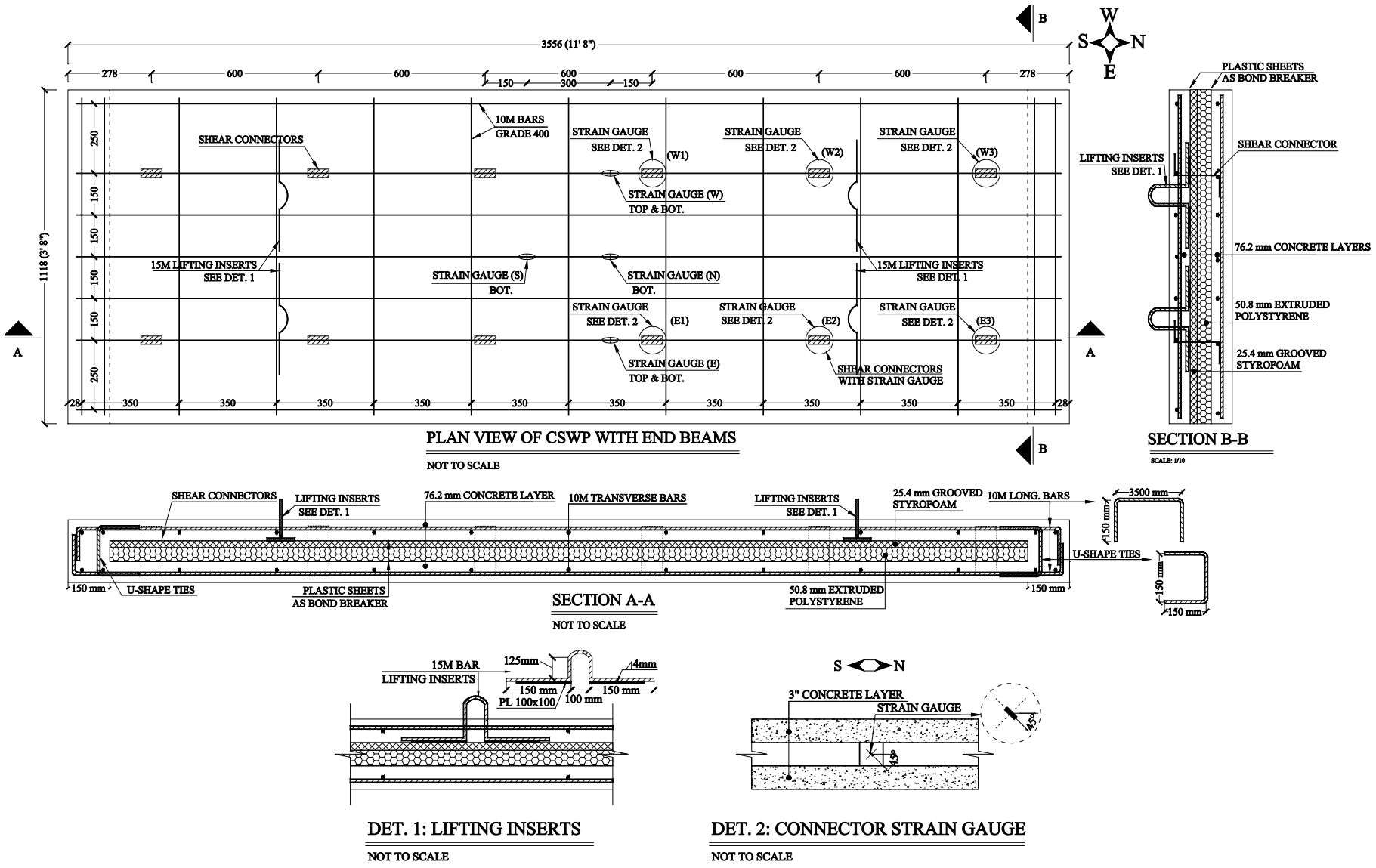

Figure 7-2: Design and instrumentation of panels with end-beams.

Figure 7-1 and Figure 7-2 show the construction details of the P- and PB-series panels, and Figure 7-3 shows one of the test panels during construction. As shown in Figure 7-1 and 7-2, the longitudinal reinforcement of the panels included seven grade 420, 10M bars and the transverse reinforcement was grade 420, 10M bars spaced at 600 mm. The panels of the PB-series were enclosed at the ends by 150 mm wide beams. These beams were reinforced by one 10M bar at each corner and U-shape 10M bars along the length of the beam.

Two rows of ZSPC were installed across the panels; each row had six ZSPC spaced at 600 mm. Since the bending moment is constant between the point loads, the interlayer shear transfer between the point loads is zero according to Bernoulli beam theorem, i.e. the shear force in the connectors between the point loads are zero. Bernoulli beam theorem, however, assumes rigid interlayer shear behavior, i.e. infinite interlayer shear stiffness. Therefore, Bernoulli beam theorem does not accurately apply to PICP since the interlayer mechanical connectors are not rigid, thus the interlayer shear stiffness of PICP is not infinite. But the ZSPC between the two point loads are expected to absorb less shear force than the other ZSPC in the tested panels. These intermediate connectors were installed to transfer the out-of-plane loads from the top concrete layer to the bottom concrete layer.

To maximize the pry-out resistance of the connector-concrete connection, the connectors' flanges were hooked to the longitudinal bars as shown in Figure 7-3. Plastic sheets were laid between the insulation and the concrete to eliminate the undesirable transfer of interlayer shear forces through concrete-insulation bonding. Moreover, to ensure the shear forces were not transferred through the legs of the lifting inserts, the lifting inserts were only embedded in the top concrete layer, i.e. they did not penetrate through the insulation.

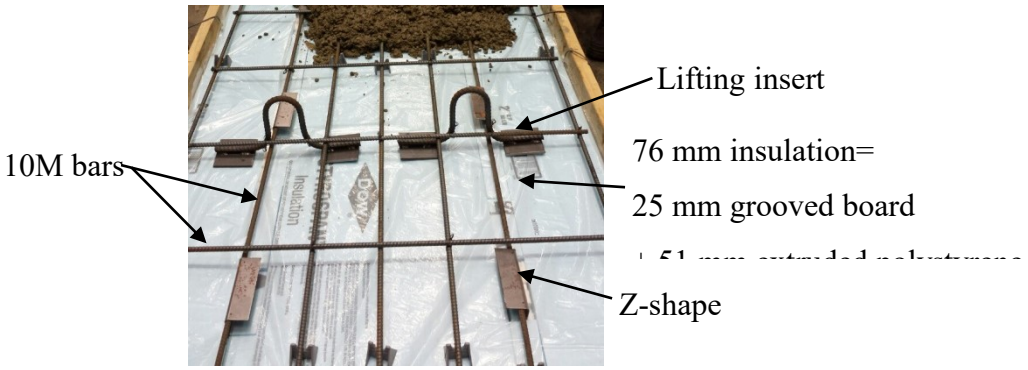

Figure 7-3: Construction of PICP specimens.

As shown in Figure 7-1 and Figure 7-2 in each panel, four strain gauges were installed on the longitudinal reinforcement of the bottom concrete layer, and two were installed on the longitudinal reinforcement of the top concrete layer. These figures also show that six strain gauges were installed on the web of the connectors at 45 degrees angle from the width of ZSPC along the expected compressive stresses induced by interlayer shear forces. These strain gauges were only meant to show the instance of buckling of the compression diagonal of the connectors. It is expected that sudden drops or jumps in the recorded strains would be associated with buckling.

For each concrete layer of the panels, the compressive behaviour of concrete at 28 days of age and on testing day was measured as per ASTM C39/C39M-14. The 28-day compressive strength, modulus of elasticity and Poisson's ratio of the top concrete layer, were 35.55 MPa, 25.61 GPa and 0.18, respectively. And the 28-day compressive strength, modulus of elasticity and Poisson's ratio of the bottom concrete layer, were 26.24 MPa, 21.6 GPa and 0.15, respectively. The 28-day tensile strength of concrete for each concrete layer was measured by split tests as per ASTM 496/496M-11. The 28-day tensile strengths of the top and bottom concrete layers were 2.78 MPa and 3.53 MPa, respectively. The properties of the bottom and top concrete layers on testing day are given in Table 7-2.

The tensile behaviour of the bars was determined by tension testing of three coupons in accordance with ASTM A370-15. The tensile stress-strain relationships for the tested coupons are shown in Figure 7-4. The yield and ultimate strengths, and modulus of elasticity of the bars were 423 MPa, 588 MPa and 194.3 GPa, respectively.

The panels were placed horizontally on two support beams as shown in Figure 7-5. Each support beam was sitting on one rocker and roller support at each end. The clear span of the panels was 3,175 mm. As shown in Figure 7-5, the loading was applied to the panel using a 520 kN hydraulic jack and two distribution beams 1,219 mm apart. A transfer beam was used to transfer the jack's force to the distribution beams. The connection between the transfer beam and the distribution beams was knife-edge and roller supports to allow rotation and horizontal movement of the two loading points. A photograph of the test setup is shown in Figure 7-6.

Table 7-2: Concrete properties of the flexural test specimens on testing day

Panel designation	Bottom concrete layer			Top concrete layer		
	f_c (MPa)	E_c (GPa)	ν	f_c (MPa)	E_c (GPa)	ν
P3-16	27.93	21.74	0.156	37.19	24.72	0.158
P4-16	29.30	21.26	0.163	40.28	26.23	0.153
P6-16	28.52	21.57	0.150	36.65	26.00	0.167
P4-10	27.11	22.82	0.177	40.21	25.77	0.165
PB3-16	27.26	24.18	0.154	36.45	22.08	0.150
PB6-16	30.89	24.71	0.164	40.28	26.85	0.152

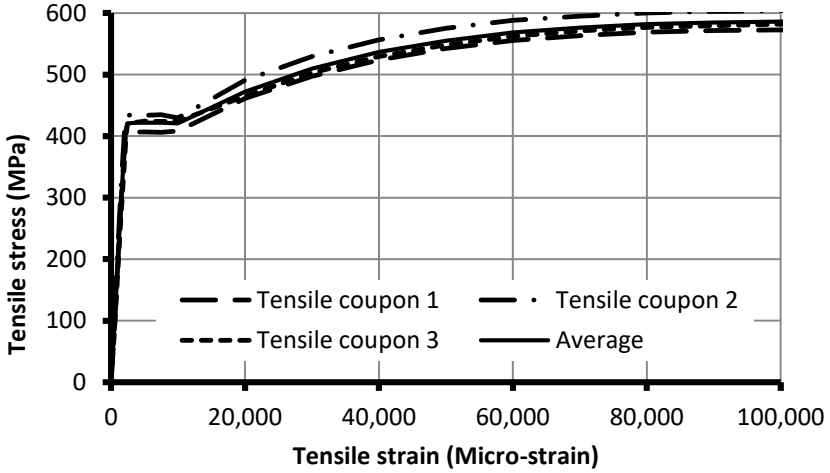

Figure 7-4: Tensile stress – strain relationship for steel bars.

As shown in Figure 7-6, four clinometers were installed at 203 mm away from the mid-span of the panels. The readings of these clinometers were used to derive the experimental curvature of the panels throughout loading. Two Linear Variable Displacement Transducers (LVDT) were installed at each end of the panels to record the relative slippage between the concrete layers due to shear deformation of the Z-shaped connectors. As shown in Figure 7-6, the mid-span deflection of the panels and the horizontal displacements of the roller supports and rollers of the loading points were recorded using cable extension transducers. The recorded horizontal displacements of the rollers were used to calculate the true mid-span bending moment of the panels.

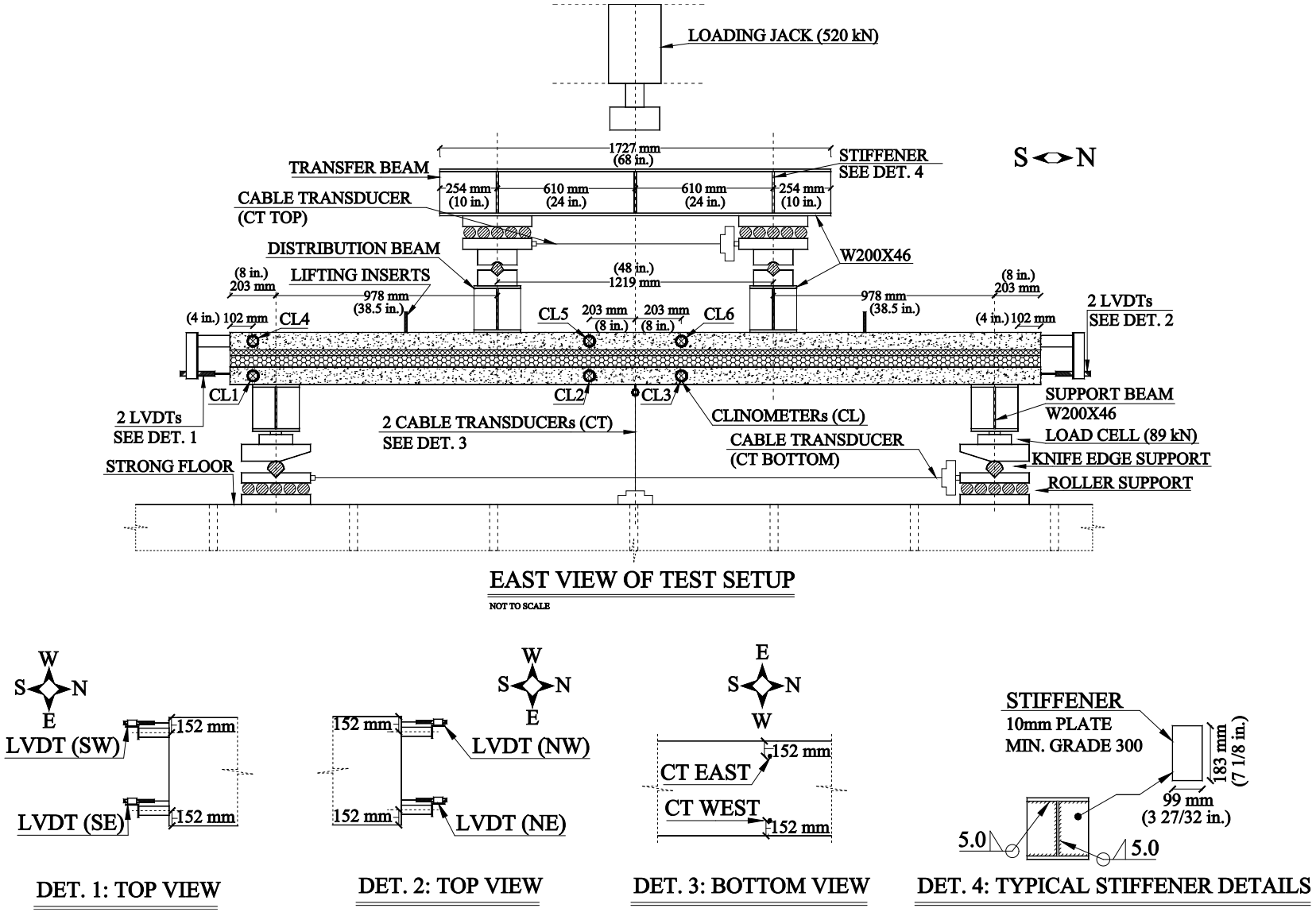

Figure 7-5: Design of test setup and instrumentation of the flexural tests.

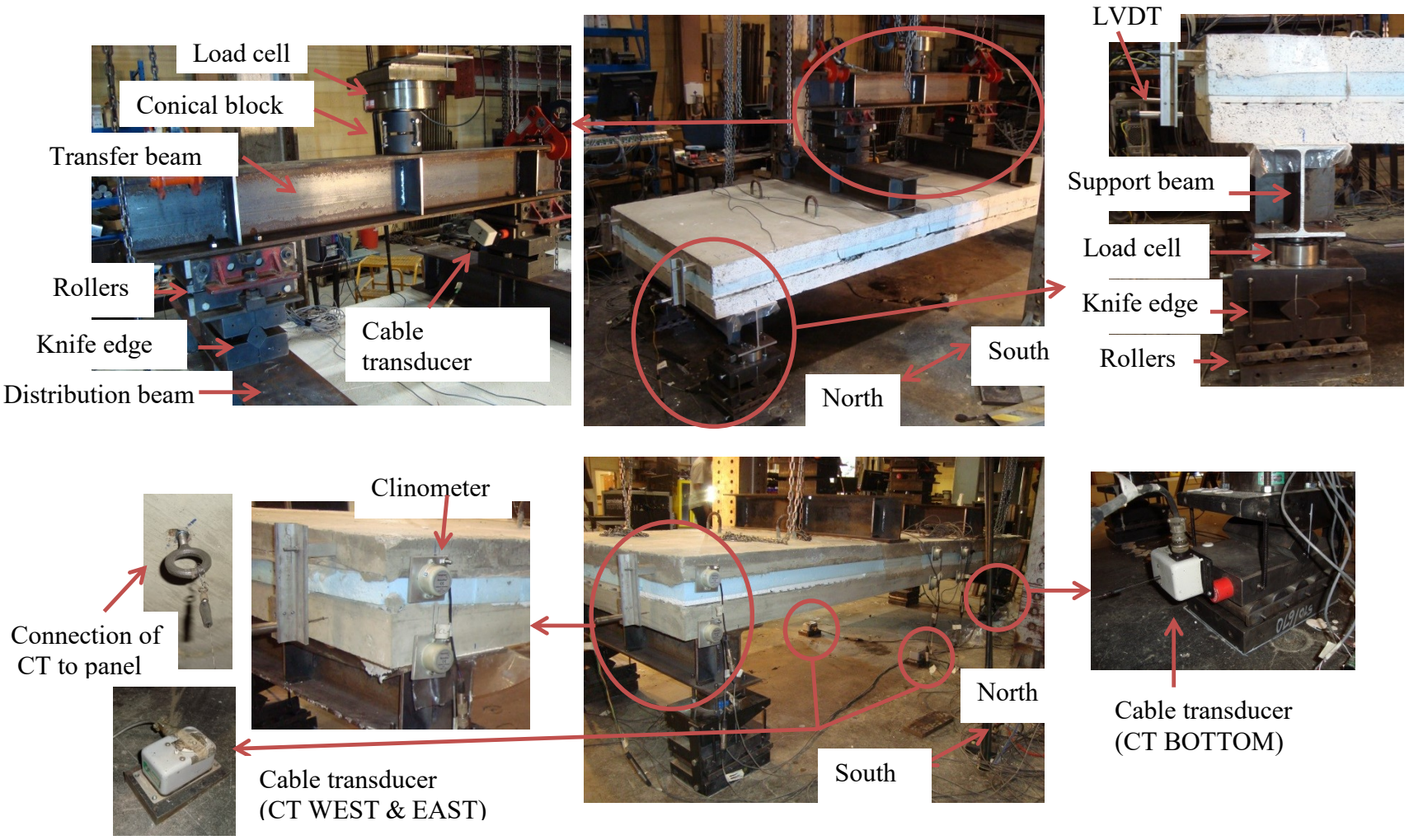

Figure 7-6: Test setup and instrumentation of flexural tests.

7.3. Flexural Test Results and Discussion

7.3.1. Cracking Pattern of the Panels

During the flexural tests of the P-series panels the first flexural cracks appeared in the mid-span of the bottom concrete layer. With increased loading, flexural cracks occurred at the underside of the mid-span of the top concrete layer. In the PB-series panels, as demonstrated in Figure 7-7, flexural cracks first appeared at the ends of the bottom concrete layer (cracks labelled as 1 in Figure 7-7), then at the mid-span of the bottom concrete layer (cracks labelled as 2 in Figure 7-7). With increased loading, similar flexural cracks occurred at the ends and mid-span of the top concrete layer (cracks labelled as 3 and 4 in Figure 7-7, respectively). For all panels, as the loading was increased, the flexural cracks spread throughout the panels and opened wider while the panel was deflecting. Loading was continued until it had to be stopped due to safety issues caused by excessive displacement of the support rollers. During testing no crushing of the concrete layers and no shear cracking were observed.

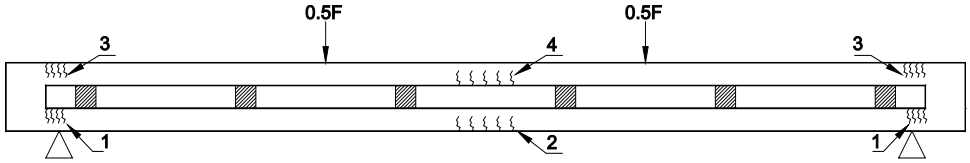

Figure 7-7: Cracking pattern of tested PICP with end-beams.

7.3.2. Out-of-Plane Behaviour of the Panels

During the flexural tests the reaction points moved farther from the mid-span and the loading points moved closer to the mid-span, which increased the shear span, and thus changed the mid-span bending moment derived from static equilibrium. The increase in the shear span was calculated using the measured horizontal displacements of the reaction and loading points during the tests. The length of the increased shear span was then used to calculate the true mid-span bending moment. Figure 7-8 and Figure 7-9 shows the total vertical load P and the true mid-span bending moment, respectively, against the mid-span deflection Δ_v of the tested panels. In these graphs the initial loads including the weight of the panel, transfer beam, distributor beams, knife edge and rollers are added to the readings of the loading jack.

Figure 7-8 and Figure 7-9 show that P3-16 and P4-16, made of ZSPC with shear strength of around 14 kN, have the same load and bending moment resistance throughout loading. But, at every

vertical deflection, P6-16 and P4-10 made of ZSPC with 22 kN and 36.6 kN shear strengths, respectively, carry larger load and bending moments than P3-16 and P4-16. Similarly, PB6-16 made of ZSPC with 22 kN shear strength have larger resistance than PB3-16 made of ZSPC with 14.22 kN shear strength. Also the resistance of PB-series panels are larger than that of P-series panels due to additional interlayer shear strength of PB-series panels provided by the end-beams. These results suggest that larger interlayer shear strength improves the out-of-plane load resistance of PICP.

As shown in Figure 7-8, the total load of P3-16 and P4-16 increases to around 39 kN at Δ_v of about 12 mm. After this Δ_v , the load-deflection behaviour makes a plateau that continues up to Δ_v of about 27 mm. After this deflection, the load starts increasing again at a small rate. The same plateau is observed for P6-16, for which the plateau extends from Δ_v of about 20 mm to 45 mm. Figure 7-8 shows that for P4-10, PB3-16 and PB6-16, the load increases continually without forming any plateau. In these panels, the load increases almost linearly up to Δ_v of 5.0 mm, after which the load-deflection behaviour becomes nonlinear until it reaches the maximum strength. For all panels the loading was stopped due to safety concerns caused by the excessive displacement of the supporting rollers.

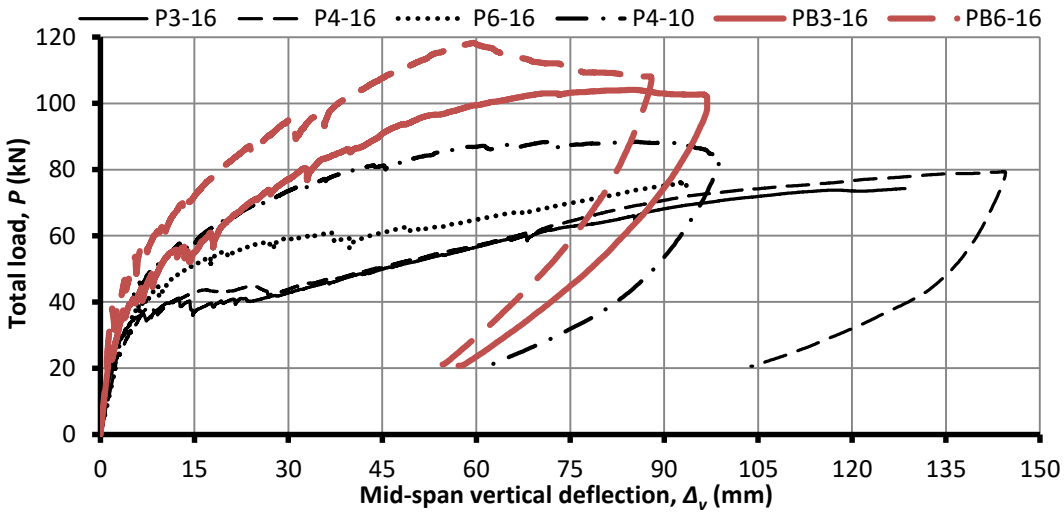

Figure 7-8: Total vertical load against mid-span vertical deflection of the tested flexural panels

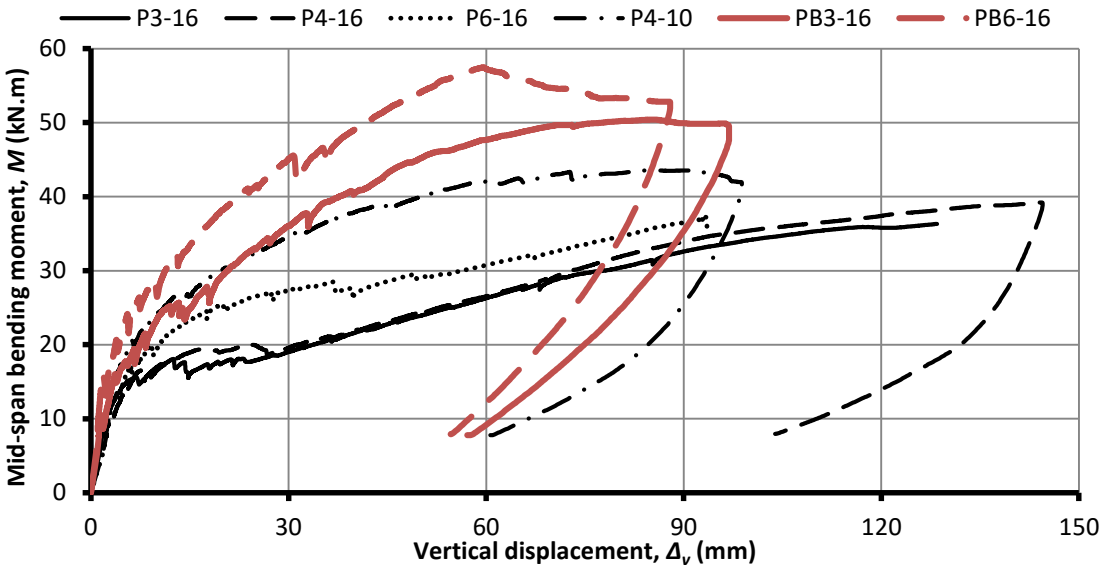

Figure 7-9: True mid-span bending moment against mid-span vertical deflection of the tested flexural panels

7.3.1. Moment-Curvature Diagrams of the Tested Panels

Figure 7-10 shows the mid-span bending moment, M, versus the mid-span curvature, φ, for the top and bottom layers of the panels. The mid-span curvature is derived from the difference in angles of rotation at two points of the mid-span divided by their distance. The angles of rotation at two points of the mid-span were recorded by clinometer CL2 and CL3 for the bottom layer, and by CL5 and CL6 for the top layer. Figure 7-10 compares the M-φ curves of the panels with that of the theoretical fully-composite and non-composite panels. The theoretical fully-composite and non-composite M-φ graphs are derived by flexural analysis of the cross section of the panels assuming fully-composite cross section and non-composite cross section, respectively. In these flexural analyses the concrete was assumed to have a parabolic compressive behaviour, as proposed by Hognestad (1951), and the bars were modeled using the average tensile stress-strain relationship shown in Figure 7-4. Tension stiffening of concrete was considered in deriving the M-φ graphs using the procedure outlined by Collins and Mitchell (1997). As shown in this figure, the M-φ relationships for the bottom concrete layer have some fluctuations between 10 kN.m to 25 kN.m. This behaviour might be related to cracking of the bottom concrete layers. These layers are under combined effect of tensile forces and bending moment, which increases the width and number of cracks in the bottom concrete layers. As the cracks spread and got wider, it might have wiggled

the clinometers, leading to fluctuations in the moment-curvature graphs of the bottom concrete layers.

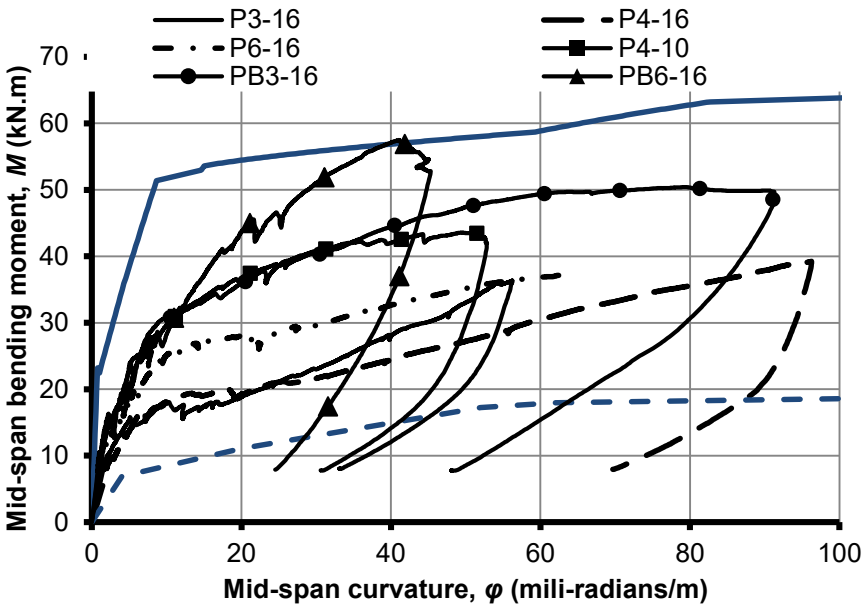

a.

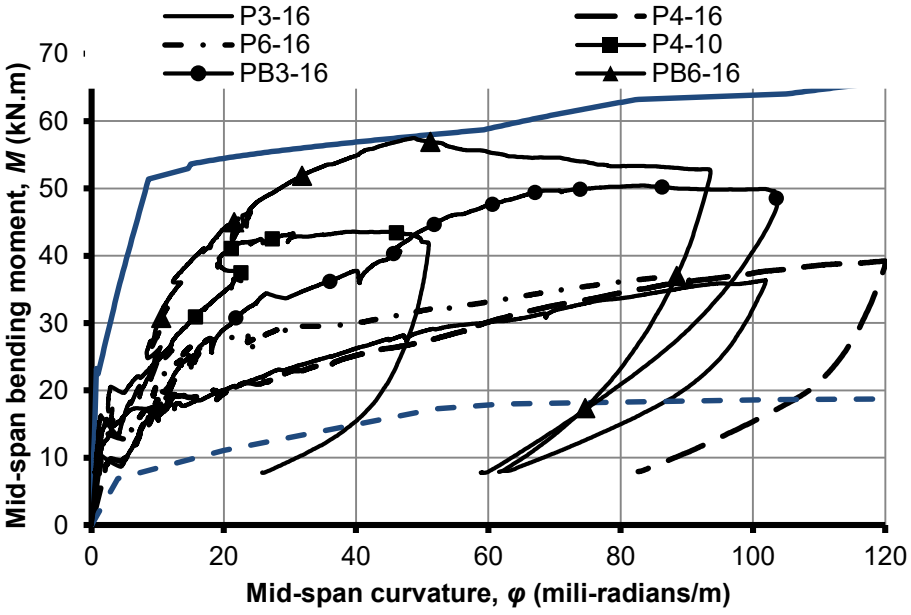

b.

Figure 7-10: Moment-curvature behaviour of a. top concrete layer, b. bottom concrete layer, of the tested PICP

Figure 7-10 shows that all panels have an initial stiffness larger that the theoretical non-composite panel. As the load increases, the M-φ relationships become nonlinear and continue to resist load with reduced tangent stiffness. The out-of-plane stiffness of P4-10, PB3-16 and PB6-16 consistently decreases with increased loading. But the out-of-plane stiffness of P3-16, P4-16 and P6-16 panels decreases to a small value at about 15 mili-radians/m forming a plateau, also observed in the out-of-plane load-deflection behaviour (Figure 7-8). After this plateau, the out-of-plane stiffness of these three panels picked up again at about 20 mili-radians/m, but remained smaller than the initial stiffness. These three panels continued to resist load without any further changes in stiffness up to a point where the test had to be stopped due to excessive horizontal displacements of the rollers under the support beams. The descending portion of the M-φ graphs in Figure 7-10 relates to the unloading of the panels. The M-φ graphs of P4-10, PB3-16 and PB6-16 do not exhibit such plateau regions; instead they nonlinearly progressed up to the maximum bending moment resistance after which the panels were unloaded due to excessive displacement of the support rollers. The plateau regions for panels P3-16, P4-16 and P6-16 can be attributed to the shear failure of ZSPC; i.e. when the connector had reached its shear strength. This shear strength was shown to exceed the theoretical plastic shear strength of ZSPC (Chapter 6). After shear failure of the ZSPC, the tension field mechanism observed in the shear tests provided residual shear strength for the connectors as discussed in Section 4.3, which may be the reason for the second ascending portion of the M-φ graphs. This argument will be revisited in Section 7.3.3 and will be examined by numerical studies in Chapter 8.

Figure 7-10 shows that the mid-span out-of-plane bending moment carried by the panels at every curvature varies substantially depending on the ZSPC type and the presence of end-beams. Since the ultimate moment resistance for P3-16, P4-16 and P6-16 could not be reached due to excessive displacement of the support rollers, the ultimate moment resistance of these panels could not be compared. Instead, the mid-span out-of-plane bending moment of the tested panels at the curvature that corresponds to the design maximum deflection limit is compared with each other. According to CAN/CSA A23.3-04, the out-of-plane horizontal deflection limit of the mid-height of PICP is 1/100 of the panel height, which corresponds to a curvature of 20 mili-radians/m for the tested panels.

The out-of-plane mid-span bending moment of the panels at 20 mili-radians/m of curvature, $M_{\varphi 20}$, for all tested panels is summarized in Table 7-3. This table also compares $M_{\varphi 20}$ of the tested panels

to the theoretical bending moment of a fully-composite and non-composite panel at 20 mili-radians/m curvature, $M_{c,20}$ and $M_{nc,20}$, respectively. As shown in this table, $M_{\varphi 20}/M_{c,20}$ for the P-series panels grows from 0.35 to 0.80 with increased width and thickness of ZSPC. This table also shows that $M_{\varphi 20}/M_{c,20}$ for PB3-16 and P3-16 with the same size of ZSPC are 0.66 and 0.35, respectively. This means that adding end-beams to P3-16 improved its out-of-plane bending moment at 20 mili-radians/m curvature by 88%. Similar comparison between P6-16 and PB6-16 shows that adding end-beams to P6-16 improved its $M_{\varphi 20}/M_{c,20}$ by 57%. This signifies the effect of end-beams in increasing the out-of-plane bending moment of PICP corresponding to the design maximum deflection limit. Table 7-3 also shows that $M_{\varphi 20}$ for PB6-16 is 21% larger than $M_{\varphi 20}$ of PB3-16, and $M_{\varphi 20}$ for P6-16 is 45% larger than $M_{\varphi 20}$ of P3-16; this shows that using ZSPC with increased V_r still improves $M_{\varphi 20}$ of PICP but to a lesser extent than when end-beams are added to the panel.

Table 7-3: Results of out-of-plane 4-point flexural tests on PICP

Panel Designation	$M_{\varphi 20}$ (kN.m)	$M_{\varphi 20}/M_{c,20}$	$M_{\varphi 20}/M_{nc,20}$	K_p (kN.m^2/radians)	K_p/K_{nc}
P3-16	19.3	0.35	1.74	5 220	3.03
P4-16	19.3	0.35	1.74	3 880	2.25
P6-16	28.1	0.51	2.53	6 180	3.58
P4-10	36.4	0.67	3.28	6 470	3.75
PB3-16	36.2	0.66	3.26	6 430	3.73
PB6-16	43.9	0.80	3.95	4 330	2.51

To study the effect of ZSPC and end-beams on the out-of-plane flexural stiffness of the panels, the secant stiffness of the panels between 0.1 $M_{\varphi 20}$ and 0.4 $M_{\varphi 20}$ for the tested PICP was calculated and was compared against the secant stiffness of the theoretical fully-composite and non-composite panels, K_c and K_{nc}, respectively. This chosen range ensured that the gaps between the panels and the supports were closed and that the out-of-plane flexural behaviour of the panels was still in the elastic range. Table 7-3 summarizes the secant stiffness, K_p, of the tested panels and compares them against the theoretical stiffness of a fully-composite and non-composite panel. This table also gives K_p/K_{nc} for each panel, where K_{nc} is the flexural stiffness of the theoretical non-composite panel. As shown in this table, K_p/K_{nc} for the tested panels varies between 2.25 to 3.75. This means a PICP with ZSPC can be at least 2.25 times stiffer than the theoretical non-composite panel.

As shown in Table 3, for P3-16, P6-16 and P4-10, an increase in the width and thickness of the shear connectors improved the out-of-plane secant stiffness of the panels. However, the stiffness of P4-16 with 102 mm wide ZSPC is smaller than the stiffness of P3-16 with 76.2 mm wide ZSPC. Therefore, these results are inconclusive on the effect of width of ZSPC on the out-of-plane stiffness of PICP. Also, comparing PB3-16 and P3-16 shows that the presence of end-beams improves the out-of-plane stiffness of the panel. However, PB6-16 with end-beams has a smaller out-of-plane stiffness than P6-16 without end-beams. Therefore, again these results are inconclusive on the effect of presence of end-beams on the out-of-plane stiffness of PICP with ZSPC. Hence, more investigation is needed to understand the relationship between the width of ZSPC and presence of end-beams on the out-of-plane stiffness of PICP, which will be discussed in Section 9.3.

7.3.2. Longitudinal Strains of Reinforcement

Figure 7-11 shows the longitudinal strains of reinforcement against the mid-span vertical deflection for top and bottom concrete layers. As shown in this figure for all P-series panels the strains barely reached the yielding tensile strain (2200 micro-strains) of the bars, which suggests that the bars did not yield. This agrees with the intended design of the panels where the panel failure was desired to initiate by yielding of ZSPC. The longitudinal strains of reinforcement of bottom layer of PB-series panels have exceeded the yield strain of the bars, indicating yielding of reinforcement of the bottom concrete layers of these two panels. This is because the end-beams in PB-series panels significantly contribute to the interlayer shear strength of the panels and it exceeds the tensile yield strength of the longitudinal reinforcement. The reinforcement of the top concrete layer of PB-series panels did not yield since the compressive forces of the top layer delays yielding of its reinforcement.

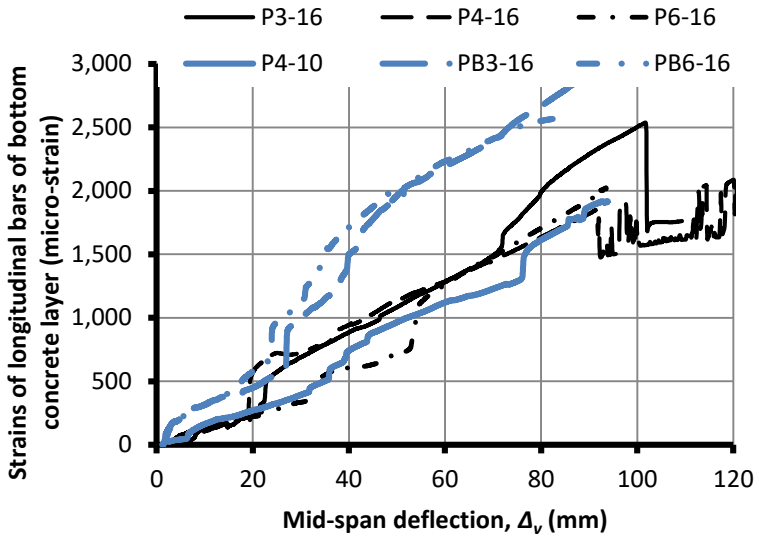

a.

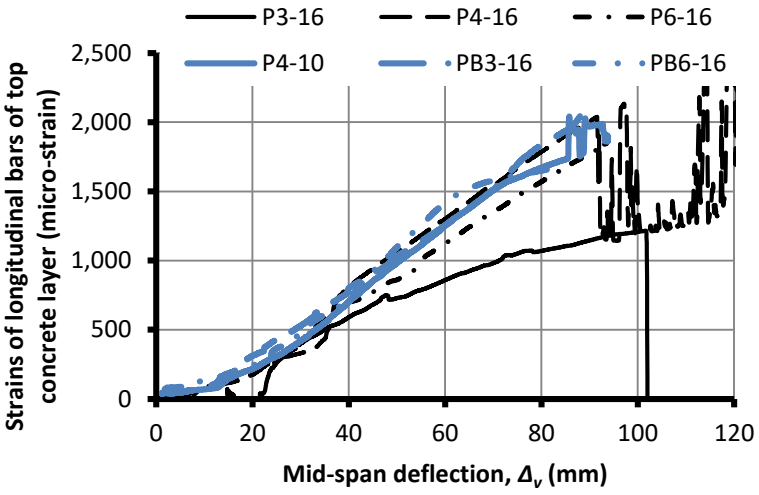

b.

Figure 7-11: Tensile strains of bars in a. top, and b. bottom concrete layers of the tested panels.

Figure 7-11 shows that longitudinal strains of the reinforcement in P-series panels have similar trends regardless of the varied width and thickness of ZSPC used in these panels. Also, the longitudinal strains of reinforcement in PB-series panels have similar trends regardless of different widths of ZSPC used in PB3-16 and PB6-16. The longitudinal strains of the bottom concrete layer of PB-series panels are larger than that of P-series panels. These results suggest that ZSPC with varied shear strength and stiffness, within the range used in these tests, did not affect the deformation mechanism of the tested panels. They did, however, affect the out-of-plane resistance of the panels as discussed in Section 7.3.2.

7.3.3. Behaviour of ZSPC during Flexural Tests

Figure 7-12 shows the deformed shape of ZSPC in P-series panels after the flexural tests. This figure also shows the location of the connectors across the panels. The connectors in row 1 are closest to mid-span and the connectors in row 3 are closest to the ends of the panel. As shown in this figure the 16 gauge connectors closest to the panel ends (row 3) underwent significant buckling. The connectors in row 2 also experienced some buckling, but the buckling deformation of gauge 16 connectors in row 2 seems smaller than that of the connectors in row 3. Figure 7-12 shows that for all the panels with gauge 16 ZSPC the connectors in row 1, closest to the mid-span, did not show any buckling deformation. This indicates that interlayer shear deformation, hence interlayer shear forces, are largest in the connectors closest to the panel ends - i.e. the regions with largest shear forces across the panel sections - and are smallest in the connectors between the point loads. This result is consistent with mechanics of materials and experimental observations by Salmon et al. (1997). As mentioned in Section 7.2, according to Bernoulli beam theorem, distribution of interlayer shear forces is proportional to the shear force distribution across the cross section of the panel. Figure 7-12 also shows that the gauge 10 ZSPC in P4-10 panel did not undergo buckling, which is consistent with the shear test results of SH4-10 specimens presented in Chapter 4.

Figure 7-13 shows the deformed shape of the various ZSPC in the PB-series panels after the flexural tests along with their location across the panels. The connectors in the second row of connectors in PB6-16 underwent the largest buckling deformation compared to the connectors in rows 1 and 3. The third row of connectors in PB3-16 underwent some buckling and the third row of connectors in PB6-16 underwent almost no buckling. This indicates that around the ends of the PB-series panels, the interlayer shear forces were primarily carried by the end-beams, thus reducing the shear force demand on the third row of connectors.

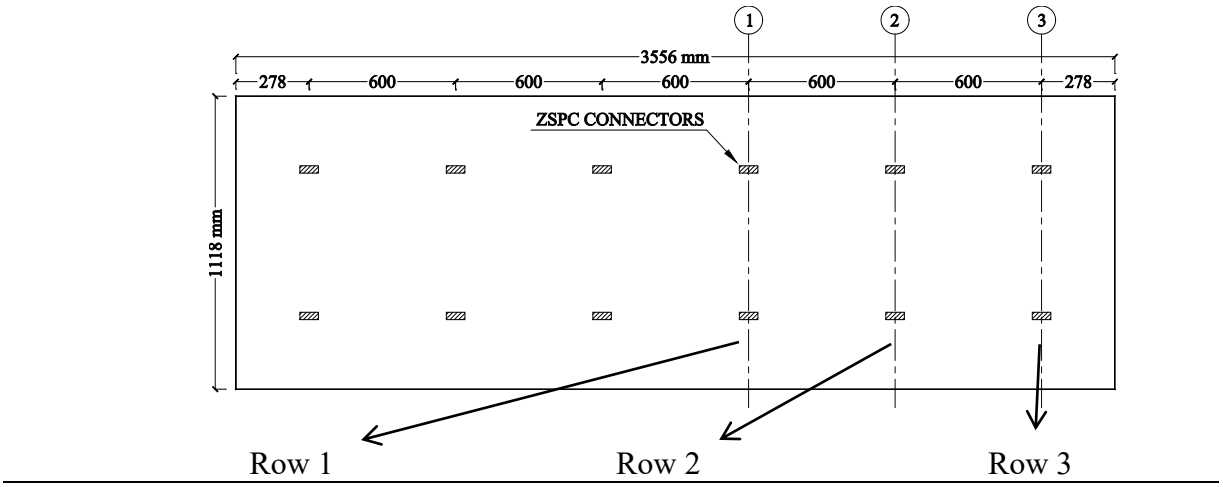

P3-16

P4-16

P6-16

P4-10

Figure 7-12: Deformed shape of ZSPC of P-series panels after flexural tests.

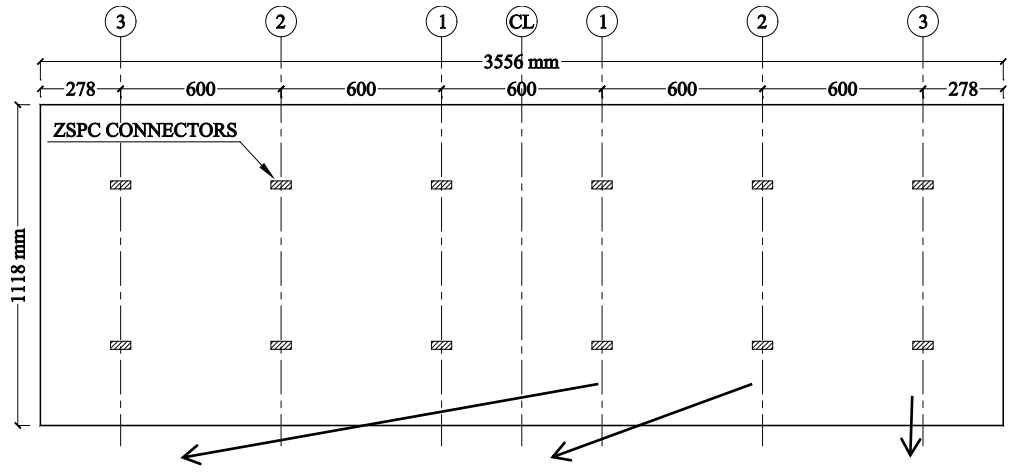

Figure 7-13: Deformed shape of ZSPC of PB-series panels after flexural tests.

Figure 7-14 shows the readings of the ZSPC strain gauges against the mid-span vertical deflection of the panels. The location, orientation and labeling of the ZSPC strain gauges are shown in Figure 7-1. The W3 and E3 strain gauges are closest to the ends of the panel and W1 and E1 strain gauges are closest to the mid-span. The readings of these strain gauges do not reflect the complex nature of the strains induced in the connectors. These strain gauges are bonded only on one face of the connectors and are localized to one spot. However, the connector's web undergoes large bending due to in-plane shear and compressive stresses producing different stresses on opposite faces of the web. However, the readings of these strain gauges can be used to spot the instance of buckling of the ZSPC where there is a sudden jump or drop in the strain readings.

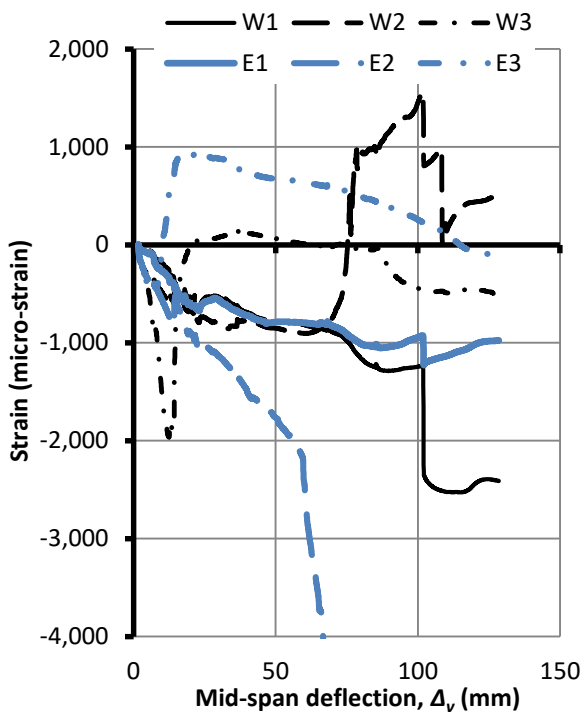

a. P3-16

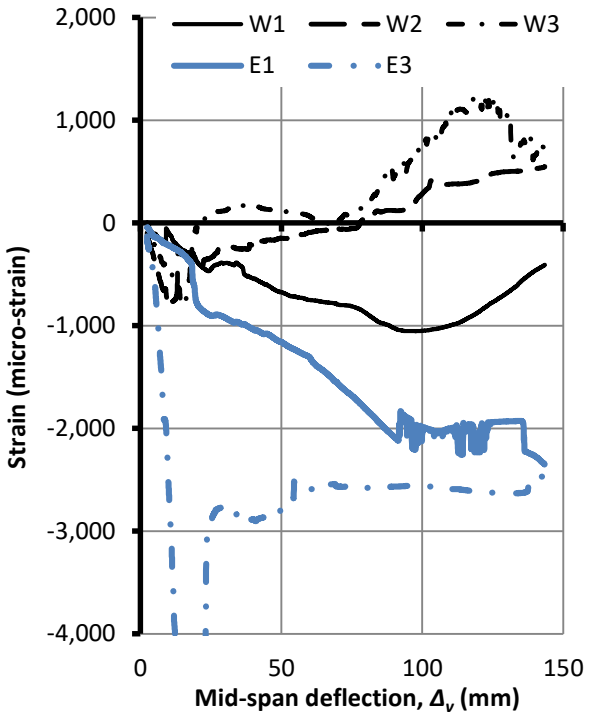

b. P4-16

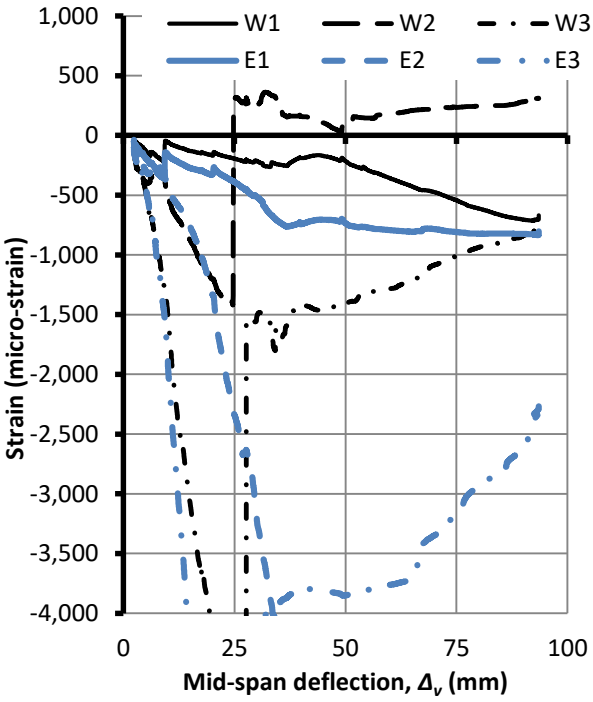

c. P6-16

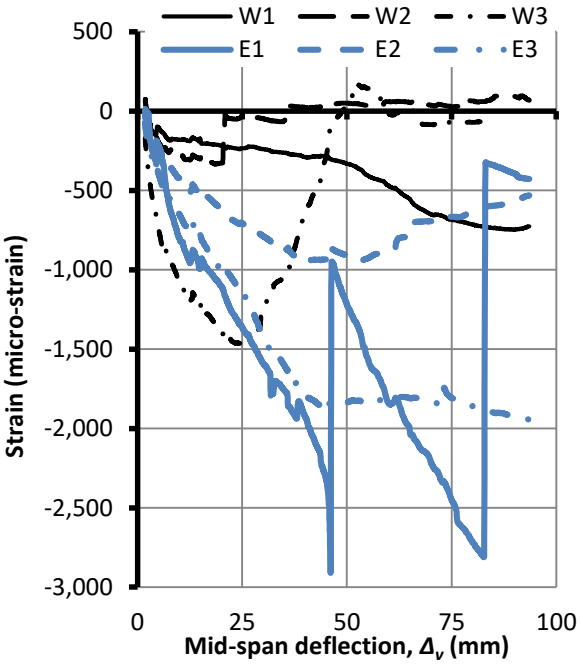

d. P4-10

Figure 7-14: Average readings of strain gauges on ZSPC of a. P3-16, b. P4-16, c. P6-16, and d. P4-10
Notes: Location, orientation and labeling of strain gauges are shown in Figure 7-1.

As shown in Figure 7-14, the strain readings of W3 in panel P3-16 shows a drop in compressive strains at Δ_v of about 15 mm. Also the strain E3 in panel P3-16 changed from compressive strains to tensile strains at Δ_v of about 12 mm. These Δ_v values are within the plateau region of P-Δ_y behaviour of P3-16 in Figure 7-7. Similarly in P4-16, strain readings of W3 shows as sudden jump in strains at Δ_v of about 12 mm, and E3 shows a sudden jump in compressive strains at Δ_v of about 10 mm, which is before the plateau region of P-Δ_v behaviour of P4-16. And in P6-16, W3 and E3 show a sudden jump in compressive strains at Δ_v of about 12 mm, which is around the beginning of P-Δ_v plateau in P6-16 (Figure 7-8). Therefore, the buckling of the connectors closest to the panel ends might have caused the plateau regions in P-Δ_v behaviour of the panels with 16 gauge ZSPC. Shear tests showed that after gauge 16 connectors reached the theoretical plastic strength, they underwent plastic buckling, which lead to decrease in shear resistance of the connectors (Section 4.3). In the panels, after the 16 gauge ZSPC reached their shear strength, they buckled, which decreased the shear resistance of the connectors; this redistributes the shear forces to other ZSPC along the panel while the panel deflects without increase in load resistance, which is depicted by the plateau regions in P-Δ_v behaviour.

After yielding of the connectors, if their shear resistance stayed constant, the interlayer shear stiffness of the panel would reduce to zero after all connectors yielded. This would make non-composite behaviour in the panel, and the out-of-plane stiffness of the panel would be equal to that of theoretical non-composite panel. In other words, the out-of-plane stiffness of the panel theoretically cannot be less than the out-of-plane stiffness of theoretical non-composite panel. For partially-composite panels, where there is non-zero interlayer shear stiffness and strength, the total mid-span bending moment is carried by sum of the bending moments in the concrete layers and the couple moment produced by the compressive and tensile forces in the top and bottom concrete layers, respectively. The axial forces of the concrete layers at mid-span should be equal to the interlayer shear forces between the mid-span and one end of the panel to maintain static equilibrium in the horizontal direction. Now, the fact that in the aforementioned plateau regions the out-of-plane stiffness of panels reaches zero suggests that under the same out-of-plane loading, the interlayer shear strength decreased, which reduced the axial forces of the concrete layers; this reduced the part of the total bending moment carried by the axial forces of the concrete layers, and thus increased the bending moment of the concrete layers. The concrete layers deflected under increased bending moment. This increased out-of-plane deformation occurs without any increase in the out-of-plane loading, which means zero out-of-plane stiffness. Therefore, the drop in shear

resistance of the 16 gauge connectors during their plastic buckling might have caused the plateau regions in the P-series panels with 16 gauge connectors. This is investigated further by numerical analysis of the panels in Chapter 8.

Figure 7-14 shows that compressive strains of W3 in P4-10 increased up to -1500 micro-strains at Δ_v of about 18 mm, then later decreased to 0.0 micro-strains at Δ_v of about 28 mm, indicating some load reversal. This increase is a gradual change of strains compared, for example, to the strain jump of E3 and W3 in P6-16 at Δ_v of about 12 mm. Also, the strains of E3 in P4-10 do not decrease throughout loading. That is, no strain reversals or abrupt changes are observed for the strain gauges of the connectors in P4-10 (Figure 7-14), which suggests that the ZSPC of P4-10 did not buckle, which is consistent with the observed deformed shape of ZSPC in P4-10 shown in Figure 7-12. This might explain why there is no plateau in P-Δ_v behaviour of P4-10 given in Figure 7-8. As noted before SH4-10 also did not show buckling and the shear behaviour of SH4-10 had high ductility. So, during loading of P4-10, when the end connectors (row 3) reached their shear strength, they showed ductile shear behaviour without any drop in shear resistance. This resulted in a nonlinear increase in P-Δ_v behaviour of P4-10 without forming any plateau.

7.3.4. Interlayer Slippage and End Rotations of the Tested Panels

Figure 7-15 shows the interlayer slippage against the vertical deflections of the panels. The interlayer slippage was recorded by LVDTs mounted at the ends of the panels. This figure shows for all panels without end-beams the interlayer slippage linearly increased to 7.5 mm at Δ_v of about 60 mm. In other words, the difference in width and thickness of the ZSPC used in these flexural tests did not affect the interlayer slippage of the panels. On the other hand, PB-series panels showed negligible (<0.1 mm) interlayer slippage due to the presence of the end-beams.

Figure 7-16 shows the end-rotation versus mid-span vertical deflection of the panels. This figure shows that the end-rotation of all panels increased almost linearly to 5 degrees at Δ_v of about 95 mm. In other words, the difference in width and thickness of the ZSPC used in these flexural tests did not affect the end rotation of the panels. The end rotations of PB-series panels are substantially smaller than that of P-series panels. For PB3-16, the end-rotation increased to a maximum value of 0.45 degrees and it decreased and showed some negative rotation. The end

rotation of PB6-16 was similar to that of PB3-16 up to Δ_v of about 30 mm. But, unlike PB3-16, the end rotation of PB6-16 increased to about 2 degrees at Δ_v of about 85 mm.

As mentioned before the critical connectors in the P-series panels are the ones closes to the panel ends. In Chapter 9, rotation angle of concrete layers is shown to be related to the shear deformation of the interlayer connectors. The panels should be designed such that shear deformation of the interlayer connectors does not exceed their failure shear deformation. Figure 7-15 suggests that if out-of-plane deflection of panel is predicted, the end rotation, and thus the shear deformation of the critical connectors in PICP without end-beams can be estimated using a linear relationship. This is further discussed in Chapter 9.

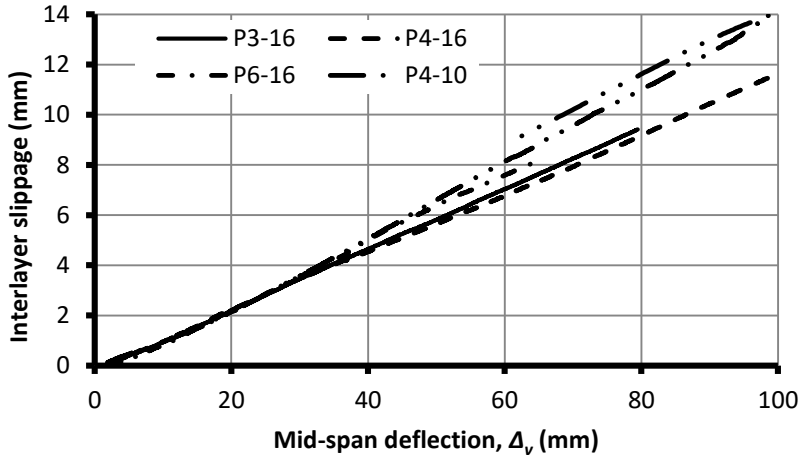

Figure 7-15: Interlayer slippage of tested PICP

Figure 7-15 and Figure 7-16 show that for P-series panels, interlayer slippage and end rotations of the panels had linear relationship with the mid-span deflection throughout loading regardless of the varied width and thickness of the interlayer ZSPC. The ZSPC used in these tests provide a certain range of interlayer shear strength and stiffness for the tested panels. This indicates that the deformation mechanism of the panels was not affected by changing the interlayer shear strength and stiffness of the panels within the chosen range of interlayer shear strength and stiffness examined in these tests. However, adding end-beams to the panels significantly changed the deformation mechanism of the panels. Presence of end-beams eliminated the interlayer slippage at the ends of the panels and significantly reduced the end-rotations of the panels.

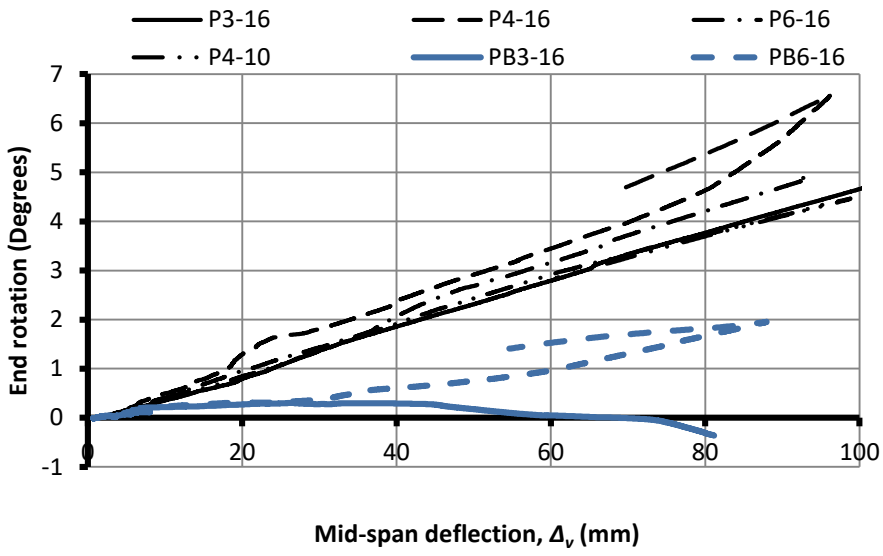

Figure 7-16: End-rotations vs. mid-span deflection of the tested PICP

7.4. Summary and Conclusion

Out-of-plane 4-point flexural tests were conducted on six PICP with Z-shaped Steel Plate Connectors (ZSPC) to study the effect of width and thickness of ZSPC and presence of end-beams on the out-of-plane behaviour of PICP. Two of these panels were enclosed with end-beams. The width of the connectors varied from 76.2 mm to 152 mm and the thickness varied from 1.47 mm to 3.22 mm.

It was found that PICP with ZSPC can attain the out-of-plane resistance of a theoretical fully-composite panel. For this to be achieved, the minimum interlayer shear strength of the panel between the locations of maximum and zero bending moments should be equal to the total yield force of the tensile reinforcement. This minimum interlayer shear strength can be achieved by designing the number, thickness and width of ZSPC across the panel. The test results demonstrated that end-beams considerably improve the out-of-plane bending moment of PICP corresponding to the design out-of-plane deflection limit specified by CAN/CSA A23.3-04. This suggests that the shear strength of end-beams significantly contributes to the interlayer shear strength of the panels, thereby improves the out-of-plane bending moment carried by PCSP. The out-of-plane flexural strength of the panels with end-beams reached the out-of-plane flexural strength of the theoretical fully-composite panel. The out-of-plane flexural strength of the panels without end-beams reached up to 77% of the out-of-plane flexural strength of the theoretical fully-composite panel.

The flexural stiffness of the tested panels was found to be 2.25 to 3.75 times the flexural stiffness of the theoretical non-composite panel. This means that using ZSPC in PICP significantly reduces its out-of-plane deflection compared to a theoretical non-composite panel. This effect of ZSPC on the flexural stiffness of PICP can be used to optimize the structural design of these panels. The results of these tests are adopted in Chapter 8 to verify the proposed method of numerical modeling to analyze PICP with different interlayer connector system.

8. Numerical Analysis of Flexural Tests on PICP

8.1. Introduction

Previous researchers have compared out-of-plane behaviour of PICP made of different interlayer mechanical connectors with the theoretical non-composite and fully-composite behaviour. And they derived approximate values for the degree of composite action for their tested PICP. However, it is shown that the degree of composite action varies with the strength and stiffness of the connectors, presence of end-beams, length of the panel and support conditions (Pfeifer and Hansen 1964, Carbonari et al. 2012). Therefore the proposed methods to predict degree of composite action in PICP do not apply to the panels with different lengths and support conditions. Previous researchers proposed analytical methods to estimate the ultimate strength of PICP (Mouser 2003, Hassan and Rizkallah 2010), but no analytical method is found by the author to estimate the out-of-plane deflection of PICP. And for tall PICP out-of-deflection is the governing design criteria. Moreover, the flexural tests in this thesis are limited to simply supported panels under 4-point loading. Thus, the moment-curvature relationships for the mid-span of the tested panels cannot be applied to PICP with different lengths, loading and support conditions.

All these problems stem from the fact that PICP are compared to and simplified as solid panels. In this Chapter, PICP is assumed as an assembly of two concrete layers and numerous interlayer mechanical connectors. Then Multistep Linear Elastic (MLE) method is developed and adopted in this Chapter to estimate the out-of-plane behaviour of PICP under any loading and support conditions with any interlayer mechanical connector system with a known shear strength and stiffness. In Section 8.3, this method is verified by the flexural tests presented in Chapter 7. This method is shown to be applicable to any PICP with any interlayer mechanical connector under any support and loading condition. The MLE method can predict the out-of-plane flexural capacity, out-of-plane deflection as well as deformation of the connectors.

8.2. Finite Element Analysis of Structures with Material Nonlinearity

8.2.1. Overview of Linear Finite Element Analysis

In Finite Element Analysis (FEA) the structure is assumed as an assembly of discrete finite elements, interconnected at nodal points on the element boundaries. The displacements within

element m, u_m are assumed to be a function of nodal point displacement vector U. Thus, u_m can be expressed as:

$$u_m = H_m . U \quad \textbf{8-1}$$

Where H_m is the interpolation matrix of element m. The strains of element m are derived by:

$$\varepsilon_m = B_m . U \quad \textbf{8-2}$$

Where B_m is the strain-displacement matrix, the rows of which are obtained by appropriately differentiating and combining rows of the matrix H_m (Bathe, 1996). The element stresses are derived by equation 8-3.

$$\sigma_m = C_m . \varepsilon_m + \sigma_{I,m} \quad \textbf{8-3}$$

Where C_m is the elasticity matrix of element m, and $\sigma_{I,m}$ is the given element initial stresses. Using the principle of virtual work the nodal load vector F can be related to the nodal point displacement vector U by (Bathe, 1996):

$$F = K . U \quad \textbf{8-4}$$

Where, K is the stiffness matrix of the structure constructed by assembling stiffness matrices of individual elements as given by equation 8-5.

$$K = \sum_m K_m \quad \textbf{8-5}$$

Where, K_m is the stiffness matrix of element m, given as:

$$K_m = \int_{V_m} B_m^T . C_m . B_m dV_m \qquad \textbf{8-6}$$

Where, V_m is the volume of the element m.

8.2.2. Materially-Nonlinear-Only (MNO) Finite Element Analysis

Nonlinear material behaviour of the elements of a structure leads to global nonlinear behaviour of the structure. This nonlinear behaviour of the structure can be determined based on the Materially-Nonlinear-Only (MNO) formulation of FEA as presented by Bathe (1996). In this formulation, loading is incrementally applied on the structure and the incremental nodal point displacements are calculated using the tangent stiffness matrix of the structure. For the next increment, the elasticity matrix of every element is modified based on its material behaviour; this changes the stiffness matrix of the structure. This modified stiffness matrix is used along with the next increment of loading to calculate the next increment of nodal point displacements. Incremental nodal point displacements are used to calculate the incremental strains and stresses of every element. The sum of incremental loading, displacements, element strains and stresses give the nonlinear behaviour of the structure.

In MNO analysis of structures, the nodal load vector *F* is applied incrementally during time *t* given as:

$$F^{(t+\delta t)} = F^{(t)} + \delta F^{(t)} \qquad \textbf{8-7}$$

Where $F^{(t)}$ and $F^{(t+\delta t)}$ are the nodal concentrated load vectors at time *t* and $t + \delta t$, where δt is the time increment; and $\delta F^{(t)}$ is the load increment at time *t.* Due to material nonlinearity of the structure, the stiffness matrix of individual elements, and thus the stiffness matrix of the structure vary with progression of loading during time *t*. Therefore, the incremental nodal point displacement and nodal load vectors at time *t* are interrelated by equation 8-8.

$$\delta F^{(t)} = K^{(t)} . \delta U^{(t)} \qquad \textbf{8-8}$$

Where, $K^{(t)}$ is the tangent stiffness matrix of the structure at time *t,* constructed by assembling the tangent stiffness matrices of individual elements $K_m^{(t)}$ given as:

$$K_m^{(t)} = \int_{V_m} B_m^T . C_m^{(t)} . B_m \, dV_m \qquad \textbf{8-9}$$

Where $C_m^{(t)}$ is the tangent elasticity matrix of element *m.* This analysis assumes that nonlinearity only stems from the variation of the C_m with time. The strains are assumed to be small and therefore, the matrix B_m is not varied and hence, geometric nonlinearity is not considered. Given the load increment, $\delta F^{(t)}$, the nodal point displacement increment, $\delta U^{(t)}$, can be derived as:

$$\delta U^{(t)} = {K^{(t)}}^{-1} . \delta F^{(t)} \qquad \textbf{8-10}$$

Then the nodal point displacement vector at $t + \delta t$, $U^{(t+\delta t)}$, can be calculated by equation 8-11.

$$U^{(t+\delta t)} = U^{(t)} + \delta U^{(t)} \qquad \textbf{8-11}$$

After finding the nodal point displacements, equations 8-148-12 and 8-158-13 give the incremental element strains and stresses, $\delta \varepsilon_m^{(t)}$ and $\delta \sigma_m^{(t)}$, respectively.

$$\delta \varepsilon_m^{(t)} = B_m . \delta U^{(t)} \qquad \textbf{8-12}$$

$$\delta \sigma_m^{(t)} = C_m^{(t)} . \delta \varepsilon_m^{(t)} \qquad \textbf{8-13}$$

The element strains and stresses, $\varepsilon_m^{(t+\delta t)}$ and $\sigma_m^{(t+\delta t)}$, can then be calculated by equations 8-14 and 8-15, respectively.

$$\varepsilon_m^{(t+\delta t)} = \varepsilon_m^{(t)} + \delta\varepsilon_m^{(t)} \quad \textbf{8-14}$$

$$\sigma_m^{(t+\delta t)} = \sigma_m^{(t)} + \delta\sigma_m^{(t)} \quad \textbf{8-15}$$

In equations 8-12 and 8-14, the small strain matrix is used to define the strain, and as long as the total displacements are small, this additive decomposition is allowed. After finding element strains and stresses at $+\delta t$, the material constitutive relationships are adopted to calculate $C_m^{(t+\delta t)}$, thereby to obtain the modified stiffness matrix of every element m, $K_m^{(t+\delta t)}$, and the modified stiffness matrix of the structure, $K^{(t+\delta t)}$. This modified stiffness matrix of the structure is used along with the next increment of nodal load vector, $\delta F^{(t+\delta t)}$, to calculate the next increment of nodal point displacement vector, $\delta U_m^{(t+\delta t)}$. These increments of nodal load and displacement vectors are then adopted to obtain the strain and stress increments at $t + \delta t$. This procedure continues until the end of loading.

8.3. Multistep Linear Elastic (MLE) Analysis of PICP

8.3.1. Overview of the Nonlinear FEA of PICP with MLE Method

The MNO formulation described in Section 8.2.2 was adopted to perform nonlinear numerical analysis on the tested PICP. For this, the nonlinear behaviour of the panels was predicted by Multistep Linear Elastic (MLE) analysis of the modeled panels. In each step, the defined stiffness of individual members of the modeled panel were based on the estimated forces and bending moments in each member.

The tested panels were modeled and analyzed in SAP 2000. The concrete layers of the panels were modeled as shell elements, and the ZSPC were modeled as shear springs between the concrete layers. The experimental material behaviour of the concrete layers (Section 7.2) and the shear behaviour of ZSPC (Section 4.3) were adopted to define the behaviour of the modeled concrete layers and shear springs of the PICP numerical models. The support and loading beams were

modeled as beam elements. The ends of the support beams were modeled as roller-pin supports, as was the case in the flexural experiments. During every loading increment, the incremental load was applied on the PICP model, linear elastic analysis was conducted, and the deformation, forces and bending moments of the concrete layers and shear connectors were recorded. Based on these forces and bending moments the axial and flexural stiffness values of different regions of the concrete layers and the shear stiffness of the shear springs were modified at the end of the increment, the next incremental loading was applied, and another linear elastic analysis was conducted to obtain the deformations, forces and bending moments of the next increment. This MLE analysis was continued to obtain the numerical out-of-plane behaviour of the tested PICP. Each tested PICP was analyzed, once, without and, the second time, with considering tension stiffening of the reinforced concrete layers. In the following sections the numerical models are described in detail and numerical results of the tested PICP are compared against the experimental results.

8.3.2. Numerical Modeling of the Tested PICP

As shown in Figure 8-1, the tested PICPs were modeled as an assembly of two concrete layers and interlayer mechanical connectors represented by shear springs. The concrete layers were modeled as shell elements with 76.2 mm thickness. The shell elements were assumed to be in the mid-thickness of the concrete layers, therefore the distance between the modeled concrete layers was 152 mm to make a 76.2 mm gap between the inner faces of the concrete layers. The end-beams of the PB-series panels were modeled as shell elements with 150 mm thickness, equal to the end-beam widths in the tests (Figure 8-2).

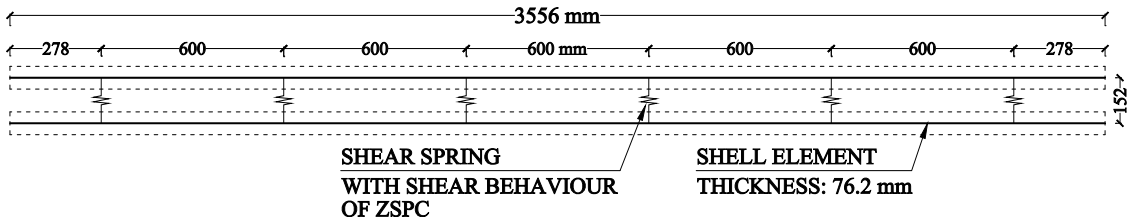

Figure 8-1: Numerical model of the tested PICP without end-beams (P-series).

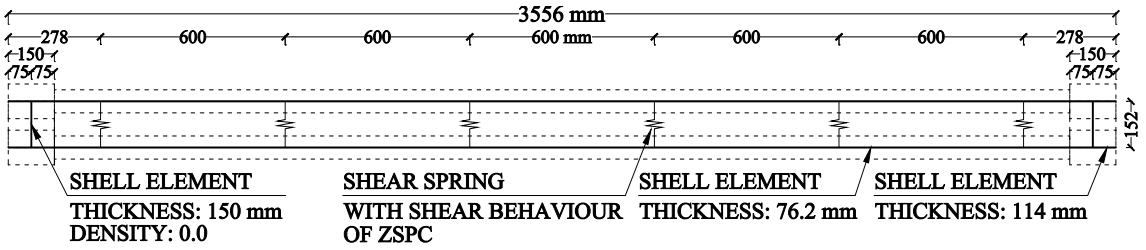

Figure 8-2: Numerical model of the tested PICP with end-beams (PB-series).

Figure 8-3 shows the schematic of the modeled PICP under 4-point loading, and Figure 8-4 shows the 3D view of the modeled PICP. As shown in Figure 8-4, the loading and support beams were modeled as beam elements with W200x46 steel section. A uniform load of 1.0 kN/m was applied on the loading beams. This unit load along with superposition principle is used in incremental loading of the modeled PICP. The boundary conditions of the ends of the support beams allowed horizontal displacement along the panel length and rotation about the longitudinal axis of the beam to simulate the pin-roller supports used in the tests (Figure 8-3). The mid-length of the concrete layers was constrained against horizontal displacement along the panel length in order to maintain static equilibrium in *x* direction in the numerical models (Figure 8-3).

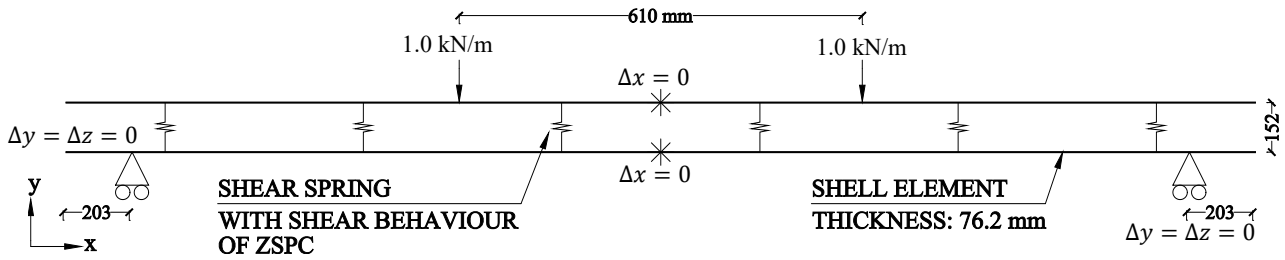

Figure 8-3: Numerical model of 4-point flexural tests.

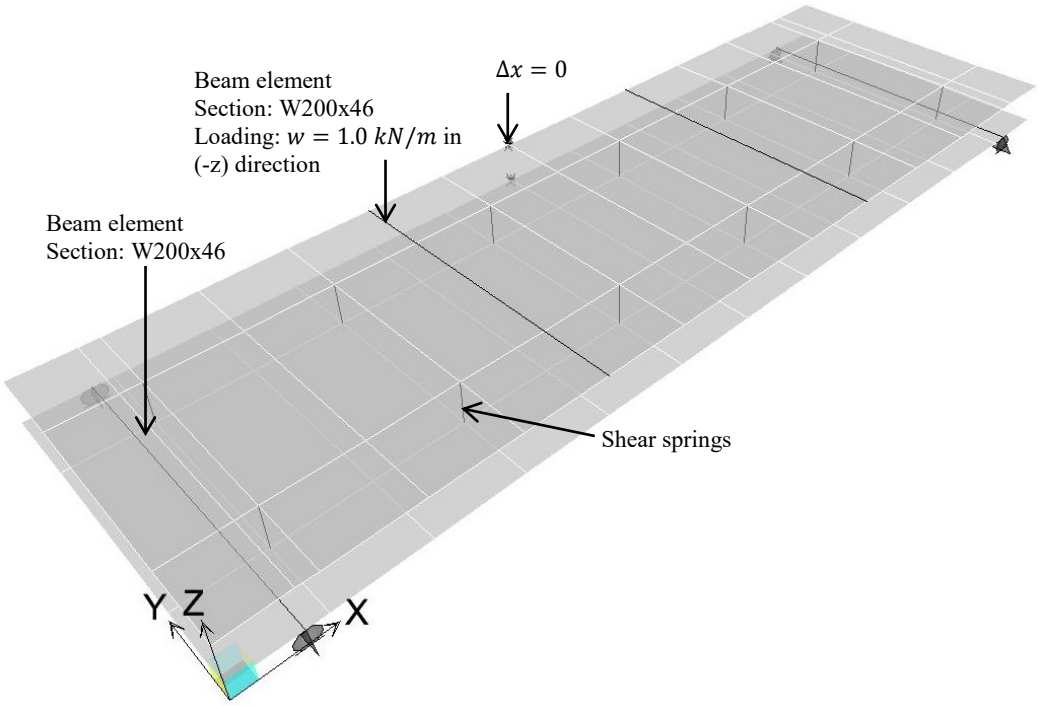

Figure 8-4: 3D view of the numerical models for the tested PICP.

The results of push-off shear tests of ZSPC presented in Section 4.3 were adopted to construct the simplified shear behaviour of ZSPC shown in Figure 8-5. These simplified shear-displacement behaviours are used in the numerical models of the PICP. Figure 8-6 shows schematic of the simplified shear behaviour of ZSPC and the modeled loading path in the numerical analyses of the tested PICP. As shown in this figure, in the simplified shear behaviour of ZSPC, the shear force increases with a shear stiffness of *K* up to a yielding point, after which the shear force remains constant but the shear deformation increases to a failure point. After failure, the shear force descends to a residual shear force, after which the shear force remains constant with increased shear deformation.

In the multistep linear elastic analysis of PICP, the initial stiffness of ZSPC was assigned to the shear springs at the early stages of loading. When any of the shear springs reached yielding, the ZSPC shear stiffness was modified to zero. Loading continued until a ZSPC reached its failure point. At failure, the descending portion of the simplified shear behaviour ZSPC require defining negative shear stiffness in the numerical analysis, which was not possible in SAP 2000.

Thus, the panel was unloaded to unload the ZSPC until the connector's shear force reached the residual shear force. The shear stiffness of ZSPC during unloading was assumed to be the same as the initial shear stiffness. This is because Z-shape connectors are made of steel, where the modulus

of elasticity of during unloading is equal to the initial modulus of elasticity. When the shear force of the connector reached the residual shear force, the shear stiffness of the ZSPC was changed to zero and loading of the panel was continued.

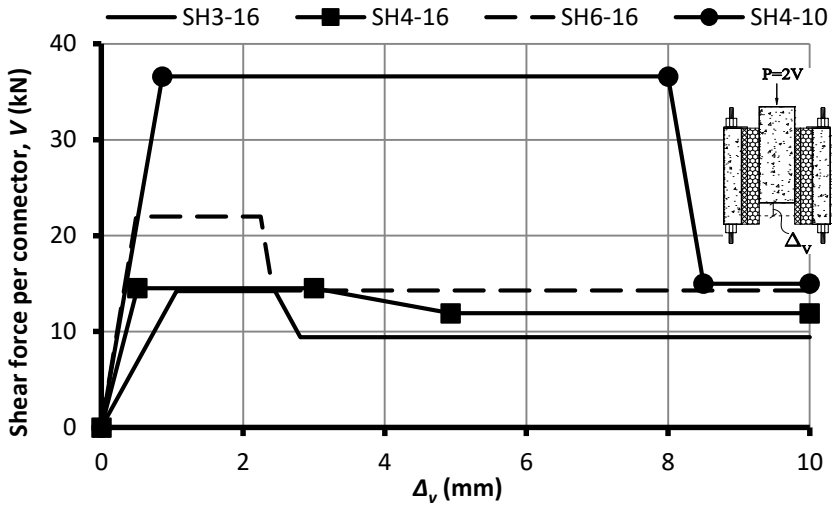

Figure 8-5: Simplified shear behaviour of ZSPC assumed in the numerical models of the tested PICP.

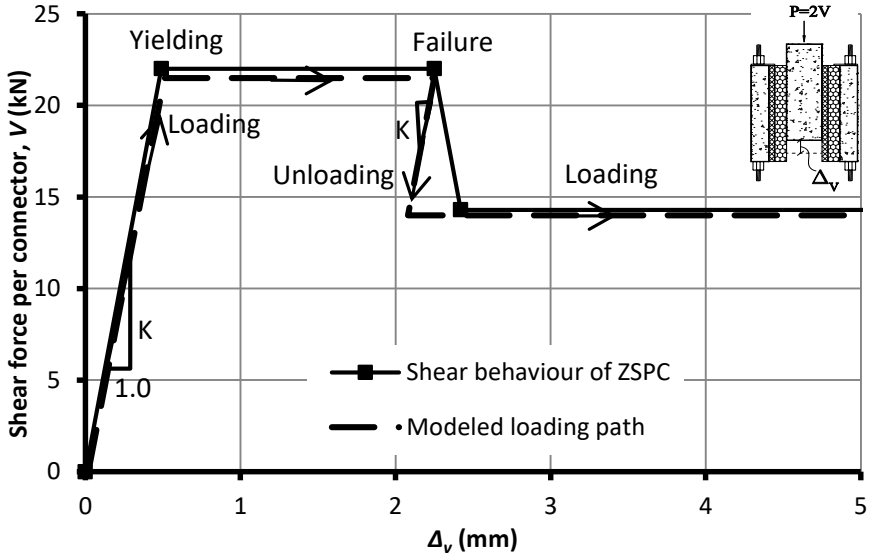

Figure 8-6: Schematic of the simplified shear behaviour of ZSPC in the numerical models of PICP.

Figure 8-7 shows the schematic of free body diagram of the modeled PICP. As shown in this figure, the concrete layers of PICP under out-of-plane loading undergo combined effects of axial force and out-of-plane bending moment. In the tested PICP, the bottom concrete layer is under the combined effect of a tensile force and an out-of-plane bending moment, and the top concrete layer

is under the combined effect of a compressive force and an out of plane bending moment. Therefore the out-of-plane moment-curvature behaviour of the concrete layers at different levels of axial force and the axial force-strain behaviour of the concrete layers at different levels of out-of-plane bending moment should be considered in the nonlinear analysis of the tested PICP.

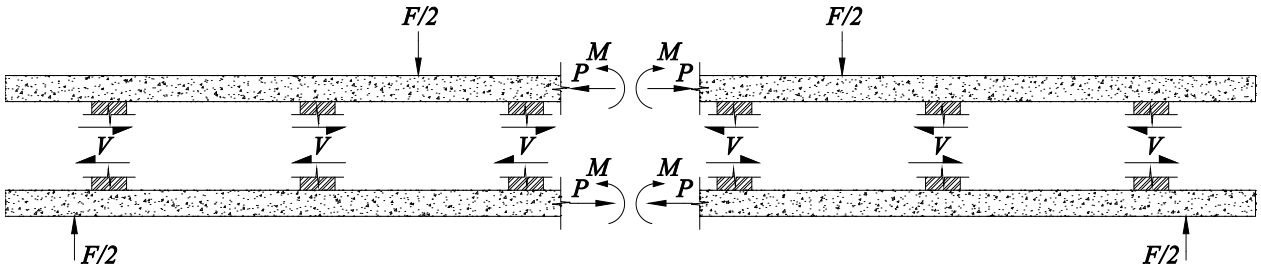

Figure 8-7: Schematic of the forces and bending moments in the tested PICP.

To assign the proper axial and out-of-plane flexural stiffness to the shell elements of the concrete layers in the numerical models of the PICP the axial force – strain (P-ε) and out-of-plane bending moment – curvature (M-φ) diagrams were constructed for the bottom and top concrete layers. The details of the calculations of the P-ε and M-φ diagrams are given in Appendix B.1. To construct the M-φ diagrams for the concrete layers, the results of the tensile testing of longitudinal bars, shown in Figure 7-4 (page 91), were used in the calculations. The elasticity moduli and compressive strengths of the concrete given in Table 7-2 (page 91) were used along with the Hognestad parabola (Hognestad, 1951) to model the compressive behaviour of concrete to construct the P-ε and M-φ diagrams of the concrete layers.

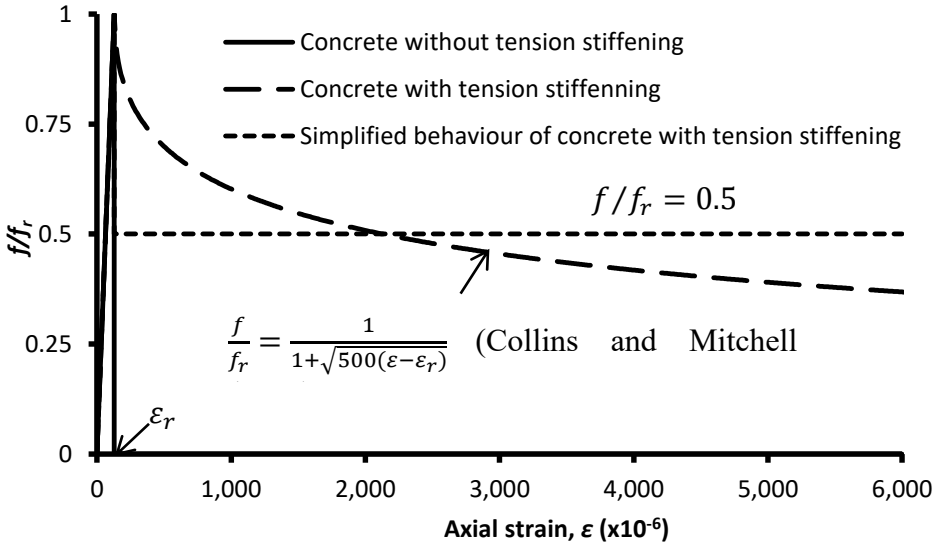

Figure 8-8: Tensile behaviour of reinforced concrete.

As mentioned earlier, each tested PICP was analyzed, once without and the second time with considering tension stiffening of the reinforced concrete layers. Therefore the *M*-*φ* diagrams were constructed once without and the second time with considering tension stiffening of the reinforced concrete layers. Figure 8-8 shows the tension stiffening of reinforced concrete using the model proposed by Collins and Mitchell (1987) for the concrete reinforced with deformed bars under short term monotonic loading. This figure also shows the assumed behaviour of concrete without tension stiffening. As shown in Figure 8-8, when tension stiffening was not considered in the numerical models of PICP, the tensile strength of concrete was assumed to drop to zero after cracking. And when tension stiffening was considered, the tensile strength of concrete was assumed to drop to half the cracking strength (f_t) as proposed by Collins and Mitchell (1997).

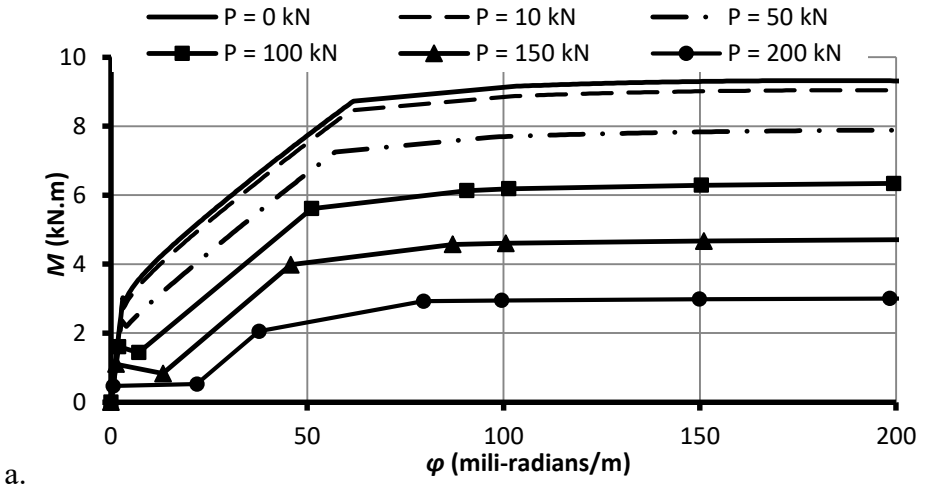

a.

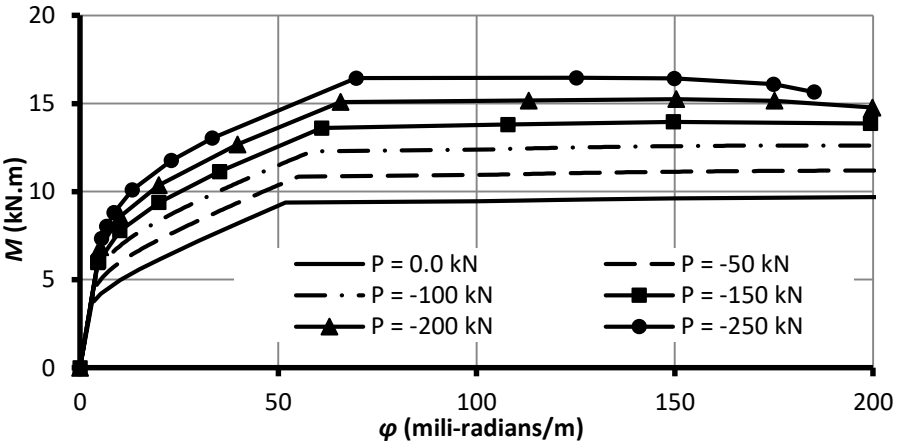

b.

Figure 8-9: Out-of-plane bending moment-curvature diagrams for a. bottom layer, and b. top layer of the tested PICP.

Figure 8-9 shows the out-of-plane bending moment-curvature (*M*-*φ*) diagrams for the bottom and top concrete layers under different levels of axial forces. These diagrams were derived using the

28-day compressive behaviour of concrete. As shown in this figure increasing tensile forces reduces the cracking flexural and ultimate out-of-plane flexural strengths of the bottom concrete layer, and increasing compressive forces improves the cracking and ultimate out-of-plane flexural strengths of the top concrete layer. Figure 8-10 shows a schematic of the *M-φ* diagram of concrete layer with and without considering tension stiffening of concrete. As shown in this figure, the out-of-plane bending moment increases with curvature until cracking of concrete. The slope of this portion of the diagram is the initial flexural stiffness of the concrete layer, $K_{f,i}$, which is equal to E_c I_0, where E_c is the concrete modulus of elasticity and I_0 is the uncracked moment of inertia of the concrete layer in the direction of the out-of-plane bending moment. If tension stiffening of concrete is considered, after cracking the bending moment keeps increasing with curvature until the reinforcing bars yield. If tension stiffening of concrete is not considered, after cracking the bending moment first drops, then increases with curvature until the yielding of reinforcing bars. The slope of this portion is the cracked flexural stiffness of the concrete layer, $K_{f,c}$, which was found to be from 0.08 to 0.11 times the initial flexural stiffness, E_c I_0.

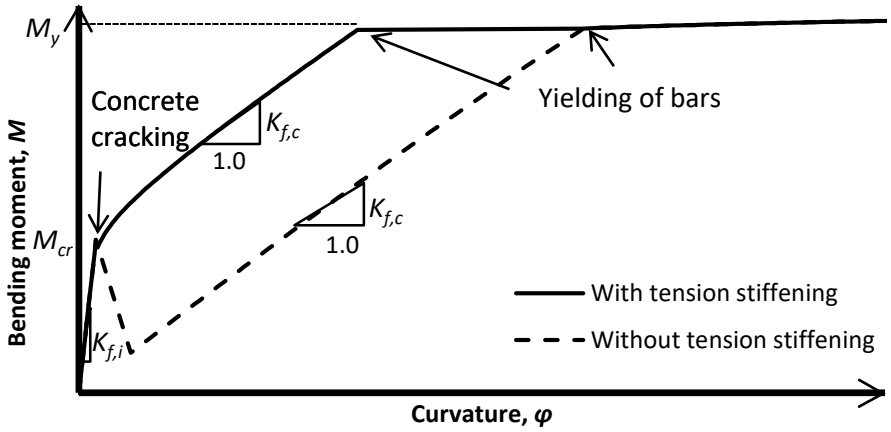

Figure 8-10: Schematic of M-ϕ diagram for concrete layer with/without tension stiffening of concrete.

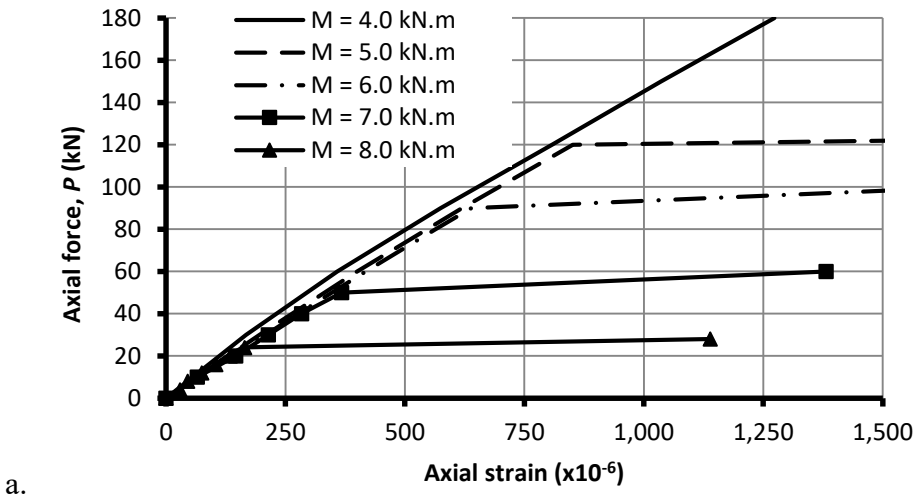

a.

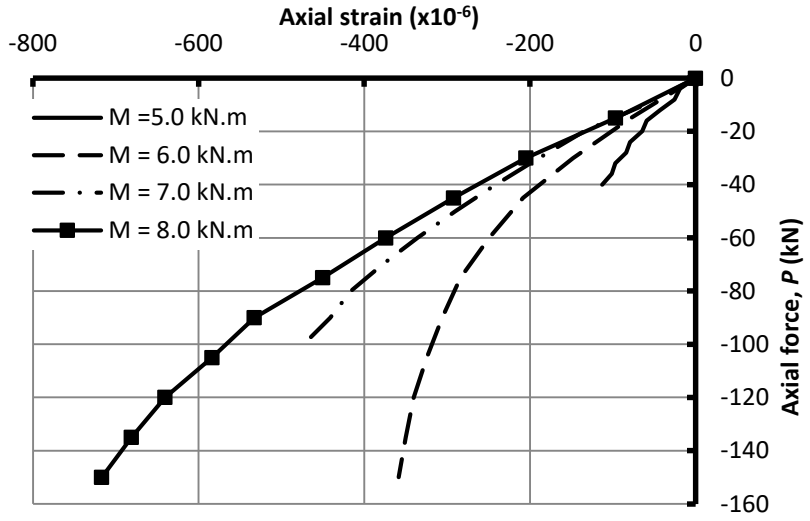

b.

Figure 8-11: Axial force vs. out-of-plane bending moment diagrams for a. bottom, and b. top concrete layer.

Figure 8-11 shows the post-cracking axial force-strain (P-ε) diagrams of the concrete layers for different values of out-of-plane bending moments (M) larger than the cracking flexural strength. The pre-cracking initial axial stiffness of the concrete layer is equal to EA_0, where E is the modulus of elasticity of concrete and A_0 is the uncracked cross sectional area of the concrete layer. The initial slope of the (P-ε) diagrams for the bottom and top concrete layers were found to be from 0.08 to 0.1 times EA_0.

As shown in Figure 8-11, the slope of the (P-ε) diagrams for the bottom concrete layer, where the axial forces are tensile, have the same slope until the yielding point, regardless of the value of the bending moment. The figure shows that as M grows larger, the bottom concrete layer yields at smaller tensile forces. Figure 8-11 shows that the compressive axial strains of the top concrete

layer grow faster as the bending moment gets larger. However, at any level of bending moment, the slope of the P-ε diagrams of the top concrete layer grows larger with increased compressive forces. This behaviour can be explained by understanding the effect of combined bending moment and compressive forces on the cross section of the concrete layer. As bending moments grows larger, larger area of the section of the concrete layer cracks, reducing the axial stiffness of the concrete layer. At the same level of bending moment, as the axial forces increase, some depth of the cracks close, restoring the axial stiffness of the concrete layer.

8.3.3. Numerical Results and Discussion

The numerical results of the tested PICP showed that the failure stages of the P-series panels include cracking of the bottom and top concrete layers, yielding and failure of ZSPC starting from the connectors farthest from the panels' mid-span. And the failure stages of the PB-series panels are the same as the failure stages of the P-series panels plus cracking and yielding of the concrete layers at the ends of the panels, where the concrete layers meet the end-beams. Table 8-1 gives different failure stages along with their acronyms. The failure stages for the concrete layers in Table 8-1 are defined by three letters, $L_1L_2L_3$. The first letter, L_1, relates either to the bottom concrete layer, B, or to the top concrete layer, T; the second letter, L_2, relates either to the mid-span, M, or to the ends, E, of the panel; the third letter, L_3, relates either to flexural cracking, C, or flexural yielding, Y, of the concrete layers. The failure stages of the connectors in Table 8-1 are defined as #L, where the number # refers to the row number of the connectors given in Figure 7-12, and the letter L refers either to the yielding, Y, or failure, F of the connectors as defined in Figure 8-6.

Table 8-1: Failure stages of the tested PICP found by numerical results.

Members	Acronym	Description
Failure stages of the concrete layers	BMC	Cracking of the mid-span of the bottom concrete layer.
	BMY	Yielding of the mid-span of the bottom concrete layer.
	BEC	Cracking of the ends of the bottom concrete layer.
	TMC	Cracking of the mid-span of the top concrete layer.
	TEC	Cracking of the ends of the top concrete layer.
Failure stages of ZSPC	#Y	Yielding of ZSPC (Figure 8-6) in the #th row of connectors (Figure 7-12).
	#F	Failure of ZSPC (Figure 8-6) in the #th row of connectors (Figure 7-12).

Numerical results of P-series panels using MLE method

Figure 8-12 shows the numerical and experimental out-of-plane total vertical load, F, against the mid-span deflection, Δ_v, for the tested P-series panels. The numerical results include two scenarios; tension stiffening of the concrete layers is considered in one scenario and neglected in the other. The numerical failure stages of the panels are also given on the graphs.

Figure 8-12 shows that failure of the P-series panels predicted using the numerical model starts with cracking of bottom layer followed by cracking of top layer. Yielding of the connectors starts from the ZSPC closest to the ends of the panel, i.e. the yielding of ZSPC occurs in the third row, second row, then first row of connectors (Figure 7-12). As an example the variation of shear forces of ZSPC vs. the mid-span deflection of the P4-16 panel is shown in Figure 8-13. As shown in this figure, ZSPC in the third row of connectors that are closest to the panel's end, have yielded first at Δ_v of 5.17 mm. Then, ZSPC in the second row yielded at Δ_v of 6.8 mm, and finally ZSPC in the first row that are closest to the mid-span yielded.

For P-series panels with 16 gauge ZSPC, the connectors in the third and second row (Figure 7-12) reached their failure point depicted by drops in the out-of-plane load resistance of the panels. These drops derived from the numerical results fall within the plateau regions observed in the experimental load-deflection graphs (Figure 7-8). This reinforces the argument discussed in

Section 7.3 that the plateau regions observed in load-displacement behaviour of the tested P-series panels with 16 gauge connectors might have happened due to failure of ZSPC.

Figure 8-12 shows that except for P3-16, all P-series panels with 16 gauge connectors reached the flexural yielding of the bottom concrete layer, after which, the out-of-plane load continued to increase due to the load resistance of the top concrete layer. As an example, Figure 8-14 shows the mid-span bending moment of the concrete layer vs. Δ_v for P4-16. As shown in this figure mid-span bending moment of the top and bottom concrete layers when tension stiffening is considered linearly increased up to their cracking flexural strength, after which the slope of graphs dropped due to reduced flexural stiffness of the concrete layers after cracking.

At Δ_v of 28 mm, where the first row of ZSPC yields (Figure 8-13), the bending moment of the top and bottom concrete layers of P4-16 starts increasing at higher rate (Figure 8-14). The reason can be explained by the free body diagram of the panels shown in Figure 8-7. As shown in this figure, the total mid-span bending moment is carried by sum of bending moment resistance of concrete layers and the couple moment produced by the axial forces of the concrete layers. Axial forces at the mid-span of the concrete layers are equal to the total shear forces carried by the connectors in half length of the panel. As the interlayer connectors start yielding from the ZSPC closest to the panel's ends, the interlayer shear stiffness decreases, after which lesser axial forces in the concrete layers are produced with increased external loading. This concept is presented in Figure 8-15, which shows the axial force at the mid-span of concrete layers vs. Δ_v for P4-16. As shown in this figure after Δ_v of 6.8 mm, where the third and second rows of connectors have yielded in the MLE model with tension stiffening, the slope of the corresponding graphs in Figure 8-15 has significantly dropped. And, after Δ_v of 28 mm, where all the connectors have yielded, the axial forces of the concrete layers stay constant, meaning the interlayer shear stiffness of panel is zero. Therefore, after Δ_v of 28 mm in MLE model of P4-16 with tension stiffening, all the added total bending moment produced by the external loading is carried by the concrete layers. And thus, after Δ_v of 28 mm the bending moment of the concrete layers starts increasing at higher rate (Figure 8-14).

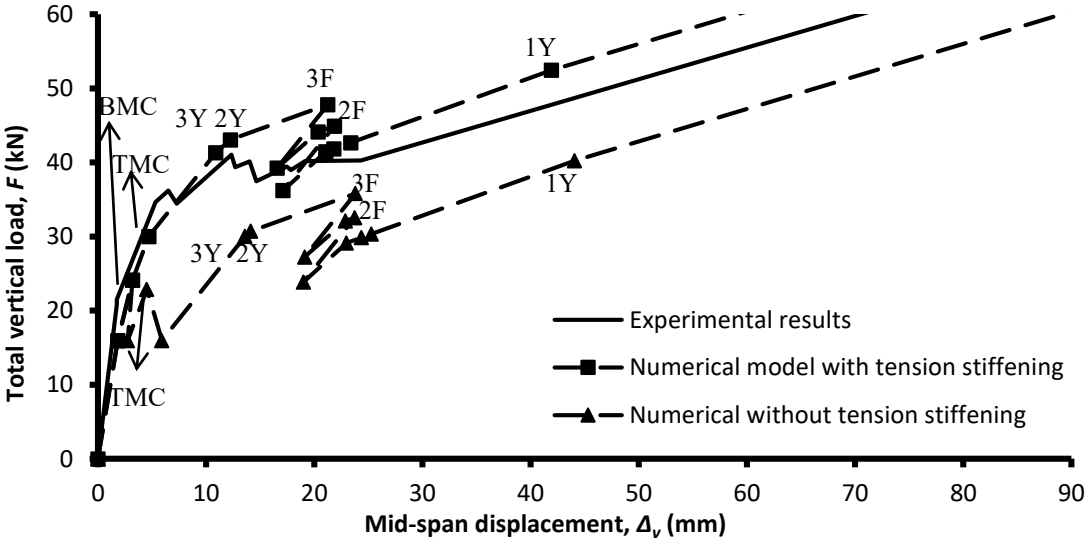

a. P3-16

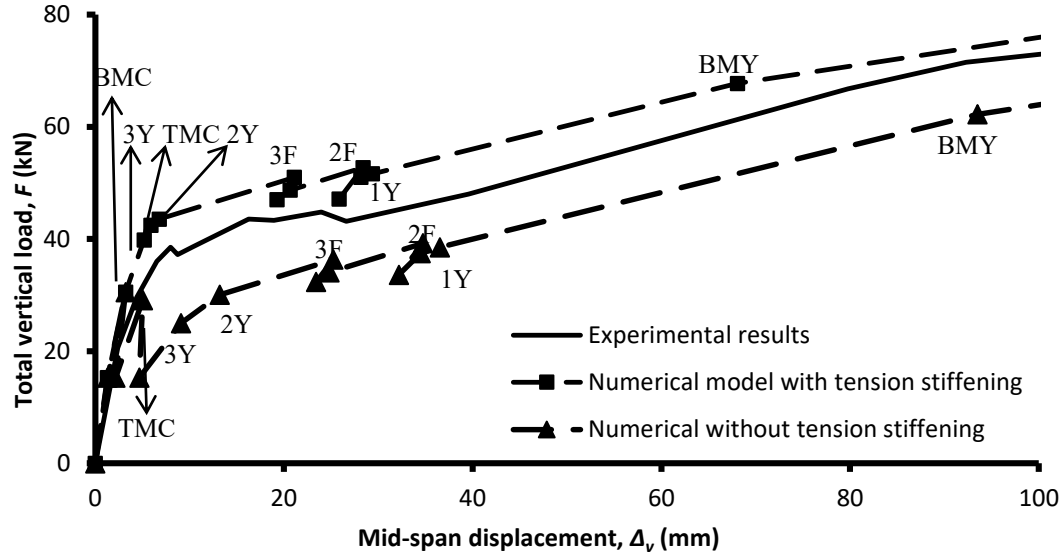

b. P4-16

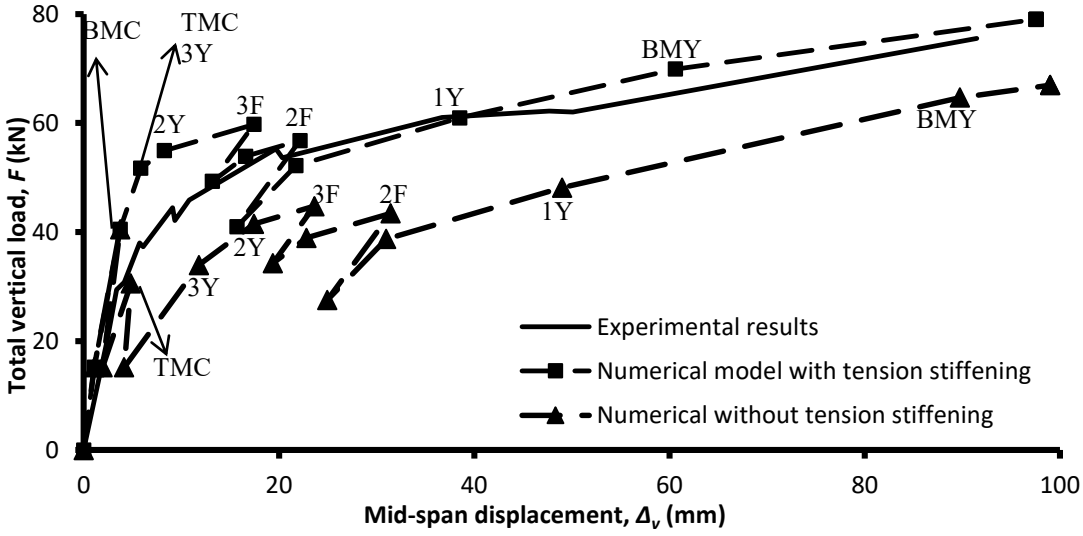

c. P6-16

Figure 8-12: Total vertical load vs. mid-span deflection for a. P3-16, b. P4-16, c. P6-16 and d. P4-10.

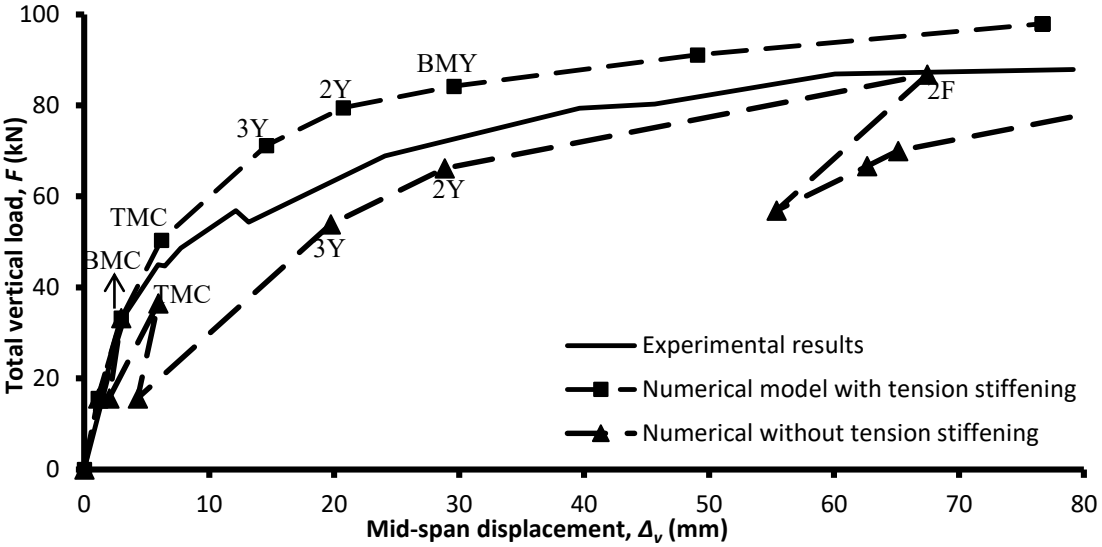

d. P4-10

Figure 8-12(Cnt'd): Total vertical load vs. mid-span deflection for a. P3-16, b. P4-16, c. P6-16 and d. P4-10.

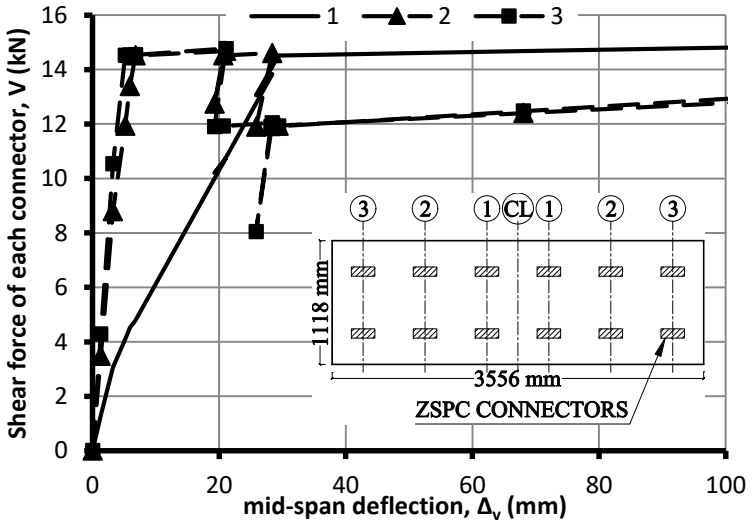

Figure 8-13: Analytical shear force of ZSPC in P4-16 vs. mid-span vertical deflection.

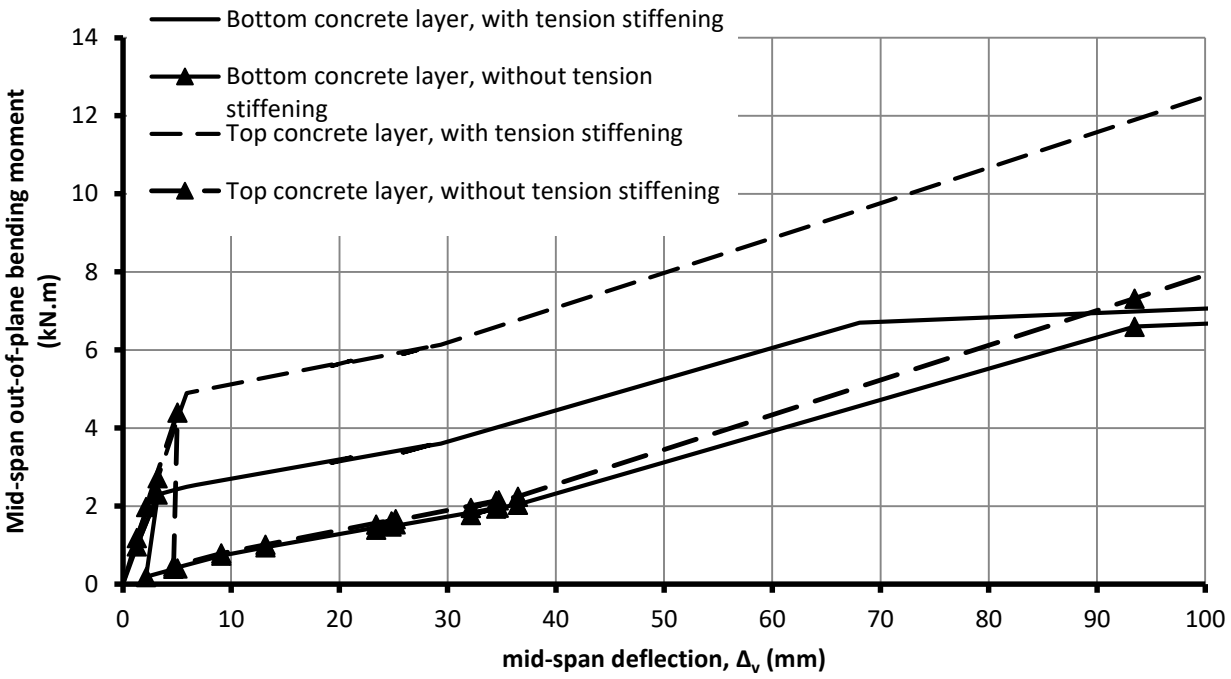

Figure 8-14: Analytical mid-span bending moment of concrete layers of P4-16 vs. mid-span deflection.

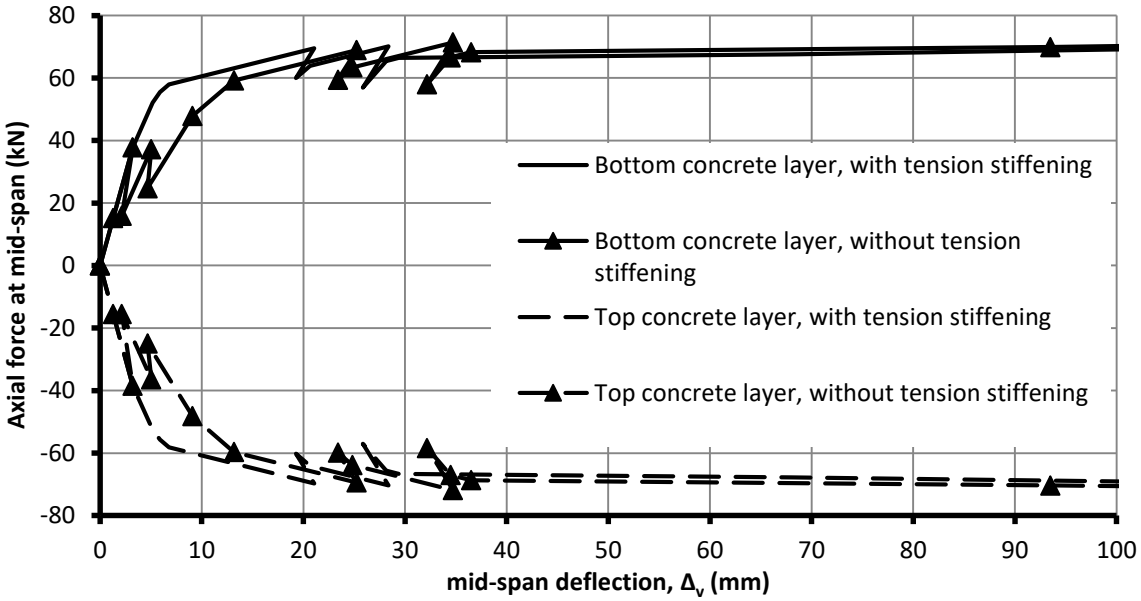

Figure 8-15: Analytical axial force of concrete layers of P4-16 vs. mid-span deflection.

Numerical results of PB-series panels using MLE method

Figure 8-16 compares the numerical results with the experimental out-of-plane load-deflection behaviour of PB-series panels. The numerical results include two scenarios; tension stiffening of the concrete layers is considered in one scenario and neglected in the other. The numerical failure

stages of the panels are also given on the graphs. The results of MLE models in Figure 8-16 shows that cracking order of PB-series panels was: cracking of the ends of the bottom concrete layer (BEC), cracking of the mid-span of the bottom concrete layer (BMC), cracking of the ends of the top concrete layer (TEC), then cracking of the mid-span of the top concrete layer (TMC). After the cracking stages of the PB-series panels the ZSPC in the second row of connectors reached their yield strengths in the numerical results. Then, the ends and mid-span of the bottom concrete layer reached their flexural yielding strength, M_y in Figure 8-10. After flexural yielding of the bottom concrete layer, the slope of the F-Δ_v diagram decreases as the flexural stiffness of the bottom concrete layer reduces to zero. Figure 8-17 shows the variation of shear forces in the ZSPC of PB3-16 and PB6-16 with respect to their mid-span deflections. This figure shows that in the PB-series panels the ZSPC in the second row of the connectors yielded first, then the ZSPC in the first and third row of connectors yielded at mid-span deflection of about 75 mm, suggesting that the interlayer shear forces around the panel's end is primarily taken by the end-beams. This might be due to the large shear stiffness of the end-beams relative to the connectors.

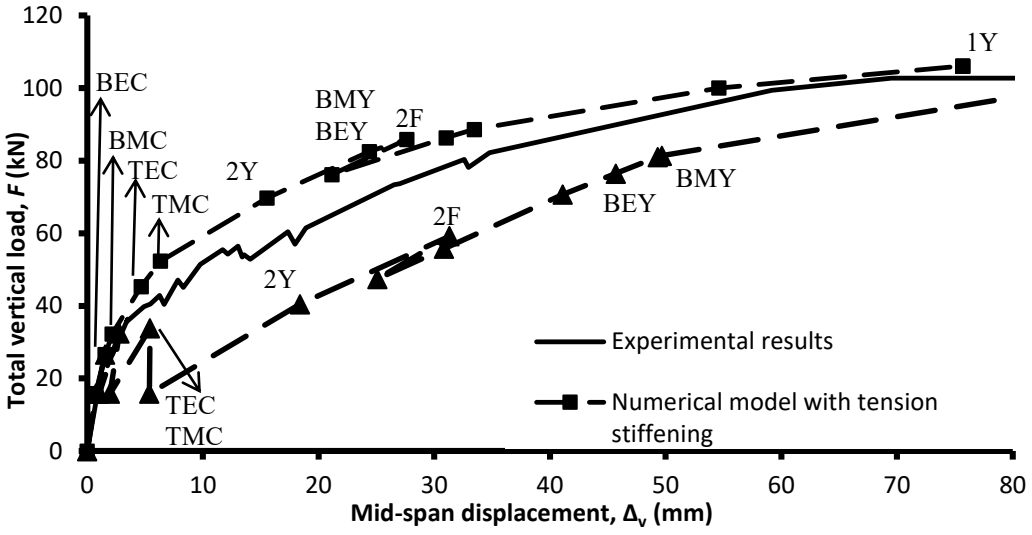

a. PB3-16

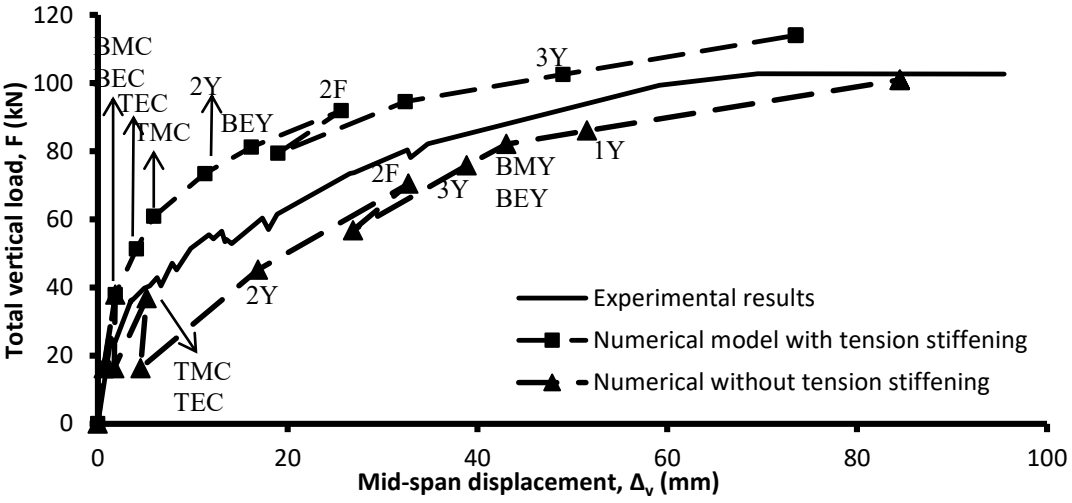

b. PB6-16

Figure 8-16: Total vertical load vs. mid-span deflection for a. PB3-16, b. PB4-16.

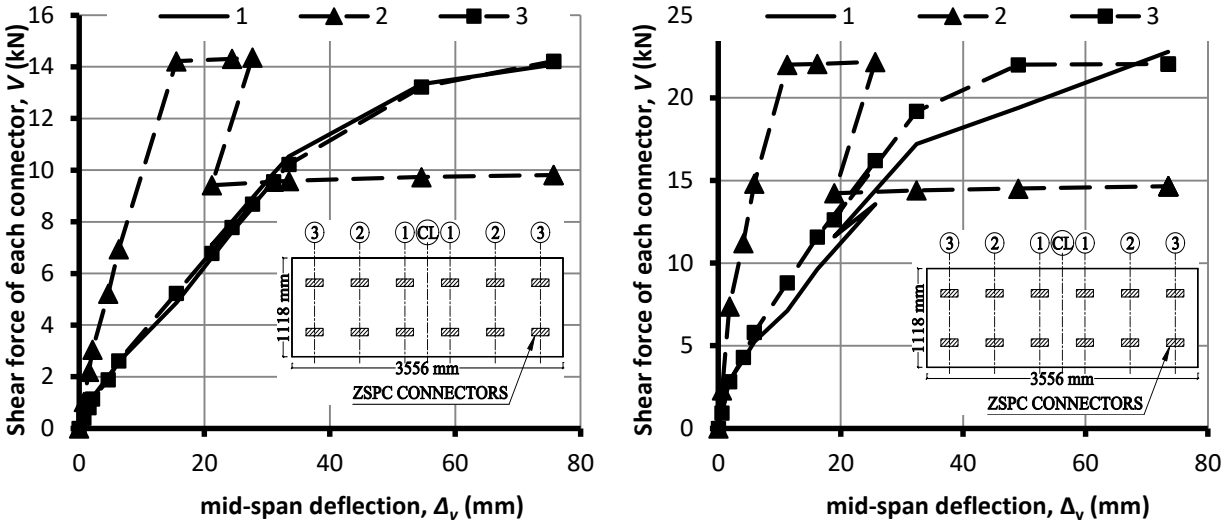

a. b.

Figure 8-17: Analytical shear force of ZSPC in a. PB3-16, and b. PB6-16 vs. mid-span vertical deflection.

Effect of tension stiffening on the numerical results of the tested panels

Figure 8-12 and Figure 8-16 show that in general MLE model with tension stiffening overestimated the load-deflection behaviour of all tested panels throughout loading. However, there are minor exceptions to this general trend. The MLE model with tension stiffening gave conservative estimates for out-of-plane load-deflection behaviour of P3-16 from zero deflection up to the deflection of about 8.0 mm. And it gave conservative estimates for load-deflection behaviour of P6-16 from the deflection of 20.0 mm to 40.0 mm. If these exceptions are neglected, the MLE model with tension stiffening can be considered as an upper bound for the out-of-plane behaviour of the tested panels. The MLE model without tension stiffening, however, gave conservative results for the out-of-plane load-deflection behaviour of the panels.

Table 8-2: Root mean square of the estimated results by the MLE model.

			Results of MLE method			
			With tension stiffening		Without tension stiffening	
Panel	$\Delta_{v,f}$ **(mm)**	**E (kJ)**	F_{rms}	**COV%**	F_{rms}	**COV%**
P3-16	65.8	2.896	4.04	9.2	9.94	22.6
P4-16	99.4	5.251	6.13	11.6	10.00	18.9
P6-16	91.4	5.428	5.15	8.7	13.76	23.2
P4-10	76.7	3.920	7.30	14.3	8.10	15.8
PB3-16	76.1	5.986	7.07	9.0	17.50	22.2
PB6-16	73.7	5.718	13.49	17.4	11.87	15.3
Average				11.7		19.7

Notes: E= Absorbed energy of the panel equal to the area under experimental load-deflection graphs. F_{rms}= Root mean square of total vertical load COV= Coefficient of variation.

Table 8-2 gives the root mean square of the predicted out-of-plane load, F_{rms}, estimated by the MLE models with and without tension stiffening. F_{rms} is calculated by the following equation.

$$F_{rms} = \sqrt{\frac{\int_{\Delta_v=0}^{\Delta_{v,f}} \left(F_{exp} - F_{MLE}\right)^2 . d\Delta_v}{\Delta_{v,f}}} \qquad \textbf{8-16}$$

Where, F_{exp} and F_{MLE} are the total out-of-plane loads from the experiments and MLE model, respectively. In this equation Δ_v is the out-of-plane mid-span deflection and $\Delta_{v,f}$ is the final out-of-plane mid-span deflection for which the experimental and numerical results are available. Table 8-2 also gives the absorbed energy of the flexural tests, E, which is defined as the area under the out-of-plane load-deflection graphs. The average experimental out-of-plane load carried by each panel throughout loading is equal to $E/\Delta_{v,f}$. The coefficient of variation, COV%, is then defined as the root mean square of the estimated out-of-plane load, F_{rms}, divided by the average experimental out-of-plane load, as given by the following equation.

$$COV\% = \frac{F_{rms}\Delta_{v,f}}{E}\% \qquad \textbf{8-17}$$

The coefficient of variation is adopted here as a measure to assess the accuracy of MLE model. Table 8-2 shows that the coefficient of variation, COV%, for MLE models with tension stiffening varies from 9.0% to 17.4% with an average value of 11.7%. The coefficient of variation for MLE models without tension stiffening varies from 15.3% to 23.2% with an average value of 19.7%. With the exception of PB6-16, the coefficient of variation for MLE models with tension stiffening is smaller than that without tension stiffening. Also, the average COV% for the MLE models with tension stiffening is 8% smaller than that without tension stiffening. This suggests that considering tension stiffening in the MLE models gives better estimates of the load-deflection behaviour of PICP; these estimates, however, are non-conservative. The MLE model without tension stiffening has lower accuracy in estimating the load-deflection behaviour of PICP and give conservative results.

8.3.4. Discussion of the Proposed Numerical Analysis

Numerical analyses conducted by previous researchers involved micro-modeling of insulated panels. In this modeling technique the concrete layers can be modeled as solid elements (Newberry et al. 2010, Lee 2003) or shell elements (Benayoune et al., 2008) and the nonlinear properties of concrete in compression and tension is considered. The reinforcing bars are modeled as truss elements with nonlinear metal properties. And truss connectors can be modeled as truss or beam elements (Benayoune et al. 2008, Bush and Wu 1998, Einea 1992). The effect of insulation can also be considered using solid elements in contact with concrete elements (Lee, 2003).

Numerical analysis of PICP using micro modeling of PICP can estimate the out-of-plane behaviour of PICP with good accuracy. However, this modeling technique slows down the numerical analysis. If the global behaviour of PICP is of interest, micro-modeling of the panels seems unnecessary. In this section, the MLE method was proposed as an alternative to micro-modeling of PICP. The MLE method gave good estimates of the out-of-plane behaviour of the tested panels. In this method, concrete layers were modeled as shell elements, and instead of modeling the

reinforcing bars, the out-of-plane moment-curvature behaviour of the concrete layers under different levels of axial forces was assigned to the shell elements.

Also, instead of modeling the Z-shaped connectors with connector-concrete interaction, the connectors were modeled as shear springs. The shear behaviour of the springs was derived from the shear tests of the connectors presented in Chapter 4. This technique of modeling interlayer connectors was also done by Newberry et al. (2010). They modeled interlayer connectors as shear springs in numerical analysis of push-off shear tests, and verified their numerical model with the results of these tests. Then, they used shear springs to model connectors in their flexural tests. Newberry et al. (2010) found that using shear springs to model interlayer mechanical connectors in numerical modeling of PICP gives good estimates of the experimental out-of-plane load displacement behaviour.

The MLE method is faster in calculating the global response of PICP, and thus can be used in design of insulated panels. This method is adopted in the next chapter to estimate the out-of-plane deflection and strength of PICP with different interlayer connector systems tested by other researchers.

8.4. Summary and Conclusion

This chapter presented the results of the nonlinear FEA analysis of the tested PICP using a newly developed Multistep Linear Elastic (MLE) method. This proposed model assumes small deformation of the panel under out-of-plane loading. In these numerical models, the concrete layers were modeled as shell elements and the ZSPC were modeled as shear springs. Interaction of axial forces and out-of-plane bending moments was considered in defining the nonlinear behaviour of the concrete shell elements. For each panel, two numerical models were developed: the first model considered tension stiffening of concrete and the second model neglected the effect of tension stiffening. The simplified experimental shear behaviour of ZSPC was considered in defining the nonlinear shear behaviour of the shear springs.

The numerical results showed that considering concrete tension stiffening gives non-conservative predictions and neglecting tension stiffening of concrete gives conservative predictions of the out-of-plane load-deflection behaviour of the tested panels. Although the predicted out-of-plane

behaviour of the panels by the numerical models with considering concrete tension stiffening was non-conservative, these models gave better predictions than the numerical models without considering concrete tension stiffening.

The failure stages of the numerical models showed that in P-series panels, concrete cracking first occurred at mid-span of the bottom concrete layer, then at the mid-span of the top concrete layer. In PB-series panels concrete cracking first occurred at the ends, then at the mid-span of the bottom concrete layer. Afterwards, concrete cracking occurred at the ends, then at the mid-span of the top concrete layer. These cracking patterns agree with the observations during the tests.

In the numerical models yielding of ZSPC of the P-series panels started from the connectors closest to the ends of the panels. However, yielding of ZSPC of the PB-series panels started from the connectors between the mid-span and the ends of the panels. This indicates that the end-beams altered the distribution of interlayer shear forces among the connectors.

9. Proposed Simplified MLE Method for Analysis of PICP

9.1. Introduction

Multistep Linear Elastic (MLE) analysis method is adopted in this chapter to propose a simplified MLE method to estimate the design parameters - out-of-plane deflection, cracking, and ultimate strengths - of PICP with different interlayer connector systems with and without end-beams. This simplified MLE method is then adopted to estimate the out-of-plane design parameters of PICP with different discrete and continuous connectors tested by previous researchers. The simplified MLE method proved to give conservative estimates of out-of-plane design parameters of PICP with good agreement with the experimental results.

The simplified MLE method is then used to develop an analytical procedure to estimate the out-of-plane design parameters of simply supported PICP under out-of-plane uniform loading. For this, a measure for degree of composite action of PICP is defined, and the variation of the degree of composite action with the interlayer shear stiffness of PICP is determined for panels with and without end-beams. Knowing the shear stiffness of interlayer mechanical connectors gives the degree of composite action of the panel, which is then used to estimate the out-of-plane design parameters of PICP. This analytical method is shown to compare well with the experimental results of PICP tested by previous researchers.

9.2. Simplified MLE Method for Analysis of PICP

9.2.1. Modeling

Insulated concrete panels can be modeled as two concrete layers, interlayer mechanical connectors and, if present, end-beams. The concrete layers are suggested to be modeled as shell elements. The distance between the shell elements are assumed to be the distance between the mid-thickness of the concrete layers (h_c). For the simplified MLE analysis of PICP, the out-of-plane flexural and axial stiffness of the shell elements of the concrete layers before and after cracking should be identified. This stiffness values can be found by performing moment-curvature analysis on the cross section of each concrete layer. In lieu of moment-curvature analysis, the uncracked flexural and axial stiffness of the cross section of individual concrete layers can be calculated as $E_c I_l$, and

E_cA_l, respectively, where E_c is the modulus of elasticity of concrete, I_l and A_l are the moment of inertia and gross area of the uncracked cross section of the concrete layer, respectively.

The cracked flexural stiffness of the concrete layers can be calculated as $E_c\ I_{l,cr}$, where $I_{l,cr}$ is the moment of inertia of the cracked cross section of the concrete layer, which is found by equations 9-1 and 9-2, respectively.

$$I_{l,cr} = Bc^3/3 + nA_s(d-c)^2 \quad \textbf{9-1}$$

$$A_{l,cr} = Bc + nA_s \quad \textbf{9-2}$$

Where B is the panel width, n is E_s/E_c, d and c are the depths of the longitudinal reinforcement and the neutral axis of the cracked section, respectively, measured from the top of the cross section as shown in Figure 9-1.

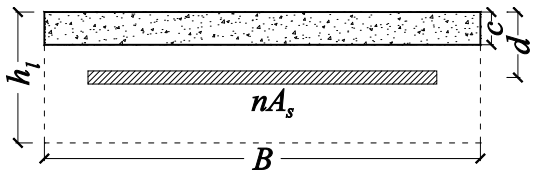

Figure 9-1: Cracked cross section of concrete layer.

Discrete interlayer mechanical connectors can be modeled as shear springs, where the shear stiffness can be derived from the shear test results available in the literature. And continuous mechanical connectors can be modeled as shell elements; the shear stiffness of these shell elements, Gtl/h_c, should be equal to the shear stiffness of the continuous connectors derived from shear test results, that is:

$$Gtl/h_c = k_s l \quad \textbf{9-3}$$

Where G is the shear modulus of elasticity of the shell element, t is the thickness of the modeled shell elements and h_c is the distance between the shell elements, equal to the distance between the mid-thickness of the concrete layers. In equation 9-3, k_s is the shear stiffness of the continuous

connector per unit length of the connector and l is the length of the connector. This equation gives the G value for the shell element as follows:

$$G = \frac{k_s h_c}{t} \qquad \text{9-4}$$

When G is calculated using equation 9-4, equation 9-3 holds true, i.e. the connector shell elements will have the same shear stiffness as the continuous shear connectors regardless of the thickness of shell elements, t. Thus, t is an arbitrary value. In this chapter t is taken as 10 mm.

The axial modulus of elasticity of the shell elements of continuous connectors along the panel, i.e. E_{xx} in Figure 9-2, is assigned infinitesimal value so they do not contribute to the flexural strength of the modeled PICP. Also, compression of insulation is not considered in this analysis, thus the axial stiffness of the shell elements along the thickness of the panel, i.e. E_{yy} in Figure 9-2, should be enough to prevent substantial reduction of h_c. In this chapter E_{yy} is assigned 200 GPa, the same as the modulus of elasticity of steel.

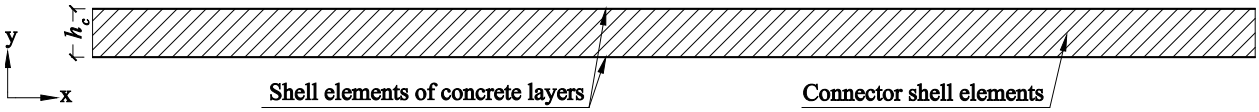

Figure 9-2: Modeling of concrete layers and continuous connectors using shell elements.

9.2.2. Out-of-Plane Cracking Strength

The panel is modeled with the concrete layers having flexural and axial stiffness of the uncracked cross section, which is $E_c I_l$ and $E_c A_l$, respectively. The service out-of-plane load, q_s, is applied on the panel and a linear elastic analysis is conducted. At every cross section of the panel, one layer undergoes compression and the other undergoes tension. To find the cracking strength of the panel the tensile stress at the critical section should be compared to the concrete tensile strength, f_t. The axial tensile force, P_t, and bending moment of the tensile concrete layer at the critical section, M_t, is derived from the linear elastic analysis, then the tensile stress is calculated as:

$$\sigma = \frac{P_t}{A_{lt}} + \frac{M_t}{S_{lt}} \quad \textbf{9-5}$$

Where S_{lt} and A_{lt} are the section modulus and the area of the uncracked cross section of the tensile concrete layer, respectively. In equation 9-5, P_t is the tensile axial force of the tensile concrete layer, thus is positive; and M_t is the bending moment of the tensile concrete layer. Now the out-of-plane uniform load corresponding to the cracking strength of PICP is calculated as:

$$q_{cr} = \frac{\sigma}{f_t} q_s \quad \textbf{9-6}$$

Where f_t is the tensile strength of concrete that can be calculated according to CAN/CSA-A23.3-04.

9.2.3. Out-of-plane Mid-Span Deflection under Service Loads

To estimate the out-of-plane deflection of PICP first the service uniform load, q_s, is applied on the panel with uncracked concrete properties, then a linear elastic analysis is conducted and the cracking strength is calculated as described in Section 9.2.2. If the cracking load is larger than the service load, the panel remains uncracked under the service load. The out-of-plane deflection is then equal to the deflection calculated by linear elastic analysis of the uncracked panel, Δ_0, thus:

$$\Delta_t = \Delta_0 \quad \textbf{9-7}$$

It should be ensured that the critical connector, i.e. the connector with the largest shear force, does not fail under service load. Thus, the shear force in the critical interlayer connector, $V_{max,}$ should be less than the shear strength of the connector found from shear test results, V_r.

$$V_{max} < V_r \quad \textbf{9-8}$$

If the cracking strength of the panel is smaller than the service load, the out-of-plane deflection of PICP will have two components: pre-cracking deflection, Δ_0, and post-cracking deflection, Δ_{cr}. The total out-of-plane mid-span deflection is the sum of pre- and post- cracking out-of-plane deflections.

$$\Delta_t = \Delta_0 + \Delta_{cr} \quad \textbf{9-9}$$

The pre-cracking deflection, Δ_0, is calculated using the results of a linear elastic analysis of uncracked PICP under q_s as follows:

$$\Delta_0 = \frac{q_{cr}}{q_s}\Delta_1 \quad \textbf{9-10}$$

Where Δ_1 is the mid-span deflection of the uncracked PICP model under q_s, and q_{cr} is the cracking strength calculated as described in Section 9.2.2.

To calculate Δ_{cr}, first the regions of both concrete layers of the panel where $\sigma > f_t$ under q_s should be assigned cracked concrete properties, where σ is calculated by equation 9-5 and is derived from the linear elastic analysis of the uncracked PICP under q_s. Then a linear elastic analysis of the cracked PICP model under service load is conducted and the mid-span deflection of the cracked PICP under q_s, Δ_2, is derived from the numerical results. The principle of superposition is then adopted to calculate the post-cracking deflection, Δ_{cr}, as:

$$\Delta_{cr} = \left(1 - \frac{q_{cr}}{q_s}\right)\Delta_2 \quad \textbf{9-11}$$

Similar to the out-of-plane deflection, the maximum shear force in the critical interlayer connector has two components: pre-cracking shear force, V_0 , and post-cracking shear force, V_{cr}. The maximum shear force in the critical interlayer shear force is then equal to:

$$V_{max} = V_0 + V_{cr} \quad \textbf{9-12}$$

Then V_{max} should be less than the shear strength of the connector (equation 9-8). The pre-cracking maximum shear force in the critical interlayer connector, V_0, is calculated using the results of a linear elastic analysis of uncracked PICP under q_s as follows:

$$\mathrm{V}_0 = \frac{q_{cr}}{q_s}\mathrm{V}_1 \qquad \textbf{9-13}$$

Where V_1 is the maximum shear force of the critical interlayer connector of the uncracked PICP model under q_s. To calculate V_{cr}, similar to Δ_{cr}, the regions of both concrete layer of the panel where $\sigma > f_t$ under q_s should be assigned cracked concrete properties. Then a linear elastic analysis of the cracked PICP model under service load is conducted and the maximum shear force of the critical interlayer connector of the cracked PICP under q_s, V_2, is derived from the numerical results. Principle of superposition is then adopted to calculate the post-cracking maximum shear force of the critical interlayer connector, V_{cr}, as:

$$\mathrm{V}_{cr} = \left(1 - \frac{q_{cr}}{q_s}\right)\mathrm{V}_2 \qquad \textbf{9-14}$$

9.2.4. Out-of-Plane Ultimate Strength

Under out-of-plane loading, one concrete layer of PICP undergoes tension and the other undergoes compression. As described in Section 8.3.3 the MLE analysis of the tested PICP showed that concrete cracking first occurs in the tensile concrete layer, then in the compressive concrete layer. If tension stiffening of concrete is considered, after cracking of compressive concrete layer the out-of-plane stiffness of PICP drops and the out-of-plane resistance of PICP keeps increasing at smaller rate without any sudden drop. As the out-of-plane loading is increased the interlayer connectors yield and, depending on shear ductility of the connectors, shear forces are redistributed to other connectors. Meanwhile, as the tensile and compressive forces in the tensile and compressive concrete layers grow larger, the reinforcement of the concrete layers start yielding, and the compressive side of the compressive concrete layer undergoes large compressive stresses. With increased loading, shear deformation of the connectors increases until it reaches the failure shear deformation of the connectors. Depending on the design of the PICP either crushing of the concrete

of the compressive layer or failure of the interlayer connectors might govern the out-of-plane strength of PICP.

Here, the analytical approach proposed by Mouser (2003) is adopted and modified to estimate the out-of-plane ultimate strength of PICP. The analytical approach by Mouser (2003) is limited to PICP where the interlayer connectors yield earlier than the longitudinal reinforcement. In the modified and extended Mouser (2003) method here, the shear strength of the interlayer connectors between the locations of minimum and maximum interlayer shear force, V_{con}, is derived by assuming an appropriate distribution of interlayer shear deformations along the panel between the locations of zero and maximum shear force over the cross section of the panel. This distribution can be derived from the numerical model of PICP. The maximum point of this distribution is taken as Δ_{sf}, failure shear deformation of connector. This failure deformation is derived from the shear test results of the connector. Then, the interlayer shear deformation and interlayer shear force of each connector can be found. The sum of these shear forces is equal to V_{con}.

Now, if the shear strength of the interlayer connectors between the locations of minimum and maximum interlayer shear force, V_{con}, is smaller than the yield force of the longitudinal reinforcement, i.e. $V_{con}<A_s f_y+A_{pr} f_{py}$, the concrete layers of the PICP model is assigned cracked concrete properties (Section 9.2.1) and the shear stiffness of the interlayer connectors are reduced by μ, i.e.:

$$K_{s,m} = (1-\mu)K_s \qquad \textbf{9-15}$$

Where $K_{s,m}$ is the reduced shear stiffness of connectors and μ is the number of yielded connectors to the total number of connectors between the minimum and maximum interlayer shear forces of the panel. The numerical model of PICP with cracked concrete layers is called *cracked model,* hereafter. The ultimate out-of-plane strength can be derived using equation 9-16.

$$M_{t0} q_u = M_{lt,r} + M_{lc,r} + V_{con} h_c, \quad V_{con} < A_s f_y + A_{pr} f_{py} \qquad \textbf{9-16}$$

Where, M_{t0} is the total bending moment across the entire cross section of the panel at the critical section under unit load. In this equation A_s and A_{pr} are the areas of non-prestressing and prestressing

reinforcement, respectively, and f_y and f_{py} are the yield stresses of the non-prestressing and prestressing reinforcement, respectively. In equation 9-16, $M_{lt,r}$ is the flexural capacity of the tensile concrete layer under a tensile force equal to V_{con}, and $M_{lc,r}$ is the flexural capacity of the compressive concrete layer under a compressive force equal to V_{con}. M_{t0} is derived from the linear elastic analysis of cracked model of PICP using equation 9-17.

$$M_{t0} = M_{lt,0} + M_{lc,0} + P_{l,0}h_c \quad \textbf{9-17}$$

Where $M_{lt,0}$ and $M_{lc,0}$ are the bending moment of the tensile and compressive concrete layers under unit load, respectively, and $P_{l,0}$ is the axial force of the concrete layers under unit load. In this equation $M_{lt,0}$, $M_{lc,0}$ and $P_{l.0}$ are derived from the linear elastic analysis of the cracked model of PICP with reduced interlayer shear stiffness under out-of-plane unit load.

The shear deformation of the critical connector under ultimate out-of-plane load, $\Delta_{s,u}$, should be less than its failure shear deformation, Δ_{sf}. $\Delta_{s,u}$ can be calculated as:

$$\Delta_{s,u} = \Delta_{s,0} + \Delta_{s,cr} \quad \textbf{9-18}$$

Where $\Delta_{s,0}$ is the shear deformation of the critical connector derived from the linear elastic analysis of the uncracked PICP model under q_{cr}, and $\Delta_{s,cr}$ is the shear deformation of the critical connector derived from the linear elastic analysis of the cracked PICP model with reduced interlayer shear stiffness under q_u-q_{cr},

If $V_{con} > A_s f_y + A_{pr} f_{py}$, the flexural reinforcement yields before failure of the critical connector. And thus, V_{con} cannot be mobilized and the interlayer shear force is bound by $A_s f_y + A_{pr} f_{py}$. Also, the tensile concrete layer cannot take any bending moment since its reinforcement has already yielded, i.e. $M_{lt,r}$ is zero. In this case, the ultimate out-of-plane strength can be derived as:

$$M_{t0} q_u = M_{lc,r} + \left(A_s f_y + A_{pr} f_{py}\right) h_c, \quad V_{con} > A_s f_y + A_{pr} f_{py} \quad \textbf{9-19}$$

Where, $M_{lc,r}$ is the flexural capacity of the compressive concrete layer under a compressive force equal to $A_s f_y + A_{pr} f_{py}$. In this equation M_{t0} can be calculated by equation 9-17, where $M_{lt,0}$, $M_{lc,0}$ and $P_{l,0}$ are derived from the linear elastic analysis of the cracked model of PICP under unit load.

9.2.5. Design of End-Beams

The shear force developed in the end-beams can be derived by the following equation:

$$V_{bm,u} = q_u V_{bm,0} \quad \text{9-20}$$

Where, $V_{bm,0}$ is the shear force of the end-beams when the panel is under out-of-plane unit load. If $V_{con} < A_s f_y + A_{pr} f_{py}$, $V_{bm,0}$ is derived from the linear elastic analysis of the cracked model of PICP with reduced interlayer shear stiffness under out-of-plane unit load and q_u is derived from equation 9-16. If $V_{con} > A_s f_y + A_{pr} f_{py}$, $V_{bm,0}$ is derived from the linear elastic analysis of the cracked model of PICP under out-of-plane unit load and q_u is derived from equation 9-19. After finding the shear force in the end-beams, $V_{bm,u}$ is compared against the shear strength of end-beams as:

$$V_{bm,u} < V_{bm,r} \quad \text{9-21}$$

Where $V_{bm,r}$ is found by the method outlined in CAN/CSA A23.3-04.

9.2.6. Comparison with Experimental Results

The proposed simplified MLE method to estimate out-of-plane design parameters of PICP is compared to eight prestressed PICP with different discrete and continuous interlayer connector systems tested by previous researchers, as given in Table 9-1. Two of the tested panels were 9.14 m and six were 3.05 m long. Five of the tested PICP had continuous interlayer connectors including FRP and steel truss connectors, GFRP grid, and expanded metal connectors. Three of the tested PICP had discrete interlayer connectors including composite pins, C-clips and M-ties. The thickness of the concrete layers of these panels varied from 63.5 mm to 82.5 mm and the insulation thickness varied from 50.8 mm to 76.2 mm.

Table 9-1: Properties of the PICP tested by previous researchers.

Panel No.	Researcher	Interlayer connector	b (m)	L (m)	t_c (mm)	t_{ins} (mm)	f_c (MPa)	Reinforcement
1	Salmon et al. (1997)	FRP truss	2.44	9.14	63.5	76.2	34.4	5-3/8" strands + 6x6 W4x4 (WWF)
2		Steel truss						
3	Naito et al. (2012)	CFRP grid	0.813	3.05	76.2	50.8	48.2	2-3/8" strands
4		Composite pin						
5		C-clip						
6	Mouser (2003)	Expanded metal	2.39	3.05	76.2	76.2	54.8	5-3/8" strands
7		Expanded metal			82.5	50.8	51.1	
8		M-tie			82.5	50.8	40.1	6-3/8" strands

Table 9-2: Mid-span deflection of previously tested PICP estimated by simplified MLE method.

Panel No.	Previous test	Interlayer connector	q kPa	Δ_e (mm)	Δ_t (mm)	$\frac{\Delta_e}{\Delta_t}$	$\Delta_t - \Delta_e$ (mm)
1	Salmon et al. (1997)	FRP truss	3.0	17.4	27.0	0.64	9.6
2		Steel truss	1.5	16.2	14.1	1.15	-2.1
3	Naito et al. (2012)	CFRP grid	18	3.0	3.4	0.88	0.4
4		Composite pin	15	3.1	5.8	0.53	2.7
5		C-clip	16	5.2	7.5	0.69	2.3
6	Mouser (2003)	Expanded metal	10	2.6	4.1	0.64	1.5
7		Expanded metal	10	3.6	2.9	1.24	-0.7
8		M-tie	10	3.4	4.1	0.83	0.7
Average						0.82	
Coefficient of variation %						31.0	

Table 9-2 compares the mid-span deflection of the PICP tested by previous researchers, Δ_e, with the analytical mid-span deflection, Δ_t, found by the proposed simplified MLE method. The uniform load q shown in this table is an arbitrary uniform load on the linear elastic region of the experimental load-displacement graphs. As given in Table 9-2, Δ_e/Δ_t ratios for the previously studied tested PICP vary from 0.53 to 1.24; and $\Delta_t - \Delta_e$ for these panels vary from -0.7 mm to 9.6 mm. It should be noted that for panel no. 2 and no. 7, Δ_e/Δ_t is larger than one, meaning the proposed simplified MLE method underestimates the experimental mid-span deflection for these two panels. However, this underestimation is only 2.1 mm and 0.7 mm for panel no. 2 and 7, respectively (Table 9-2).

Table 9-3 compares the experimental out-of-plane ultimate cracking and ultimate strengths of PICP tested by previous researchers, $q_{cr,e}$ and $q_{u,e}$, respectively, to the estimated cracking and ultimate strengths by the proposed simplified MLE method, $q_{cr,u}$ and q_u, respectively. The experimental cracking strength is taken as the out-of-plane strength beyond which there is considerable drop in the out-of-plane stiffness of the panel, i.e. considerable drop in the slope of the experimental load-deflection graph. And $q_{cr,e}$ is compared with $q_{cr,u}$, which is associated with considerable drop in the analytical out-of-plane stiffness of PICP when the compressive concrete layer cracks.

Table 9-3 shows that $q_{cr,e}/q_{cr,u}$ varies from 1.01 to 1.40 with average value of 1.14 and coefficient of variation of 10.76%; and $q_{u,e}/q_u$ varies from 0.98 to 1.50 with average value of 1.24 and coefficient of variation of 17.59%. This means that the simplified MLE method provides conservative estimates of the ultimate cracking and ultimate strength of these previously studied panels with different interlayer connector systems with 14% and 24% error, respectively.

Table 9-3: Out-of-plane cracking and ultimate strength of previously tested PICP estimated by simplified MLE method.

Panel no.	Researcher	Interlayer connector	Ultimate cracking strength			Ultimate strength		
			$q_{cr,e}$	$q_{cr,u}$	$\frac{q_{cr,e}}{q_{cr,u}}$	$q_{u,e}$	q_u	$\frac{q_{u,e}}{q_u}$
1	Salmon et al. (1997)	FRP truss	5.74	4.10	1.40	8.14	5.41	1.50
2		Steel truss	3.83	3.32	1.15	5.67	4.11	1.38
3	Naito eta al. (2012)	CFRP grid	23.4	23.3	1.01	32.7	24.0	1.36
4		Composite pin	15.2	13.9	1.09	31.7	32.33	0.98
5		C-clip	14.47	10.7	1.33	28.9	22.8	1.27
6	Mouser (2003)	Expanded metal	20.5	19.94	1.03	25.0	19.9	1.25
7		Expanded metal	17.0	15.3	1.11	23.0	19.3	1.19
8		M-tie	13.0	10.07	1.29	21.0	20.4	1.03
Average					1.14			1.24
Coefficient of variation %					11.0			18.0

9.3. Analysis of Simply Supported PICP under Out-of-Plane Uniform Loading

9.3.1. Introduction

Since the majority of PICP are simply supported at their top and bottom, the simplified MLE method for analysis of PICP are adopted in this section to develop an analytical procedure for simply supported PICP under uniform loading without the need for numerical modeling. As the interlayer shear stiffness of PICP is increased their out-of-plane flexural stiffness is improved. In Section 9.3.2 a dimensionless parameter K/K_0 is defined, where K is the total interlayer shear stiffness of PICP and K_0 is a factor called *basic interlayer shear stiffness* in this study. Then the degree of composite action is defined in terms of the out-of-plane mid-span deflection of PICP. Afterwards in Section 9.3.3 parametric analysis is conducted on PICP with and without end-beams. The PICP in these analyses vary in length, thickness of insulation and concrete layers, and shear

stiffness of interlayer mechanical connectors. The results of this parametric analysis are adopted to correlate the degree of composite action to K/K_0. This correlation is then adopted in Section 9.3.4 to estimate the out-of-plane deflection, cracking and ultimate strengths of simply supported PICP with and without end-beams under uniform out-of-plane loading. This proposed analytical model is compared against the experimental results in section 9.3.5.

9.3.2. Basic Interlayer Shear Stiffness and Degree of Composite Action

Basic interlayer shear stiffness

The out-of-plane stiffness of PICP is affected by the total interlayer shear stiffness of the panel. The total interlayer shear stiffness is defined as the shear stiffness of interlayer mechanical connectors between locations of minimum to maximum interlayer shear forces, i.e. locations of minimum to maximum cross sectional shear forces since interlayer and cross sectional shear forces are proportional to each other. Therefore, for simply supported PICP, the total interlayer shear stiffness is the total shear stiffness of interlayer mechanical connectors between one end and mid-span of the panel. In this section the dimensionless value of K/K_0 is defined, where K is the total interlayer shear stiffness of simply supported panel between one end and the mid-span of the panel, and K_0 is the basic shear stiffness. K_0 is found by idealization of the out-of-plane behaviour of the fully-composite panel. In Section 9.3.3 the degree of composite action is related to K/K_0.

In this section it is desired to relate the out-of-plane deflection and interlayer shear forces of PICP to the out-of-plane behaviour of fully-composite and non-composite panels. The out-of-plane flexural behaviour of fully-composite and non-composite panels are calculated using Bernoulli beam theorem. Based on this theorem, the interlayer shear stiffness of a panel has to be infinite so that its out-of-plane flexural behaviour can be approximated as a fully-composite panel. If the interlayer shear stiffness is insufficient, the interlayer shear deformations are substantial, and the out-of-plane flexural behaviour of the panel would deviate from that of a Bernoulli beam. In this section it is attempted to find a K_0 parameter as a measure of interlayer shear stiffness beyond which the behaviour of panel can be approximated as a Bernoulli beam. For this, the following assumptions are made:

1. Panels are simply supported at the ends.

2. Cross section of the panel and the concrete layers is constant along the length of the panel

3. Concrete layers behave as Bernoulli beams.

4. Deformations are small.

Figure 9-3 shows the free body diagram of a simply supported panel under uniform loading. As shown in this figure, out-of-plane loads produce out-of-plane bending moment in each concrete layer, tensile forces in the tensile concrete layer and compressive forces in the compressive concrete layer. The tensile and compressive forces in the concrete layers induce an internal bending moment, therefore the total bending moment at every section of the panel is obtained by:

$$M_t = M_{lt} + M_{lc} + P_l h_c \qquad \text{9-22}$$

Where M_{lt} and M_{lc} are the out-of-plane bending moments carried by the tensile and compressive concrete layers, respectively, P_l is the axial force in the concrete layers and h_c is the distance between the centroids of the concrete layers (Figure 9-3). In a simply supported panel, the axial forces of concrete layers at the panel mid-span are equal to the total interlayer shear forces between the mid-span and the panel ends, V_t.

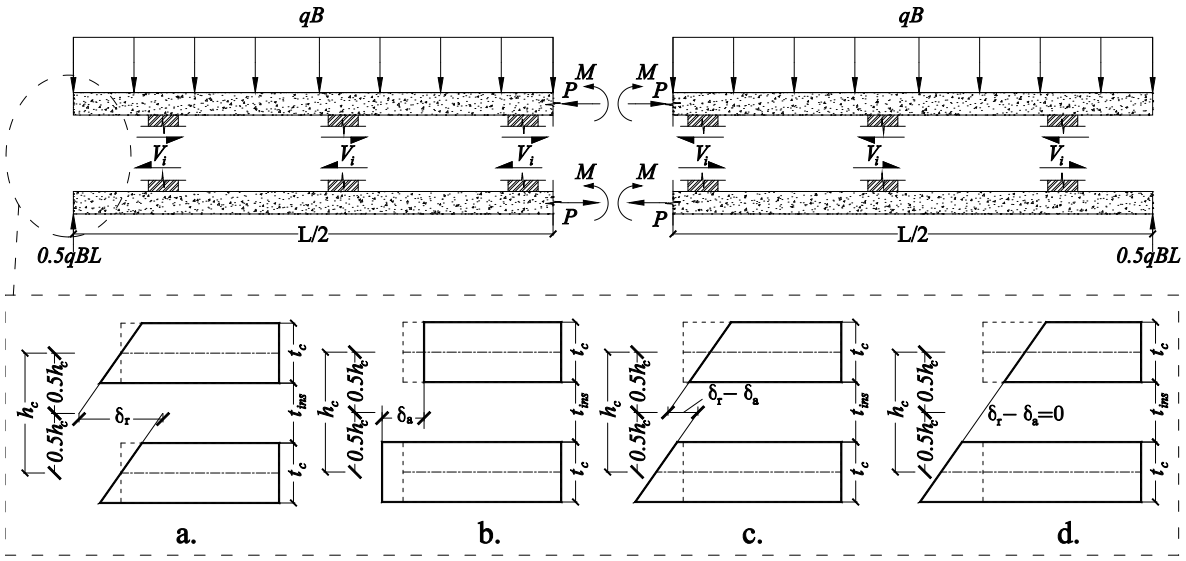

Figure 9-3: Free body diagram and idealized deformation of a simply supported PICP. Interlayer slippage due to a. flexural, b. axial and c. flexural and axial deformation of concrete layers. d. Deformation of panel ends in fully-composite PICP.

The basic shear stiffness, K_0, is defined as a value proportional to the total interlayer shear forces of a fully-composite simply supported panel, V_c, divided by the maximum interlayer shear deformation of a fully-composite panel, δ_c. The total interlayer shear forces, V_c, is the total interlayer shear forces between one end and mid-span of PICP, i.e. the locations of maximum and minimum interlayer shear forces in a panel that is simply supported at its ends. δ_c in a panel that is simply supported occurs at the ends of the panel. Therefore, K_0 is defined as V_c/δ_c. This K_0 has no physical meaning, instead it is just adopted here as a benchmark for the total interlayer shear stiffness of panels, beyond which the behaviour of PICP can be approximated as a fully-composite panel. This K_0 is used in the K/K_0 parameter to relate the behaviour of any PICP to the behaviour of theoretical non-composite and fully-composite panels. V_c is derived assuming Bernoulli beam theorem as:

$$V_c = \frac{qBL^2 A_l h_c}{16 I_c} \qquad \textbf{9-23}$$

Where q is the out-of-plane uniform load, B and L are the panel width and length, respectively. In equation 9-23, h_c is the distance between the centroids of the concrete layers, A_l is the cross sectional area of one concrete layer, and I_c is the moment of inertia of the cross section of the panel assuming fully-composite behaviour.

The maximum interlayer shear deformation of the panel is the distance between the tangential planes of the ends of the two concrete layers (Figure 9-3). This distance is equal to the horizontal distance between the tangential planes of individual concrete layers since deflections and rotations of the panel are considered to be small. In Figure 9-3, if the tangential plane of the tensile concrete layer is on the right of that of the compressive layer, the shear deformation of the interlayer connector is considered positive.

In a non-composite panel, the concrete layers only undergo out-of-plane bending moments. Since the thickness of concrete layers is considered the same, the out-of-plane bending moments produce rotations at the ends of the concrete layers of the panel, which makes a horizontal distance between the tangential planes at the ends of the concrete layers (Figure 9-3). This horizontal distance is the maximum interlayer shear deformation due to rotation only, δ_r, which is found by:

$$\delta_r = 0.5\theta_{lt}h_c + 0.5\theta_{lc}h_c \quad \textbf{9-24}$$

Where θ_{lt} and θ_{lt} are the rotation angles of the ends of the tensile and compressive concrete layers, respectively. If the out-of-plane bending moments in the panel is only produced by axial forces in the concrete layers, the maximum interlayer shear deformation due to axial deformation of the layers, δ_a, is derived by summing the shortening of the compressive layer and extension of the tensile concrete layer between one end and mid-span of the panel. The axial force in the concrete layer at every cross section is equal to the total interlayer shear force from that cross section to one end of the panel. Therefore, δ_a is equal to:

$$\delta_a = -\left(\frac{1}{E_c A_{lt}}\int_{x=0}^{0.5L} P \;\; dx + \frac{1}{E_c A_{lc}}\int_{x=0}^{0.5L} P \;\; dx\right) \quad \textbf{9-25}$$

Where, A_{lt} and A_{lc} are the cross sectional areas of the tensile and compressive concrete layers, respectively, and P is the axial force of the concrete layers at every cross section. It should be noted that δ_a is negative in this equation since the tangential plane of the tension concrete layer is on the left side of that of the compressive layer.

In a PICP the maximum interlayer shear deformation at the end of the panel is produced by superposition of rotation and axial deformation of the concrete layers, therefore the maximum shear deformation is:

$$\delta \;\; = \delta_r - \delta_a \quad \textbf{9-26}$$

The maximum interlayer shear deformation of a fully-composite panel, δ_c, can be found using equation 9-26. For a fully-composite panel using Bernoulli beam theorem the plane sections are assumed to remain plane across the entire thickness of the panel, and thus there is no distance between the tangential planes, meaning δ_c is zero. This is because in Bernoulli beam theorem the beam is assumed to be rigid in shear, i.e. infinite shear stiffness. This assumption of infinite shear stiffness does not apply to insulated panels. Therefore, the maximum interlayer shear deformation of a fully-composite panel, δ_c, is calculated as:

$$\delta_c = \delta_r - a_0\delta_a \quad \textbf{9-27}$$

To calculate δ_c by this equation, the parameter a_0 should be determined. Here, the thickness of concrete layers is assumed to be equal, and the end rotations of the concrete layers in a fully-composite panel are equal. Now, using equations 9-24, 9-25 and 9-27, δ_c can be found as:

$$\delta_c = \frac{qbL^3h_c}{24E_cI_c}\left(1 - \frac{a_0I_c}{A_lh_c^2}\right) \quad \textbf{9-28}$$

Where a_0 is a coefficient found in Section 9.3.3. Now K_0 is found as:

$$K_0 \propto \frac{V_c}{\delta_c} = \frac{1.5E_cA_l}{L\left(1 - \frac{a_0I_c}{A_lh_c^2}\right)} \quad \textbf{9-29}$$

Since only the form of K_0 is of interest to be used in the dimensionless value of K/K_0, the factor 1.5 in the numerator of equation 9-30 is dropped and K_0 is defined as:

$$K_0 = \frac{E_cA_l}{L\left(1 - \frac{a_0I_c}{A_lh_c^2}\right)} \quad \textbf{9-30}$$

Where a_0 is found to be 1.55 in Section 9.3.3 by finding the best fitting curve over the numerical results.

Degree of composite action

Different expressions have been proposed to define the degree of composite action by previous researchers including Pessiki and Mlynarczyk (2003), Culp (1994) and Salmon et al. (1997). Since the mid-span deflection of panel is of prime interest the expression by Pessiki and Mlynarczyk (2003) is adopted, which is in terms of the moment of inertia of non-composite and fully-composite panel. The expression by Pessiki and Mlynarczyk (2003) for the degree of composite action is modified as follows:

$$\beta = \frac{\Delta_{nc} - \Delta}{\Delta_{nc} - \Delta_c} \qquad \text{9-31}$$

Where Δ_c and Δ_{nc} are the out-of-plane mid-span deflection of PICP assuming fully- and non-composite behaviour, respectively. The advantage to this modified expression is that β found by equation 9-31 is equal to V_t / V_c as shown in Section 9.3.3, where V_t is the total interlayer shear forces between one end and mid-span of the panel, while V_c is the total interlayer shear force in a fully-composite panel derived by equation 9-23.

9.3.3. Parametric Study of Simply Supported PICP under Uniform Loading

Linear elastic analyses were conducted on different PICP with and without end-beams. The studied simply supported PICP varied in length, thickness of insulation and concrete layers, and shear stiffness of the interlayer connectors. The width of the studied panels was 2.0 m and the width of the end-beams was 150 mm.

Since the maximum in-plane interlayer shear forces of PICP occurs at the ends of the panels, the out-of-plane flexural behaviour of PICP is expected to be affected by the shear stiffness of the end-beams. This shear stiffness is determined by the depth and width of the end-beams. In this parametric study, since the overall thickness of the panels, which is equal to the depth of the end-beams, was variable, the in-plane shear stiffness of the end-beams along the length of the panels was variable as well. Thus, the results of this parametric study cover the effect of shear stiffness of the end-beams on the out-of-plane flexural behaviour of PICP.

Continuous connectors were modeled as 10 mm thick shell element with infinitesimal modulus of elasticity along the length of panel, E_{xx}, to eliminate contribution of the longitudinal stresses of the shell elements to the flexural behaviour of the panel. Discrete connectors were modeled as shear springs. Figure 9-4 and Figure 9-5 show the details of the modeled PICP with continuous and discrete interlayer connectors, respectively. As shown in these figures, the spacing of the continuous discrete connectors were taken as 700 mm and 500 mm, which is the common spacing of connectors in PICP (Mouser 2003, Naito 2012, Salmon et al. 1997).

Matrix of analyzed PICP

Table 9-4 shows the attributes of the numerical PICP models studied in this section. In this table the thickness of concrete and insulation layers of PICP is denoted by #1-#2-#3, where #1 is the thickness of the compressive concrete layer, #2 is the insulation thickness and #3 is the thickness of tensile concrete layer in inches. The stiffness of the continuous connectors is given in kN/mm per unit length of the connector. As given in this table the length of the studied panels varied from 6.0 m to 16 m, which is the common length range used in industry (PCI, 2011). The overall thickness of the studied PICP varied from 127 mm to 229 mm.

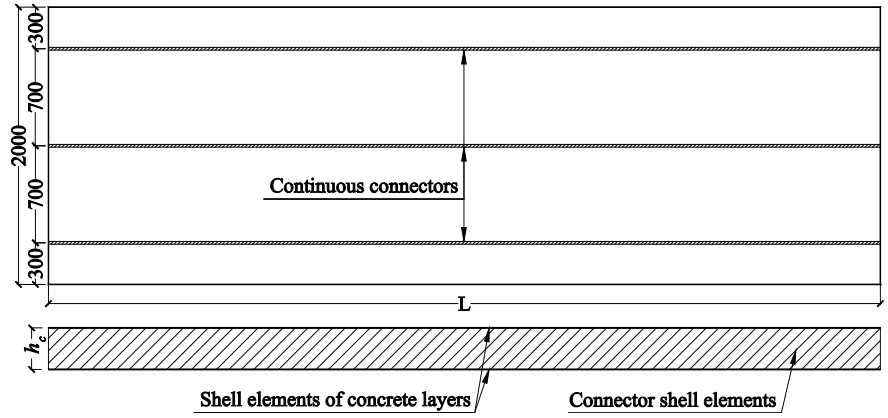

Figure 9-4: Analytical model of the studied PICP with continuous interlayer connectors.

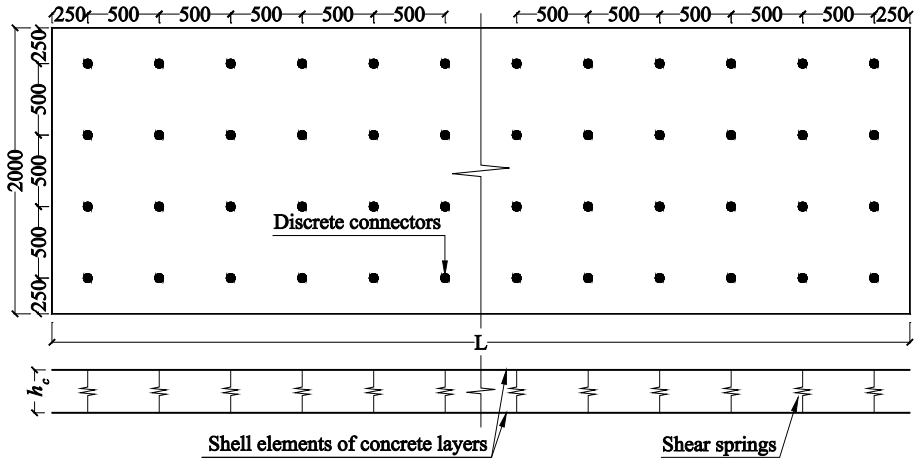

Figure 9-5: Analytical model of the studied PICP with discrete interlayer connectors.

Table 9-4: Matrix of the studied PICP using the proposed analytical modeling.

Length (m)	Thickness of PICP layers	K_s (kN/mm/m)	K_s (kN/mm)
6	P2-2-2	10, 20, 40, 60, 80, 100	10, 20, 40, 60, 80, 100
8	P3-2-3	10, 20, 40, 60, 80, 100	10, 20, 40, 60, 80, 100
12	P3-3-3	10^{-3}, 10^{-2}, 0.1, 1.0, 2.0, 4.0, 6.0, 8.0, 10, 12, 14, 16, 18, 20, 40, 60, 80, 100, 10^3, 10^5	1.0, 2.0, 4.0, 6.0, 8.0, 10, 12, 14, 16, 18, 20, 40, 60, 80, 100,
12	P3-2-3	40, 60, 80, 100	10, 20, 40, 60, 80, 100
12	P3-1-3	1.0, 40, 60, 80, 100	10, 20, 40, 60, 80, 100
12	P2-1-2	10, 20, 40, 60, 80, 100	10, 20, 40, 60, 80, 100
12	P2-2-2	10, 20, 40, 60, 80, 100	10, 20, 40, 60, 80, 100
16	P2-1-2	10, 20, 40, 60, 80, 100	10, 20, 40, 60, 80, 100

Degree of composite action for PICP without end-beams

Figure 9-6 shows the degree of composite action β of PICP without end-beams against K/K_0, where K_0 is calculated by equation 9-30 with $a_0 = 1.55$. The value of 1.55 for a_0 was obtained using a trial-and-error approach to obtain the best curve fitting model to estimate β. When a_0 is 1.55, β for PICP without end-beams can be estimated by equation 9-32 with 99.98% coefficient of determination (R-squared)

$$\beta = \frac{21.02\, K/K_0}{21.02\, K/K_0 + 0.6418} \qquad \textbf{9-32}$$

Figure 9-6 shows that β for PICP without end-beams grows fast with increasing K/K_0, such that at K/K_0 of 0.1, β is 0.78. As K/K_0 grows larger the rate of increase in β decreases and the β values approach 1.0, i.e. fully-composite behaviour. Figure 9-6 also shows that V_t/V_c for the studied

panels, where V_t is the total interlayer shear force between one end and mid-span of the panel, is equal to β defined using equation 9-30. Therefore, the degree of composite action can be defined as:

$$\beta = \frac{\Delta_{nc} - \Delta}{\Delta_{nc} - \Delta_c} = \frac{V_t}{V_c} \qquad \textbf{9-33}$$

It should be noted that V_t/V_c was previously defined as degree of composite action by Hassan and Rizkallah (2010). Equation 9-33 shows that the definition of β given by Hassan and Rizkallah (2010) is related to the out-of-plane mid-span deflection. Estimated out-of-plane deflection of PICP by equation 9-33 can be compared to the out-of-plane deflection limits specified in the design codes. Figure 9-6 shows that as the total interlayer shear stiffness K increases, the mid-span deflection and the total interlayer shear forces of PICP approach those of a fully-composite panel. With increased interlayer shear stiffness, β increases at high rate up to K/K_0 of 0.1, afterwards the rate of increase in β slows down.

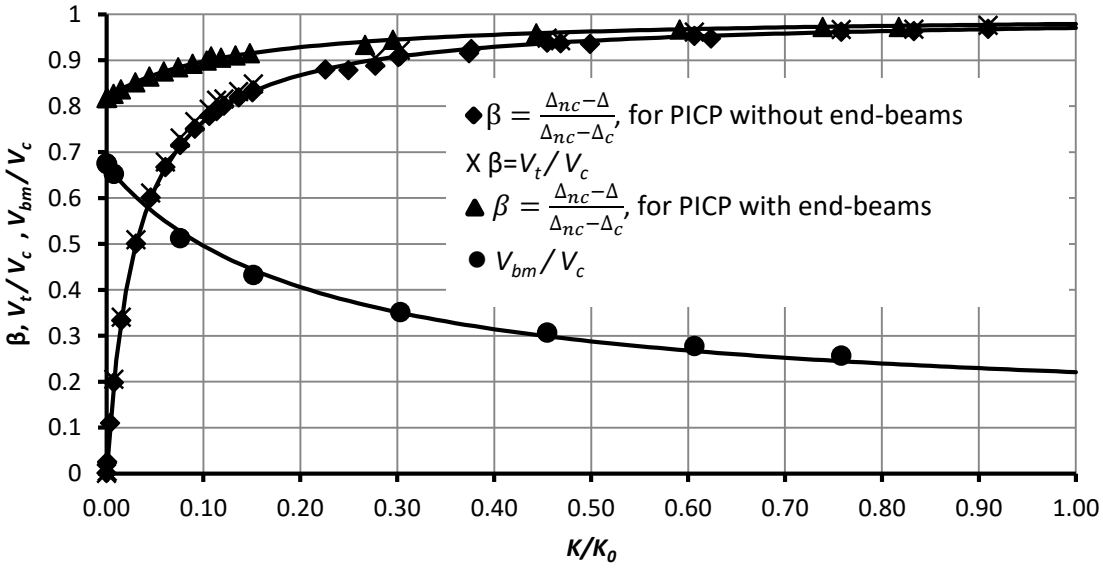

Figure 9-6: β, V_t/V_c and V_{bm}/V_c against K/K_0.

As mentioned earlier, V_t is equal to the axial force at the mid-span of the concrete layers, P_l. Therefore, after V_t is determined using equation 9-33, it can be substituted for P_l in equation 9-22 to calculate the out-of-plane bending moment carried by the concrete layers. The axial force and

bending moment in each concrete layer can then be used to calculate the cracking and ultimate strength of supported PICP as explained in Section 9.3.4.

The basic shear stiffness defined in equation 9-30 and the β- K/K_0 graphs shown in Figure 9-6 reveal the effect of different parameters on the degree of composite action. As given by equation 9-30, K_0 decreases proportionally with the panel length. Also as the panel length increases K increases proportionally since the number of interlayer connectors is increased proportionally. Therefore, K/K_0 exhibits quadratic growth with panel length, and leads to improved degree of composite action. Also as the overall thickness of the panel increases, K_0 increases, leading to decreased K/K_0 which lowers the degree of composite action. Therefore, with the same interlayer shear stiffness, thicker PICP has smaller degree of composite action.

Effect of end-beams

Figure 9-6 shows β for PICP with end-beams against K/K_0. As shown in this figure for a panel with zero interlayer shear stiffness, i.e. zero K/K_0, the degree of composite action is 0.8, which suggests significant contribution of end-beams to the degree of composite action in PICP. As K/K_0 increases, values of β for PICP with and without end-beams converge and approach 1.0. The degree of composite action for PICP with end-beams, β_{EB}, can be estimated using equation 9-34 with 99.8% coefficient of determination (R-squared).

$$\beta_{EB} = \frac{7.728\ K/K_0 + 0.8177}{7.728\,K/K_0 + 1} \qquad \textbf{9-34}$$

Figure 9-6 also shows the interlayer shear force taken by the end-beams, V_{bm}, as a ratio of total interlayer shear force between the end and mid-span of a composite panel, V_c, given by equation 9-23. As shown in this figure, when the total interlayer shear stiffness, K, is zero, V_{bm}/V_c is about 0.67. As K increases, a part of the interlayer shear forces is taken by the interlayer connectors, and thus V_{bm}/V_c decreases. The rate of this decrease slows down as K/K_0 increases. V_{bm}/V_c can be estimated using equation 9-35 with 99.7% coefficient of determination.

$$V_{bm}/V_c = \frac{0.588\ K/K_0 + 0.669}{4.70\,K/K_0 + 1.0} \quad \textbf{9-35}$$

When V_{bm} is determined using equation 9-35, the total interlayer shear forces taken by the interlayer connectors, V_{con}, can be calculated as:

$$V_{con} = V_t - V_{bm} \quad \textbf{9-36}$$

If equation 9-36 is divided by V_c, and V_t/V_c is replaced by β_{EB}, then V_{con}/V_c is found to be:

$$V_{con}/V_c = \beta_{EB} - V_{bm}/V_c \quad \textbf{9-37}$$

Although using end-beams alone induce 80% degree of composite action, some interlayer mechanical connectors across the panel are still needed to transfer the loads from the windward layer to the leeward layer. These connectors can be non-shear connectors that can only carry axial forces.

It should be noted that end-beams create thermal bridges between concrete layers of PICP, thus reduce the thermal performance of the panels. Therefore, if thermal insulation of the building is a governing design parameter, end-beams in PICP should be avoided. Otherwise, end-beams can be used in PICP to optimize the number of interlayer connectors.

Distribution of interlayer shear forces

Figure 9-7 shows the interlayer shear force distribution in three panels without end-beams, and the same three panels with end-beams. These three panels vary in length and thickness of insulation and concrete layers. As shown in this figure, the interlayer shear forces of PICP without end-beams linearly increases to its maximum value, V_m, at the end of the panel, i.e. when $X = 0.5L$ (Figure 9-7). This result agrees with the distribution of interlayer shear forces estimated by principles of mechanics of materials. For the same three panels, when end-beams are added, the interlayer shear

forces carried by the connectors reach their maximum value between the reduce to zero at the end of the panel, where the interlayer shear forces are primarily carried by the end-beams.

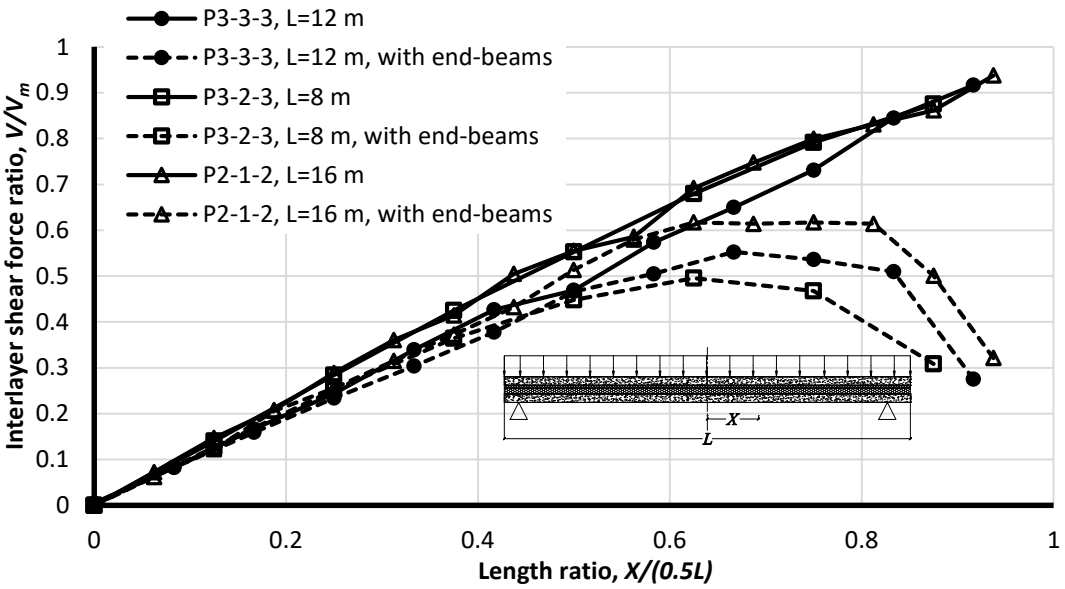

Figure 9-7: Distribution of interlayer shear forces for PICP with and without end-beams.

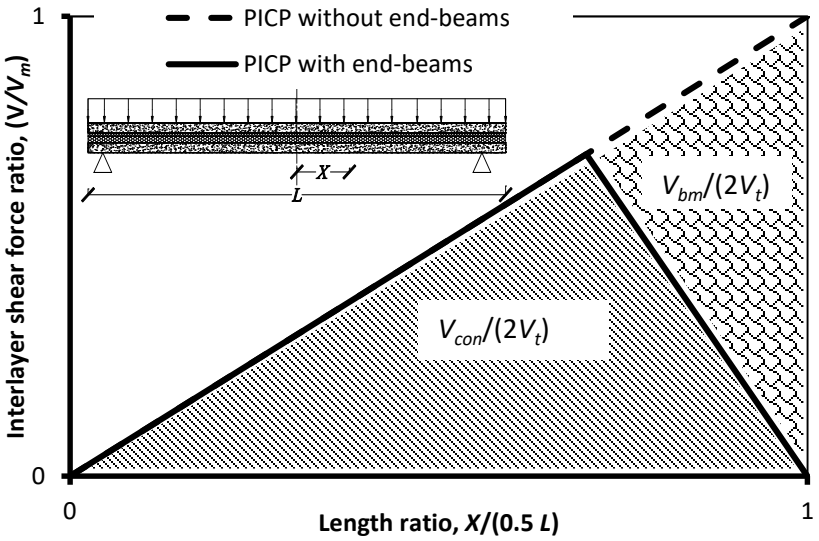

Figure 9-8: Simplified distribution of interlayer shear forces of simply supported PICP under uniform loading.

Figure 9-8 shows the simplified distribution of interlayer shear forces for simply supported PICP with and without end-beams. As shown in this figure the distribution of interlayer shear forces for PICP without end-beams is assumed to be linear from zero to its maximum value at the panel's end. This distribution of interlayer shear forces gives the maximum interlayer shear force at the

end of the panel. For this, first the degree of composite action is determined, then the total interlayer shear force, V_t, is calculated by equation 9-33. Afterwards, the maximum interlayer shear force at the end of the panel is calculated by equating V_t to the total interlayer shear force assuming linear distribution. For continuous connectors the total interlayer shear force with linear distribution is $0.5v_mL/2$, and thus v_m for continuous connectors is found by:

$$v_m = \frac{V_t}{0.25L} \quad \textbf{9-38}$$

For discrete connectors the total interlayer shear force is $\sum V_i$, and thus the maximum shear force of the discrete connector, V_m, which occurs in the connector closest to the panel's end is found by solving the following equation.

$$\sum_{i=1}^{n} V_i = V_t \quad \textbf{9-39}$$

Where i=1 is for the closest connector to the mid-span and i=n is for the closest connector to the panel's end. Therefore, V_n is equal to the maximum shear force of the connector, V_m. Since the distribution of shear forces are linear V_i is related to V_n as:

$$V_i = \frac{x_i}{x_n} V_n \quad \textbf{9-40}$$

Where x_i and x_n are the distances of connectors i and n from the mid-span of the panel.

As shown in Figure 9-8, for PICP with end-beams V_m does not occur in the connector closest to the panel's end. For PICP with end-beams the distribution of interlayer shear forces is assumed to be bilinear, i.e. the interlayer shear forces are assumed to increase linearly to a maximum value, V_m, before the panel's end, then linearly reduces to zero (Figure 9-8). To find the maximum interlayer shear force, first β_{EB} is determined, then V_t and V_{bm} are calculated by equations 9-33 and 9-35, respectively. Then, the maximum shear force in continuous connectors, v_m, is found by equating the total interlayer shear force carried by the connectors, V_{con}, found as V_t - V_{bm}, to V_{con}

assuming linear distribution of interlayer shear forces from zero to v_m, i.e. $0.5v_m$ $L/2$. Therefore, v_m can be found as:

$$v_m = \frac{V_t - V_{bm}}{0.25L} \quad \textbf{9-41}$$

For discrete connectors the total interlayer shear forces carried by the connectors, V_{con}, is equal to $\sum V_i$, and thus the maximum shear force of the discrete connectors, V_m, is found by solving the following equation.

$$\sum_{i=1}^{n} V_i = V_t - V_{bm} \quad \textbf{9-42}$$

Where i=1 is for the closest connector to the mid-span and i=n is for the closest connector to the panel's end. In equation 9-42, V_i can be related to V_m assuming bilinear distribution of shear forces shown in Figure 9-8.

9.3.4. Analysis of Simply Supported PICP using Degree of Composite Action

The relationships for the degree of composite action and the interlayer shear forces carried by the end-beams in terms of K/K_0 presented in Section 9.3.3 are adopted here to calculate the out-of-plane deflection, cracking and ultimate strengths of simply supported PICP with and without end-beams under uniform loading. The analytical model in this section is based on assuming equal thickness for the concrete layers of PICP. To analyze simply supported PICP using degree of composite action, first, the K/K_0 parameter is determined, where K_0 is calculated by equation 9-30. If the degree of composite action of cracked panel is required, the cracked properties of the cross section - $I_{l,cr}$ and $A_{l,cr}$ found by equations 9-1 and 9-2, respectively - should be used in equation 9-30 to calculate K_0. And I_c in equation 9-30 is replaced by the moment of inertia of cracked fully-composite panel, $I_{c,cr}$, calculated as:

$$I_{c,cr} = 2I_{l,cr} + 0.5A_{l,cr}h_c^2 \quad \textbf{9-43}$$

The degree of composite action is then found by equation 9-32 or 9-34 for PICP without and with end-beams, respectively. In these equations, if K_0 is calculated using cracked properties of the cross section, the results is called *degree of composite action of cracked panel*, β_{cr}. In the following analytical model, where β_{cr} is used, the cracked geometric properties of the panel's cross section - $A_{l,cr}$, $I_{l,cr}$, $I_{c,cr}$- should be used in equation 9-33 to calculate Δ_c, Δ_{nc} and V_c. The out-of-plane deflection, cracking and ultimate strengths can be calculated as explained in the following sections.

Out-of-plane cracking strength

To find the cracking strength of the panel the tensile stress at the mid-span, σ, should be compared to the concrete tensile strength, f_t as given by equation 9-6:

$$q_{cr} = \frac{\sigma}{f_t} q_s \qquad \textbf{9-6}$$

Where q_s is the uniform out-of-plane service load. The maximum tensile stress of the mid-span of the panel is calculated as:

$$\sigma = \frac{P_l}{A_l} + \frac{M_l}{S_l} \qquad \textbf{9-44}$$

Where P_l and M_l are the axial force and bending moment in the concrete layer, and A_l and S_l are the area and section modulus of the cross section of the concrete layer. As mentioned earlier P_l is equal to V_t, where V_t is related to the degree of composite action by equation 9-33. Since the concrete layers are assumed to have equal thickness in this section the bending moment in the concrete layers are equal, and thus M_l can be found by rewriting equation 9-22 as:

$$M_t = 2M_l + V_t h_c \qquad \textbf{9-45}$$

Where M_t is the total out-of-plane bending moment of the PICP at the mid-span, which is found by:

$$M_t = 0.125 q_s b l^2 \quad \textbf{9-46}$$

Out-of-plane mid-span deflection under service loads

If the cracking load, q_{cr}, found earlier is larger than the service load, q_s, the mid-span deflection is found by 9-7:

$$\Delta_t = \Delta_0 \quad \textbf{9-7}$$

Where Δ_0 is found by equation 9-33 when Δ is replaced by Δ_0 and Δ_{nc} and Δ_c are calculated under service load, q_s.

If the cracking strength of the panel is smaller than the service load, the out-of-plane deflection of PICP will have two components: pre-cracking deflection, Δ_0, and post-cracking deflection, Δ_{cr}. The total out-of-plane mid-span deflection is the sum of pre- and post- cracking out-of-plane deflections as given by equation 9-9.

$$\Delta_t = \Delta_0 + \Delta_{cr} \quad \textbf{9-9}$$

Where Δ_0 is found by equation 9-33 when Δ is replaced by Δ_0 and Δ_{nc} and Δ_c are calculated under cracking load, q_{cr}. In equation 9-9, Δ_{cr} is found by equation 9-33 when Δ and β is replaced by Δ_{cr} and β_{cr}, respectively, and Δ_{nc} and Δ_c are calculated under, q_s - q_{cr}.

Out-of-plane ultimate strength

The out-of-plane ultimate strength of simply supported PICP under uniform load can be derived by equation 9-47, if $V_{con} < A_s f_y + A_{pr} f_{py}$.

$$0.125q_uBL^2 = M_{lt,r} + M_{lc,r} + V_{con}h_c, \quad V_{con} < A_sf_y + A_{pr}f_{py} \qquad \textbf{9-47}$$

Where V_{con} is derived by the procedure outlined in Section 9.2.4 9.3.3, assuming a linear distribution of interlayer shear deformations similar to the distribution of interlayer shear forces described in Section 9.3.3.

The shear deformation of the critical connector under ultimate out-of-plane load, $\Delta_{s,u}$, should be less than the its failure shear deformation, Δ_{sf}. $\Delta_{s,u}$ can be calculated using equation 9-18.

$$\Delta_{s,u} = \Delta_{s,0} + \Delta_{s,cr} \qquad \textbf{9-18}$$

Where $\Delta_{s,0}$ is the shear deformation of the critical connector of the uncracked PICP under q_{cr}. $\Delta_{s,cr}$ is the shear deformation of the critical connector of the cracked PICP with reduced interlayer shear stiffness under q_u-q_{cr}. The amount of reduction in the interlayer shear stiffness is as described in Section 9.2.4. As explained in Section 9.3.2, the shear deformation of the connector is produced by the rotation angle and axial deformation of the concrete layers (equation 9-26). Since axial deformation of the concrete layers reduces the shear deformation of the connector, it is conservatively neglected. Therefore, $\Delta_{s,cr}$ is calculated considering only the rotation angle of the panel's end. Using Bernoulli beam theorem, the ratio of the rotation angle of the end of a beam to the mid-span deflection is found to be $3.2/L$. Here, the thickness of the concrete layers are assumed to be the same, therefore $\Delta_{s,cr}$ is found by:

$$\Delta_{s,cr} = \theta_{cr}h_c = 3.2\frac{h_c}{L}\Delta_{cr} \qquad \textbf{9-18}$$

Where θ_{cr} and Δ_{cr} are the rotation angle and mid-span deflection of cracked PICP with reduced interlayer shear stiffness under q_u-q_{cr}. Δ_{cr} can be found using degree of composite action for cracked PICP with reduced interlayer shear stiffness.

If $V_{con}>A_sf_y+A_{pr}f_{py}$ the flexural reinforcement yields before failure of the critical connector. And thus, V_{con} cannot be mobilized and the interlayer shear force is bound by $A_sf_y+A_{pr}f_{py}$. Also, the

tensile concrete layer cannot take any bending moment since its reinforcement has already yielded, i.e. $M_{lt,r}$ is zero. In this case, the ultimate out-of-plane strength can be derived as:

$$0.125 q_u B L^2 = M_{lc,r} + \left(A_s f_y + A_{pr} f_{py}\right) h_c, \quad V_{con} > A_s f_y + A_{pr} f_{py} \qquad \textbf{9-48}$$

Where, $M_{lc,r}$ is the flexural capacity of the compressive concrete layer under a compressive force equal to $A_s f_y + A_{pr} f_{py}$.

Design of end-beams

Using Timoshenko beam theorem the maximum interlayer shear transfer occurs at the ends of simply supported PICP, thus interlayer shear forces taken by the end-beams in simply supported PICP are larger than other interlayer mechanical connectors across the panel. With presence of end-beams, even after failure of the interlayer mechanical connectors, the end-beams carry the interlayer shear forces; and as presented in Section 9.3.3 end-beams alone can mobilize about 80% degree of composite action in simply supported PICP. To ensure that simply supported PICP with end-beams reach fully-composite out-of-plane flexural strength, the end-beams are assumed to carry the total interlayer shear forces for fully-composite out-of-plane flexural strength. The fully-composite out-of-plane flexural strength occurs when the tensile reinforcement of the tensile concrete layer has yielded. The yield force of this reinforcement should be transferred to the compressive concrete layer through the end-beams. Therefore, the shear force in the end-beams at ultimate flexural strength, $V_{bm,u}$, in simply supported PICP can be calculated as:

$$V_{bm,u} = A_s f_y + A_{pr} f_{py} \qquad \textbf{9-49}$$

After finding the shear force in the end-beams, $V_{bm,u}$ is compared against the shear strength of end-beams as given by equation 9-21.

9.3.5. Comparison with Experimental Results

Table 9-5 compares the mid-span deflection of the PICP tested by previous researchers, Δ_e, with the analytical mid-span deflection, Δ_t, estimated using degree of composite action described in Section 9.3.4. The uniform load q shown in this table is an arbitrary uniform load on the linear elastic region of the experimental load-displacement graphs. As given in Table 9-5, Δ_e/Δ_t ratios for the previously studied tested PICP vary from 0.52 to 1.12; and $\Delta_t - \Delta_e$ for these panels vary from -2.0 mm to 2.8 mm. It should be noted that for panels no. 1, 2 and 7 Δ_e/Δ_t is larger than one, meaning the proposed analytical method underestimates the experimental mid-span deflection for these three panels. This underestimation is maximum 14% for panel no. 2.

Table 9-5: Mid-span deflection of previously tested PICP estimated using degree of composite action.

Panel No.	Previous test	Interlayer connector	q kPa	Δ_e (mm)	Δ_t (mm)	$\frac{\Delta_e}{\Delta_t}$	$\Delta_t - \Delta_e$ (mm)
1	Salmon et al. (1997)	FRP truss	3.0	17.4	16.5	1.05	-0.90
2		Steel truss	1.5	16.2	14.2	1.14	-2.00
3	Naito (2012)	CFRP grid	18	3.0	3.9	0.77	0.90
4		Composite pin	15	3.1	5.9	0.52	2.80
5		C-clip	16	5.2	7.1	0.73	1.90
6	Mouser (2003)	Expanded metal	10	2.6	2.7	0.96	0.10
7		Expanded metal	10	3.6	3.2	1.12	-0.40
8		M-tie	10	3.4	5.0	0.68	1.60
Average						0.87	
Coefficient of variation %						26.0	

Table 9-6 compares the experimental out-of-plane ultimate cracking and ultimate strengths of PICP tested by previous researchers, $q_{cr,e}$ and $q_{u,e}$, respectively, to the estimated cracking and ultimate strengths by the proposed analytical method, $q_{cr,u}$ and q_u, respectively. The experimental cracking strength is taken as the out-of-plane strength beyond which there is considerable drop in the out-of-plane stiffness of the panel, i.e. considerable drop in the slope of the experimental load-deflection graph. And $q_{cr,e}$ is compared with $q_{cr,u}$, which is associated with considerable drop in the analytical out-of-plane stiffness of PICP when the compressive concrete layer cracks.

Table 9-6 shows that $q_{cr,e}/q_{cr,u}$ varies from 1.12 to 1.57 with average value of 1.26 and coefficient of variation of 11.3%; and $q_{u,e}/q_u$ varies from 1.01 to 1.32 with average value of 1.17 and

coefficient of variation of 9.07%. This means the proposed analytical method using degree of composite action gives conservative estimates of the ultimate cracking and ultimate strength of these previously studied panels with different interlayer connector systems with 57% and 32% error, respectively.

Table 9-6: Out-of-plane strength of previously tested PICP estimated using degree of composite action.

Panel no.	Researcher	Interlayer connector	Ultimate cracking strength			Ultimate strength		
			$q_{cr,e}$	$q_{cr,u}$	$\frac{q_{cr,e}}{q_{cr,u}}$	$q_{u,e}$	q_u	$\frac{q_{u,e}}{q_u}$
1	Salmon et al. (1997)	FRP truss	5.74	4.77	1.20	8.14	6.30	1.29
2		Steel truss	3.83	3.13	1.22	5.67	4.76	1.19
3	Naito (2012)	CFRP grid	23.4	14.9	1.57	32.7	27.0	1.21
4		Composite pin	15.2	13.6	1.12	31.7	31.5	1.01
5		C-clip	14.47	10.9	1.33	28.9	25.5	1.13
6	Mouser (2003)	Expanded metal	20.5	17.5	1.17	25.0	21.4	1.17
7		Expanded metal	17.0	14.5	1.17	23.0	17.44	1.32
8		M-tie	13.0	10.1	1.29	21.0	19.8	1.06
Average					1.26			1.17
Coefficient of variation %					11.3			9.07

9.4. Discussion of the Proposed Analytical Model

9.4.1. Degree of Composite Action

As mentioned earlier various definitions of degree of composite action were proposed by previous researchers as given by Table 9-7. The definition of β by Culp (1994) is in terms of the initial slope of the moment-displacement graph of the panel. The definitions of β by Pessiki and Mlynarczyk (2003) and Salmon et al. (1997) are in terms of the moment of inertia of the insulated panel. These

definitions can be used to only estimate the mid-span deflection of insulated panels, not the out-of-plane cracking and ultimate strengths of these panels. The definition of β proposed by Wade and Porter (1988) is in terms of the bending moments of the concrete layers, by which the axial forces can also be calculated. Therefore, this definition can be used to estimate the out-of-plane cracking strength of PICP, but not the out-of-plane deflection. These researchers calculated β for their tested insulated panels, but did not propose any methodology to estimate β for PICP with different dimensions or interlayer connector systems. The degree of composite action given by Mouser (2003) can be estimated knowing the shear strength of the interlayer connector system, which is derived by shear test results. However, β defined by Mouser (2003) is only useful to estimate ultimate out-of-plane strength of PICP, but not the out-of-plane deflection.

Table 9-7: Definitions of degree of composite action by previous researchers.

Researcher	β	Definition of parameters
Culp (1994)	$\frac{S - S_{nc}}{S_c - S_{nc}}$	S is the slope of the linear elastic portion of the moment-displacement graph of PICP. S_{nc} is equal to S for theoretical non-composite panel. S_c is equal to S for theoretical fully-composite panel.
Mouser (2003)	$\frac{V_{con} + V_{ins}}{A_p f_{pr}}$	V_{con} is the total shear strength of connectors in one half of the simply supported panel. V_{ins} is the total shear strength of insulation in one half of the simply supported panel. A_p is the area of the prestressing strands. f_{pr} is the effective stress in the prestressing strands
Pessiki and Mlynarczyk (2003)	$\frac{I - I_{nc}}{I_c - I_{nc}}$	I is the moment of inertia of the panel. I_c and I_{nc} are the moment of inertia of the theoretical fully-composite and non-composite panels, respectively.
Hassan and Rizkallah (2010)	V_t/V_c	V_t is the total interlayer shear force V_c is the total interlayer shear force in a fully-composite panel
Salmon et al. (1997)	I_e/I_g	I_e is the effective moment of inertia of the panel. I_g is the gross moment of inertia of the theoretical fully-composite panel.
Wade and porter (1988)	$\frac{M_t - (M_{lt} + M_{lc})}{M_t}$	M_t is the total mid-span bending moment. M_{lt} is the bending moment of the concrete layer in tension. M_{lc} is the bending moment of the concrete layer in compression.

The advantage of the β defined in Section 9.3.2 over other definitions given in Table 9-7 is that it is related to out-of-plane deflection and is equal to the β given by Hassan and Rizkallah (2010), so it can be adopted to estimate the out-of-plane deflection and cracking and ultimate strengths of PICP with different geometries and interlayer connector systems. Moreover, the β defined in Section 9.3.2 can be estimated by the ratio of the total interlayer shear stiffness, derived from the shear tests, to the basic interlayer shear stiffness of PICP defined in Section 9.3.2.

9.4.2. Estimating Out-of-Plane Deflection and Strength

The existing design method to estimate out-of-plane deflection and strength of PICP assumes either non-composite or fully-composite behaviour (PCI 2011, CPCI 2007). Assuming non-composite action leads to conservative design of PICP, and thus increases the thickness of the panels. If fully-composite action is considered the interlayer shear strength and stiffness of the interlayer connectors should be sufficient to mobilize fully-composite behaviour. The existing design codes and manual including CPCI 2007 and CAN/CSA A23.3-04 do not give any guideline on how to determine the adequacy of interlayer shear strength and stiffness of PICP. Instead, in practice, the interlayer connectors are categorized into shear and non-shear connectors. Shear connectors are assumed to mobilize fully-composite action. Although this method of designing PICP might give conservative designs for majority of panels, it does not consider the dimensional effect of the panel on the degree of composite action. Also, it does not consider the behaviour of partially-composite panels. The degree of composite action defined in 9.3 and its relationship to the interlayer shear stiffness of connectors and basic interlayer shear stiffness is believed to give a more rational approach to estimating out-of-plane deflection and strength of PICP.

In this research the degree of composite action of PICP is related to the shear stiffness of interlayer connectors. Using this relationship presented in Section 9.3, the shear stiffness of connectors is determined, then the out-of-plane deflection and cracking strength of PICP can be estimated without the need to conduct numerical analysis or flexural tests on the panel. The research by Naito et al. (2012) was the only study found in literature that related the composite behaviour of PICP to the shear stiffness of interlayer mechanical connectors. Naito et al. (2012) conducted shear tests on the common interlayer connectors and proposed tri-linear relationships for their shear behaviour. Then, they proposed an analytical procedure to derive the out-of-plane load-displacement graph of PICP by finding the moment-curvature relationship at multiple cross

sections between the end and mid-span of the panel. At every cross section the linear elastic relationship of the moment-curvature graph is derived by comparing the shear stiffness of the connector to the shear stiffness corresponding to full composite and non-composite action, as given by equation 9-50.

$$\frac{M_t - M_{nc}}{M_c - M_{nc}} = \frac{K - K_{ins}}{K_{max} - K_{ins}} \qquad \textbf{9-50}$$

In equation 9-50, M_{nc} and M_c are the bending moment of theoretical non-composite and fully-composite panel, respectively, and M_t is the bending moment of the partially-composite panel. In this equation, K is the shear stiffness of the connector, K_{ins} is the shear stiffness of insulation and K_{max} is the maximum shear stiffness of connectors found in shear tests by Naito et al. (2012). So, for every curvature, M_{nc} and M_c can be calculated by principles of mechanics of materials. Then, given K of the interlayer connector, M_t can be calculated using equation 9-50.

Equation 9-50 assumes that the shear stiffness of fully-composite panel is the largest shear stiffness value found in the shear tests of common interlayer connector system (Naito et al., 2012), and constant for all panels with different dimensions. The investigations in Section 9.3, however, showed that the degree of composite behaviour of PICP not only depends on the interlayer shear stiffness, but also on the geometric properties of the panel. So, in the analytical investigation presented in Section 9.3, the measure of total interlayer shear stiffness corresponding to fully-composite behaviour is given by K_0 factor which is a function of the geometric properties and modulus of elasticity of panel.

Moreover, Equation 9-50 assumes that the behaviour of partially-composite panel varies linearly with the interlayer shear stiffness. This relationship, however, was shown in Section 9.3 to be nonlinear. As presented in Section 9.3 the out-of-plane behaviour of panel, measured by β, starts from non-composite behaviour for zero value of K/K_0 to 0.8 at K/K_0 of 0.1, then asymptotically approaches to fully-composite behaviour, i.e. $\beta = 1$. Therefore, assuming linear variation of composite behaviour underestimates the degree of composite behaviour of partially-composite panels, and thus leads to unnecessary increase of panel thickness in structural design of PICP under out-of-plane loading.

After finding the analytical cracking moment of partially-composite panel, the analytical method by Naito et al. (2012) gives the moment-curvature relationship of the cross section by calculating the interlayer shear deformation at that section. This interlayer shear deformation is found by estimating the interlayer shear force and using the tri-linear shear relationships proposed by Naito et al. (2012). In this method the interlayer shear force is derived by M_t / h_c, where M_t is the total bending moment found by static equilibrium of the simply supported panel. This calculation for interlayer shear forces, however, seems inconsistent with the principles of mechanics of materials. For the extreme case where the panel in non-composite, for example, there should be no interlayer shear force, but large interlayer shear deformation occurs due to rotation angle of concrete layers (Section 9.3.2). And for fully-composite panel some part of the total bending moment is taken by the concrete layers as given by equation 9-22. Therefore, the load-displacement relationship of the panel derived by Naito et al. (2012) method is expected to have some errors arising from assumptions that are inconsistent with the principles of mechanics of materials.

To avoid the aforementioned problem in the analytical model proposed by Naito et al. (2012), the MLE method presented in Section 8.3 is proposed to find the load-displacement relationships for PICP. The MLE method relies on FEM in which the concrete panel is modeled as an assembly of concrete layers and interlayer connectors. When the behaviour of the concrete layers and the interlayer connectors are known, the MLE method was shown to estimate the load-displacement behaviour of PICP along with the failure stages. The estimates of the MLE method are in good agreement with the tested panels in this research. Comparison of the results of this method with eight PICP with different connector systems tested by previous researchers showed that this method gives good estimates of the out-of-plane deflection and ultimate strength of the tested panels. Therefore, the MLE method can be applied to different panels with any type of interlayer connector.

In Section 9.3 the analytical approach proposed by Mouser (2008) was modified to estimate the ultimate out-of-plane strength of PICP. The analytical method proposed by Mouser (2008) is given by the following equation.

$$M_r = M_{lt} + M_{lc} + (V_{con} + V_{ins})h_c \qquad \textbf{2-6}$$

Where, M_r is the moment capacity of the insulated panel found by static equilibrium of simply supported PICP, M_{lt} and M_{lc} are the moment capacities of the tensile and compressive concrete layers, respectively, and V_{con} and V_{ins} are shear capacities of the connectors and the concrete-insulation bonding, respectively. In this equation, h_c is the distance between the centres of the concrete layers. This equation assumes that at ultimate out-of-plane loading the flexural capacity of the panel is the sum of the flexural capacities of the concrete layers and the bending moment carried by the interlayer shear forces.

Equation 2-6 proposed by Mouser (2003) to estimate ultimate out-of-plane strength of PICP is consistent with the free body diagram of the concrete layers shown in Figure 9-3. This equation, however, does not account for different modes of failure, and thus needs to be modified. In equation 2-6, the term ($V_{con} + V_{ins}$) is the total interlayer shear strength of the panel. If the yield strength of the flexural reinforcement of the tensile concrete layer is less than this ($V_{con} + V_{ins}$), the total interlayer shear strength is not mobilized at ultimate loading. In this case, equation 2-6 overestimates the ultimate out-of-plane strength of PICP. Also, M_{lt} would be zero since the reinforcement of the tensile concrete layer has already yielded under tensile forces, therefore the flexural capacity of the tensile concrete layer is zero. So, when the total yield strength of the flexural reinforcement of the tensile concrete layer ($A_s f_y + A_{pr} f_{py}$) is less than ($V_{con} + V_{ins}$) equation 2-6 should be modified as:

$$M_r = M_{lc} + \left(A_s f_y + A_{pr} f_{py}\right) h_c, \qquad A_s f_y + A_{pr} f_{py} < V_{con} + V_{ins} \tag{9-51}$$

Also, as mentioned earlier the distribution of interlayer shear forces is not uniform, which means interlayer connectors at different locations along the panel length reach their shear strength at different levels of out-of-plane loading. So, if the interlayer connector system lacks adequate shear ductility, the critical connectors, i.e. the ones closest to the ends of the panel in simply supported PICP, will fail before other connectors reach their shear strength, and the expected total interlayer shear strength of the panel cannot be reached.

9.5. Summary and Conclusion

In this section the steps of MLE method was reduced and a simplified MLE method was proposed to estimate the out-of-plane deflection, cracking and ultimate out-of-plane strengths of PICP of varying dimensions and with different interlayer connector systems. The summary of this method is presented in Table 9-8. The proposed simplified analytical method was compared with PICP tested by previous researchers and was found to give conservative estimates for the out-of-plane deflection and ultimate out-of-plane strength of PICP with 18% and 24% error, respectively.

For the specific case of simply supported PICP parametric linear elastic analyses were conducted to develop an analytical method to estimate the out-of-plane design parameters- i.e. deflection, cracking and ultimate strengths- of PICP. For this, the degree of composite action is defined in terms of the out-of-plane deflection of theoretical fully- and non-composite panel. And the basic interlayer shear stiffness is defined in terms of the geometric and material properties of PICP. The degree of composite action was then related to the ratio of the total interlayer shear stiffness to the basic interlayer shear stiffness. The total transferred interlayer shear force was found to be related to the degree of composite action. In the proposed analytical model for the simply supported PICP, given the shear stiffness of the interlayer connector system, the degree of composite action and the total transferred interlayer shear force is calculated and is adopted to estimate the out-of-plane design parameters of PICP. The procedure of this analytical model is summarized in Table 9-9.

Out-of-plane deflection and strengths of eight PICP tested by previous researchers were compared with those estimated by the proposed analytical model using degree of composite action. The tested PICP varied in length, thickness of concrete and insulation layers, and interlayer connector system. The proposed analytical model gave conservative estimates for out-of-plane deflection and ultimate strength with 13% and 18% error.

Table 9-8: Summary of simplified MLE method to estimate out-of-plane design parameters of PICP.

Design parameter	Parameter (derived from linear elastic analysis of PICP model under q_s, or calculated by an equation)	Design parameter
Cracking	1. P_t, M_t (Uncracked PICP) 2. σ (equation 9-5)	q_{cr} (equation 9-6)
Out-of-plane deflection	If $q_s < q_{cr}$: 1. Δ_0 , V_{max} (Uncracked PICP)	$\Delta_t = \Delta_0$, $V_{max} < V_r$
	If $q_s > q_{cr}$: 1. Δ_1, V_1 (Uncracked PICP) 2. Δ_2, V_2 (Cracked PICP) 3. Δ_0 (equation 9-10) 4. Δ_{cr} (equation 9-11) 5. V_0 (equation 9-13) 6. V_{cr} (equation 9-14)	Δ_t (equation 9-9) V_{max} (equation 9-12) < V_r
Ultimate strength	If $V_{con} < A_s f_y + A_{pr} f_{py}$: 1. M_{t0} (Cracked PICP with reduced interlayer shear stiffness).	
	2. $M_{lt,r}$, $M_{lc,r}$ (CAN/CSA A23.3-04) 3. $\Delta_{s,u}$ (equation 9-18)	q_u (equation 9-16) $\Delta_{s,u} < \Delta_{sf}$
	If $V_{con} > A_s f_y + A_{pr} f_{py}$: 1. M_{t0} (Cracked PICP)	q_u (equation 9-19)
End-beams	If $V_{con} < A_s f_y + A_{pr} f_{py}$: 1. q_u (equation 9-16)	$V_{bm,u}$ (equation 9-20)
	If $V_{con} > A_s f_y + A_{pr} f_{py}$: 1. q_u (equation 9-19)	$V_{bm,r}$ (CAN/CSA A23.3-04) $V_{bm,u} < V_{bm,r}$

Table 9-9: Proposed procedure to estimate out-of-plane design parameters of simply supported PICP.

Design parameter	**Parameter** (derived from linear elastic analysis of PICP model under q_s, or calculated by an equation)	**Design parameter**
Cracking	1. P_l , M_l (equations 9-33 and 9-45) 2. σ (equation 9-44)	q_{cr} (equation 9-6)
Out-of-plane deflection	If $q_s < q_{cr}$: 1. Δ_0 (equation 9-33)	$\Delta_t = \Delta_0$, $V_{max}<V_r$
	If $q_s > q_{cr}$: 1. Δ_{cr} (equation 9-33), Use cracked properties for PICP.	Δ_t (equation 9-9)
Ultimate strength	If $V_{con}<A_s f_y+A_{pr} f_{py}$: 1. $M_{lt,r}$, $M_{lc,r}$ (CAN/CSA A23.3-04) 2. $\Delta_{s,cr}$ (equation 9-18) 3. $\Delta_{s,u}$ (equation 9-18)	q_u (equation 9-47) $\Delta_{s,u}<\Delta_{sf}$
	If $V_{con}>A_s f_y+A_{pr} f_{py}$:	q_u (equation 9-48)
End-beams	$V_{bm,u}$ (equation 9-49) $V_{bm,r}$ (CAN/CSA A23.3-04)	$V_{bm,u}<V_{bm,r}$

Part 4: Summary and Conclusion

10. Summary, Conclusion and Recommendations for Future Research

10.1. Introduction

Precast Insulated Concrete Panels (PICP) consist of one insulation layer sandwiched between two concrete layers. These panels are widely used in North America to enclose buildings to provide thermal insulation and protect the building envelope against moisture ingress. These panels are under out-of-plane wind and seismic loading. Under out-of-plane loading, the out-of-plane deflection, cracking and ultimate strengths of these panels should meet the design requirements. The concrete layers are attached to each other through interlayer mechanical connectors. The shear strength and stiffness of these connectors significantly affect the out-of-plane behaviour of PICP. Larger shear strength and stiffness of these connectors results in larger shear transfer between the concrete layers, thus more flexural composite action is mobilized between the concrete layers. And as the flexural composite action of PICP in increased the out-of-plane strength and stiffness is improved. In practice, PICP are sometimes enclosed at the top and bottom with reinforced concrete beams. These end-beams can increase transfer of interlayer shear forces, hence improve flexural composite action between the concrete layers.

The most common interlayer mechanical connectors with large shear strength and stiffness include truss and grid connectors, made of steel or composite materials. While these connectors are capable of mobilizing composite action in PICP, they are susceptible to buckling. Thus shear failure of these connectors occurs before the plastic strength of their material is reached.

Experimental and analytical research was conducted by previous researchers on the effect of different interlayer mechanical connectors on the out-of-plane flexural behaviour of PICP. However, the existing experimental and analytical research on the effect of end-beams on the out-of-plane behaviour of PICP is not enough and conclusive. Moreover, the existing proposed analytical approaches to estimate the out-of-plane behaviour of PICP are too cumbersome for design purposes and are not applicable to all types of PICP.

In this research the shear strength and stiffness of a newly developed connector system made of Z-shaped steel plates was investigated. These Z-shaped Steel Plate Connectors (ZSPC) were shown

to possess larger shear strength than existing shear connectors. In this research the shear behaviour of ZSPC was determined using experimental and numerical studies, and an analytical approach was proposed to determine the shear strength and stiffness of ZSPC. Moreover, the effect of ZSPC and end-beams on the out-of-plane flexural behaviour of PICP was identified by experimental and analytical studies. And an analytical approach was developed to estimate the out-of-plane flexural behaviour of PICP with different interlayer mechanical connector systems with and without end-beams. The results of the proposed analytical approach compared well with the experimental results of PICP tested by previous researchers.

10.2. Summary and Conclusion

10.2.1. Shear Behaviour of ZSPC

In this research eleven push-off shear tests were conducted on ZSPC used in small-scale PICP to determine the shear strength and stiffness of ZSPC with different widths and thicknesses. The connector width varied from 76.2 mm to 152 mm and the connector thickness varied from 1.47 mm to 3.21 mm. The flange width of ZSPC in these tests was 50 mm. The thickness of insulation and concrete layers was 76.2 mm. The experimental results were complemented by parametric finite element analyses to develop analytical equations to estimate the shear strength and stiffness of ZSPC. The results of this experimental and analytical study is valid for ZSPC with dimensions within the aforementioned limits used in PICP with 76.2 mm thick concrete layers and 76.2 mm thick insulation layer. The conclusions of this study are as follows:

1. The shear stiffness of ZSPC is adversely affected as the thickness-to-width ratio of the Z-shaped connectors increases. This is because ZSPC with large thickness-to-width ratios transfer large shear forces to concrete layers, inducing micro cracking around the connector-concrete connection.

2. The Z-shaped connector can be idealized as a rectangular plate between the two concrete layers. The length and width of this idealized plate is equal to the insulation thickness and connector width, respectively. The shear strength of Z-shaped connectors within the dimensional range studied here can be estimated as the plastic shear strength of the idealized rectangular plate using the Tresca yield criterion and considering the interaction of in-plane shear forces and bending moments at the face of the concrete layers.

3. With the same volume of material, the shear strength of ZSPC was shown to exceed the shear strength of steel truss connectors, that are the most common interlayer mechanical connector.

4. The shear stiffness of ZSPC within the dimensional range studied in this research can be estimated using the proposed modified equation for the in-plane shear stiffness of an idealized rectangular plate between the faces of the concrete layers.

10.2.2. Flexural Behaviour of PICP under Out-of-Plane Loading

Six 4-point out-of-plane flexural tests were conducted on PICP with ZSPC to determine the effect of ZSPC and end-beams on the out-of-plane flexural behaviour of PICP. Two of the tested panels were enclosed by 150 mm wide reinforced concrete end-beams. The connector width varied from 76.2 mm to 152 mm and the connector thickness varied from 1.47 mm to 3.21 mm. The flange width of the ZSPC was 50 mm. Thickness of insulation was 76.2 mm. Multistep Linear Elastic (MLE) analysis method was proposed to analyze the tested PICP. The proposed numerical model was verified by the experimental results. The results of this study on the out-of-plane flexural behaviour of PICP is valid for PICP under one-way out-of-plane bending without end-beams or with 150 mm wide end-beams. Based on the experimental and numerical results of the tested PICP, the following conclusions are derived.

1. The out-of-plane strength of PICP with ZSPC can reach that of a fully-composite panel.

2. The out-of-plane strength of PICP with end-beams can reach that of a fully-composite panel even with the smallest size of ZSPC used in the tested PICP.

3. Insulated concrete panels with discrete interlayer mechanical connectors can be modeled as two layers of shell elements representing the concrete layers and discrete shear springs representing the connectors. The shear stiffness of these shear springs should be equal to the experimental shear stiffness of the connectors. Continuous connectors can be modeled as shell elements whose shear stiffness is equal to the experimental shear stiffness of continuous connectors. End-beams can be modeled as shell elements with a thickness equal to the width of the end-beams.

4. The Multistep Linear Elastic analysis method gives good estimation of the out-of-plane behaviour of PICP with different interlayer mechanical connectors with and without end-beams.

5. The analytical results of PICP with the MLE method showed that the end-beams were found to carry a large portion of the interlayer shear forces thus reducing the shear demand on the interlayer connectors.

6. The analytical results of PICP with the MLE method showed that the interlayer shear forces of PICP with end-beams is at least 0.8 times that of a fully-composite panel.

7. For design purposes, the simplified MLE method was proposed to estimate the out-of-plane deflection, cracking, and ultimate strengths of PICP with different interlayer mechanical connectors with and without end-beams.

8. An analytical approach based on the simplified MLE method was proposed to estimate the out-of-plane deflection, cracking and ultimate strengths of simply supported PICP with and without end-beams. This analytical approach uses graphs of the degree of composite action to estimate the out-of-plane behaviour of PICP.

10.3. Recommendations for Future Research

The results of this research help to understand the shear behaviour of ZSPC and the out-of-plane behaviour of PICP with and without end-beams. However, the conducted experimental and analytical studies in this research had some limitations which can be overcome with the following proposed future research.

10.3.1. Shear Behaviour of Interlayer Mechanical Connectors

1. The shear tests conducted on ZSPC in this research were limited to Z-shaped connectors with 1.47 mm to 3.21 mm thickness and 76.2 mm to 152 mm width. In addition, the insulation thickness of the shear test specimens was 76.2 mm. It is recommended that shear tests be conducted on small scale PICP with ZSPC with different widths and thicknesses, and with different thickness of insulation. This is because smaller thickness of insulation is expected to delay plastic buckling of ZSPC, and thus might provide higher ductility. Higher ductility of shear connectors can be used in PICP under extreme loading like an explosion or seismic forces.

2. The proposed equations to estimate the shear strength and stiffness of ZSPC are recommended to be compared with experimental results of the extensive shear tests recommended in item 1 and, if necessary, modifications should be made to the proposed equations.

3. It is recommended that more extensive shear tests are conducted on truss and girder connectors and analytical approaches be proposed to estimate their shear strength and stiffness.

10.3.2. Flexural Behaviour of PICP

1. The out-of-plane flexural tests on non-loadbearing PICP conducted in this research were limited to Z-shaped connectors with 1.47 mm to 3.21 mm thickness and 76.2 mm to 152 mm width. And the insulation thickness of the flexural test specimens was 76.2 mm. It is recommended that out-of-plane flexural tests are conducted on PICP with ZSPC with wider range of insulation thickness, and with different widths and thicknesses of ZSPC.

2. Similar tests as mentioned in item 1 are recommended to be conducted on loadbearing PICP under out-of-plane loading.

3. Similar tests as mentioned in item 1 is recommended to be conducted on PICP under in-plane shear loading to study the effect of ZSPC on in-plane shear strength and stiffness of PICP that are used as shear walls.

4. The PICP with end-beams studied in this research had fixed width of 150 mm. Further experimental study is recommended on PICP with end-beams of varying widths to investigate the effect of width of end-beams on the out-of-plane behaviour of PICP.

5. The flexural tests and the proposed analytical models for PICP in this study were limited to one-way bending, which applies to common PICP systems. However, in some PICP systems the panel is under two-way bending. Therefore, flexural tests are required to examine the effect of ZSPC on out-of-plane behaviour of PICP under two-way bending.

10.3.3. Multistep Linear Elastic (MLE) Analysis Method

Although the MLE method was proposed and adopted in this research to analyze PICP under out-of-plane loading, this method seems to be applicable to other types of structures as well. The MLE method relies on macro modeling of the structure using the nonlinear behaviour of the elements. It is recommended that the MLE method be investigated in more depth and be examined for other

types of structures including: PICP under gravity and shear loading, concrete slabs, composite slabs, concrete domes and vaults under gravity loading, etc.

10.3.4. Basic Interlayer Shear Stiffness and Degree of Composite Action

The analytical approach adopted in Section 9.3 to derive the basic interlayer shear stiffness and estimate the degree of composite action of PICP can be expanded to other composite systems. It is recommended to investigate the application of degree of composite action derived in Section 9.3 to other composite systems including composite slabs, composite steel columns, and other types of sandwich panels.

Bibliography

ABAQUS by Simula Inc., Dassault Systemes brand. (2009). "General Purpose Finite Element Software."Ver. 6.9, Providence, RI, USA.

Ahmad, I., Mohamad, N., (2011). "Structural Behaviour of precast lightweight concrete sandwich panel under eccentric load: an overview," The International Conference on Civil and Environmental Engineering Sustainability (IConCEES 2011), 3-5 April, Johor Bahru, Malaysia.

Allen, G.H. (1993). "Analysis and design of structural sandwich panels," Pegamon Press Ltd., London, United Kingdom, 283 p.

American Concrete Institute. (2008). "Building code requirements for structural concrete and commentaries." ACI 318, Farmington Hills, MI, USA.

American Concrete Institute. (2012). Guide for Precast Concrete Wall Panels. ACI 533R-11, Farmington Hills, MI, USA.

ASHRAE (2013). "2013 ASHRAE Handbook – Fundamentals," American Society of Heating, Refrigeration and Air Conditioning Engineers, Atlanta, 1000 p.

ASTM (2010). ASTM C469/C469M-10: Standard Test Method for Static Modulus of Elasticity and Poisson's Ratio of Concrete in Compression. ASTM International, West Conshohocken, PA, 5 p.

ASTM (2011). ASTM C496/C496M-11: Standard Test Method for Splitting Tensile Strength of Cylindrical Concrete Specimens. ASTM International, West Conshohocken, PA, 5 p.

ASTM (2012). ASTM C165-07: Standard Test Method for Measuring Compressive Properties of Thermal Insulations. ASTM International, West Conshohocken, PA, 5 p.

ASTM (2013). ASTM A370-13: Standard Test Methods and Definitions for Mechanical Testing of Steel Products. ASTM International, West Conshohocken, PA, 48 p.

ASTM (2014). ASTM C39/C39M-14: Standard Test Method for Compressive Strength of Cylindrical Concrete Specimens. ASTM International, West Conshohocken, PA, 7 p.

Basunbul, I. A., Saleem, M., Al-sulaimani, G. J., (1991). "Flexural Behaviour of Ferrocement Sandwich Panels," Elsevier, Cement & Concrete composites, Vol. 13, pp. 21-28.

Bathe, K. J. (1996). “Finite Element Procedures,” Prentice Hall Inc., Englewood Cliffs, New Jersey, U.S.

Benayoune, A., Samad, A.A.A., Abang Ali, A.A., Trikha, D.N., (2007), “Response of Precast Reinforced Composite Sandwich Panels to Axial Loading,” Elsevier, Construction and Building Materials, Vol. 21, pp. 677-685.

Benayoune, A., Samad, A.A.A., Trikha, D. N., AbangAli, A. A.,Ashrabov, A.A., (2006). “Structural Behaviour of Eccentrically Loaded Precast Sandwich Panels,” Elsevier, Construction and Building Materials, Vol. 20, pp. 713-724.

Benayoune, A., Samad, A.A.A., Trikha, D.N., Abang Ali, A.A., Ellinna, S.H.M., (2008). “Flexural behaviour of Precast Concrete Sandwich Composite Panel-Experimental and Theoretical Investigation,” Elsevier, Construction and building Materials, Vol. 22, pp. 580-592.

Benyoune, A., Abang Ali, A.A., Abdul Samad, A.A., Trikha, D.N., (2007). “Flexural Analysis of Composite One- and Two-Way Sandwich Slabs with Truss-Shaped Connectors,” The Institution of Engineers, Vol. 68, No. 1, March, pp. 53-60.

Bunn, W. G. (2011). “CFRP Grid/Rigid foam shear transfer mechanism for precast, prestressed Precast Concrete Sandwich Panels,” M.S. thesis, North Carolina State University, Raleigh, NC., USA.

Bush, T. D., Jr., Stine, G. L., (1994). “Flexural Behaviour of Prestressed Sandwich Panels with Continuous Truss Connectors,” PCI Journal, V. 39, No. 2, March-April, pp. 112-121.

Bush, T.D., Wu, Z., (1998). “Flexural Analysis of Prestressed Concrete Sandwich Panels with Truss Connectors,” PCI Journal, pp. 76-86.

Canadian Precast/Prestressed Concrete Institute (CPCI), (2007). “Design Manual: Precast and Prestressed Concrete,” 4th edition. CPCI, Ottawa, Ontario, Canada.

Carbonari, G., Cavalaro, S.H.P., Cansario, M.M., Aguado, A., (2012). “Flexural Behaviour of Light-Weight Sandwich Panels Composed by Concrete and EPS,” Construction and Building Materials, Elsevier, Vol. 35, pp. 792-799.

Challamel, N., Bernard, F., Casandjian, C. (2010). “Out-of-Plane Behaviour of Partially Composite or Sandwich Beams by Exact and Finite Element Methods,” Thin-Walled Structures, Elsevier, Vol. 48, pp. 561-580.

Chaudhari, S.V., Chakrabarti, M.A. (2012). "Modelling of Concrete for Nonlinear Analysis Using Finite Element Code Abaqus," International Journal of Computer Applications, Vol. 44, No. 7, pp. 14-18

Collins, M. P., Mitchell, D. (1997). "Prestressed Concrete Structures," Response Publications, Toronto, ON., 766 p.

Collins, M. P., Mitchell, D., (1987). "Prestressed Concrete Basics," Canadian Prestressed Concrete Institute.

Cornelissen, H. A. W., Hordijk, D. A., and Reinhardt, H. W. (1986). "Experimental Determination of Crack Softening Characteristics of Normal Weight and Lightweight Concrete," Heron Journal, Vol. 31, No. 2, pp. 45-56.

CSA (2009). CAN/CSA-A23.1-09/A23.2-09: Concrete Materials and Methods of Concrete construction/Test Methods and Standard Practices for Concrete. Canadian Standard Association, Mississauga, Ontario, 674 p.

CSA (2009). CAN/CSA-A23.4-09: Precast Concrete – Materials and Construction. Canadian Standard Association, Mississauga, Ontario, 78 p.

CSA (2009). CAN/CSA-S16-09: Design of steel structures. Canadian Standard Association, Mississauga, Ontario, 198 p.

CSA (2004). CAN/CSA-A23.3-04: Design of Concrete Structures. Canadian Standard Association, Mississauga, Ontario, 352 p.

Culp T. (1994)."Full scale testing of thermally and structurally efficient precast concrete sandwich panels," M.S. thesis, University of Nebraska.

Dassault Systemes Simulia Corp. (2012). Abaqus/CAE version 6.12-1 [computer software]. Providence, RI, USA.

Drucker, D. C. (1956). "The effect of shear on the plastic bending of beams." Journal of Applied Mechanics, Vol. 23, pp. 509-514.

Einea, A.A., (1992). "Structural and Thermal Efficiency of Precast Concrete Sandwich Panel Systems," PhD Thesis, University of Nebraska, Lincoln, Nebraska, USA, 201 p.

Einea, A.A., Salmon, D. C., Tadros, M. K., Culp, T., Fogarasi, G. J. (1991). State-of-the-Art of Precast Concrete Sandwich Panels. PCI Journal, Vol. 36, No. 6, pp. 78-98.

Fero Corporation. 15305-117 Ave. NW, Edmonton, AB T5M 3X4, Canada. www.ferocorp.com.

Frankl, B.A. (2008). Structural Behaviour of Insulated Precast Prestressed Concrete Sandwich Panels Reinforced with CFRP Grid. M.S. Thesis, North Carolina State University.243 p.

Frankl, B.A., Lucier, G., Rizkalla, S., (2008). "Structural Behaviour of Insulated Prestressed Concrete Sandwich Panels Reinforced with FRP Grid," 4th Intl. Conference on FRP Composites in Civil Engineering (CICE2008), 6 p.

Frankl, B.A., Lucier, G.W., Hassan, T.K., Rizkalla, S.H., (2011). "Behaviour of Precast, Prestressed Precast Concrete Sandwich Panels Reinforced with CFRP Shear Grid," PCI Journal, pp. 42-54.

Frostig, Y. and Baruch, M. (1990). "Bending of sandwich beams with transversely flexible core," American Institute of Aeronautics and Astronautics (AIAA) Journal, Vol. 28, No. 3, pp. 523-531.

Gara, F., Ragni, L., Roia, D., Dezi, L., (2012). "Experimental Tests and Numerical Modelling of Wall Sandwich Panels," Elsevier, Engineering Structures, Vol. 37, pp. 193-204.

Gordaninejad, F., Bert, C.W. (1989). "A New Theory for Bending of Thick Sandwich Beams," International Journal of Mechanical Sciences, Vol. 31, No. 11/12, pp. 925-934.

Goudarzi, N., Hatzinikolas, M. and Korany, Y. (2014). "Out-of-Plane Behavior of Precast Concrete Sandwich Wall Panel Systems." Proceedings, 4th Annual International Conference on Civil Engineering. Athens, Greece: The Athens Institute for Education and Research.

Hassan, T., Rizkalla, S. (2010). "Analysis and Design Guidelines of precast prestressed Concrete, Composite Load-Bearing Sandwich Wall Panels Reinforced with CFRP Grid," PCI Journal, Vol. 50, No. 3, pp. 16-25.

Hognestad, E. 1951. A study on combined bending and axial load in reinforced concrete members. University of Illinois, Urbana-Champaign, Illinois, US.

Holmberg, A. and Plem, E. (1986). "Behaviour of load bearing sandwich-type structures," Handout No. 49, State Institute for Construction research, Lund, Sweden.

Hotta, H., Kihara, H., Takiguchi, K. (1998). “A Fundamental Study on Shear Bond Strength of Steel Encased Reinforced Concrete Members,” 3rd Conference of Fracture Mechanics for Concrete Structures (FraMCoS-3), Gifu, Japan, pp. 1321-1330.

Leabu, V.F. (1965). “Precast Concrete Wall Panels: Design Trends and Standards,” American Concrete Institute,”Special Publication, SP-11, American Concrete Institute (ACI), Farmington Hill, MI, USA, pp. 31-44.

Lee, B. J., Pessiki, S. (2007). “Design and Analysis of Precast, Prestressed Concrete, Three-Wythe Sandwich Wall Panels,” PCI Journal, July-August, pp. 70-83.

Lee, B., Pessiki, S. (2008). “Experimental Evaluation of Precast, Prestressed Concrete, Three-Wythe Sandwich Wall Panels,” PCI Journal, V. 53, No. 2, pp. 95-115.

Lee, B., Pessiki, S. 2006. “Thermal Performance Evaluation of Precast Concrete Three-Wythe Sandwich Wall Panels. Energy and Buildings, V. 38, No. 8, pp. 1006-1014.

Lee, B.J. (2003). Development of a Precast Prestressed Concrete Three-Wythe sandwich Wall Panel.Ph.D.Dissertation, Lehigh University, 398 p.

Lee, B.J., Pessiki, S. (2004). “Analytical investigation of thermal performance of precast concrete three-wythe sandwich wall panels,” PCI Journal, July-Aug., pp. 88-101.

Lee, B.J., Pessiki, S. (2006). “Thermal behaviour of precast prestressed concrete three-wythe sandwich wall panels,” Building Integration Solutions, pp. 1-15.

Lubliner, J., Oliver, J., Oller, S. and Onate, E. (1989). “A Plastic Model for Concrete.” International Journal of Solids and Structures, Vol. 25, pp. 299-329.

Maximos, H. N., Pong, W. A., Tadros, M. K., Martin, L. D. (2007). Behaviour and Design of Composite Precast Prestressed Concrete Sandwich Panels with NU-Tie.University of Nebraska, Lincoln, USA.28 p.

McCall, W. (1985). “Thermal Properties of Sandwich Panels,” Concrete International, Vol. 7, No. 1., pp. 35-41.

Mohamad, N., Omar, W., Abdullah, R., (2012). “Structural Behaviour of Precast Lightweight Foamed Concrete Sandwich Panel as a Load Bearing Wall,” International Journal of Sustainable Development, 05:03, pp. 49-58.

Mouser, L.A.D. (2003). Partially Composite concrete Sandwich Panels. M.S. Thesis, University of Alberta, 122 p.

Muir, L. S. and Thornton, W. A. (2004). "A Direct Method for Obtaining the Plate Buckling Coefficient for Double-Coped Beams." Engineering Journal, AISC, 3rd Quarter, pp. 133-134.

Naito, C., Beacraft, M., Hoemann, J., (2010). "Design Limits for Precast Concrete Sandwich Walls Subjected to External Explosions," Proc., ASCE Structures Congress, pp. 1794-1804.

Naito, C., Beacraft, M., Hoemann, J., (2010). "Design Limits for Precast Concrete Sandwich Walls Subjected to External Explosions," Rep., AFRL-RX-TY-TP-2010-0013, Air Force Reseaerch Laboratory, Tyndall Air Force Base, Fl.

Naito, C., Hoemann, J., Beacraft, M., Bewick, B., (2012). "Performance and Characterization of Shear Ties for Use in Insulated Precast Precast Concrete Sandwich Panels," J. of Structural Engineering, ASCE, Vol. 138, pp. 52-61.

Naito, C., Howmann, J., Bewick, B., Hammons, M. (2009). "Evaluation of Shear Tie Connecotrs for Use in Insulated Concrete Sandwich Panels," Rep. AFRL-RX-TY-TR-2009-4600, Air Force Research Laboratory, Tyndall Air Force Base, Fl.

Newberry, C., Davidson, J., Hoemann, J., Bewick, B., (2010). "Simulation of Prestressed Concrete Sandwich Panels Subjected to Blast Loads," Rep., AFRL-RX-TY-TP-2010-0014, Air Force Reseaerch Laboratory, Tyndall Air Force Base, Fl.

Newmark, N.M., Siess, C.P., viest, I.M. (1951). Tests and Analysis of composite beams with incomplete interaction. Proceedings of the society for experimental stress analysis," V.9, No. 1, pp. 75-92.

NRC. (2010). "National Building Code of Canada," Associate Committee on the National Building Code (NBC 2010). Ottawa, Ontario, Canada: National Research Council of Canada.

Pantelides, C.P., Reaveley, L.D., McMullin, P.W. (2003). "Design of CFRP composite connector for precast concrete elements," Journal of Reinforced Plastics and Composites, V. 22, No. 15, pp. 1335-1351.

Pavese, A., Bournas, D. A., (2011). "Experimental assessment of the Seismic Performance of a Prefabricated Concrete Structural Wall System," Engineering Structures, Elsevier, Vol. 33, pp. 2049-2062.

PCI Committee on Precast Sandwich Wall Panels (2011). “State of the Art of Precast/Prestressed Sandwich Wall Panels.” PCI Journal, Spring, pp. 131-142.

Pessiki, S., Mlynarczyk, A., (2003), “Experimental Evaluation of Composite Behaviour of Precast Precast Concrete Sandwich Panels,” PCI Journal, March-April, pp. 54-71.

Pfeifer, D. W., Hansen, J. A. (1964). “Precast Concrete Wall Panels: Flexural Stiffness of Sandwich Panels,” Special Publication, SP-11, American Concrete Institute (ACI), Farmington Hill, MI, USA, pp. 67-86.

Richmond, J. (1997). Unit shear tests on M tie connectors, Research project at University of Alberta.

Rizzo, S., Fazio, P., (1983). “Sandwich-Panel Assemblies: Analytical Model,” Journal of Structural Engineering, Vol. 109, No. 11, November, pp. 2715-2732.

Salmon, D. C., Al-Einea, A., Tadros, M. K., Culp, T. D., (1997) “Full Scale Testing of Precast Concrete Sandwich Panels,” ACI Structural Journal, Vol. 94, No. 4, pp. 354-362.

Salmon, D.C., Einea, A., (1995). “Partially Composite Sandwich Panel Deflections,” Journal of Structural Engineering, Vol. 121, No. 4, April, pp. 778-783.

Soriano, J., Rizkalla, S., (2013). “Use of FRP Grid for the Composite Action of Concrete Sandwich Panels,” 11th Intl. Symposium on Fiber Reinforced Polymer for Reinforced Concrete Structures (FRPRCS11), 12 p.

Stine, G.L. (1992). “Flexural behaviour of composite prestressed sandwich panels,” M.S. thesis, University of Oklahoma, Norman, OK, 133 p.

Stine, G.L., Bush, T.D. (1991). “Flexural behaviour of composite prestressed sandwich panels,” Research ReprotNo.FSEL/PCI 91-01, University of Oklahoma, Norman, OK, 122 p.

Tadros, M. K.,Ghali, A., and Dilger, W. H., (1977). “Time-Dependent Analysis of Composite Frames,” Journal of Structural Division, American Society of Civil Engineers, V. 103, No. ST4, April, pp. 871-884.

Wade, G., Porter, M., and Jacobs, D. (1988). “Glass fiber composite connectors for insulated concrete sandwich walls,” Iowa State University Report ISU-ERI-Ames-88202, Ames, IA, 205 p.

Woltman, G., Tomlinson, D., Fam, A., (2013). “Investigation of Various GFRP Shear Connectors for Insulated Precast Precast Concrete Sandwich Panels,” Journal of Composites for Construction, 35 p.

Wu, Z. (1993). “Analysis of flexural behaviour of prestressed concrete sandwich panels,” M.S. thesis, University of Oklahoma, Norman, OK, 104 p.

A. Shear Behaviour of ZSPC

Shear load-deformation behaviour of tested ZSPC

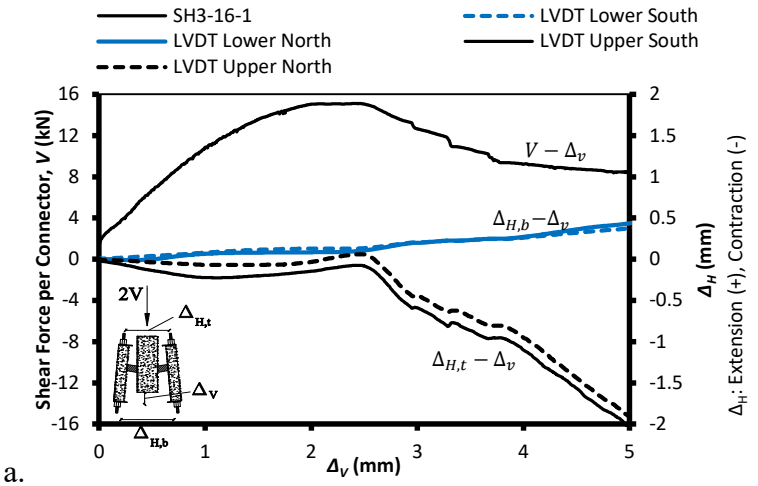

a.

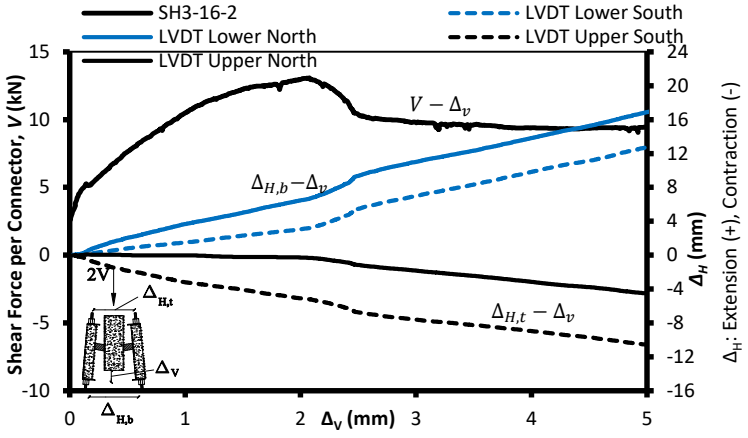

b.

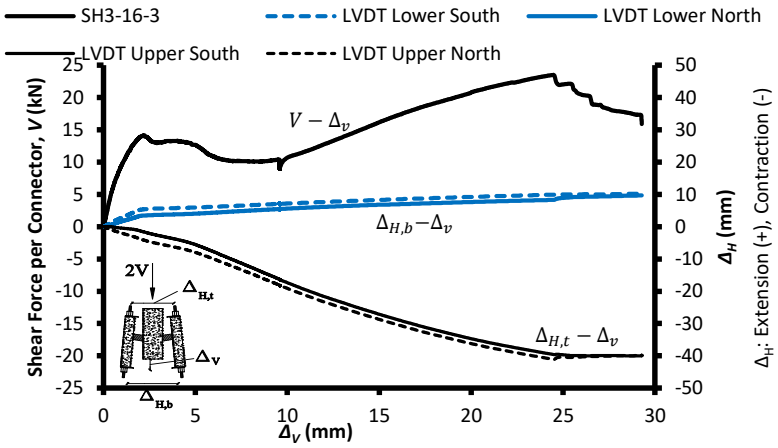

c.

Fig. 1: Shear load-deformation behaviour for a. SH3-16-1, b. SH3-16-2, and c. SH3-16-3.

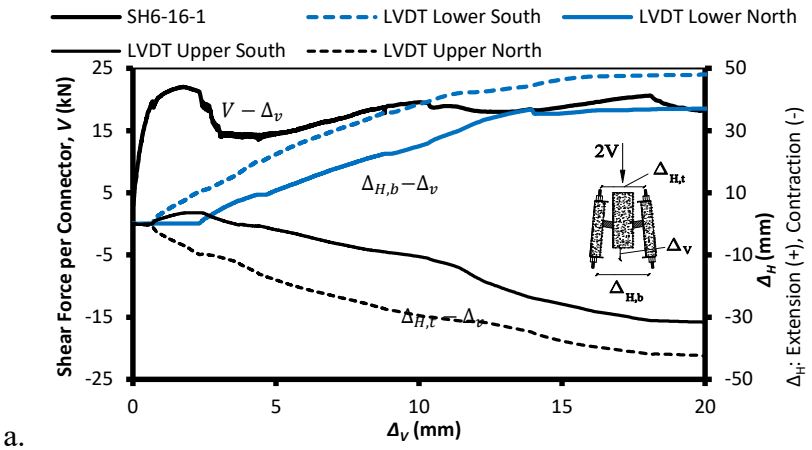

a.

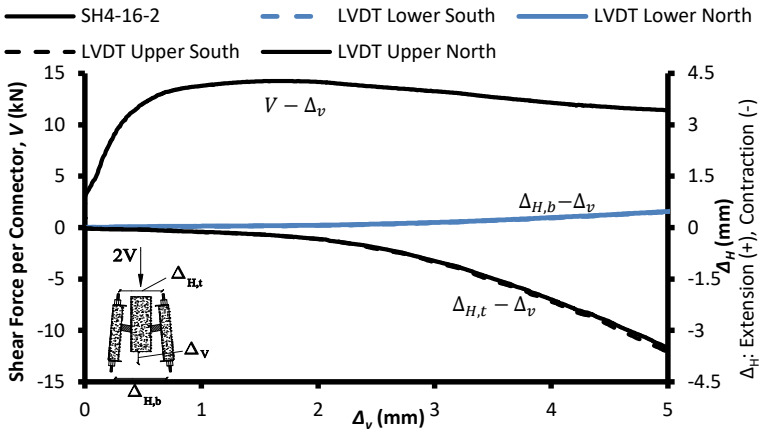

b.

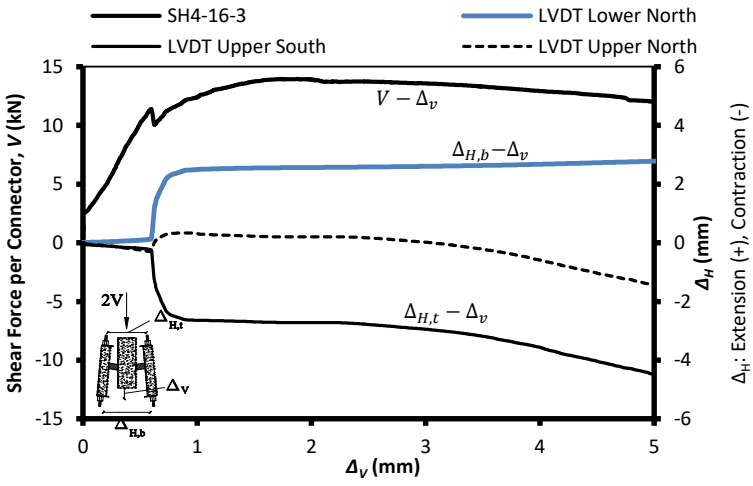

c.

Fig. 2: Shear load-deformation behaviour for a. SH4-16-1, b. SH4-16-2, and c. SH4-16-3.

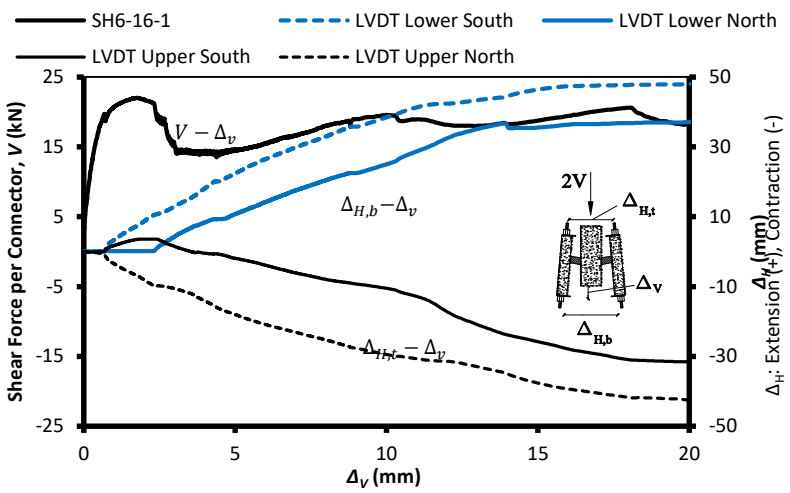

Fig. 3: Shear load-deformation behaviour for SH6-16-1.

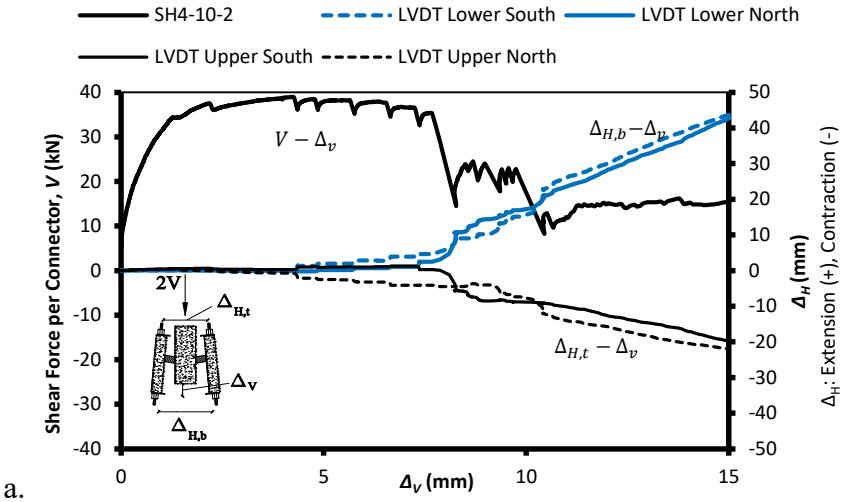

a.

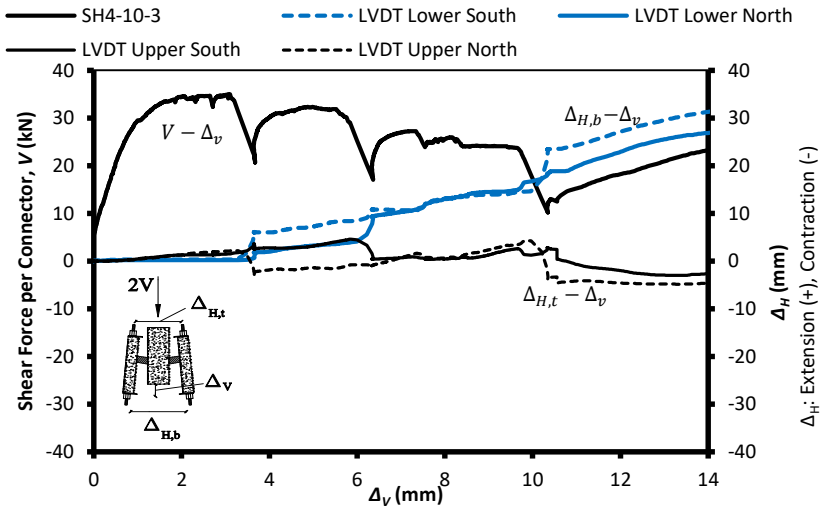

b.

Fig. 4: Shear load-deformation behaviour for a. SH4-10-2, and b. SH4-10-3.

B. Flexural Behaviour of PICP with ZSPC

B.1. Moment-Curvature Analysis

To derive the M-φ and P-ε relationships of concrete layers, axial strains are assumed to have linear distribution, based on which the stress in concrete and reinforcing bars at the cross section of the concrete layers can be calculated. Fig. 5 shows the schematic of axial strain and stress distributions, and resultant forces and bending moment across the cross section.

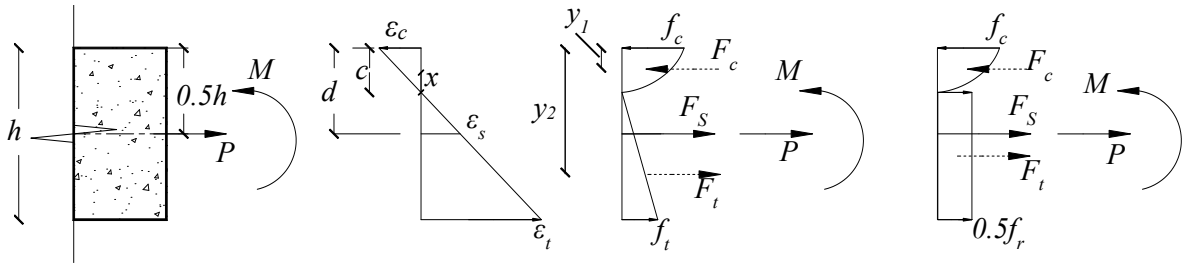

Fig. 5: Forces and stresses over the cross section of concrete layers.

Based on this figure the equilibrium of forces along the panel gives:

$$-F_c + F_s + F_t = P \qquad \textbf{E. 1}$$

where F_c is the compressive force in the concrete that is calculated using the distribution of compressive stresses over the cross section shown in Fig. 5. The compressive stress of concrete is assumed to have parabolic relationship to the compressive strain as proposed by Hognestad (1951) as follows:

$$f = f_c[2\,\varepsilon/\varepsilon_0 + (\varepsilon/\varepsilon_0)^2] \qquad \textbf{E. 2}$$

where ε_0 is taken as 0.0019 based on the results of the compressive tests of concrete cylinders. Also ε is calculated by:

$$\varepsilon = \frac{x}{c}\varepsilon_c \qquad \textbf{E. 3}$$

Where c is the depth of neutral axis to the top of the cross section. The total compressive force over the cross section, F_c, is calculated as:

$$F_c = \int_{x=0}^{c} fB.dx \qquad \textbf{E. 4}$$

The distance between the top of the concrete cross section and the compressive force on the concrete, y_1, is calculated as:

$$y_1 = c - \frac{\int_{x=0}^{c} fBx.dx}{\int_{x=0}^{c} fB.dx} \qquad \textbf{E. 5}$$

The tensile strain in the steel is equal to:

$$\varepsilon_s = \frac{d-c}{c}\varepsilon_c \qquad \textbf{E. 6}$$

And the tensile stress of the steel bars is found by the following equation based on the results of the tensile tests on three coupons.

$$f_s = \begin{cases} E_s\varepsilon_s & , \quad \varepsilon_s < \varepsilon_y \\ f_y & , \quad \varepsilon_y < \varepsilon_s < \varepsilon_{sh} \\ f_y + (f_u - f_y)\left[1 - \dfrac{1}{1 + 47.69(\varepsilon_s - \varepsilon_{sh}) + 713{,}911(\varepsilon_s - \varepsilon_{sh})^4}\right], & \varepsilon_s > \varepsilon_{sh} \end{cases} \qquad \textbf{E. 7}$$

In this equation E_s is 180.93 GPa, f_y is 415.6 MPa and f_u is 558 MPa. Also, strain-hardening strain, ε_{sh}, is equal to 0.00995 according to the results of the tensile tests on reinforcing bar specimens. The total tensile force of the longitudinal bars is equal to:

$$F_s = f_s A_s \quad \text{E. 8}$$

Where A_s is the total areal of seven 10M bars, which was calculated using the measured diameter of the bars as 682 mm^2.

The tensile force carried by the concrete, F_t, is calculated based on the tensile strain of the bottom fibre. If $\varepsilon_t < f_r/E_c$, F_t is calculated as:

$$F_t = 0.5 E_c \varepsilon_t (h - c) \quad \text{E. 9}$$

And the distance between the top of the cross section and the tensile force carried by concrete, y_2, is calculated by:

$$y_2 = h - 1/3\,(h - c) \quad \text{E. 10}$$

If $\varepsilon_t > f_r/E_c$ and tension stiffening of reinforced concrete is not considered, F_t is taken as zero. But if $\varepsilon_t > f_r/E_c$ and tension stiffening of reinforced concrete is considered, the tensile stress of the concrete is taken as $0.5f_r$ (Fig. 5) as suggested by Collins and Mitchell (1997) and the tensile force carried by the concrete is calculated using the procedure described by Collins and Mitchell (1997) as:

$$F_t = 0.5 f_r (h - c) \times 2 n_b \times 7.5 d_b \quad \text{E. 11}$$

Where n_b is the number of bars, which is equal to 7, and d_b is the diameter of the bars which was measured as 11.14 mm. Then y_2 is found by:

$$y_2 = h - 0.5(h - c) \quad \text{E. 12}$$

Now, for any value of ε_c, the only unknown in equation E. 1 is c, which can be found by solving equation E. 1 using numerical methods. Then the bending moment on the cross section is found by summing the moments of all forces about the top of the cross section.

$$M = F_t y_2 + F_s d - 0.5Ph - F_c y_1 \quad \textbf{E. 13}$$

The curvature is found by:

$$\varphi = \varepsilon_c / c \quad \textbf{E. 14}$$

Since the axial force is acting on the mid-height of the cross section, the axial strain of the concrete layer under combined effect of axial force and bending moment is taken as the axial strain of the mid-height of the cross section when P is acting minus the axial strain the mid-height when P is zero, i.e.:

$$\varepsilon_a = \frac{0.5h - c}{c} \varepsilon_c - \varepsilon_{a0} \quad \textbf{E. 15}$$

Where ε_{a0} is the axial strain of the mid-height of the cross section when P is zero. Now, M-φ and P-ε graphs can be constructed to be incorporated in MLE analysis of PICP.

B.2. Steps of MLE Analysis for P4-16

Here, the steps of MLE analysis of P4-16 are presented as an example to elaborate on how the proposed MLE analysis is performed. The ZSPC in P4-16 are 101.2 mm wide and 1.47 mm thick. The shear behaviour of ZSPC in P4-16 comes from the results of the shear test specimens SH4-16 and is simplified as shown in Figure 8-5. The parameters of this shear behaviour used in MLE modeling are:

Shear strength: V_r= 14.52 kN

Secant shear stiffness: K_s = 28.65 kN/mm

Yield shear deformation: $\Delta_y = Vr/K_s$ = 0.51 mm

Shear deformation at failure: Δ_f = 3.0 mm

Residual shear strength: V_{res} = 11.9 kN

In the MLE model, unit load is applied on the loading beams. The step of MLE analysis is shown in table T 2. The parameters in this table are as follows.

T 1: Definition of parameters used in MLE model.

Parameter	Definition	Calculation for step *i*
ρ	Load multiplier applied to the unit load on the loading beams	
$\delta\Delta_v$	Increment of mid-span deflection	From MLE model
Δ_v	Mid-span deflection	$\Delta_{v,i}= \Delta_{v,i-1} + \rho\delta\Delta_{v,i-1}$
ΔP	Increment of vertical load	From MLE model
P	Vertical load	$\Delta_{v,i}= \Delta_{v,i-1} + \rho\delta\Delta_{v,i-1}$
ΔV_n	Increment of shear force of ZSPC in the n^{th} row of connectors (Figure 7-12)	From MLE model
V_n	Shear force of ZSPC in the n^{th} row of connectors (Figure 7-12)	$V_{n,i} = V_{n,i-1} + \rho\Delta V_{n,i-1}$
$\delta\Delta_{sn}$	Increment of shear deformation of ZSPC in the n^{th} row of connectors (Figure 7-12)	From MLE model
Δ_{sn}	Shear deformation of ZSPC in the n^{th} row of connectors (Figure 7-12)	$\Delta_{sn,i}= \Delta_{sn,i-1} + \rho\delta\Delta_{sn,i-1}$
ΔF_{lt}	Increment of axial force in the bottom (tensile) concrete layer	From MLE model
F_{lt}	Axial force in the bottom (tensile) concrete layer	$F_{lt,i} = F_{lt,i-1} + \rho\Delta F_{lt,i-1}$
ΔM_{lt}	Increment of bending moment in the bottom (tensile) concrete layer	From MLE model
M_{lt}	Bending moment in the bottom (tensile) concrete layer	$M_{lt,i} = M_{lt,i-1} + \rho\Delta M_{lt,i-1}$

ΔF_{lc}	Increment of axial force in the top (compressive) concrete layer	From MLE model
F_{lc}	Axial force in the top (compressive) concrete layer	$F_{lc,i} = F_{lc,i-1} + \rho \Delta F_{lc,i-1}$
ΔM_{lc}	Increment of bending moment in the top (compressive) concrete layer	From MLE model
M_{lc}	Bending moment in the top (compressive) concrete layer	$M_{lc,i} = M_{lc,i-1} + \rho \Delta M_{lc,i-1}$

In the MLE analysis in this example, the increments of out-of-plane mid-span deflection, total vertical force on the panel, forces and bending moments in the concrete layers, and shear force and deformation in the connectors are derived from linear elastic analysis of the modeled panel under unit load. Then, the load multiplier, ρ is solved such that the most critical element reaches its failure or yielding point. Then, the stiffness of that element is modified, and another linear elastic analysis is performed. The critical element in every step is different. In table T 2 the value of the critical element in every step is underlined. Table T 2 shows the calculation for each step and table T 3 gives the description of each step.

T 2: Steps of MLE analysis for P4-16 with tension stiffening of the reinforced concrete.

		Step							
Parameter		**1**	**2**	**3**	**4**	**5**	**6**	**7**	**8**
ρ			6.65	4.07	1.15	0.48	3.25	-1.75	0.75
$\delta\Delta_v$	mm	1.3	0.3	0.5	0.6	1.9	4.4	1.0	1.9
Δ_v	mm	1.3	3.2	5.2	5.9	6.8	21.1	19.3	20.7
ΔP	kN	15.3	2.3	2.3	2.3	2.3	2.3	2.3	2.3
P	kN	15.3	30.5	39.8	42.4	43.5	51.0	47.0	48.7
ΔV_3	kN	4.3	0.9	1.0	0.0	0.0	0.1	1.6	0.0
V_3	kN	4.3	10.5	**14.5**	14.5	14.5	14.8	**11.9**	11.9
$\delta\Delta_{s3}$	mm				0.1	0.3	0.7	0.1	0.3
Δ_{s3}	mm			0.5	0.6	0.7	**3.0**	2.9	3.1
ΔV_2	kN	3.5	0.8	0.8	1.3	2.4	0.1	1.1	2.4
V_2	kN	3.5	8.8	11.9	13.4	**14.5**	14.7	12.7	**14.5**
$\delta\Delta_{s2}$	mm						0.5	0.0	0.1
Δ_{s2}	mm					0.5	2.1	2.1	2.1
ΔV_1	kN	1.3	0.3	0.3	0.4	0.5	1.8	0.3	0.5
V_1	kN	1.3	3.1	4.1	4.5	4.8	10.8	10.2	10.6
$\delta\Delta_{s1}$	mm								
Δ_{s1}	mm								
ΔF_{lt}	kN/m	15.2	3.4	3.5	2.9	5.2	3.6	5.4	5.2
F_{lt}	kN/m	15.2	37.8	52.1	55.5	57.9	69.5	60.0	63.9
ΔM_{lt}	kN.m/m	1.0	0.2	0.0	0.0	0.1	0.2	0.1	0.1
M_{lt}	kN.m/m	1.0	**2.3**	2.4	2.5	2.5	3.2	3.1	3.2
ΔF_{lc}	kN/m	-15.5	-3.5	-3.5	-2.8	-5.2	-3.6	-5.5	-5.2

F_{lc}	kN/m	-15.5	-38.5	-52.5	-55.7	-58.2	-69.7	-60.2	-64.1
ΔM_{lc}	kN.m/m	1.2	0.2	0.4	0.5	0.1	0.2	0.1	0.1
M_{lc}	kN.m/m	1.2	2.7	4.3	**4.9**	4.9	5.7	5.6	5.7

T 2 (Cnt'd): Steps of MLE analysis for P4-16.

Parameter		Step 9	10	11	12	13	14
ρ		1.76	-2.44	1.68	0.28	7.04	4.00
$\delta\Delta_v$	mm	4.4	1.0	1.4	4.4	5.5	8.9
Δ_v	mm	28.4	25.8	28.2	29.4	68.1	103.7
ΔP	kN	2.3	2.3	2.3	2.3	2.3	2.3
P	kN	52.7	47.1	51.0	51.6	67.7	76.9
ΔV_3	kN	0.1	1.6	2.3	0.1	0.1	0.1
V_3	kN	12.0	8.0	**11.9**	11.9	12.5	13.0
$\delta\Delta_{s3}$	mm	0.7	0.1	0.1	0.7	0.8	1.2
Δ_{s3}	mm	4.4	4.2	4.4	4.5	10.1	15.1
ΔV_2	kN	0.1	1.1	0.0	0.1	0.1	0.1
V_2	kN	14.6	**11.9**	11.9	11.9	12.4	12.8
$\delta\Delta_{s2}$	mm	0.5	0.0	0.1	0.5	0.7	1.0
Δ_{s2}	mm	**3.0**	2.9	3.1	3.3	7.9	12.0
ΔV_1	kN	1.8	0.3	0.6	1.8	0.0	0.0
V_1	kN	13.8	13.1	14.0	**14.5**	14.7	14.8
$\delta\Delta_{s1}$	mm					0.2	
Δ_{s1}	mm				0.5	2.1	
ΔF_{lt}	kN/m	3.6	5.4	5.1	3.6	0.2	0.4
F_{lt}	kN/m	70.1	56.9	65.4	66.4	67.5	69.3
ΔM_{lt}	kN.m/m	0.2	0.1	0.1	0.2	0.4	0.1
M_{lt}	kN.m/m	3.6	3.4	3.5	3.6	**6.7**	**7.1**
ΔF_{lc}	kN/m	-3.6	-5.5	-5.2	-3.6	-0.2	-0.4
F_{lc}	kN/m	-70.4	-57.0	-65.7	-66.6	-67.8	-69.2
ΔM_{lc}	kN.m/m	0.2	0.1	0.1	0.2	0.5	0.8
M_{lc}	kN.m/m	6.1	5.9	6.1	6.1	9.6	12.8

T 3: Description of steps in MLE analysis of P4-16.

Step	Description
1	Dead load of the panel is applied. ρ should be one since the self-weight is not increased during loading.
2	Loading is applied on the loading beams. Critical element is found to be the bottom concrete layer. ρ is set such that the bottom concrete layer reaches its cracking moment of 2.3 kN.m under 37.8 kN of tensile force (Figure 8-9). Then EI of this layer is set to the slope of the M-φ curve after cracking, and EA is set to the slope of the P-ε graphs (Figure 8-11). The modified stiffness values were found as: EI = 94.94x10^9 N.mm^2 and EA= 141x10^6 N/strain.
3	Loading is applied on the loading beams. Critical element is found to be the connectors in the third row of ZSPC, that are closest to panel's end (Figure 7-12). ρ is set such that the shear force in these connector reaches V_r which is 14.52 kN. Then the stiffness of these connectors is set to 0.01 times the initial stiffness, instead of zero shear stiffness. This is because if zero shear stiffness is assigned to the connectors the FEA model would have numerical instability.
4	Loading is applied on the loading beams. Critical element is found to be the top concrete layer. ρ is set such that the top concrete layer reaches its cracking moment of 4.9 kN.m under 55.7 kN of compressive force (Figure 8-9). Then EI of this layer is set to the slope of the M-φ curve after cracking, and EA is set to the slope of the P-ε graphs (Figure 8-11). The modified stiffness values were found as: EI = 109.42x10^9 N.mm^2 and EA= 203x10^6 N/strain.
5	Loading is applied on the loading beams. Critical element is found to be the connector in the second row of ZSPC (Figure 7-12). ρ is set such that the shear force in these connector reaches V_r which is 14.52 kN. Then the stiffness of these connectors is set to 0.01 times the initial stiffness, instead of zero shear stiffness. This is because if zero shear stiffness is assigned to the connectors the FEA model would have numerical instability.
6	Loading is applied on the loading beams. Critical element is found to be the connector in the third row of ZSPC (Figure 7-12). ρ is set such that the shear deformation in these

connectors reaches Δ_{sf}, which is 3.0 mm. After Δ_f there will be a drop in the shear force of these connectors. So next step should be unloading.

7 Loading is applied on the loading beams. Panel should be unloaded until V_3 reaches V_{res} of 11.9 kN. For this The stiffness of all ZSPC is restored to their secant shear stiffness of 28.65 kN/mm. Then, ρ is set as a negative value such that the shear force in the third row of connectors reaches the V_{res} of 11.9 kN.

8 Loading is applied on the loading beams. The shear stiffness of the third row of connectors is set to $0.01K_s$. Panel is reloaded in this step such that V_2 reaches V_r again, similar to step 5.

9 Loading is applied on the loading beams. Critical element is found to be the connector in the second row of ZSPC (Figure 7-12). ρ is set such that the shear deformation in these connectors reaches Δ_{sf}, which is 3.0 mm. After Δ_f there will be a drop in the shear force of these connectors. So next step should be unloading.

10 Loading is applied on the loading beams. Panel should be unloaded until V_2 reaches V_{res} of 11.9 kN. For this, the stiffness of all ZSPC is restored to their secant shear stiffness of 28.65 kN/mm. Then, ρ is set as a negative value such V_2 reaches 11.9 kN.

11 Loading is applied on the loading beams. The shear stiffness of the second row of connectors is set to $0.01K_s$. Panel is reloaded in this step such that V_3 reaches V_{res} again.

T 3 (Cnt'd): Description of steps in MLE analysis of P4-16.

Step	Description
12	Loading is applied on the loading beams. Critical element is found to be the connector in the first row of ZSPC (Figure 7-12). ρ is set such that the shear force in these connector reaches V_r which is 14.52 kN. Then the stiffness of these connectors are set to 0.01 times the initial stiffness, instead of zero shear stiffness
13	Loading is applied on the loading beams. Critical element is found to be the bottom concrete layer. ρ is set such that the bottom concrete layer reaches its yielding moment

of 6.7 kN.m under 67.5 kN of tensile force (Figure 8-9). Then *EI* of this layer is set to the slope of the *M*-φ curve after yielding and *EA* is set to the slope of the *P*-ε graphs (Figure 8-11). The modified stiffness values were found as: $EI = 13.16 \times 10^9$ N.mm^2 and $EA = 9.87 \times 10^6$ N/strain.

14 Loading is continued up to 103 mm of vertical deflection, which is the end of the experimental data from the flexural test.

B.3. Calculation Examples for the Proposed Analytical Models

Panel with truss girder connector Salmon et al. (1997)

Geometric properties:

Width	B=	2440	mm
Span length	L=	9144	mm
Insulation thickness	t_{ins}=	76.2	mm
Thickness of concrete layer	t_l=	63.5	mm

Concrete properties:

Compressive strength	f_c=	34.45	MPa
Modulus of elasticity	E_c=	30,522	MPa
Tensile strength	f_t=	3.52	MPa

Reinforcement properties:

Area of prestressing strands	A_{ps}=	258	mm^2
5-3/8 in. strands			
Ultimate tensile strength	f_{pu}=	1860	MPa
Yield tensile strengt.	f_{py}=	1674	MPa
Effective stress	f_{pr}=	1310	MPa
Area of non-prestressing reinforcement	A_s=	412.8	mm^2
Yield strength	f_y=	448	MPa

Properties of the interlayer shear connectors:

Shear strength	V_r=	54.11	kN/m
Shear stiffness (kN/mm per meter of length)	k_s=	61.63	kN/mm/m
$\Delta_y = V_r / K_s$	Δ_y =	0.88	mm
shear deformation at failure	Δ_f =	8.9	mm

B.2.1. Analytical Method using Simplified MLE

Out-of-plane deformation

The shear modulus of elasticity of the shell elements that represent the truss connector, G, is: $G = \frac{k_s h_c}{t}$	G=	861	MPa
t is the thickness of shell element taken as 10 mm.			
In the MLE model, the uniform is 1.5 kPa. then:	Δ=	14.2	mm

Cracking strength:

$P_s = A_{pr} f_{pr}$	P_s=	337,980	N
Tensile strength of concrete is modified to account for the beneficial effect of prestressing. $f_{tm} = f_t + P_s/A_l$	f_{tm}=	5.7	MPa
Tension force from the model, P	P =	65.7	kN/m of width
Bending moment in the tensile concrete layer	M_{lt} =	0.63	kN.m/m of width
For 1.0 m of width: $A = 1000 \times t_l$ $S = 1000 \times t_l^3/6$	σ =	1.97	MPa

$\sigma = P/A + M_{lt}/S$

$q_{cr} = q \times f_{tm}/\sigma$ $q_{cr} =$ 2.9 kPa

Out-of-plane strength:

Check $(A_s f_y + A_{pt} f_{py})$< or > V_t $A_s f_y + A_{pt} f_{py} =$ 616.8 kN

V_t at ultimate is calculate by considering linear distribution of interlayer shear deformation of interlayer connectors such that the shear deformation of the critical connector is less than Δ_f. The following figure shows the distribution of interlayer shear forces and deformations among connectors. Based on this figure the following calculation shows how to find the total interlayer shear force that can be mobilized between the panel mid-span and one end of the panel.

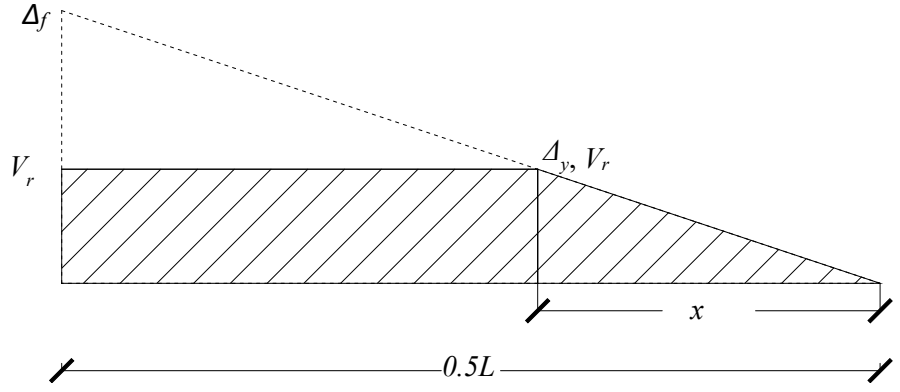

$\frac{\Delta_f}{0.5L} = \frac{\Delta_y}{x}$ $x =$ 451 mm

$V_t = V_r(0.5L - x) + 0.5 \times V_r \times x$ $V_t =$ 940 kN

$(A_s f_y + A_{pt} f_{py}) < V_t$, therefore the maximum interlayer shear force is V_t.

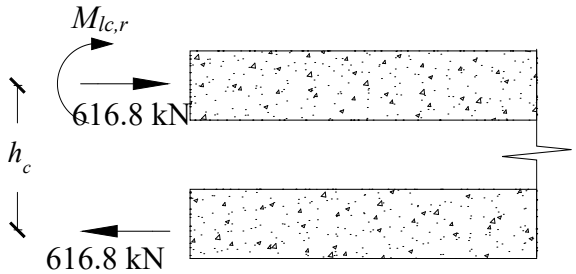

$\alpha = .85 - .0015 f_c$ $\alpha =$ 0.8

$\alpha f_c B a = A_s f_y + A_{pr} f_{py} + 616.8$ $a =$ 18.4 mm

axial force and reinforcement are assumed to be at the mid-thickness of concrete layer.

The moment about mid-thickness of concrete layer:

$M_{lc,r} = \alpha f_c B a (d - 0.5a)$ $M_{lc,r} =$ 27.83 kN

Total moment under q=1.0 kPa, M_t, is:

$M_t = M_{lt} + M_{lc} + P h_c$

Where M_{lt}, M_{lc} and P are derived from the FEA results of linear elastic analysis of PICP with cracked concrete layers.

M_{lt}= $M_t =$ 25.47 kN.m

$M_{lc,r} + 616.8 \times h_c = M_t \, q_u / q$ $q_u =$ 4.47 kPa

Two experiments were conducted on PICP with truss connectors by Slamon et al. (1997). The results of the experiments are as follows:

$q_{u,e1}$=5.02 kPa, $q_{u,e2}$=6.28 kPa

Average experimental ultimate strength $q_{u,e} =$ 5.65 kPa

Difference between the experimental results. $\Delta q_{u,e}/q_{u,e} =$ 22.3 %

$$(\Delta q_{u,e}/q_{u,e})\% = (|q_{u,e2} - q_{u,e1}|)/q_{u,e} \times 100\% =$$

Error of estimated ultimate strength $err\% =$ 20.9 %

$err\% = |q_{u,e} - q_u|/q_{u,e} \times 100\%$

B.2.2. Analytical Method using Degree of Composite Action

Out-of-plane deflection:

Moment of inertia of composite panel	I_c=	1.616E+09	mm^4
$h = 2t_l + t_{ins}$, $I_c = B(h^3 - t_{ins}^3)/12$			
Moment of inertia of non-composite panel	I_{nc}=	5.206E+07	mm^4
$I_{nc} = 2Bt_l^3/12$			
Out-of-plane uniform load	q=	1.5	kPa
$\Delta_c = \frac{5qBL^4}{384E_cI_c}$	Δ_c=		mm
$\Delta_{nc} = \frac{5qBL^4}{384E_cI_{nc}}$	Δ_{nc}=		mm
$A_l = Bt_l$	A_l=		
Distance between centroids of concrete layers	h_c=		
$h_c = t_{ins} + t_l$			
$K_0 = \frac{E_cA_l}{L\left(1 - \frac{1.55I_c}{A_lh_c^2}\right)}$	K_0=	3.013E+06	N/mm
Total interlayer shear stiffness	K=	1.127E+06	N/mm
4 truss girders used across the width			
$K = 4 \times 0.5Lk_s$			
	K/K_0 =	0.37	
$\beta = \frac{21.02\ K/K_0}{21.02\ K/K_0 + 0.6418}$	β =	0.92	
$\beta = \frac{\Delta_{nc} - \Delta}{\Delta_{nc} - \Delta_c}$	Δ=	14.2	mm

Cracking strength:

$P_s = A_{pr} f_{pr}$	P_s=	337,980	N
Tensile strength of concrete is modified to account for the beneficial effect of prestressing.	f_{tm}=	5.7	MPa
$f_{tm} = f_t + P_s/A_l$			
$V_c = \frac{qbL^2 A_l h_c}{16 E_c I_c}$	V_c=	2.562E+05	N
$M_t = 0.125 qBL^2$	M_t=	38,252,826	N.mm
$\beta = V_t/V_c$	V_t=	2.368E+05	N
$M_t = 2M_l + V_t h_c$	M_l=	2.585E+06	N.mm
$\sigma = \frac{V_t}{A_l} + \frac{M_l}{S_l}$	σ =	3.105	MPa
$S_l = \frac{I_l}{0.5 t_l}$			
$q_{cr} = q \times f_{tm}/\sigma$	q_{cr}=	2.755	kPa

Out-of-plane strength:

From Appendix B.2.1. ($A_s f_y + A_{pt} f_{py}$)< V_t , therefore the maximum interlayer shear force is $A_s f_y + A_{pt} f_{py}$= 616.8 kN.

And flexural capacity of the compressive concrete layer from Appendix B.2.1. is: $M_{lc,r}$=27.83 kN.m

$M_{lc,r} + 616.8 \times h_c = 0.125 q_u BL^2$	q_u=	4.47	kPa

Two experiments were conducted on PICP with truss connectors by Slamon et al. (1997). The results of the experiments are as follows:

$q_{u,e1}$=5.02 kPa, $q_{u,e2}$=6.28 kPa

Average experimental ultimate strength	$q_{u,e}$=	5.65	kPa
Difference between the experimental results.	$\Delta q_{u,e}/q_{u,e} =$	22.3	%

$$(\Delta q_{u,e}/q_{u,e})\% = (|q_{u,e2} - q_{u,e1}|)/q_{u,e} \times 100\% =$$

Error of estimated ultimate strength	$err\% =$	20.9	%

$$err\% = |q_{u,e} - q_u|/q_{u,e} \times 100\%$$